# UNIVERSITÉ DE STRASBOURG

École Doctorale des Sciences de la Vie et de la Santé ED 414

Luxembourg Institute of Health (LIH)

Laboratory of Experimental Cancer Research

**THÈSE** présentée par:

Antoun Al Absi

Soutenue le : **06 Juillet 2018**

pour obtenir le grade de: **Docteur de l'Université de Strasbourg**

Discipline/ Spécialité: Aspect moléculaire et cellulaire de la biologie / Oncologie - Immunologie

## Role of the actin cytoskeleton in breast cancer cell resistance to natural killer cells

**THÈSE dirigée par :**
Dr. Clément THOMAS                    LIH, Luxembourg

**Rapporteurs externes :**
Dr. Jacques ZIMMER                    LIH, Luxembourg
Dr. Juan J. GARCIA VALLEJO            VUMC, Amsterdam

**Examinateur interne :**
Dr. Catherine-Laure TOMASETTO         IGBMC, Strasbourg

**Membre invité :**
Dr. Bassam JANJI                      LIH, Luxembourg

**To the greatest family one could ever have,**
**To Syria...**

# Acknowledgement

*First, I would like to express my gratitude to all the members of the jury, Dr. Catherine-Laure Tomasetto, Dr. Juan J. Garcia Vallejo and Dr. Jacques Zimmer for accepting to evaluate my thesis work. Thank you for your time and your effort. I am grateful to Dr. Hélène Heagel and Dr. Andreas Girod for being members of my mid-thesis committee.*

*This work was completed at the Laboratory of Experimental Cancer Research, at the Luxembourg Institute of Health (LIH). It was a pleasure for me to work with all the great people at the LIH. I am very grateful to Dr. Guy Berchem for offering me the chance to proceed with my PhD thesis in his laboratory. I am also thankful to "Fond National de la Recherche" for funding my PhD project.*

*Clément, thank you for being a great (and cool) supervisor. You integrated me in your laboratory and you were always my first supporter. We worked hard together to make a successful project. I wasn't always perfect, I had my ups and downs but I hope I made you proud of me. I am sure we will cross paths again, and until we do, I wish you and your family all the best.*

*Thank you, Bassam, for your support during my thesis. I remember you telling me I will achieve great work when we first met, I hope that I was at your expectation.*

*My colleagues in Cytoskeleton and Cancer Progression team, I cannot thank you enough. MERCI. Flora, with your positive energy, you were always eager to help me and I would be lost in the lab without you. I learned a lot from you and I will be always grateful! Céline, you transmit to me your passion for the microscope. Thank you for always being there to enhance my work. Hannah, thank you for all your help last year. I am sure you will do a great PhD. Good luck in all your endeavors. Thank you XianQing for not only being a colleague but a friend too. Josh, thank you for being a source of motivation. Carla, Ludo and Florian, I really enjoyed working with you all. I am grateful for your help.*

*Etienne, Jerome, Sandrine, Delphine, Marina, Anne, Ernesto and each member of TSI and TM teams, it was really a pleasure to work with you. Thank you for all the sweet and funny moments we shared together. A special thank you for Maman Mano, Nassera and Victoria for your kindness and care. Malina, we met not long time ago but I am sure that we will laugh together again. Alexandra, Rita, Massimo, Sandrine, Angelina, Vanessa and Ning, each one of you took a different professional way but your presence around me during my PhD made my days. Thank you.*

*Thank you Malou for supporting me and helping all the PhD students from the bottom of your heart.*

*Joanna, thank you a lot for all the support you gave me. I think we can make a comedy movie about our first 3 months in the lab! Hehe*

*My gratitude also goes to my colleagues in NorLux lab. I really enjoyed working with you. Sabrina, Anna, Katrin, and my dear Monika thank you for everything. Mohammad, you are the coolest colleague I ever had. Keep it up.*

*Coralie, I cannot thank you enough for all the support you have given to me. You let me discover new aspects that made my PhD a successful project. Lea, Maira and Anna, thank you a lot.*

*Takouhie, thank you for every single funny moment we spent together. I smiled each time we talked and this smile will never go away. Thank you, Kris, for listening to me and helping me each time. Audrey, each Monday repeat the same sentence I used to say to you. Elodie, I will miss every single little thing we did together. Thank you for being a true friend.*

*Tsolère (TsoTso), we began the PhD together, finish it together and we will stay always together. You are not just a colleague or a friend, you are my sister.*

*My close friends, thank you from the bottom of my heart for supporting me in every single step. I am lucky to have each one of you in my life. Yasmine, Mohammad and Kamel, thank you for giving me hope, support and fun.*

*My undying gratitude is to my big family for their support and encouragement. Even though war separated us from each other, I always felt your support. Nayla, my lovely aunt, I would have never achieved anything without your love and care. Thank you for being always by my side and most caring person.*

*One personal "Thank you" for a very special person in my life, because you were beside me since the first day we met. Francesco, my love, my friend and my partner, thank you for supporting me each day more. We are strong together. I love you.*

*Even through distance, our hearts have remained together. My dad Farid and my mom Rouyida, you are my real heroes. I wouldn't have achieved nothing in my life without your love and support. I know you sacrificed a lot for me and my brothers to receive the best education. While I was doing my PhD, you were under fire in Syria. Every time I called you, you would still find the strength to support me. I am lucky I have parents like you. My brothers, Dany and Naji, thank you for always encouraging me. You are the real reason for me to smile.*

*My lovely little family, this PhD is dedicated to you. I hope I made you proud of me.*

**Antoun AL ABSI**

UNIVERSITÉ DE STRASBOURG

LUXEMBOURG
INSTITUTE
OF HEALTH
RESEARCH DEDICATED TO LIFE

# Rôle du cytosquelette d'actine dans la résistance des cellules de cancer du sein à la lyse induite par les cellules «natural killer»

## Résumé

L'évasion immunitaire tumorale joue un rôle central dans la progression tumorale et représente un obstacle majeur au succès des immunothérapies. Dans cette Thèse nous avons étudié le rôle du cytosquelette d'actine dans la résistance des cellules de cancer du sein à la lyse induite par les cellules "natural killers" (NKs). Nous avons trouvé que les cellules de cancer du sein résistantes échappent à l'attaques des cellules NKs par une accumulation importante et rapide d'actine près de la synapse immunologique, un processus que nous avons nommé "réponse actine". Nos analyses mécanistiques suggèrent que la réponse actine induit la polarisation d'autophagosomes vers la synapse immunologique et facilite ainsi la dégradation des molécules cytotoxiques sécrétées par les cellules NKs, tel que le ganzyme B, par autophagie. De plus, la réponse actine est associée au regroupement de ligands inhibiteurs à la synapse, suggérant qu'elle est au centre de plusieurs mécanismes de résistance. Dans leur ensemble, nos résultats constituent une base pour le développement d'approches thérapeutiques visant à interférer avec la réponse actine et à restaurer une réponse immunitaire anti tumorale efficace.

Mots-clés : Cancer du sein, cellules Natural Killer, cytosquelette d'actine, Cytotoxicité, évasion immunitaire, granzyme B.

## Résumé en anglais

Tumor immune evasion plays a central role in cancer progression and is a major hurdle to effective immunotherapy. In this Thesis, we examine the role of the actin cytoskeleton in breast cancer cell resistance to natural killer (NK) cell-mediated cell lysis. We found that resistant breast cancer cells escape from NK-cell attack through a rapid and prominent accumulation of actin near the immunological synapse, a process we termed the "actin response". Our mechanistic investigations suggest that the actin response drives autophagosome polarization toward the immunological synapse and thereby facilitates the autophagy-mediated degradation of NK cell-derived cytotoxic molecules such as granzyme B. In addition, the actin response was associated with inhibitory ligand clustering at the immunological synapse, suggesting that it is a common driver of different immune evasion mechanisms. Taken together, our data lays the groundwork for therapeutic approaches aimed at interfering with the actin response and restoring an effective anti-tumor immune response.

# Table of Contents

# Table of figures (Excluding the figures of the articles)

# Abbreviations

| | |
|---|---|
| α-SMA | α-smooth muscle actin |
| ABC | ATP-binding cassette |
| ABP | Actin-binding proteins |
| ADCC | Antibody-dependent cellular cytotoxicity |
| ADP | Adenosine 5'-diphosphate |
| AF | Actin filament |
| AML | Acute myeloid leukemia |
| Apaf-1 | Apoptotic peptidase activating factor 1 |
| aPKC | Atypical protein kinase C |
| Arl8b | ADP-ribosylation factor-like 8b |
| ARPC | ARP complex component |
| ATG | Autophagy related genes |
| ATP | Adenosine 5'-triphosphate |
| BAG-6 | Bcl-2associated athanogene 6 |
| BC | Breast cancer |
| Bcl-2 | B-cell lymphoma-2 |
| BCR | B cell receptors |
| bHLH | Basic helix-loop-helix |
| Bid | BH3 interacting domain |
| BMI1 | B lymphoma Mo-MLV insertion region 1 homologue |
| BTLA | B and T lymphocyte attenuator |
| C9 | Component C |
| CAR | Chimeric antigen receptors |
| CARMIL | Capping protein Arp2/3 mysoin I linker |
| CCD | Coiled-coil domain |
| CCR4 | CC chemokine receptor 4 |
| CFP | Complement factor P |
| CIP4 | Cdc42-interacting protein-4 |
| CLP | Common Lymphoid progenitor |
| CMA | Chaperone-mediated autophagy |
| CQ | Chloroquine |
| CRIB | CDC42 and Rac interactive binding |
| CTBP | C-terminal-binding protein |
| CTLA-4 | Cytotoxic T lymphocyte-associated protein 4 |
| DAD | Diaphanous auto-inhibitory domain |
| DC | Dentritic cells |
| DCIS | Ductal carcinoma in situ |
| DDR2 | Discoidin domain receptor 2 |
| DID | DAD-interacting domain |

| | |
|---|---|
| DISC | Death-inducing signaling complex |
| DLG | Discs large |
| DR | Death receptor |
| ECD | Evolutionary conserved domain |
| EGFR | Epiermal growth factor receptor |
| EMT | Epithelial-to-mesenchymal transition |
| ER | Estrogen receptor |
| ERK | Extracellular signal-regulated kinases |
| EZH2 | Enhancer of zeste homologue 2 |
| FADD | Fas-associated death domain |
| FAK | Focal adhesion kinase |
| FGFR | Fibroblast growth factor receptor |
| FH1 and 2 | Formin homology domain 1 and 2 |
| FHL | Familial haemophagocytic lymphohitiocytosis |
| FIP200 | FAK-family interacting protein of 200 kDa |
| FLIP | FLICE-like inhibitory protein |
| FOX | Forkhead box |
| FoxP3 | X-linked forkhead/winged-helix transcription factor box P3 |
| FSH | Follicle-stimulating hormone |
| G-actin | Globular actin |
| GABARAP | Gamma-aminobutyric acid receptor-associated protein |
| GAPs | GTPase activating proteins |
| GBD | GTPase binding domain |
| GDIs | Guanine-nucleotide dissociation inhibitors |
| GEP | Guanine-nucleotide exchange factor |
| GHL2 | Grainyhead-like-2 |
| GITR | Glucocorticoid-induced TNF receptor family-related gene |
| GM-CSF | Granulocyte-macrophage colony-stimulating factor |
| GSK3 | Glycogen synthase kinase-3 |
| GVHD | Graft-versus-host-disease |
| HDAC | Histone-deacetylase |
| Her2/neu | Human epidermal growth factor receptor/neu |
| HIF-1$\alpha$ | Hypoxia-inducible factor-1$\alpha$ |
| HLA | Human leukocyte antigen |
| HS1 | Haematopoietic lineage cell-specific protein 1 |
| HVEM | Herpes virus entry mediator |
| IAF | Iodoacetamido-fluorescein |
| ICAM-1 | Intercellular adhesion molecule-1 |
| ID | Inhibitor of differentiation |
| IDC | Invasive ductal carcinoma |
| IL | Interleukin |
| ILC | Innate lymphoid cell |
| IQGAP1 | IQ containing GTPase-activating protein 1 |

| | |
|---|---|
| ITAM | Immuno-receptor tyrosine-based activation motif |
| ITIM | Immuno-receptor tyrosine-based inhibitory motif |
| JAK | Janus Kinase |
| KIR | Killer cell immunoglobulin-like receptor |
| KLRG1 | Killer cell lectin-like receptor G1 |
| LAG3 | Lymphocyte activation gene 3 |
| LAMP | Lysosome associated membrane protein |
| LATS2 | Large tumor suppressor 2 |
| LC3 | Light chain 3 |
| LFA-1 | Lymphocyte function associated antigen-1 |
| LGL | Lethal giant larvae |
| LH | Lutenizing hormone |
| LILR | Leukocyte immunoglobulin like receptors |
| LIMK | LIM kinase |
| LSD1 | Lys-specific demethylases 1 |
| MACEP | Membrane-attack-complex/PRF protein |
| MAGES | Melanoma-associated antigens |
| mDia | Mammalian Diaphanous formin |
| MET | Mesenchymal-to-epithelial transition |
| MHC | Major histocompability complex |
| MICA/B | MHC class I-related chain A and B |
| miR | microRNA |
| MLL5 | Mixed-lineage leukemia-5 |
| MMPs | Metalloproteinases |
| MTOC | Microtubule organizing center |
| MTORC1 | mammalian TOR complex |
| N-CAM | Neural-cell adhesion molecule |
| N-WASP | Neural-WASP |
| NCRs | Natural cytotoxicity receptors |
| NK | Natural killer |
| NKEXO | Natural killer cell-derived exosomes |
| NKG2 | Natural killer group 2 |
| NPF | Nucleation-promoting factor |
| NSCLC | Non-small-cell lung carcinoma |
| NUMA | Nuclear mitotic apparatus protein A |
| PAK | p21-activated kinase |
| PALS1 | Protein associated with Lin-7 1 |
| PAMPs | Pathogen-associated molecular patterns |
| PAP | Prostatic acid phosphatase |
| PARP-1 | Poly ADP-ribose polymerase 1 |
| PATJ | PALS1-associated tight junction protein |
| PCAF | p300/CBP-associated factor |
| PD1 | Programmed cell death 1 |

| | |
|---|---|
| PDGF | Platelet-derived growth factor |
| PE | Phosphatidylethanolamine |
| PEGPH20 | PEGylated recombinant hyaluronidase 20 |
| PI3K | Phosphatidylinositol 3-kinase |
| PKD1 | Protein kinase D 1 |
| PLC | Phosphoinositide phospholipase C |
| PR | Progesterone receptor |
| PRC2 | Polycomb repressive complex 2 |
| PRD | Prolin-rich domain |
| PRR | Pattern recognition receptors |
| PSGL-1 | P-selectin glycoprotein ligand-1 |
| Regulatory T cells | Tregs |
| ROCK | Rho-associated coiled-coil containing protein kinase |
| ROS | Reactive oxygen species |
| RTKs | Receptor tyrosine kinases |
| S1P5 | Sphingosine-1-phosphate receptor 5 |
| SH2 and 3 | Src homology 2 and 3 |
| SIP1 | Smad-interacting protein 1 |
| SMAC | Supramolecular activation cluster |
| SNARE | Soluble NSF attachement protein receptor |
| SOX | SRY box |
| STAT | Signal transducer and activator of transcription |
| STING | Stimulator of interferon genes |
| STX17 | SNARE protein syntaxin 17 |
| SWI/SNF | Switch/sucrose non-fermentable |
| T-VEC | Talimogene laherparepvec |
| TCR | T cell receptors |
| TGF-β | Transforming growth factor-β |
| Th1 | T helper type 1 |
| TIGIT | T cell immunoglobulin and ITIM domain |
| TIM3 | T cell immunoglobulin and mucin domain-containing 3 |
| TME | Tumor microenvironment |
| TNBC | Triple-negative breast cancer |
| TNF | Tumor necrosis factor |
| TRAIL | Tumor necrosis factor-related apoptosis-inducing ligand |
| ULBP | UL16-binding protein |
| ULKF | Unc-51-like kinase family |
| UVRAG | UV radiation resistance-associated gene protein |
| VISTA | V-domain immunoglobulin suppressor of T cell activation |
| WASP | Wiskott-aldrich syndrome protein |
| WH1 and 2 | WASP homology 1 and 2 |
| WHAMM | WASP homologue associated with actin, membranes and microtubules |

| WIP | WASP-interacting protein |
| WISP2 | Wnt-inducible signaling pathway protein 2 |
| ZO1 | Zonula occludens 1 |

# List of publications

**Actin cytoskeleton remodeling drives breast cancer cell escape from natural killer cell lysis.**

<u>Antoun Al Absi</u>, Hannah Wurzer, Coralie Guerin, Celine Hoffmann, Flora Moreau, Xianqing Mao, Joshua Brown-Clay, Rémi Petrolli, Monika Dieterle, Jean-Paul Thiery, Salem Chouaib, Guy Berchem, Bassam Janji and Clément Thomas. *Cancer Research*. 2018.

**Hypoxia promotes breast cancer cell invasion through HIF-1α-mediated up-regulation of the invadopodial actin bundling protein CSRP2.**

Xianqing Mao, Celine Hoffmann, Joshua Brown-Clay, Flora Moreau, <u>Antoun Al Absi</u>, Hannah Wurzer, Barbara Soussa, Fernando Schmitt, Guy Berchem, Bassam Janji and Clément Thomas. *Scientific Reports*. 2018.

**CRP2, a new invadopodia actin bundling factor critically promotes breast cancer cell invasion and metastasis.**

Hoffmann C, Mao X, Dieterle M, Moreau F, <u>Al Absi A</u>, Steinmetz A, Oudin A, Berchem G, Janji B and Thomas C. *Oncotarget*. 2016.

**Hypoxia: a key feature of the tumor microenvironment triggers several mechanisms of evasion from natural killer and cytotoxic T lymphocytes surveillance.**

Mgrditchian T, Arakelian T, Paggetti J, Viry E, <u>Al-Absi A</u>, Medves S, Moussay E, Berchem G, Thomas C and Janji B. *Journal of Immunology Research*. 2014.

# Summary of the thesis in French

## Introduction

Les cellules natural killers (NKs) sont des sentinelles du système immunitaire inné qui patrouillent à travers l'organisme pour détecter et détruire les cellules tumorales ainsi que les cellules infectées par des agents pathogènes. Contrairement aux cellules cytotoxiques du système immunitaire adaptatif, telles que les lymphocytes T cytotoxiques CD8^{+}, les cellules NKs détruisent leurs cibles de manière rapide et sans nécessiter de pré-activation par exposition préalable aux antigènes. Ainsi les cellules NKs sont souvent considérées comme la première ligne de défense immunitaire anti-tumorale.

Les cellules NKs sont équipées de récepteurs activateurs et inhibiteurs qui peuvent reconnaître leurs ligands au niveau de la membrane des cellules cancéreuses. La balance entre les signaux inhibiteurs et activateurs régule l'activation de la cytotoxicité des cellules NKs. Suite à la reconnaissance d'une cellule cible, les cellules NKs s'engagent dans une série d'étapes aboutissant à l'exocytose de granules cytolytiques contenant des agents lytiques tels que la perforine et les granzymes. Une étape clé de ce processus est la formation d'une interface entre la cellule NK et sa cible nommée "synapse immunologique". L'établissement d'une synapse lytique est un processus hautement contrôlé qui implique plusieurs phases. Lors de la phase de reconnaissance, la cellule NK établie un conjugué avec sa cible via l'interaction de récepteurs et molécules d'adhésion. La formation du conjugué « cellule NK-cellule cible » requiert une réorganisation importante du cytosquelette d'actine dans la cellule NK, ainsi que la polarisation du centre d'organisation des microtubules (MTOC) et des granules cytolytiques vers la synapse. Lors de l'étape effectrice, les granules cytolytiques sont secrétés vers la cellule cible et induisent l'apoptose. Enfin, lors de l'étape de terminaison, la cellule NK se détache de sa cible morte et régénère son potentiel cytolytique.

Certaines cellules tumorales parviennent à échapper à la lyse cellulaire induite par les cellules NKs et contribuent ainsi la progression de la maladie. Par ailleurs, les mécanismes d'évasion immunitaire limitent l'efficacité des immunothérapies, tels que le transfert adoptif de cellules NKs ou les inhibiteurs de checkpoints immunitaires. Il est donc primordial de mieux caractériser les mécanismes moléculaires de la résistance au système immunitaire, notamment aux cellules NKs, afin d'élaborer de nouvelles

approches thérapeutiques visant à interférer avec ces mécanismes et à restaurer une réponse immunitaire anti-tumorale efficace.

De précédents travaux ont permis de caractériser en détail le rôle clé du cytosquelette d'actine des cellules NKs dans la formation et l'activité de la synapse immunologique. Par exemple, des études d'imagerie à haute résolution ont montré qu'une accumulation d'actine filamenteuse près de la synapse est nécessaire à la polarisation du MTOC et des granules cytolytiques vers la cellule cible. Contrairement à notre connaissance approfondie de l'organisation et des fonctions du cytosquelette d'actine des cellules NKs lors de la reconnaissance et la lyse des cellules cibles, le rôle du cytosquelette d'actine dans les cellules tumorales au cours de ces processus reste énigmatique.

# Objectifs et approches

Mon travail de thèse a consisté à atteindre deux objectifs principaux : 1) documenter l'organisation et la dynamique du cytosquelette d'actine dans les cellules tumorales au cours de leur attaque par les cellules NKs et 2) évaluer le rôle du cytosquelette d'actine des cellules tumorales dans la résistance à la lyse induite par les cellules NKs. Pour atteindre ces objectifs, j'ai focalisé mes travaux sur le cancer du sein dont plusieurs lignées cellulaires différant par leur susceptibilité aux cellules NKs étaient disponibles au laboratoire.

J'ai introduit dans chacune de ces lignées un marqueur du cytosquelette d'actine constitué d'un petit peptide (17 acides aminés) dérivé d'une protéine de Saccharomyces cerevisiae et fusionné à la GFP (LifeAct-mEGFP). L'utilisation combinée de la microscopie confocale de dernière génération et de la cytométrie de flux en image m'a permis de révéler, pour la première fois, les changements de configuration du cytosquelette d'actine dans la cellule tumorale au cours de l'attaque par les cellules NKs avec une haute résolution spatiale and temporelle, et de générer des résultats statistiquement significatifs.

# Résultats

Les données que j'ai obtenues au cours de ma thèse indiquent que le remodelage du cytosquelette d'actine joue un rôle majeur dans le processus de résistance des cellules de cancer du sein à la lyse induite par les cellules NKs. Les principaux résultats de cette étude sont énumérés ci-dessous :

Certaines cellules de cancer du sein répondent à l'attaque des cellules NKs par une rapide et massive accumulation d'actine filamenteuse dans la région de la synapse immunologique, un processus que nous avons nommé « réponse actine ». Toutes les lignées cellulaires de cancer du sein que nous avons analysées comportent une sous-population de cellules capables de répondre à l'attaque des cellules NKs par une réponse actine. En outre, l'abondance relative de cette sous-population dans une lignée donnée est directement liée à la susceptibilité globale de cette lignée à la lyse induite par les cellules NKs. Les lignées cellulaires avec une sous-population abondante de cellules compétentes pour la réponse actine présentent une faible susceptibilité aux cellules NKs. Les lignées cellulaires avec une sous-population réduite de cellules compétentes pour la réponse actine présentent une susceptibilité élevée aux cellules NKs.

Les lignées cellulaires de type mésenchymal contiennent une plus large sous-population de cellules compétentes pour la réponse d'actine et sont plus résistantes à la lyse induite par les cellules NKs que les lignées cellulaires de type épithélial. Une induction expérimentale de l'EMT augmente simultanément la sous-population des cellules compétentes pour la réponse d'actine et la résistance à la lyse induite par les cellules NKs.

La réponse d'actine est responsable de la résistance des cellules tumorales à la cytotoxicité induite par les cellules NKs. L'analyse de cellules au microscope confocal procure une preuve directe que les cellules tumorales avec une réponse d'actine survivent à l'attaque des cellules NKs (et ce, plusieurs heures après le détachement des cellules effectrices), alors que les cellules tumorales sans réponse d'actine sont efficacement lysées. En accord avec ces résultats, nous avons établi que le taux d'apoptose est significativement réduit dans les cellules tumorales présentant une réponse d'actine, par rapport aux cellules sans réponse d'actine. Enfin, l'inhibition de la réponse d'actine induite par la déplétion de régulateurs clés de la polymérisation d'actine est suffisante pour convertir des lignées cellulaires fortement résistantes en lignées très sensibles.

La réponse d'actine est associée à une réduction de la quantité de Granzyme B (GzB) dans la cellule cible. Le blocage de la dynamique de l'actine (par traitement pharmacologique ou ablation génétique de Cdc42 ou N-WASP) suffit à restaurer une quantité élevée de GzB dans les cellules cibles.

La réponse d'actine entraîne la polarisation d'autophagosomes au niveau de la région synaptique dans les cellules cibles. Ce processus pourrait être à l'origine d'une dégradation facilitée du GzB dérivé des cellules NKs dans les cellules tumorales. En accord avec cette hypothèse, l'inhibition de la formation d'autophagosomes augmente simultanément la quantité de GzB dans les cellules tumorales et la susceptibilité cellulaire à la lyse induite par les cellules NKs.

La réponse à l'actine et ses effets protecteurs ont pu être validés à l'aide de cellules NKs primaires dérivées de donneurs sains

# Conclusions

Mes travaux de thèse ont permis d'établir le rôle clé du cytosquelette d'actine dans la résistance des cellules de cancer du sein à la lyse par les cellules NKs. Au-delà d'une meilleure compréhension des interactions entre les cellules du système immunitaire et les cellules tumorales, nos résultats ouvrent des perspectives pour le développement de stratégies innovantes visant à cibler la réponse actine afin de restaurer une réponse immunitaire anti-tumorale efficace et/ou améliorer l'efficacité des immunothérapies. Dans cette optique, il serait intéressant de caractériser le mécanisme par lequel la réponse actine induit le recrutement d'autophagosomes à la synapse et d'identifier les principaux régulateurs de la réponse d'actine.

Compte tenu de la rapidité de l'établissement de la réponse d'actine lors de l'attaque des cellules NKs, nous anticipons que des modifications post-traductionnelles, telles que la de/phosphorylation, sont à l'origine de l'activation de protéines du cytosquelette responsables du « burst » local de polymérisation d'actine à la synapse. Ainsi, il est envisagé au laboratoire de conduire des analyses phospho-protéomiques visant à identifier les protéines du cytosquelette d'actine et de signalisation dont le statut de phosphorylation est modifié au cours de l'établissement de la réponse actine. Les candidats les plus prometteurs, notamment ceux pour lesquels il existe des inhibiteurs cliniquement

approuvés ou en phase d'évaluation, seront validés dans des tests *in vitro* puis dans des modèles murins de cancer du sein.

# Introduction

# 1. NK cells in the anti-tumor immune response

## 1.1. The immune system

The immune system is composed of different and complementary networks of cells, tissues and organs that interact together for the purpose of protecting the host from pathogens and clearing infected and diseased cells such as cancer cells. In the absence of functional immune defenses, minimal infections can have dangerous effects on the organism. The innate and adaptive immune cells are commonly considered the two arms comprising the immune system[1] (Figure 1).

### 1.1.1. Adaptive immunity

The adaptive immune system is more specific to pathogens than the innate immune system and it needs more time to become protective and functional. Its specificity relies on the recognition of antigens present on target cells via antigen-specific receptors. The sophistication of the system derives from its ability to memorize and have an effective immune response upon re-infection with the same antigen[2]. The two major effector-adaptive cells types are the T cells expressing T-cell receptors (TCRs), and B cells, which express B cell receptors (BCRs).

T cells are derived from bone marrow, migrate as immature thymocytes and mature in the thymus where they undergo gene rearrangements that lead to the development of TCRs. They recognize the major histocompatibility complex (MHC) molecules referred to as human leukocyte antigens (HLAs). HLA class I includes HLA-A, B and C while HLA class II contains HLA-DP, DQ and DR[3]. The TCR is a disulfide-linked heterodimeric membrane protein composed of a constant region and a variable region with two polypeptide chains, $\alpha$ and $\beta$, responsible of antigen recognition. T cells are CD3$^+$ as well as CD4$^+$ or CD8$^+$. Additionally, a fraction of T cells is composed of TCRs with $\gamma$ and $\delta$ chains and are referred to as $\gamma\delta$ T cells. They are CD4$^-$ and CD8$^-$ and share innate and adaptive features.

CD4$^+$ T cytotoxic cells represent a low frequency subpopulation of T cells in the circulation, which increase upon chronic inflammation. They have a lytic function against MHC class II-presenting cells. CD8$^+$ cells are the most cytotoxic T cell subpopulation, able to eliminate pathogens and aberrant cells. T cell-mediated cell death occurs upon contact with antigen-presenting cells, which leads to the secretion of lytic granules[4].

Naïve CD4$^+$ T cells differentiate into four types of CD4$^+$ T-helper cells Th1, Th2, Th17, and regulatory T cells (Treg). Th1 cells are characterized by the expression of the transcription factor Tbet as well as by the production of IFN-ɣ and IL-2. They participate in the elimination of intracellular pathogens, regulation of inflammation, and healing tissue injuries. Th2 cells express the transcription factor GATA3 and secrete cytokines, including IL-4, IL-5, IL-6, IL-10, and IL-13. They are involved in the clearance of extracellular pathogens as well as in mediating humoral immunity[5]. Th17 cells develop in response to TGFβ, IL-6, and IL-21, and they are responsible for IL-17 secretion. They are characterized by their expression of the transcription factor RORɣt and provide protection against bacteria and fungi. Moreover, Th17 cells recruit neutrophils and macrophages to the site of infection, stimulate cytokine production and regulate T-cell proliferation[6]. Tregs are a subset of T cells expressing CD25, cytotoxic T lymphocyte-associated antigen 4 (CTLA-4), glucocorticoid-induced TNF receptor family-related gene (GITR) and the X-linked forkhead/winged-helix transcription factor box P3 (FoxP3). Treg cells can secrete inhibitory cytokines and can suppress the expansion and activation of immune cells[7].

Natural killer T (NKTs) cells are a T-cell subset that bridges the innate and adaptive immune system. They express CD1d and NK cell-surface marker NK1.1 (CD161) as well as the T-cells marker CD3 and the αβ TCR[8]. They are defined as CD1d-restricted T cells that express an invariant TCR with a variable (V) and joining (J) Vα24-Jα18 repertoire combined with a limited TCR-β chain repertoire.  They modulate immunity against bacteria and viruses as well as in allergy and autoimmunity by producing cytokines within minutes[9].

B cells are derived from bone marrow where they remain until maturation with a unique BCR expressing the IgM and IgD isotypes. Activation promotes isotype substituting, resulting in the development of antibodies with different heavy chains. Most of B cells are activated via the binding of BCRs and an antigen followed by ligation between CD40 on the B cells and the CD40-ligand on T-helper cells. Upon activation, B cells differentiate into the short-lived plasma cells responsible for producing specific antibodies. Microbes are attacked by B cell-derived antibodies making them accessible for phagocytosis by macrophages. These antibodies can also neutralize toxins and viruses. In addition, B cells can differentiate into a small fraction of memory cells that can become active in the case of re-infection[10].

## 1.1.2. Innate immunity

The first line of defense that responds immediately against invading tumors and pathogens is the non-specific innate immune system. It is composed of three main components: 1) anatomic barriers, which involve the skin, saliva, tears, mucus and cilia; 2) the humoral barriers, including a number of small proteins synthesized in the liver; and 3) cellular barriers that comprise different types of cells with distinct and complementary functions. Innate immune cells express pattern-recognition receptors (PRRs) that detect pathogen-associated molecular patterns (PAMPs), which are motifs that are unique to microorganisms[11].

Mononuclear cells, including monocytes and macrophages, are a type of phagocyte that finds and digests foreign microorganisms. Monocytes are derived from the bone marrow and circulate in the blood at a steady state. They can migrate to tissues to engulf cells and toxic molecules. During development, monocytes differentiate into dendritic cells (DCs) or macrophages, which are long-lived cells that can survive within the body for months and even years. Their function is essential to phagocytizing apoptotic erythrocyte cells and cellular debris as well as for the secretion of pro-inflammatory cytokines such as IL-6 and tumor necrosis factor (TNF). Macrophages also induce the proliferation of other immune cells[12].

Dendritic cells are the granular antigen-presenting sentinels of the innate immune system. In the skin, DCs are called Langerhans cells, whereas immature DCs with phagocytic properties circulate in the blood. Upon infection, DCs migrate to the lymph nodes where they interact with adaptive immune cells to shape the immune response[13].

Neutrophils along with eosinophils and basophils are known as granulocytes due to the presence of multiple granules in their cytoplasm. They are polymorphonuclear cells, having lobed nuclei. Neutrophils are the most abundant phagocytic cells, and they are usually the first to arrive at a site of infection to kill bacteria and fungi. When activated, neutrophil granules containing a variety of cytotoxic compounds are released. Basophils and eosinophils release histamine, an important mediator of allergic reactions and a defense against parasites. Mast cells are morphologically and functionally very similar to basophils, but they are more particularly involved in wound healing, immune tolerance and angiogenesis[14].

Complement proteins are small polypeptides synthesized in the liver that circulate in the blood in an inactive state. When stimulated, proteases cleave the complement proteins into fragments[15]. The role of these proteins is to enhance the ability of antibodies and phagocytes to eliminate pathogens and damaged cells[16]. As I focused on this innate cell type during my research, Section 1.2 describes NK-cell properties and functions in more detail.
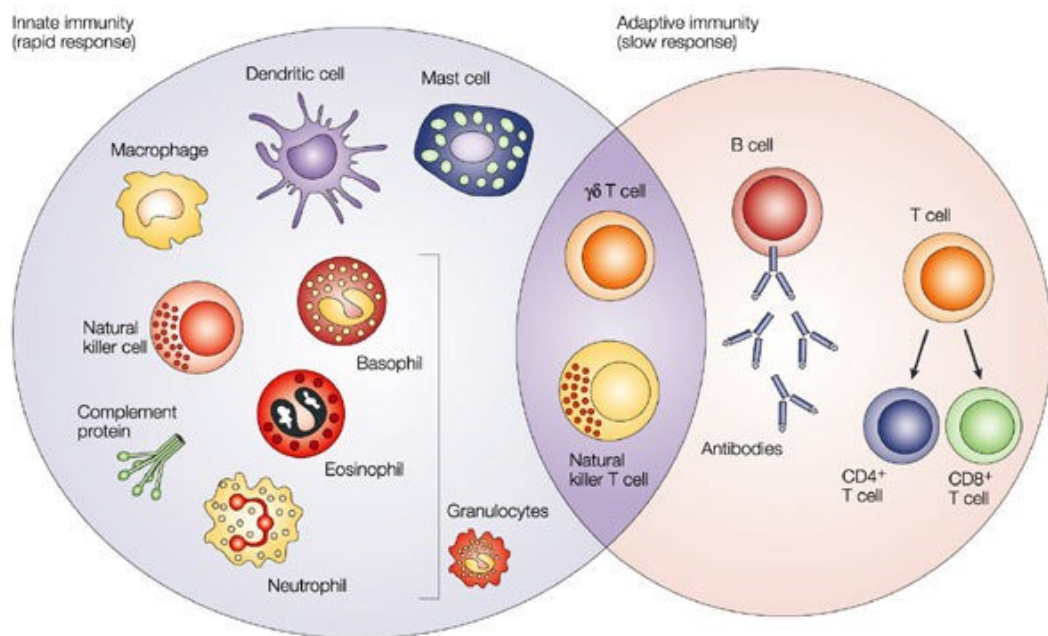


**Figure 1 | The innate and adaptive immune systems**

The innate immune response functions as the first line of defense against infection. It consists of soluble factors, such as complement proteins, and diverse cellular components including granulocytes (basophils, eosinophils and neutrophils), mast cells, macrophages, dendritic cells and natural killer cells. The adaptive immune response is slower to develop, but manifests as increased antigenic specificity and memory. It consists of antibodies, B cells, and CD4^{+} and CD8^{+} T lymphocytes. NKT cells and γδ T cells are cytotoxic lymphocytes that straddle the interface of innate and adaptive immunity. Adapted from Dranoff, 2004.

## 1.1.3. Innate immune system specificity: recent paradigm changes

Until recently, the innate system was considered as a non-specific arm of the immune system that detects and eliminates aberrant cells without education or specificity. The discovery of the specificity in some innate immune responses in the last 20 years has shifted our understanding of the of immune system classifications. These observations led researchers to re-think about the simplistic classification of immune cells into the innate and adaptive arms[17]. In this section, I summarize some of the recent discoveries about the adaptive arm of innate immunity.

Sensing Gram-negativity by a host through the detection of lipopolysaccharides and other components by the host was the first observation of a specific innate response against infectious agents. Further, the stress sensing pathway was found to induce innate immunity in some species such as nematodes[18]. Mammalian stress signaling was also reported in the induction of inflammatory responses involving heme, which is abundant in red blood cells. Heme functions to activate TLR4 on innate immune cells and in initiating an oxidative stress response. An adaptive response re-occurs following red blood cell damage[19].

Studies have shed light on the non-apoptotic regulated cell death of certain innate immune cells. One of the best-described example is the formation of the neutrophil extracellular traps, a process known as NETosis. Neutrophils and other granulocytes can undergo a self-immune cell death and release their own chromatin as an anti-microbicidal response. It has been well established that bacteria, viruses and fungi can be trapped and killed by the released network of histones, DNA and granular proteins. The implication of this type of innate immune-cell death revealed a high specificity toward pathogen infections[20]. Moreover, the Fc receptors of basophils and mast cells show an adaptive functionality, as the generated signaling pathways have an adaptive response toward allergic reactions that can be regulated and tuned[21].

Relevant to my work is the recent discovery of Innate Lymphoid Cells (ILCs), which include NK cells as well as the recently discovered subsets, ILC1, ILC2, and ILC3. Whereas NK cells share the cytolytic molecules, IFN-γ and Eomes, with CD8$^+$ T cells, ILCs share common transcription factors with T cells that give rise to strikingly similar effector functions, such as cytokine production. Profiling the subsets has revealed that ILC1 shares the expression of T-bet and IFN-γ with Th1 cells, ILC2 shares GATA-3, IL-5 and IL-13 with Th2 cells and ILC3 shares RORγt, IL-17 and IL-22 with Th17/Th22

cells. The link between T cells and the ILC groups is still not fully understood, but recent studies support the importance of ILCs in protecting of epithelial and mucosal surfaces when T cells are inefficient or absent[22] (Figure 2). Upcoming studies will establish the precise biological functions of such responses in specifically regulating the host defense immune system.
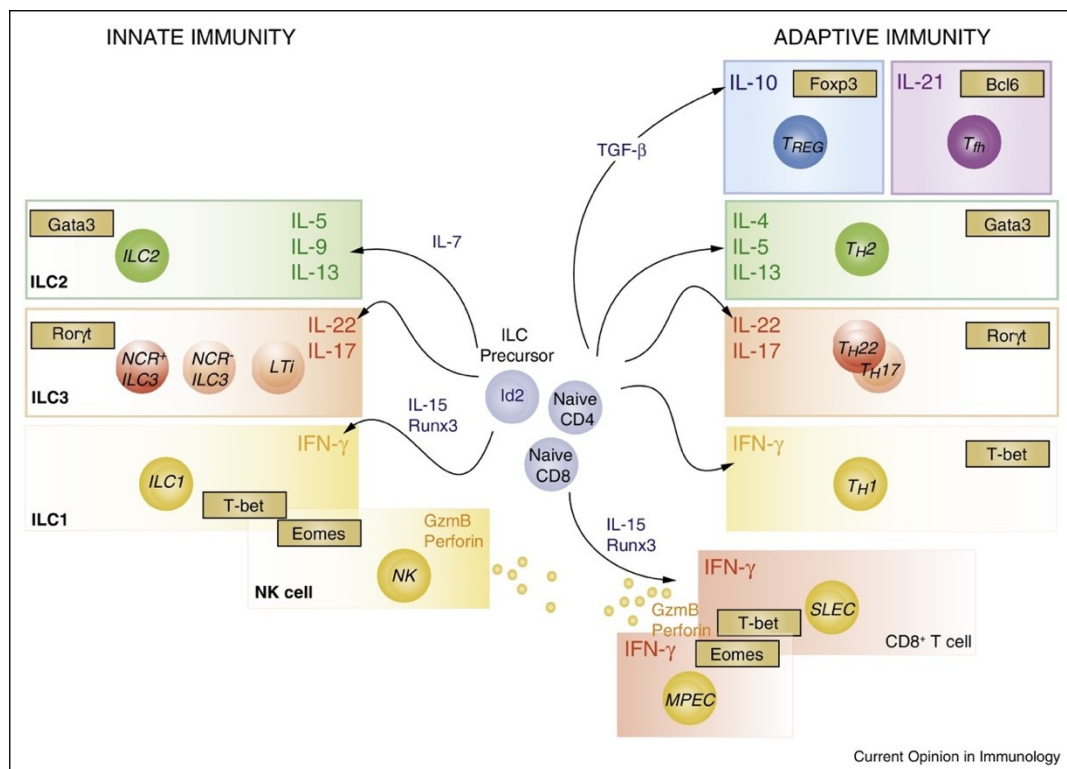


**Figure 2 | Parallels between innate and adaptive immune lineages**

Innate lymphoid cells share a number of features with T cells including the cytokines and transcription factors necessary for differentiation and the effector cytokines produced by each subset. SLEC, short-lived effector CD8+ T cells; MPEC, memory precursor CD8+ T cells; GzmB, GzB. Adapted from Huntington et al., 2016.

## 1.2. NK cells: generalities

A fraction of effector lymphocytes was originally considered as typical, with high cytotoxicity and cytokine secretion capability but without education[23]. The intense focus on the role of these cells led to the identification of a new sub-population of cells defined as natural killer cells. Natural Killer cells are granular lymphocytes in the ILC group and a part of the innate immune system. They have the ability to lyse aberrant cells, including tumor and pathogen-infected cells, without prior sensitization. The NK cell employs sophisticated mechanisms to discriminate between abnormal and healthy cells[24]. Moreover, NK cells provide a source of immunoregulatory cytokines. This regulatory function of the NK cells, in addition to their cytotoxicity, holds promise for improvements in immunotherapy, autoimmune and inflammatory diseases and organ transplantation[25].

The NK-cell membrane expresses a variety of germline-encoded activating and inhibitory cell surface receptors whose engagement leads to target recognition. The activation of NK cells derives from the complex system that detects activation and inhibitory ligands on the target surface. Thus, the signals derived from the interaction of receptors on the NK surface and their corresponding ligands on neighboring cells governs the "dynamic" equilibrium regulating NK-cell activation and inhibition[26].

In this chapter, the biology and features of NK cells will be described in detail, with particular emphasis on the critical roles played by NK-cell receptors and the different components of NK cell-mediated cell-death receptors.

## 1.3. NK cells: a historical perspective

From 1970 until the present, much progress has been made on elucidating NK-cell functionality, which is not limited to cell lysis and elimination, but also includes reciprocally regulating of the activity of other immune cells[27]. That NK cells represent a separate cell lineage took long to be established because their ability to kill tumor target cells was considered as an artifact. However, in the early 1970s, Rolf Kiessling, a PhD student from the Karolinska Institute in Stockholm, discovered a new type of lymphocytes in the spleen of BALB/c mice with the capacity to kill aberrant cells without prior stimulation. Theses remarkable cells were described as naturally occurring killer lymphocytes with a specificity to mouse Moloney leukemia and with unique surface and functional properities[23,28]. The lysis of tumor cells occurred within one to four hours after

contact with the effector cells *in vitro*, a more rapid induction than that of other adaptive immune cells. "The killer cells involved would seem to be neither T nor B lymphocytes as classified by conventional markers but rather belong to yet a third group of lymphocytes", Kiessling stated. In 1976, Hugh Pross identified the same immune cell population in peripheral human blood[29]. Studies on NK cells began to attract growing interest, and in the same year, Ronald Herberman published data confirming the functionality of the new cell type to kill target cells without any previous sensitization[30-32]. The number of studies continued to rise, and Thornthwaite eventually showed how the newly discovered cells kill P815 cells, a mastocytoma tumor model, under a microscope for the first time[33]. After the discovery of NK cells, experiments were conducted on whole peripheral blood mononuclear cells (PBMCs) because there were no efficient isolation methods. In 1980, however, Timonen and Saksela isolated NK cells with the use of a density gradient, allowing them to visualize the cells under a microscope and characterized them as large granular lymphocytes[34].

## 1.4. The biology of NK cells

Consistent with their innate immune function as the first line of defense against aberrant and pathogen-infected cells, NK cells are widespread throughout lymphoid and non-lymphoid tissues. The NK cell lineage is generated from the common lymphoid progenitor (CLP), and they further develop in the bone marrow as well as in the liver and the thymus. The lineage's development fundamentally relies on the secretion of cytokines such as interleukin (IL)-15 or IL-12 and on the expression of transcription factors such as Nfil3, PU.1 and Tox. During the maturation process, NK cells acquire the ability to recognize cells lacking self-recognizing MHC class I molecules[35].

Human NK cells are defined by the positivity for the CD56 antigen, an isoform of the human neural-cell adhesion molecule (N-CAM), and by their negativity for CD3. In human peripheral blood, NK cells represent from 2% to 18% of the total lymphocytes. Studies on mice have shown that the percentage of NK cells defined as $NK1.1^+ CD32^-$ is about 2% in mice spleen, 5% of PBMCs, and about 8% to 10% in mice lung and liver[36,37]. In humans, NK cells are divided into two subsets with different roles and functions based on the expression levels of the unique CD56 markers, CD56^{bright} and CD56^{dim}. The largest fraction of NK cells (~90% of PBMCs and spleen NK cells) is the highly cytotoxic CD56^{dim} subpopulation, which expresses high levels of the Fcγ receptor III (Fcγ RIII,

CD16^{+})[38]. In contrast, NK cells are CD56^{bright}CD16^{−} in lymph nodes and tonsils. This subpopulation is known to be non-cytotoxic in comparison to the CD56^{dim} NK cells due to the absence of perforin (detailed in section 1.6.3.2). However, the CD56^{bright}CD16^{−} subpopulation secretes high levels of cytokines after being activated by monocytes. Interestingly, the recently discovered cell subpopulation of CD56^{dim}CD16^{dim} NK cells has been found to be present in higher in numbers than the bright subsets in more immature cells[39].

The distribution and trafficking of NK cells in an organism are regulated by chemokine-receptor expression on the NK-cell membrane. The expression of some of these receptors is dependent on the maturation and the activation level of the cell[40]. Immature NK cells express the chemokine receptors CXCR3, CXCR4 and CXCR6 until maturation, when they gain the ability to express CX3CR1 and sphingosine-1-phosphate receptor 5 (S1P5), mainly responsible for NK cell egress from the bone marrow and lymph nodes. Once NK cells enter the periphery, they are directed to the site of action via chemotaxis[41]. All NK cells express high levels of CXCR4, a receptor for CXCL12, and SDF-1α/β, a receptor for CXCL12. CD16^{+} cells express high levels of CXCR1 and CX3CR1, low levels of CXCR2 and CXCR3 and no CXCR5. These cells migrate in response to CXCL8 and CX3CL1[42]. By contrast, CD56^{bright}CD16^{−} NK cells express high levels of CXCR3, CCR5 and CCR7, but have no CXCR1, CXCR2, or CXCR5 expression. Accordingly, they migrate in response to CCL19, CCL21, CXCL10, and CXCL11[43].

The NK cell membrane expresses a wide variety of activating and inhibitory receptors that determine the NK cell's killing activity and interactions with other immune cells. The receptors are divided into several groups based on their corresponding ligands. Healthy cells are not affected by NK-cell activity as they express the inhibitory ligands MHC class I molecules while downregulating the activating ligands. Conversely, NK cells can detect the overexpression of activating ligands and the absence of MHC class I on the surface of target cells. In addition, the NK cell membrane expresses the death receptor ligand tumor necrosis factor-related apoptosis-inducing ligand (TRAIL) or CD95-L, which can ligate with the corresponding receptor on a target cell and initiate target cell apoptosis[44] (Figure 3).

a

TOLERANCE

NK cell   Inhibitory   MHC   Healthy cell
receptor   class I

Activating
ligand

NK cell inhibition

Activating
receptor

b

MISSING SELF

Activated NK cell   Tumour cell

Loss of MHC molecule
expression promotes
killing of tumour cell

NK cell activation

Cytokines and
cytotoxic mediators

c

STRESS-INDUCED SELF

Activated NK cell   Tumour cell

Upregulation of
stress-induced
ligands promotes
killing of tumour cell

NK cell activation

Cytokines and
cytotoxic mediators

Nature Reviews | Immunology

### recognition of tumor cells

a) NK cells are tolerant to normal self-cells as the 'strength' of activating signals is dampened by engagement of inhibitory receptors. b) NK cells are selectively activated by stressed cells as they express a density of cell surface ligands for activating receptors which overcomes signaling via inhibitory receptors. c) NK cell activation leads to tumor elimination directly (cytotoxicity) or indirectly (production of cytokines such as IFN-γ). Adapted from s

## 1.5. Activating and inhibitory NK-cell receptors

NK cells express a repertoire of activating and inhibitory receptors on their cell membrane. The inhibitory receptors expressed on the NK-cell surface are divided into different classes: killer cell immunoglobulin-like receptors (KIRs); NKG2/CD94 receptors, which are type II glycoproteins with a C-type lectin scaffold; and leukocyte immunoglobulin-like receptors. The activating receptors include natural cytotoxicity receptors, the activating form of KIRs, immunoglobulin gamma FcγRIII and C-type lectin receptors. The balance between signals generated by the ligation of inhibitory and activating receptors with their cognate ligands controls NK-cell activity. The section below presents a more detailed description of the different receptor classes on the NK-cell membrane [44] (Figure 4). Immune-checkpoint receptors are described in the chapter on immunotherapy.

## 1.5.1. Killer cell immunoglobulin-like receptors (KIRs)

The KIR receptor class (also known as CD158) comprises 7 activating and 7 inhibitory receptors. KIRs are monomeric type I glycoproteins whit two or three Ig-like domains (KIR2D or KIR3D) in the extracellular region[45]. All inhibitory KIR receptors contain one or more an immune-receptor tyrosine-based inhibitory motifs (ITIM) that recognizes MHC class 1 ligands[44]. Upon the engagement of KIRs with HLA-A, B or C, the ITIM domain is phosphorylated by Src family protein kinases. This phosphorylation promotes the formation of a docking space and the recruitment of the SHP-1/2 protein kinase phosphatases, which in turn, leads to the suppression of the activating receptor signals. All activating KIR receptors lack ITIMs and instead, express the DAP12 protein that delivers activating signals through the immune-receptor tyrosine-based activation motif (ITAM)[46,47].

## 1.5.2. Natural killer group 2 (NKG2) receptors

NKG2 receptors are a group in the C-type lectin family that contains six heterodimers (NKG2A, B, C, E, F and H) coupled to CD94 and a non-coupled NKG2D. They are predominantly expressed and divided into activating and inhibitory receptors. Both activating and inhibitory NKG2/CD94 receptors bind to the corresponding non-classical MHC HLA-E ligand expressed on target cells[44]. The receptor subtypes NKG2A and B are classified as inhibitory receptors as they contain 2 ITIM domains that drive inhibitory

signal cascades. NKG2C, E and H associate with DAP-12 and accordingly generate activating signals. NKG2F is classified as an orphan receptor because its expression and function on NK cells is not well established. Nevertheless, it is usually accepted that NKG2F can associate with DAP-12 and therefore functions as an activating receptor[48].

The most critical member of the NKG2 class is the NKG2D receptor, which is expressed on a wide range of cytotoxic cells, including NK cells, and $\gamma\delta^+$ and $CD8^+$ T-cells. NKG2D is encoded by KLRK1 gene, located on the chromosome 12 in humans[49]. In contrast to the other NKG2 class members, NKG2D does not form a heterodimer with CD94, but instead is expressed as a homodimeric receptor. NKG2D monomers associate with DAP-10 dimers, which transduce activation signals[50]. Due to their short binding site, NKG2D receptors recognize many different types of ligands. Importantly, the MHC class I-related chain A and B (MICA/B) and the family of six UL16-binding protein (ULBP1-6)[51-53]. The ligation of NKG2D with MICA/B or ULBPs and the subsequent activating signals represent an important regulatory axis of cancer immune surveillance. Cellular stress ligands expression is regulated by DNA damage and heat shock response pathways, which are increased accordingly in cancer cells[54,55]. Nevertheless, healthy cells also express NKG2D ligands but at a baseline level[56]. Experiments on Eµ-myc mice, which lack NKG2D receptors, have shown the importance of these receptors in the immune response.

### 1.5.3. Leukocyte immunoglobulin-like receptors (LILRs)[44]

The LILRs subfamily B or CD85 is widely expressed on NK cell membranes. These receptors are type I transmembrane glycoproteins with an extracellular Ig-like domain. Upon binding to MHC class I molecules, and more particularly to the HLA-G ligands from tumor cells, the 5 isoforms of the receptors (LILRB1-5) transduce signals via ITIMs that recruit the SHP-1/2 protein kinase, leading to the inhibition of NK-cell activity[57]. This interaction reportedly serves as an immune checkpoint, although its impact on tumor immune escape is less documented than that of CTLA4 or PD-1[58].

### 1.5.4. Natural cytotoxicity receptors (NCRs)

Another important class of activating receptors on NK-cell membranes is the Ig-superfamily called natural cytotoxicity receptors (NCRs)[59]. Their role in promoting NK cell mediated-tumor cell lysis was discovered following the combined knockout of each

receptor in mice or through the use of specific blocking monoclonal antibodies[44]. NKp30, NKp44 and NKp46 are the identified activating receptors that were identified and shown to bind to viral-, parasite-, bacterial- and tumor-derived ligands [60]. NKp30 and NKp46 are constitutively expressed on the membrane of both resting and activated NK cells whereas NKp44 is only expressed upon IL-2 stimulation[61].

NKp30 is a major receptor that mediates NK cell-meditated DC maturation as well as virus-infected cell and tumor lysis[62]. Studies are still ongoing to uncover the precise role of NKp30 in the anti-tumor immune response[63]. Recent studies have shown that the nuclear factor HLA-B-associated transcript 3, tumor antigen B7-H6, Bcl-2-associated athanogene 6 (BAG-6) and heparin sulfate proteoglycans can bind to NKp30 resulting in cell lysis[64,65]. To date, only a few studies have shed the light on the NKp46 receptors, their ligands, and their implications in tumor recognition and elimination[60]. Viral ligands such as the influenza virus's hummagglutinin were the first ligands identified to bind to NKp46[66]. Viral, parasite and bacterial ligands were later shown to have the capacity for signal induction after NKp46 binding[67]. Although the ligands of NKp44 on tumor cells remain to be identified, *in vivo* studies in NKp44 KO mice provide evidence that NKp44 is implicated in tumor immune surveillance[61]. A cellular ligand of NKp44 has been recently identified as NKp44L. This ligand is a novel isoform of the mixed-lineage leukemia-5 protein (MLL5) and has been shown to control NK cell-mediated cell lysis[68,69].

### 1.5.5. 2B4 receptors

2B4 or CD244 is a non-MHC multifunctional binding receptor that is abundant on NK cells, monocytes, basophils and a subpopulation of T cells. There are two isoforms, 2B4-A and 2B4-B, which differ in their affinity for CD48, a ligand expressed on all hematopoietic cells. Depending on the maturation stage of the NK cell, activating or inhibitory signals can derive from these receptors upon ligation with CD48. A recent study has reported that the interaction between 2B4-A and CD48 leads to increased intracellular calcium release, induces IFN-ɣ secretion, and contributes to initiating of the cytotoxicity process[70].

### 1.5.6. Killer cell lectin-like receptor G1 (KLRG1)

Killer cell lectin-like receptor G1 (KLRG1) is an abundant receptor on both NK cells and T cells. They were originally defined as inhibitory receptors that induce inhibitory signals through an ITIM domain. The ligands for KLRG1 receptors include the cadherin family members (E-, N-, and R-cadherins), which are abundant on healthy cells and are downregulated on malignant mesenchymal tumors. Thus, NK cells implicate KLRG1 receptors in playing an important role in preventing healthy cell damage and lysis[71].

### 1.5.7. Co-stimulatory receptors

The co-stimulatory DNAM-1 (also known as CD226) receptors are expressed on 50% of NK cells and they bind to CD155 (PVR) and CD112 (PVRL2, nectin-2), which are expressed on tumor cells[60]. Beside their role in lymphocyte migration, DNAM-1 is involved in tumor cell recognition and adhesion[72].

T-cell immunoglobulin and the ITIM domain (TIGIT) are co-inhibitory receptors of the Ig superfamily expressed on NK cells, and they bind to CD155 with a higher affinity than to DNAM-1. Remarkably, the interaction between DNAM-1 and CD155 is inhibited by TIGIT[73]. Another group of co-stimulatory receptor is the NKR-P1 receptors (NK1.1 in mice), which are classified into 5 isoforms. NKR-P1 B/D inhibits NK-cell activation through the ITIM domain, while the NKR-P1 C has an ITAM domain[74]. In addition, B and T lymphocyte attenuator (BTLA) and CD160 are immunoglobulin inhibitory receptors that bind to herpes virus entry mediator (HVEM)[75]. The ligation between HVEM and the TNF suprafamily 14 (TNFSF14, also known as LIGHT) co-stmulatory receptors induces activating signals[76]. Sialic acid-binding immunoglobulin-like lectin is another inhibitory receptor that binds to sialylated glycan to induce inhibitory signals[77].
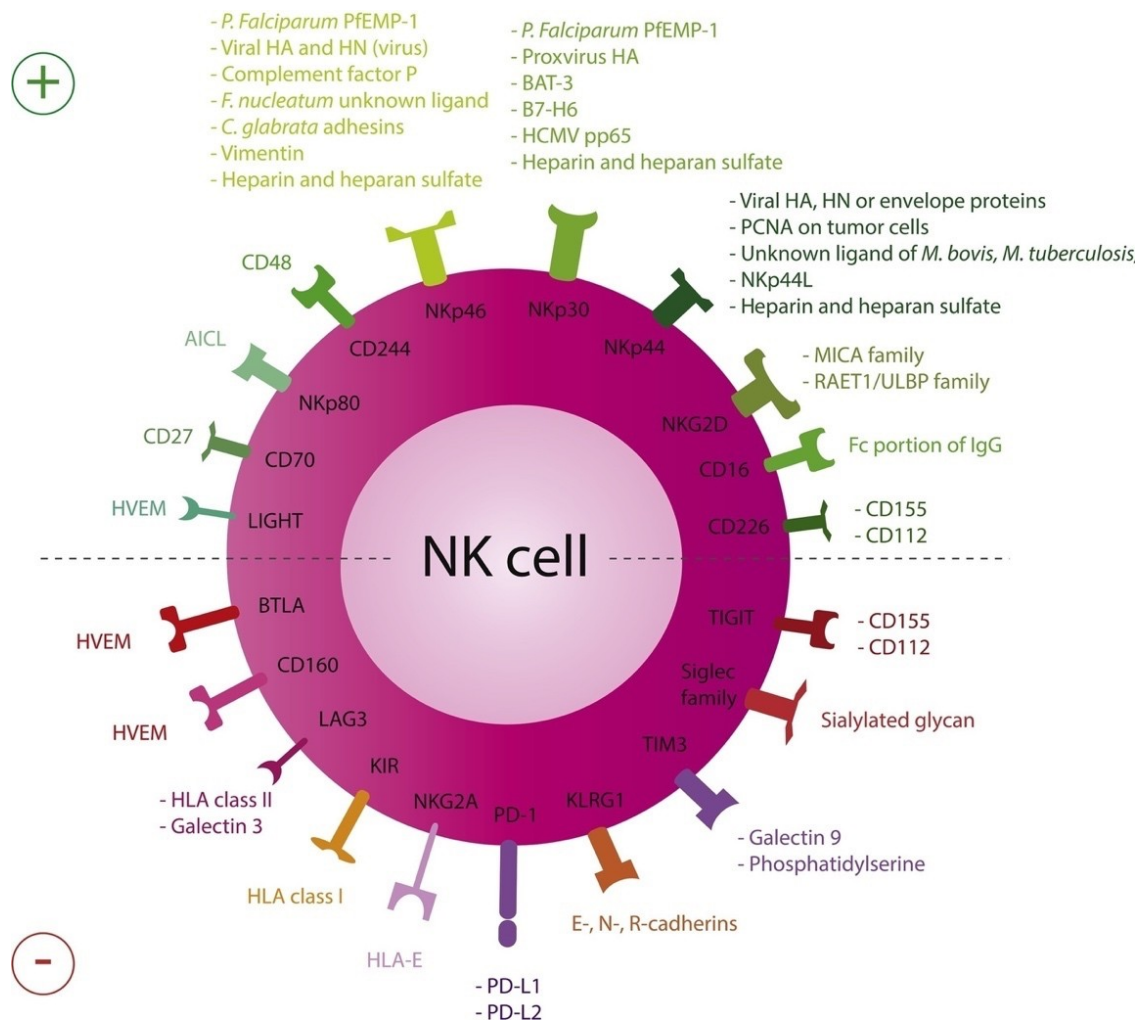
**Figure 4 | NK cell activating and inhibitory receptors**

Major activating (green) and inhibitory (red) receptors expressed by human NK cells and their corresponding ligands are represented. Adapted from Chiossone et al., 2017.

## 1.6. NK cell-mediated-cell death

The main function of NK cells is as a defense against tumor and virally-infected cells via different and well-established lytic mechanisms[24]. These mechanisms include (1) death receptor pathways[31] (2) NK cell-mediated antibody-dependent cellular cytotoxicity (ADCC)[78], and (3) the lytic granule-dependent pathway[79]. Along with these well-defined lysis mechanisms, NK cells release exosomes that are known to play a significant role in immune-surveillance[80]. NK cell-derived exosomes (NKEXOs) have been reported to have lytic properties when they enter tumor cells. They express the exosomal markers Rab5B and CD63 as well as the CD56, NKp30, NKp46, and NKp44, NK-cell markers[81]. Importantly, NKEXOs contain cytolytic proteins such as Fas ligand and perforin[82].

### 1.6.1. Death receptor pathways

NK cells contribute to the suppression of tumor growth and metastasis via death-receptor pathways independently from the cytotoxic granule pathway[83]. This pathway is activated upon the ligation of death ligands with their corresponding death receptors, which promotes caspase-dependent death pathways[84] [31,85].

### 1.6.1.1.  The Fas receptor-Fas ligand pathway

FasL (also known as CD95L, APO-1, or TNFRSF6) and its receptor Fas (also known as CD95, APO-1, or TNFRSF6) are members of the TNF and TNF-receptor family[86]. Fas is a type I transmembrane protein containing a death domain in its cytoplasmic region that is responsible for inducing apoptosis[87]. Not all tumor cells express the death receptor on their membrane. Nevertheless, NK cells can stimulate Fas expression on target cells via the secretion of IFN-ɣ. This 40 kDa Fas ligand is expressed at the surface of both NK and cytotoxic T-lymphocyte (CTL) cells and its ligation with Fas allows for recruitment of the protein Fas-associated death domain (FADD). FADD promotes the formation of the death-inducing signaling complex (DISC) and the activation of caspases 8 and 3. Moreover, the anti-apoptotic FLICE/ caspase-8-like inhibitory protein (FLIP) blocks Fas pathway-mediated cell lysis by disturbing the formation of the DISC[88]. Of note, metalloproteinases can split FasL into a soluble inactive form that competes with the FasL on the membrane[89,90].

## 1.6.1.2. The TNF-related apoptosis-inducing ligand (TRAIL) pathway

TRAIL (also known as APO-2 ligand) is a type II transmembrane protein that belongs to the TNF superfamily. Five TRAIL receptors have been identified in human cells, but only two of them, DR4 and 5, are capable of inducting apoptotic signals due their death domain[31]. The high expression of TRAIL on NK-cell membranes is stimulated by with IL-2, IL-15, and IFNs. Like Fas receptors, the activation of DR 4 or 5 induces DISC assembly. FADD then translocates to the DISC, where it interacts with the death domain of the receptor[91]. FADD recruits pro-caspases 8 and 9 to the DISC where they are activated. In some types of cells, DISC also activates the mitochondrial pathway. The BH3 interacting-domain death agonist (BID) is then cleaved to tBid by caspases 8 and 10 and translocated to the mitochondrial. tBID activates Bax and Bak resulting in cytochrome-C release and the activation of caspases 9 and 3[91-93].

## 1.6.2. Antibody-dependent cellular cytotoxicity (ADCC)

ADCC is a mechanism of the cell-mediated immune response whereby an NK cell detects and lyses a target cell whose membrane antigens are bound to specific antibodies. NK cells and hematopoietic cells (except most T cells) express three types of Fcγ receptors, which bind to the Fc part of the IgG antibodies. FcγRI (CD64) is expressed on the membranes of neutrophils and macrophages and binds to human IgG1 and 3[94]. The second type is FcγRII (CD32), which comprises two isoforms that function as activating or inhibitory receptors. The third type is FcγRIII, which has two isoforms, FcγRIIIa with an ITAM domain and FcγRIIIb with an ITIM domain[95]. The balance between the activating and inhibitory signals of FcγRs and their antibody-affinity thresholds control the efficacy of ADCC.

NK cells represent an important model of ADCC as the activating FcγRIIIa is highly expressed on CD56$^{dim}$ CD16$^+$ NK cells, while inhibitory FcγRIIIb is absent. The binding of FcγRIIIa to the IgG1 and IgG3 subclasses induces a potent activating signal. NK-cell activation triggers cytotoxic granule polarization and secretion. ADCC has been implicated in tumor elimination in several *in vivo* studies[78]. Antibodies specifically engineered to prevent Fc binding to FcγRIIIa and human epidermal growth factor receptor 2/neu (Her2/neu, CD240) induce a potent inhibition of the ADCC pathway and lead to increased tumor size in BC xenograft-mouse models. It is worth mentioning that

vaccination and monoclonal antibody-based immunotherapies takes advantage of the ADCC mechanism[96,97].

### 1.6.3. The lytic granule-dependent death pathway

Upon target recognition, the main elimination pathway is the secretion of the cytolytic granules into the target cells and the subsequent induction of apoptosis[98]. Whereas CTLs have TCRs that recognize MHC class I, NK cells mainly recognize their targets via a set of activating and inhibitory receptors. Despite NK cells and CTLs having different target recognition mechanisms, the following lytic granule-dependent killing mechanism is conserved in both cell types. The lytic granules are electron-dense organelles that contain the pore-forming protein perforin, the serine protease proteins called granzymes, and the lipid-disrupter granulysin[99]. Once NK cells are activated, $Ca^{+2}$ concentration increases in the cytosol, the microtubule organizing center (MTOC) moves toward the target cell and the cytotoxic granules are polarized along with the MTOC toward the immunological synapse (IS)[100]. Perforin and granzymes synergize to induce apoptosis in the target cells[101] (Figure 5).
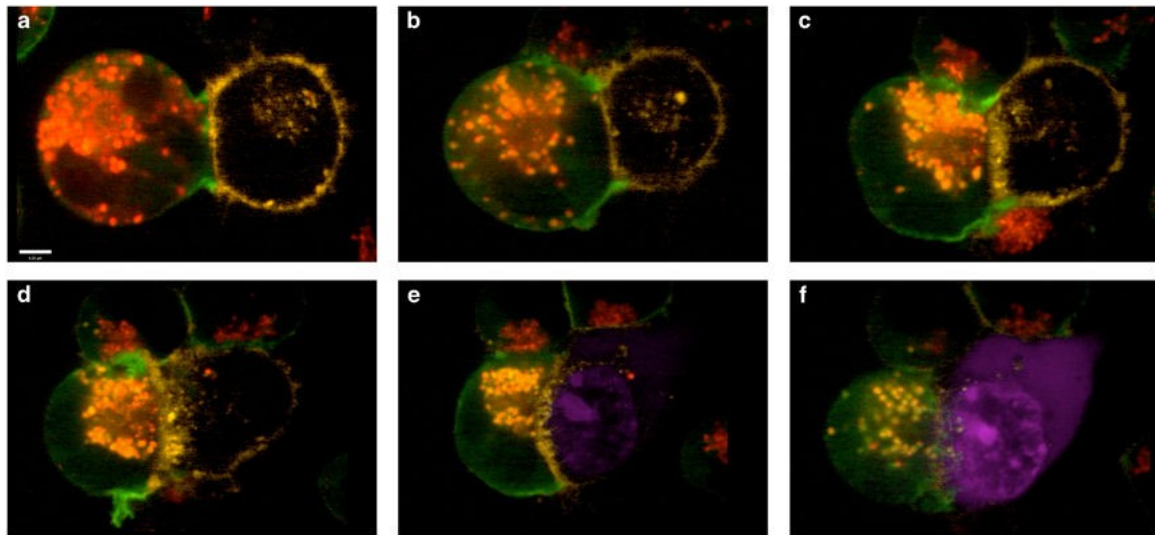
**Figure 5 | Stepwise stages during NK cell-mediated cytotoxicity**

YTS GFP-actin (green) cells were labeled with Lysotracker Red (red) to selectively label lytic granules and co-incubated with CellMask-labeled (Life Technologies, Carlsbad, CA, USA) (yellow) 721.221 target cells in the presence of SYTOX Blue (Life Technologies) (blue) for detection of cell death. Conjugates were imaged by spinning disk confocal microscopy for a total of 90 min. The images shown are frames acquired approximately every 15 min. a) The NK cell is conjugated to the target cell and lytic granules are dispersed. b) Granules are converged at the MTOC. c) The MTOC along with converged lytic granules are polarized at the immune synapse. F-actin is evidently reorganized from a to c. d) More F-actin reorganization is observed and lytic granules are docked at the plasma membrane. e) Target cell death begins as SYTOX Blue enters the cell. f) Target cell undergoes apoptosis and NK prepares for detachment as shown by reversal of shape change. Scale bar=4 μm. Adapted from Mace, 2014.

### 1.6.3.1. Granzymes

Granzymes constitute a family of serine proteases whose members differ in their substrate specificity and functionality. Five granzymes have been identified in humans, granzymes A, B, H, K and M [102,103]. Granzymes reportedly to cleave both intracellular and extracellular proteins. However, there is a gap in our knowledge regarding their extracellular functions. Granzyme A-mediated cell death is not related to the caspase-activation pathways, but rather involves a loss of the mitochondrial inner membrane, the release of reactive oxygen species (ROS), and nuclear histone cleavage [104,105]. The mode of action of granzymes H and K are not well characterized, but recent studies support that granzyme H-induced cell death is also independent of caspase activation [84]. In contrast to granzyme H, granzymes K and M mediate cell death through caspase pathway activation and ROS production [106].

Granzyme B (GzB) is the most abundant protein and the best functionally characterized among the other forms of cytolytic granules. GzB is responsible for the rapid induction of caspase-dependent apoptosis in target cells promoting directly or by indirectly caspase activation. Although its relative importance to tumor cell elimination remains unclear, caspase-independent cell death has also been reported after GzB is internalized [107].

### 1.6.3.1.1. Granzyme B structure and synthesis

GzB was discovered in 1987 by Schmid and Weissmann as an abundant serine protease in human leukocytes [108]. In 1991, Poe et al., showed that the 32 kDa GzB could be purified from the granules in human cytolytic lymphocytes, and that they established its enzymatic activity [109-111]. The protein is composed of two 6-stranded β-sheets which are connected by three trans domains. In the first step, GzB is first synthesized as a pre-proenzyme before being transported into the endoplasmic reticulum. The subsequent pro-GzB is then transported in specific vesicles into the Golgi apparatus, where it is modified by mannose-6-phosphate [112]. Once modified, the pro-GzB is ready to be activated by dipeptidyl peptidase I or cathepsins C and H in secretory granules, which are stored in association with the proteoglycan serglycin-containing chondroitin sulphate [113].

### 1.6.3.1.2. Granzyme B delivery to and internalization in the target cell

At steady state and in the absence of target cells, CTLs and NK cells constitutively synthesize GzB. A major difference between the NK cells and CTLs is that NK cells secrete and release GzB in its active form while CTLs secrete the inactive form. The regulators of cytotoxic granules such Rab-27A, Munc13-4, and synaptotagmin VII play an essential role in granzyme maturation and the fusion with the plasma membrane[114,115]. Additionally, NK cells can recycle a fraction of the secreted GzB via clatherin-dependent endocytosis. The entry of GzB into the target cells can be achieved either by co-entry into the cytoplasm with perforin or via the mannose-6-phosphate receptor[116].

### 1.6.3.1.3. Granzyme B-induced apoptosis

The exposure of target cells to nanomolar concentration of GzB is rapidly followed by apoptosis (within 5-8 minutes). Granzyme B's entrance into the target cell's cytoplasm is followed by the recognition of a broad range of intracellular signaling components that directly or indirectly promote cell death[107]. These pathways are briefly described below.

BID is an important molecular target of GzB. The proteolysis of Bid leads to the translocation of its C terminal into mitochondria and the subsequent permeabilization of the mitochondrial membrane via Bak or Bax protein oligomerization[117]. In addition, GzB is responsible for the cleavage of anti-apoptotic B-cell lymphoma-2 (Bcl-2) and myeloid cell leukemia sequence 1 (Mcl-1)[118]. Both mechanisms lead to the release of the mitochondrial cytochrome C and diablo homolog (Smac/diablo) into the cytosol[119]. Cytochrome C, together with apoptotic peptidase activating factor 1 (Apaf-1), directly activates caspases 9 and 3. Additionally, GzB is capable of directly cleaving caspases 8, 10, 3, and 7 and indirectly cleaving caspases 2, 6 and 9[120].

The indirect induction of target cell death involves the activation of Rho-associated coiled-coil-containing protein kinase 2 (ROCK2) and results in membrane blebbing[121]. In addition, GzB cleaves α-tubulin, leading to cytoskeleton collapse and microtubule polymerization[122]. GzB also directly cleaves nuclear components such as lamin A/C, lamin B, and nuclear mitotic apparatus protein A (NUMA1), which results in lamina disruption and a loss of nuclear integrity[123,124]. Moreover, GzB-dependent targeting of the poly (ADP-ribose) polymerase 1 (PARP-1) or the DFF45/ICAD (cytoplasmic DNA fragmentation factor 45) alpha peptide promotes apoptosis via DNA fragmentation.

Finally, GzB can negatively affect fibroblast growth factor receptor 1 (FGFR1) and notch homolog 1 translocation-associated (Notch/NEXT) to enhance apoptosis[125].

### 1.6.3.2. Perforin

The 67 kDa multi-domain protein perforin was discovered in 1980 by 3 groups of scientists: Henkart et al., Okumura et al., and Podack et al[126]. Perforin is a pore-forming member of the membrane-attack-complex/perforin (MACPF) protein family that induces transmembrane tubules[127]. Additionally, it can oligomerize into membrane-spanning pores at neutral pH and when $Ca^+$ is present [2128]. Such pores allow the passive diffusion of the GzB into the target cells[129]. The amino-terminal MACPF domain is followed by an epidermal growth factor (EGF) domain. The C-terminal domain of perforin is related to the $Ca^{+2}$-dependent C2 domain family and is extremely important to its activity. Perforin is an essential key for granzyme-dependent apoptosis, as noted by the loss of perforin in mice abolishing targeted cell death[130]. It is also associated with various human diseases such familial haemophagocytic lympho-histiocytosis (FHL; a congenital perforin deficiency), hematological malignancies, and protracted viral infections[131].

### 1.6.3.3. Granulysin

The saponin-like protein family contains the 15 kDa member granulysin. In addition to perforin and granzymes, secretory granules also contain the granulysin, which is responsible for the lysis of microbes and tumor cells[132]. Interestingly, there is no homolog of granulysin in mice, and no *in vivo* studies have been conducted to elucidate its functionality. However, it has shown *in vitro* that granulysin kills a spectrum of parasites, fungi, and bacteria, particularly Mycobacterium tuberculosis[133].

## 1.7. Structure and function of the immunological synapse (IS)

Target cell lysis by NK cells depends mainly on a lytic granule-dependent apoptotic pathway. This process relies on strict and well defined biological steps to ensure the precise targeting of the lytic molecules[134]. A key element governing NK cell-mediated cell lysis is the formation of the IS, which is a specialized cell-cell interface characterized by the tight apposition between the membrane of an immune cell and its target. Originally the IS was defined between a T cell and an antigen-presenting cell, but studies have

shown the critical role of NK-IS upon target recognition[135]. For the first time, in 1983, Abraham Kupfer showed the polarization of the Golgi apparatus and MTOC in an NK cell towards its target. Originally the interface was named after the neuronal synapse due to their having the function of connecting two cells in common[136]. Studies on the NK-IS have improved our understanding about its multiple functions. The IS serves first as a region of contact between the membranes of the two cells, creating a critical zone for ligand-receptor ligation[137]. Upon target recognition, the purpose of the IS is first to ensure the adhesion and stability of the connection between the two cells. Subsequently, the direct secretion of cytolytic granules into the target cells guarantees their elimination and lysis. Highly regulated steps, components, and pathways participate in the formation of a functional IS[138]. Importantly, the sizes of the activating and inhibitory clefts are similar, between 10 and 30 nm. The lytic clefts between the effector and opposing cells play a major role in preventing the leakage of lytic granules into the surrounding tissue and ensure targeted secretion.

## 1.7.1. Stepwise stages of IS formation and activity

Defining the steps required to establish an IS is crucial for our understanding of the NK cell-mediated cell lysis. Of note, any dysregulation of one of the main stages or detailed steps is critical and may present a high risk of immune deficiency and malignancy[139,140] (Figure 6).

### 1.7.1.1.  Target recognition and adhesion stage

Resting or primed NK cells are able to recognize their targets via either tethering or a more potent adhesion component on their cell membrane, but before the adhesion receptors engage in the process, heterogeneous structures called nanotubes are rapidly formed to guide the NK cell toward its target and to transmit signals over long distances[141]. Subsequently, selectin family members on the NK membrane such as L-selectin and P-selectin glycoprotein ligand-1 (PSGL-1), initiate the adhesion with the target. Lymphocyte function associated antigen-1 (LFA-1/CD11B/CD18) and CD2 are also implicated in the creation of a firm junction[142]. LFA-1 ligation with the intercellular adhesion molecule-1 (ICAM-1) on the surface of a target cell leads to a tight junction. This adhesion step induces downstream signals via the phosphorylation of the guanine nucleotide exchange factor Vav1 by an Src-family kinase, Rac1 activation, and cytoskeletal rearrangement[143,144]. Ligand-receptor ligation is strengthened and activated

upon engagement of the activating receptors DNAM-1, NKG2D, and NCRs along with their corresponding ligands, giving rise to the initiation of the cytotoxic process[72]. Afterwards, the lytic granules move along microtubules in a dynein-dependent manner and converge upon the MTOC polarization [145].

### 1.7.1.2.  Effector stage

The most important stage for the lytic process is the effector stage when the degranulation of the cytotoxic granules occurs. This stage is marked by a rearrangement of the cytoskeleton, MTOC polarization and lytic protein secretion[146]. The mature activating IS contains a region called the supramolecular activation cluster (SMAC) that is divided into a central (cSMAC) and a peripheral (pSMAC) forms. The SMAC serves as a region for surface receptors and actin filaments (AF) to cluster[147].  The $\beta2$ integrin LFA-1 receptors and AF cluster at the pSMAC, while perforin polarizes to at the cSMAC[148].

Dynamic AF polymerization is crucial for the establishment of a lytic IS through MTOC polarization and the delivery of cytotoxic granules[149]. Importantly, AF polymerization drives the maintenance of adhesion molecules at synaptic region during the effector stage. Pharmacological- or gene-targeting of the actin cytoskeleton at the NK-IS has been found to impair IS development, cleft size, receptor distribution, and MTOC polarization[150]. Actin filament dynamics at the synapse are discussed in detail in Section 5.4.

Activating and inhibitory receptors also cluster at the SMAC. One key to an inhibitory synapse is the domination of signals derived from inhibitory receptors and the functionality of phosphatases, especially SHP-1[45,151]. These inhibitory signals swiftly act to disrupt multiple IS checkpoints such as target-cell adhesion, LFA-1 stimulation, the phosphorylation state of Vav1, activating receptor clustering, and Ca+2 flux[152,153].

It is well established that activating receptors, such as NKG2D and 2B4, cluster at the periphery of the synapse suggesting a more potent activating signal transmission. Interestingly, the inhibitory receptor KIR2DL1 also clusters at the synapse but its concentration is highly reduced when NKG2D signaling is dominant. Two main axes of activating signaling occur after NK cell activation: the phosphatidylinositol 3-kinase/extracellular signal-regulated kinases (PI3K/ERK) pathway and the phosphoinositide phospholipase Cɣ-/c-Jun NH(2)-terminal kinase (PLC ɣ-JNK) pathways. An early marker of NK cell activation is the calcium flux from the

endoplasmic reticulum (ER), which is mediated by an IP3 channel downstream of PLCy signaling. The ER likewise polarizes toward the synapse to ensure a sustained $Ca^{+2}$ flux during the lytic process[54,154].

Following activation and actin rearrangement, the MTOC is reoriented toward the synapse accompanied by the lytic granules. The movement of MTOC depends on either microtubule growth (push) or on microtubule shrinkage (pulling). Signals that direct MTOC polarization are derived from the LFA-1-derived Vav1[155]. Moreover, the actin cytoskeleton is linked to the microtubule network via Cdc42-interacting protein-4 (CIP4), the formin hDia, and the IQ-containing GTPase-activating protein 1 (IQGAP1) to ensure MTOC polarization[156,157]. Previous studies have also shown that the ADP-ribosylation factor-like 8b (Arl8b) interacts with kinesin-1 and regulates MTOC polarization[158,159]. This process is directed and regulated by the factor Munc13-4 and its ligation to Rab27a, a Rab GTPases member that regulates subcellular compartment trafficking[114]. Myosin IIA is likewise associated with lytic granules movement to the plasma membrane[160]. The lytic granules must traverse an actin meshwork by identifying actin hypo-density areas where the actin is remodeled again to provide the way[161]. Afterwards, Munc13-4 and rab27a mediates granule docking and fusion with the plasma membrane as directed by the target-soluble NSF attachment protein receptor (SANRE)[162].

NK cell mediated cell lysis is achieved by granule exocytosis in the cleft of the target[163]. Notably, proteinase inhibitor and cathepsin B are upregulated at the synapse to protect the NK cells from self-suicide or self-destruction from the released lytic proteins in the cleft[164].

### 1.7.1.3.  Lysis and elimination stage

The final stage of the cytotoxicity process is target cell lysis. Upon lytic granule delivery into the target, effector cells detach and either reinitiate the lysis of another target with granules still converged at the MTOC or they return to a resting state. Phosphatidylserine is exposed on the target-cell surface after perforin protrusion and is responsible for the signal transmitted to the inhibitory CD300a on the NK cell membrane that stops the process[127,165]. Detachment from the target cell is faster when the target cell lysis is the result of this process rather than a non-lytic IS, but it can leave the NK cells in a state of exhaustion state[40]. However, the exposure of NK cells to an activator and stimulator such as IL-2 could reinitiate their activity[166].
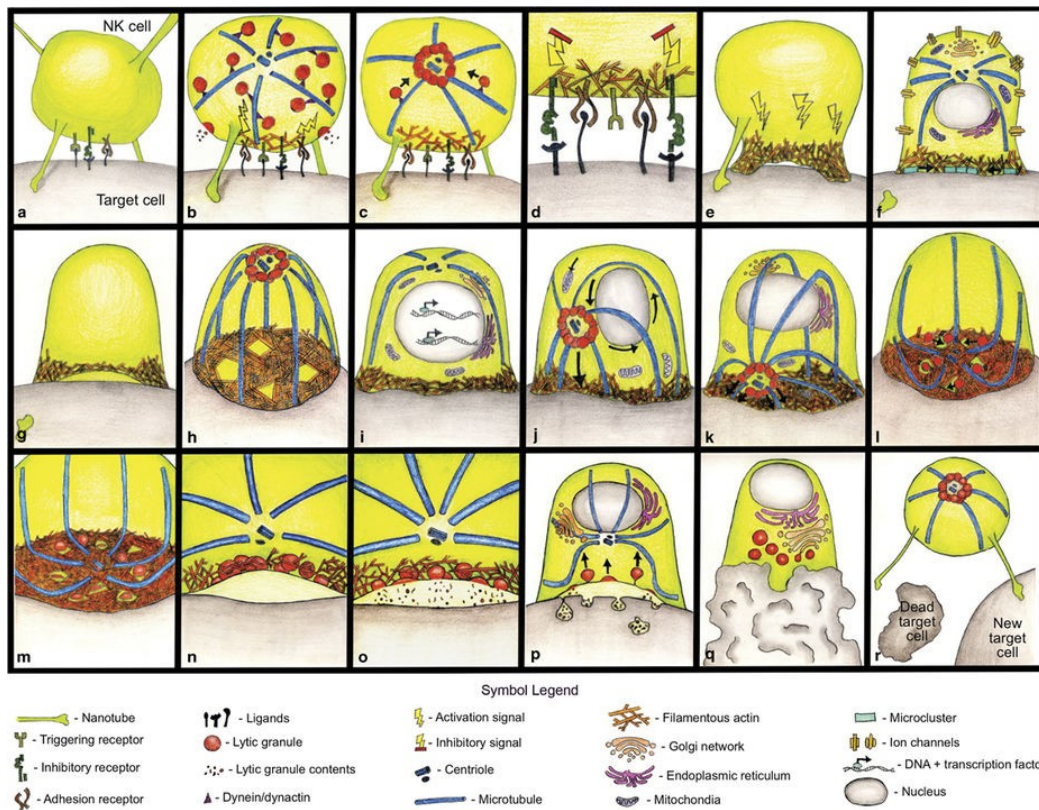
**Figure 6 | Stepwise molecular progression through NK cell cytotoxicity**

NK cell cytotoxicity can be broken down into three main stages: recognition (a–d), effector (d–p) and termination (q, r). During the recognition stage, the NK cell is particularly sensitive to inhibitory signaling (d). Key events include lytic granule convergence (c), the actin-dependent firm adhesion of the NK cell (e) and subsequent F-actin conduit formation (h), MTOC polarization (j) and LG fusion and exocytosis (o). This is followed by vesicle recycling (p), a period of relative inactivity (q) and detachment and subsequent serial killing (r). Adapted from Mace, 2014.

## 1.8. NK-cell regulation and cross-talk with immune cells

It is well established that the immune function of NK cells is defined by cytokine secretion and the elimination of aberrant cells. However, a large number of events occur between NK cell trafficking to the site of action and their activation. The maturity and functionality of the NK-cell response generally depends on constant signals from their microenvironment, including cytokine secretion and interactions with other immune cells[167].

### 1.8.1. Cytokine regulation of NK cells

The main activators of NK activity are type I IFN, IL-12, IL-18, and IL-15. IL-15 ligates with a high affinity to the IL-15Rα receptor, and the derived signal plays an important role in NK survival through regulation of the anti-apoptotic family Bcl2[168]. It is also a key element in priming NK cells to react more rapidly and efficiently by establishing a stock of lytic granules. Furthermore, IL-15 is required for IFN-ɣ secretion and NK-cell maturation and proliferation[169].

*In vitro*, IL-2 is a powerful activator for NK-cell proliferation and functionality[170]. The receptor IL-2R on NK-cell membranes is triggered upon ligation with IL-2, which activates the downstream signals JAK1 and STAT4. The role of IL-2 is well established as promoting NK cell proliferation, cytokine secretion, and cytotoxicity[171]. Together, IL-12/IL-18 principally affect IFN-ɣ secretion, while IL-18 plays a role in the expression of CCR7 and the secretion of CCL3[172,173]. However, some cytokines such as IL-21 act negatively to inhibit the proliferation of NK cells while increasing their cytotoxic effect[174]. IL-4 also inhibits NKG2D expression and the production of TNFα, IFN-ɣ, and granulocyte-macrophage colony-stimulating factor (GM-CSF)[175]. Type I IFN induces the proliferation and cytotoxicity of NK cells. IFNs ligate with their corresponding receptor IFNAR, and the absence of that receptor provokes an activation failure. The role of TGF-β in decreasing the activation and proliferation of NK cells by affecting NKG2D expression has also been established. In contrast, inhibiting TGF-β signaling increases the capacity of NK cells to secrete cytokines. The majority of cytokine receptors activate JAK/STAT signaling pathways, where the Janus kinase (JAK) allows for the recruitment and phosphorylation of signal transducer and activator of transcription (STAT), which migrates to the nucleus to regulate transcription factors[175].

## 1.8.2. NK cells: beyond natural killing

An effective immune response relies on rapid and flexible coordination between the innate and adaptive immune systems. Cytokine secretion and direct interactions between immune cells control the maturation, development, and activity of each cell population. Besides the cytolytic function of NK cells, their functions go beyond killing. Indeed, NK cells play a critical role in shaping other immune cells by mediating a refined and developed activity that impacts innate and adaptive immune cell function[176].

One of their primary important effects is regulating the function of the antigen-presenting DC[177]. The interaction between the two cell types is considered reciprocal as the cells regulate one another, and the generated results are required for an appropriate immune response[178]. Studies have shown that the depletion of NK cells affects the functionality of DCs and that NK cells kill immature DCs lacking MHC class I via the lytic or death-receptor pathway. The NK cell-mediated maturation of DCs depends on TNF-$\alpha$ and IFN-$\gamma$ secretion upon direct contact[179]. In lymph nodes, CD4$^+$ T cell-derived IL-2 activates NK cells, while CD4$^+$-derived TGF-$\beta$ inhibits NK-cell functions and suppresses their cytotoxic effect[180]. CD4+ T-helper type 1 (T$_H$1) cells are primed by NK cell-derived IFN-$\gamma$ in the lymph nodes[181]. Indirectly, T$_H$1 polarization is enhanced via the maturation of DCs. However, NK cells induce the CD8+ T-cell response via DC activation. The role of CD4$^+$CD25$^+$ Treg in suppressing immune cells is well studied. Interestingly, Treg can negatively affect various aspects of NK-cell functions such as the cytolytic process, proliferation, and cytokine production [182].

NK cells also induce the differentiation of CD14$^+$ monocytes into DCs through direct contact with CD56$^{bright}$ NK cells and the production of GM-CSF. Moreover, macrophage cross-talk with NK cells has proven to be inducible, as cytokine secretion increases upon interaction[178].

# 2. Immune-based cancer treatment

Immunotherapy is a form of cancer treatment with the intent of empowering the immune system against tumor cells, either by energizing the immune cells themselves or by ending break-off and resistance against the immune system. Cancer immunotherapy is favorably evolving and can now be considered a primary choice of therapy, joining such classical therapies as surgery, radiation, chemotherapy, and targeted therapy. With the development of immune-based therapy, attention is not only on targeting the tumor itself, but on targeting immune cells in the tumor microenvironment (TME) to reinforce their intrinsic immunological killing[183]. Thus, immunotherapy relies on the insight that the innate and adaptive immune systems recognize and eradicate tumor cells. Interestingly, some types of tumors show a dramatic and efficient response, while others do not respond at all[184]. Cancer immunotherapy seeks to reinforce the patient's immune mechanisms against tumor cells with an aim of having fewer side effects by not targeting healthy cells. Unfortunately, therapy strategies such as chemotherapy and radiation are unable to distinguish between healthy and malignant cells when they kill[184].

## 2.1. Types of immunotherapy

Approaches to stimulate immune cells involve vaccination with tumor antigen or increasing the number of antigen presentations. Adoptive cell therapy (ACT) is an additional strategy that involves the direct uptake of activated immune cells. Moreover, administering oncolytic viruses has proven to be highly efficacious in initiating anti-tumor immunity. Recombinant proteins that either block immune checkpoints or stimulate immune cells are also used[185].

### 2.1.1. Cancer vaccination

For decades, the idea of developing therapeutic cancer vaccines similar to those used against infectious agents has been of interest to researchers[186]. The objective of cancer vaccination is to stimulate immune cells to elicit an immune response against tumors. Although many vaccines have shown the capacity to activate immunity, their clinical efficiency has remained less than expected[187]. Activating host T cells against tumors was one the first targeted approaches. Vaccines are composed of antigens and adjuvants that

elicit the activation of the antigen-presenting cells responsible for shaping the immune cells. Whole cells, cell lysates, and purified antigens are sources for tumor antigens. However, the main obstacle is finding the optimal and suitable antigen that can stimulate immunity. The first cancer vaccine to be approved by the FDA was in 2010 for sipuleucel-T, a treatment for metastatic castration-resistant prostate cancer. The vaccine is made from a patient's PBMCs and enriched ex vivo. The cells are subsequently fused with prostatic acid phosphatase (PAP) and GM-CSF[188].

DCs are the most effective antigen-expressing cells that bridge the innate and adaptive immune systems[183]. The strategy is to provide a high quantity of appropriate antigens to load onto the DCs, and accordingly, allow the tumor cells to break the tolerance to immune cells. A DC-based vaccine strategy relies on isolating DCs from a patient's PBMCs and activating them with tumor antigens before re-infusing them into the patient[189].

## 2.1.2. Oncolytic virus

The therapeutic outcomes for oncolytic viruses derive either from the ability of some viruses to induce tumor killing or by their stimulation of immune-based lysis[190]. The viruses are engineered to limit their lytic activity exclusively to cancer cells[191]. Talimogene laherparepvec (T-VEC), a modified herpes simplex virus type 1 and the first oncolytic virus approved by the FDA (in 2015), is for the treatment of advanced myeloma[192].

## 2.1.3. Adoptive cell therapy (ACT)

Immunotherapy's exploitation of the cytotoxic granule activity in immune cells has revolutionized immune-based cancer treatment. For instance, ACT is taking advantage of the perforin and granzyme pathways. The concept of ACT is to isolate a patient's PBMCs, expand them ex-vivo, and re-infuse them back into the patient[193]. The lymphocytes can be isolated from peripheral blood, lymph nodes, or tumor tissue. In melanoma patients, depleting immunosuppressive cells such as Treg cells or co-injecting IL-2 has improved the efficiency and clinical outcome of ACT for tumor infiltrating lymphovytes[194]. Another strategy is to transfer T cells engineered and generated ex vivo. One example involves the expression of the TCR $\alpha$ and $\beta$ chains that ligate with HLA ligands[195]. Another approach is the transfer of chimeric antigen-receptor (CAR) cells,

which are an antibody-recognition domain fused to a TCR-constant domain. This new FDA-approved strategy has shown promise in treating patients with hematological malignancies such as acute B-cell lymphoblastic leukemia and B-cell lymphoma[196-198].

### 2.1.4. Immune checkpoint blockade

Immune checkpoints play a critical role in controlling the immune response against pathogens and cancers[199]. A plethora of immune inhibitory pathways are generated upon contact with cancer cells. Any blockage to inhibitory checkpoints, and therefore their derived inhibitory signals, is a promising approach for triggering an anti-tumor immune response[200]. Here we focus on the main approved checkpoint inhibitors for cancer immunotherapy[201].

The first inhibitory checkpoint to be targeted was cytotoxic T lymphocyte-associated protein 4 (CTLA-4), also known as CD152, an inhibitory receptor and negative regulator expressed on regulatory T cells[202]. CTLA-4 is a homolog of the co-stimulatory receptor CD28, but with a high affinity to CD80 (B7-1) or CD86 (B7-2) ligands on the membranes of antigen-presenting cells. Ligation with B7 molecules leads to a net negative signal, which limits IL-2 production and T-cell survival[200]. In 2011, the anti-CTLA-4 monoclonal antibody ipilimumab was approved by the FDA for treating metastatic melanoma. Clinical trials for CTLA-4 with prostate, bladder, and non-small-cell lung carcinoma (NSCLC) are ongoing. Results have shown T-cell compartment activation, tumor regression, and overall survival improvement[203].

The programmed cell death 1 (PD1) receptor expressed on activated T-cell membranes is among the important inhibitory checkpoints. Activation of PD1 (also known as CD279) after it interacts with its ligands regulates the antigen response threshold of T and B cells and thus, inhibits cell proliferation, cytokine release, and cytotoxicity[204]. PD-L1 and PD-L2, expressed on tumor cells, are ligands that bind to PD1 receptors. Blocking this interaction can enhance T-cell anti-tumor activity[202].

Pembrolizumab and nivolumab antibodies target PD1 and are approved by the FDA to treat melanoma, head and neck squamous cell carcinoma, and NSCLC[205]. Additionally, due to the high clinical response it has shown, nivolumab was also approved for Hodgkin lymphoma and renal cell carcinoma. Moreover, atezolizumab, avelumab, and durvalumab are antibodies against PD-L1. Atezolizumab produces a therapeutic response in many

types of cancers such as melanoma and colon, lung, gastric, and head cancers. It was approved by the FDA in 2016 for the treatment of NSCLC and urothelial carcinoma[184].

V-domain immunoglobulin suppressor of T cell activation (VISTA) is an inhibitory immune checkpoint that downregulates CD4$^+$ and CD8$^+$ T-cell activation[206,207]. It is expressed on naïve CD4$^+$ and CD8$^+$ cells, Foxp3$^+$CD4$^+$ regulatory cells, and DCs. VISTA blockage could soon be a target for novel therapies[200,208]. Lymphocyte activation gene 3 (LAG3) is a selective marker and cell surface molecule on the membrane of T, B and NK cells. It has been reported that this ligand downregulates the proliferation and activation of T cells and plays a role in the suppressive function of Tregs. Targeting LAG3 reverses T-cell exhaustion and thus, enhances anti-tumor activity[209]. T-cell immunoglobulin and mucin domain-containing 3 (TIM3) is another immune checkpoint expressed on NK cells, DCs, and various T-cell populations. Its co-expression with PD1 in CD8+ cells makes it a potent therapeutic target[210]. The TIGIT receptor is strongly expressed on lymphocytes. The blockade of TIGIT in combination with a PD1 mAb resulted in the improvement of CD8+ T-cell functionality and tumor rejection. Anti-TIGIT can also be combined with anti-LAG3 or anti-TIM3 to confer anti-tumor immunity[73].

## 2.2. NK cell-based immune editing

Although immunotherapy studies have focused more on T cell-based therapy, recent studies have shed light on the potential of NK cells as a powerful directed immunotherapy approach. Overcoming the immunosuppressive microenvironment and inducing anti-tumor activity in NK cells have been exploited to cure cancers in different approches[211].

### 2.2.1. Adoptive NK-cell therapy

The first approach is adoptive NK-cell therapy whereby NK cells from healthy donors (allogenic NK cells) or the patient (autologous NK cells) are isolated and re-infused into the patient after ex vivo expansion and activation with cytokines (IL-2, IL-12, IL-15, and IL-18) or stimulatory molecules. Cytokines, and especially IL-2, are administrated after the re-infusion in repeated injections at low doses. Allogenic NK-cell transfer shows a higher efficacy and optimal anti-tumor effect than autologous NK-cell transfer due to the KIR mismatch (haploidentical). Furthermore, NK cells don't exert graft-versus-host-disease (GvHD)[212]. The disadvantage of this method is the poor proliferation and persistence of NK cells in the patient. Given the donor-dependent variability of NK cells,

studies have shown the high efficiency of infusing NK-cell lines such as NK-92, which lacks the KIR inhibitory receptor and therefore is highly cytotoxic[213,214].

Genetic modifications to NK cells have also proven to enhance NK-cell anti-tumor activity. The infusion of CAR T, CAR-NK, or CAR-NK-92 cells is a promising approach at the preclinical stage that involves increasing tumor specificity in NK cells for the treatment of B-lineage acute lymphoblastic leukemia[215] (Figure 7).
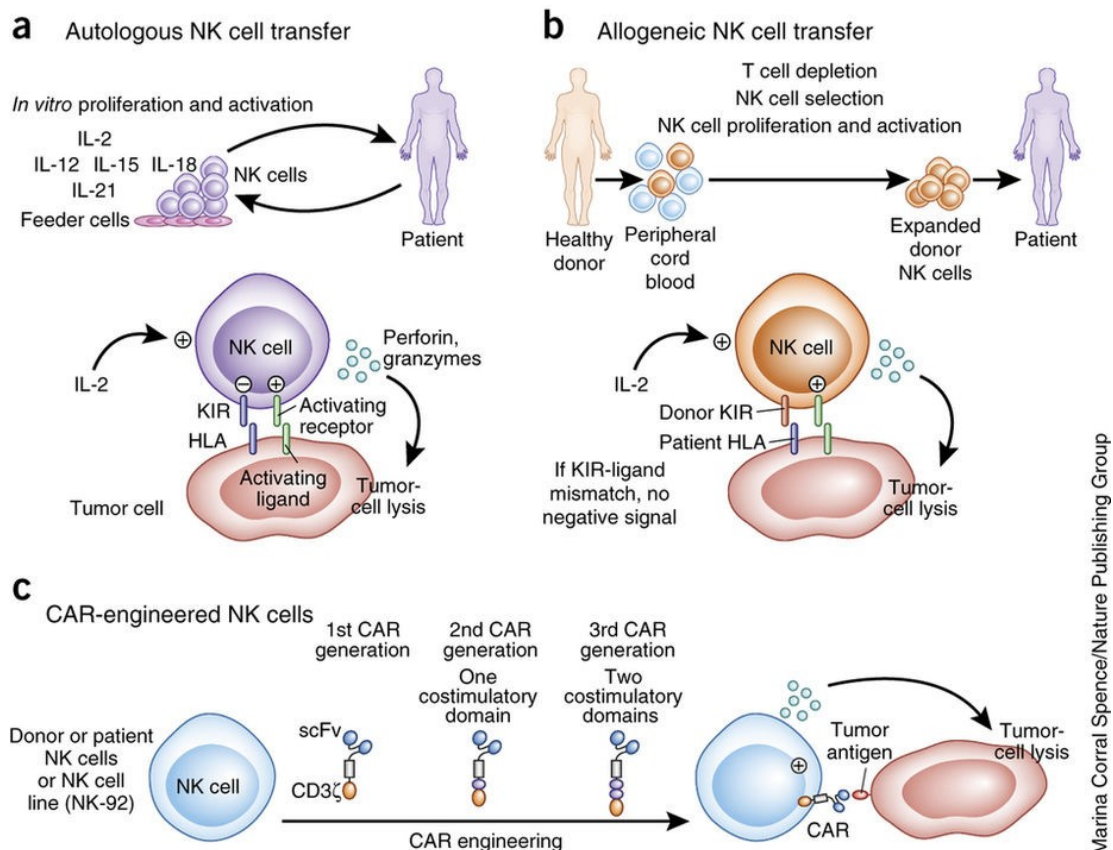


**Figure 7 | NK cell transfer**

a) In autologous transfer, NK cells from the patient are activated and expanded *in vitro* in the presence of cytokines. Combination of IL-12, IL-15 and IL-18 might generate NK cells and feeder cells such as K562 can be added to the culture. The expanded and activated NK cells are then transferred back into the patient, who generally receives cytokine administration to sustain the expansion and function of the infused NK cells. b) In allogeneic transfer, NK cells can be obtained from HLA-matched or haploidentical (partially matched) donors. In this setting, the best responses are obtained when haploidentical donors do not express KIRs that recognize the patient's HLA molecules, because donor NK cells do not receive an inhibitory signal from the patient's cancer cells. c) CARs can be engineered in autologous or allogeneic NK cells or in NK cell lines such as NK-92. Adapted from Guillerey et al., 2016.

## 2.2.2. Tumor antigen-specific antibody administration

Targeting tumor-associated antigens with therapeutic antibodies plays a role in inducting NK cell-mediated ADCC. The chimeric monoclonal antibody (mAb) anti-CD20 (rituximab) is indicated for the treatment of chronic lymphocytic leukemia and non-Hodgkin lymphoma. The Fc portion of rituximab mediates ADCC as well as CDC, and thus enhances NK-cell cytotoxicity[96,216]. Cetuximab, an anti-epidermal growth factor receptor (EGFR) mAb, is used for colorectal cancer, NSCLC, and head and neck cancer[217]. Besides inhibiting EGFR, one of the mechanisms of action is considered to be the ADCC triggering by Fcγ-R on the NK cells[218]. Moreover, recent studies have focused on increasing the activity of ADCC by increasing the affinity of the activating receptor FcγRIIIa. Mogamulizumab, which is a mAb that binds to CC chemokine receptor 4 (CCR4) is such a treatment[219]. The drug is used for T-cell leukemia-lymphoma, and research has shown it enhances anti-tumor activity via ADCC by removing fucose residues from the Fc region[220].

## 2.2.3. NK cell genetic modifications

Clinical studies with NKG2D- or TRAIL-overexpressing NK cells showed they have improved tumor recognition and lysis capability after re-infusion in the patient. Immunosuppressive cytokines such TGF-β are secreted into the TME to downregulate the activity of NK cells. Studies show that NK cells engineered with TGF-β dominant-negative receptor II protect NK cells and improve their survival. In addition to the genetic modification of NK cells, clinical trials with TGF-β inhibitors and adenosine A2A agonists are ongoing[215].

## 2.2.4. Supplement cytokine uptake

IL-2, IL-12, and IL-15 are activator cytokines for NK cells, and their uptake could enhance the anti-tumor response. In melanoma and metastatic renal cell carcinoma, the combined administration of IL-15 or IL-2 with lymphokine-activated killer cells has a 20% response rate[215].

## 2.2.5. NK-cell immune checkpoint targeting

An important approach to treating cancer is to empower the lytic mechanisms of endogenous NK cells by blocking inhibitory receptors with specific mAbs, thus banning

the inhibitory signals. Indeed, a few inhibitory receptors are currently being targeted in clinical or pre-clinical development. Furthermore, classical immune checkpoints are present on the NK cell membrane, and their blockade reverts the NK inhibitory state[211,221].

The inhibitory pathway of NK cells depends largely on KIR receptors and their interactions with HLA class I on target cells. The negative effects of this ligation influence NK-cell activity, cytokine production, and cytotoxicity. Studies have shown that blocking KIR receptors with specific antibodies induces NK-cell cytotoxicity to acute myeloid leukemia (AML) cells. This promising result led to the development of lirilumab, a recombinant IgG4 mAb against KIR2DL1, KIR2DL2, and KIR2DL3. Clinical trials have been conducted for lirilumab as a monotherapy for AML patients and in combination with elotuzumab for multiple myeloma, with rituximab for chronic lymphocytic leukemia, and with nivolumab for head and neck carcinoma[211].

An important receptor of the NKG2 family is the A form that binds to HLA-E to generate inhibitory signals. NKG2A expression on effector cells is constant and unaffected by the microenvironment. Blocking NKG2A receptors with the mAb monalizumab led to an increased proportion of lymphocytes that infiltrated to the tumor site and enhanced cytotoxicity in oral squamous cell carcinoma and gynecological malignancies. Clinical trials are now being conducted for monalizumab in combination with cetuximab and durvalumab[222].

PD1, the most promising immune checkpoint receptor, is expressed on the NK-cell membrane and is associated with the inhibition of NK-cell lysis. *In vitro*, blocking PD1 on NK cells with mAbs relieves this inhibition. Clinical responses to nivolumab have been observed by rescuing the anti-tumor NK-cell response[199].

The expression of LAG3 on NK cells is crucial for NK-cell function. Nevertheless, targeting LAG3 with mAbs enhanced Fas-mediated apoptosis in NK and melanoma cells. Similar to LAG3, targeting TIM3 shows a promising result in increasing NK activity. In lung adenocarcinoma, TIM3 mAbs act to increases IFN-ɣ production and the cytotoxicity of NK cells. Clinical trials with LAG3 and TIM3 mAbs are ongoing. Of note, the administration of a TIGIT mAb in combination with other immune checkpoints is being tested in clinical trials on various solid tumors[222].

### 2.2.6. Immunomodulatory drugs

Immunomodulatory drugs can regulate NK-cell function and anti-tumor activity. Thalidomide and its derivate lenalidomide have proven to be efficient in multiple myeloma by increasing IL-2 secretion[223]. Equally, tyrosine-kinase inhibitors, proteasome inhibitors, and serine-threonine kinase GSK3 have direct effects on NK cell-mediated cell activity[224] and thus their combination with anti-cancer drugs could be a promising way to enhance NK-cell function[222] (Figure 8).
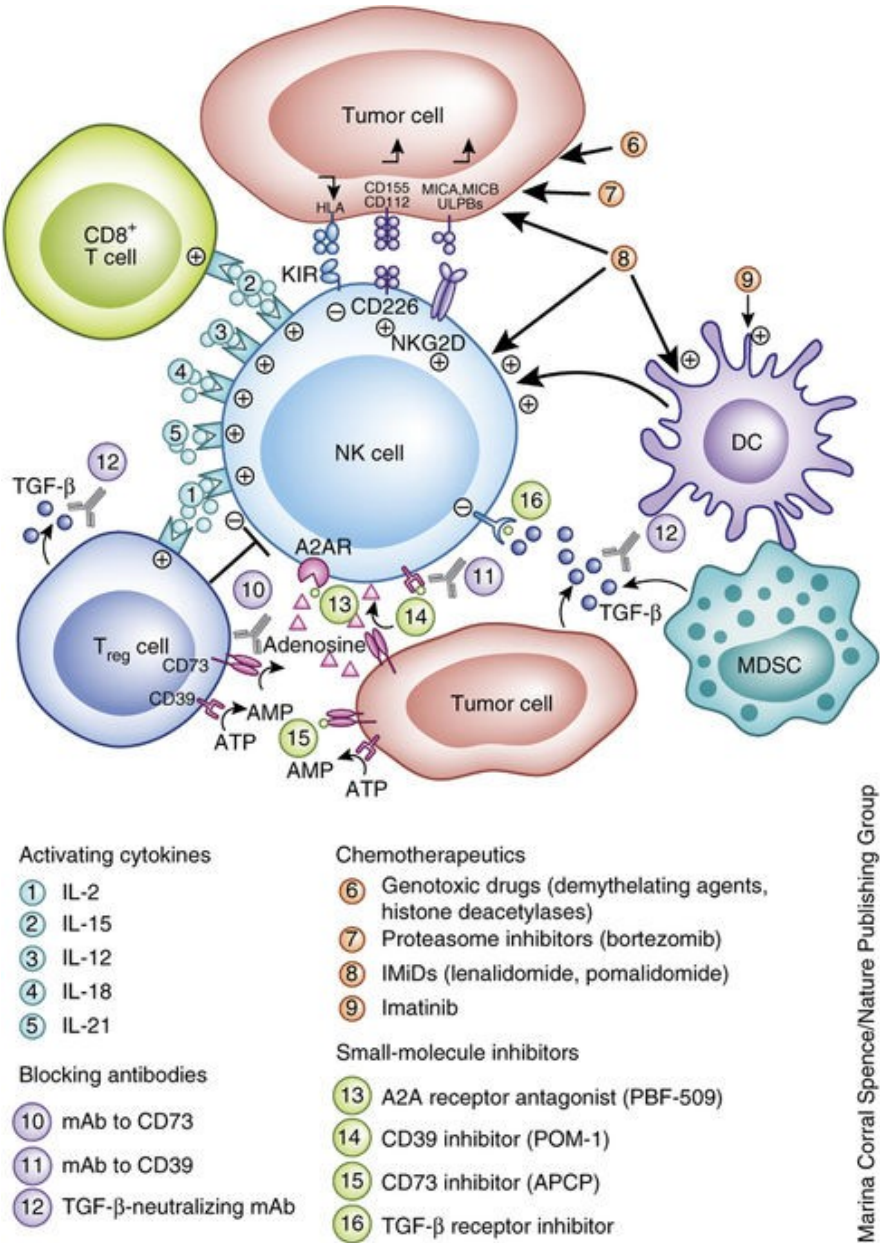


**Figure 8 | Targeting the tumor microenvironment to improve NK cell responses**

Various strategies can be adopted to create a microenvironment favorable to NK cells to improve the efficacy of NK cell–based therapies including the administration of activating cytokines, blocking antibodies, chemotherapeutics and small-molecule inhibitors. Adapted from Guillerey et al., 2016.

# 3. Breast cancer and immune evasion

## 3.1. A general overview of breast cancer

Breast cancer (BC) is the second most common form of cancer behind lung cancer. It is the first common cancer and accounts for 30% of all new diagnoses in women. Each year, 1.3 million cases are reported worldwide[225]. Although advanced treatment strategies are applied, BC is still the second leading cause of death related to cancer in women today. Several risk factors are implicated in BC such as inheritance, age, hormonal status, and origins[226].

Mammary glands are made of individual lobes that are regulated upon puberty in response to the endocrine system and secreted hormones. Each gland consists of a central duct connected to many branched ducts. These ducts and lobules are connected and surrounded by the stroma, which is made up of fatty connective tissues as well as blood and lymphatic vessels. Breast cancer that starts in the epithelial lining of milk ducts is termed ductal carcinoma. However, in some cases, it can also start in the milk-producing glands (lobules). Two forms of ductal carcinoma exist: ductal carcinoma in situ (DCIS) and invasive ductal carcinoma (IDC). The latter tends to spread to other parts of the breast and body via neighboring lymph nodes. Less common types of BC also occur such as inflammatory BC, medullary carcinoma, mucinous carcinoma, and tubular carcinoma[227,228].

Mammary glands develop due to ovarian hormones as well as pituitary hormones and growth factors. Luteinizing hormone (LH) and follicle-stimulating hormone (FSH) are secreted from the pituitary gland and stimulate the ovaries to secrete the female sex steroid hormones estrogen (estradiol) and progestin (progesterone). These hormones are a key element in the development of mammary glands and tumorigenesis[229].

## 3.2. Types of breast cancer

Breast cancer shows a high level of heterogeneity in terms of biomarkers, histological grades, and morphology. The classification of BC is defined by the expression or lack of expression of three distinct protein receptors: estrogen receptor (ER), progesterone

receptor (PR), and HER2. Breast cancer is also classified based on the tumor size, lymph node implications, and age.

The ER$^+$ group represents the most varied group with regard to genetic diversity, but it responds well to treatment. This group is also categorized as luminal A, which is ER-$\alpha$ positive with a low histological grade, or luminal B, which is low ER-$\alpha$ positive with a high histological grade. The luminal A phenotype responds to anti-estrogen therapy better than the luminal B phenotype. The second group is the HER2$^+$ group, which is characterized by the high expression of HER2 receptors and accounts for 30% of all BCs[230]. Compared to the ER$^+$ group, HER2$^+$ has shown better prognoses and clinical outcomes. The basal-like phenotype of cells lacking the three receptors is defined as a triple-negative breast cancer (TNBC). TNBCs tend to be the more aggressive form, as generally this group does not respond to targeted treatments such as anti-estrogen or anti-HER2 antibodies[231]. Nevertheless, the complicity and heterogeneity of BC groups limit the possibility of a common therapeutic effect for treatment[232].

## 3.3. Breast cancer therapeutic strategies

Breast cancer is becoming a major area of interest for researchers due to its high malignancy in women. Traditional therapies such as radiation and chemotherapy are becoming less effective, as they harm the healthy tissues of the body. Surgery is also considered to have a limited effect due to the rapid metastasis of BC after prognosis. Alternative therapies, especially immune-based therapies, are emerging as promising therapeutic strategies[233].

### 3.3.1. General treatments

Owing to the heterogeneity of BC, the choice of an appropriate and optimal therapy option relies on many factors such as the type and stage of the tumor, genomic markers, patient age, menopausal status, and the presence of mutations. Likewise, the biology of the cancer and its size affect the decision on a strategy. Several therapeutic approaches can be used such as surgery, chemotherapy, radiation, hormone therapy, targeted therapy, and immunotherapy.

Surgery is the choice for DCIS and early stage invasive BC. Lumpectomy is the removal of the tumor and the tissue surrounding it, whereas mastectomy is the removal of the entire breast. The removal of lymph nodes is also one of the surgical choices. Usually

surgery is followed by radiation therapy (ionizing irradiation) as an adjuvent[234,235]. Systemic chemotherapy is one powerful treatment option because it destroys cancer cells and their ability to grow and divide. There are many common drugs used to treat BC, alone or in combination with other adjuvant therapies. Methotrexate, cisplatin, fluorouracil, cyclophosphamide, and doxorubicin are commonly used chemotherapeutic agents[227].

Endocrine or hormonal therapy is one of the most effective treatments for the corresponding cancer type that can be used alone or as an adjuvant therapy. Blocking hormones can lead to the prevention of cancer growth and recurrence. Tamoxifen acts as an antagonist and blocks the effect of estrogen by binding to estrogen receptors. It is the drug of choice for ER$^+$ patients and has proven to lower the growth, recurrence, and risk of developing cancer[236]. Aromatase inhibitors are used to decrease the amount of estrogen by blocking the enzymatic activity of aromatase, which is responsible for converting the male hormone androgen into estrogen[229].

### 3.3.2. Breast cancer immune-based treatment

Although BC has been considered a non-immunogenic tumor type, studies have shown that certain types of BC are highly infiltrated by immune cells and have a high response rate to immune checkpoint inhibitors. These are the TNBC and the HER2$^-$ BCs. Clinical trials using immunotherapy have resulted in good therapeutic outcomes in TNBC patients, who have no targeted-therapy options[231]. Targeting PD1/PD-L1 to treat BC is also showing promising results with tumor regression and the improvement of patient outcomes. Pembrolizumab (a PD1 inhibitor), atezolizumab, and avelumab (PD-L1 inhibitors) enhance the local anti-tumor response. They can also be combined with MAP2K and GITR in TNBC cases to provide a more therapeutic outcome[237]. In a pre-clinical study, co-treatment with mAbs against TIM3/PD-L1 showed complete BC regression in the majority of treated mice[210]. The new fusion protein M7824 is an innovative drug that blocks both PD-L1 and TGF-β, and thus, activated CD8$^+$ T cells and NK cells. Preclinical studies in a BC model have shown enhanced anti-tumor activity and reduced metastasis. Moreover, an increase in the buildup of hyaluronan, a glycosaminoglycan, was observed in the breast cancer TME, leading to a delay in immune cell and antibody infiltration to the tumor. In a preclinical study with a BC

model, the depletion of hyaluronan by PEGylated recombinant hyaluronidase 20 (PEGPH20) enhanced the delivery of PD-1 and PD-L1[238,239].

It has also been shown that tamoxifen enhances NK-cell ADCC in HER2/neu BC cells[240]. The use of trastuzumab and pertuzumab, anti-HER2 mAbs, in HER2^{+} BC cases improves the overall survival of patients via the recruitment of NK cells and the induction of NK cell ADCC[241].

Another new approach that shows a clinical outcome in BC studies is the use of stimulator of interferon genes (STING). STING induces interferon production and DC activation, promoting the priming of cytotoxic CD8^{+} T cells. The injection of ADU-S100, a STING agonist, in combination with PD1 mAb administration produced a delay in tumor progression and tumor clearance in TNBC and HER2^{+} BC[232].

The epigenetic modification of immune recognition is one of the mechanisms of tumor evasion. Inhibitors against histone-deacetylase (HDAC) have proven to be effective by priming the anti-tumor immune response in a variety of BCs, especially in the ER[+] group. Etinostat, a selective HDAC-1 inhibitor, has also been shown to increase the T cell-mediated cell death of BC cell lines *in vitro*[239].

## 3.4. Mechanisms of immune evasion in breast cancer

While an immune response is directed to eradicate cancer, tumor cells can induce resistance among the immune cells and evade the elimination process. To withstand the growth of a tumor, a suppressive TME is necessary to neutralize the activation of immune cells and stop the elimination process. The majority of immune-cell types can infiltrate into or to the edge of a tumor, with the infiltration rate varying depending on the type and stage of the tumor. Remarkably, the hypoxic milieu and the stabilization of hypoxia-inducible factor 1-$\alpha$ (HIF1-$\alpha$) proteins in tumor cells mediate the adjustment of cells to the TME through phenotypic, genetic, or metabolic transformations[242].

The immunoediting of BCs and other solid tumors is a dynamic process in which immune cells lyse the tumor cells. It comprises three distinct stages: elimination, equilibrium, and escape. During the elimination stage, immune cells destroy tumor cells after infiltration and activation. Cells that manage to resist and survive this killing enter into the equilibrium phase. The escape stage represents the final stage of the process, when tumor cells keep progressing, spreading, and becoming clinically detectable. The

microenvironment of the tumor at this stage tends to be suppressive, and tumors have diverse mechanisms of resistance[243].

In BC, tumor cells escape from the immunosurveillance of the innate and adaptive immune cells. Immunotherapy approaches have significantly increased remission and overall survival in patients. Nevertheless, the high proportion of non-responders represents a tough and serious challenge in the cancer field. Remarkably, many biological processes are implicated in tumor immune evasion as well as in resistance to various therapies. The mechanisms used by tumor cells for immune evasion fall under many categories and include tumor-related immune evasion and microenvironment alteration as well as morphological and cellular changes[242]. Recent findings have well established that cellular heterogeneity and plasticity, e.g., the induction of autophagy or the epithelial-to-mesenchymal transition (EMT), have a serious impact on tumor evasion from T and NK cells.

The next section will provide insight into the various processes with a focus on the implications of the EMT and autophagy to better understand how cancer cells escape immune surveillance and resist T and NK cell attacks.

### 3.4.1. Intrinsic tumor resistance

Immune cells recognize tumors via antigens and ligands presented on the surface of the tumor. Breast cancers express surface antigens distinct from normal cells, triggering immune cells to recognize them. Melanoma-associated antigens (MAGEs) are a family of cancer/testis antigens expressed on the surface of BC cells, but not on normal cells (only in testis and placenta). MAGE-A9 is highly expressed in ductal BC and is associated with negative consequences. However, MAGE-A9 is expressed less in ER $^-$ and HER2 $^-$ BC[244,245]. Another antigen is mesothelin, a cell-surface glycoprotein highly expressed on the surface of TNBC. It is considered a tumor marker and can modify TCRs. Moreover, HER2/neu is known to be overexpressed in HER2$^+$ BC, and higher levels of HER2/neu were found in patients with BCs possessing a more aggressive phenotype[246]. Moreover, β2 microglobulin, calnexin, and transporter-associated antigen processing 1 are downregulated in metastatic BC and negatively affect CTL infiltration. The MHC class I expression level is also significantly downregulated in BC cells, leading to evasion of the T cell-dependent immune response, but also the simultaneous activation of NK cell-mediated cell lysis by the "missing self" signal[247]. To avoid T cell- and NK cell-mediated

killing, BC cells express HLA-G on the cell surface. HLA-G is considered a biomarker for identifying metastatic BC and hence, for targeting. It is a potent immunotherapeutic strategy.

Controlling the apoptotic pathway is considered an important mechanism for tumor cells to evade the immune response. Any disruption of one of the components in the pathway can block the apoptotic process, leading to endless proliferation. Breast cancer cells can either downregulate the Fas receptor on the surface of their membrane or stimulate the immune cell apoptotic pathway by overexpressing FasL, which binds to Fas receptors on the immune cell surface[248]. In addition to the Fas pathway, high levels of Bcl-2 in BC cells inhibit the TRAIL-dependent pathway, leading to a prolonged life span for the tumor cells[249]. The overexpression of downstream proteins such as survivin in the apoptotic pathway plays a significant role in BC resistance in advanced grades[250].

BC cells express both PD1 and PD-L1 on their membranes. The interaction between PD-L1 on the BC-cell membrane and the receptor on immune cells leads to downregulation of the immune response due to the induction of T-cell and NK-cell apoptosis. The N-glycosylation and ubiquitination of the PD-L1 ligand on BC cells have direct positive effects on its suppressive activity[251]. Blocking PD-L1 or destabilizing it can significantly attenuate T-cell apoptosis. Moreover, a high correlation has been found between PD-L1 expression and increased FoxP3$^+$ Treg infiltration in the high histological grade BCs (ER $^-$, PR $^-$, and TNBC). They work synergistically to promote BC immune evasion[252]. Additionally, the overexpression of CD80 and CD86 on TNBCs leads to the inactivation of T cell-mediated cell death, immunosuppressive-cell infiltration, and a reduction in cytokine production via interaction with the inhibitory CTLA-4 receptors[253].

### 3.4.2. Immune cell suppression

Tumor progression and metastasis is not only restricted to modifications in tumor cells, but also to the TME. Recent studies have shown a tight association between the BC microenvironment and tumor evolution. The activation of infiltrated immune cells depends largely on chemokines and cytokines produced by the tumor[254]. Due to the impact of the inhibitory environment, T cells could ignore tumor antigens presented on BC cells. A high rate of Treg infiltration and proliferation has been observed in TNBCs. This recruitment is dependent on CCR4, CCL22, and CCL17 and modulated by compounds secreted from the BC cells and DCs[255]. Using MAPK/ERK inhibitors leads to

blocking the TGF-β-dependent induction of Treg[256]. Tumor cells can also suppress the activity of NK cells that have infiltrated to the BC microenvironment.

One immune-evasion strategy consists of shedding ligands that bind to NKG2D receptors or the secretion of transforming growth factor-β (TGF-β), which downregulates NKG2D-receptor expression. Additionally, tumor secretion of NKG2D ligands can saturate and abolish the activity of NK-cell receptors[257,258]. Furthermore, BC can produce soluble factors that induce the expression of NKG2D ligands on the immune-cell surface, thereby evading immunity[154].

BC cells produce numerous cytokines during the elimination stage to evade anti-tumor responses. The IL-6 secreted by BC cells affects NF-κB, leading to EMT induction and more resistant and invasive tumor cells. Secreted IL-33 activates the production of GM-CSF and myeloid-derived suppressor cells. IL-19 and IL-20 enhance the proliferation and metastasis of tumor cells, while IL-23 affects CD8+ T-cell infiltration and activation[242] (Figure 9).
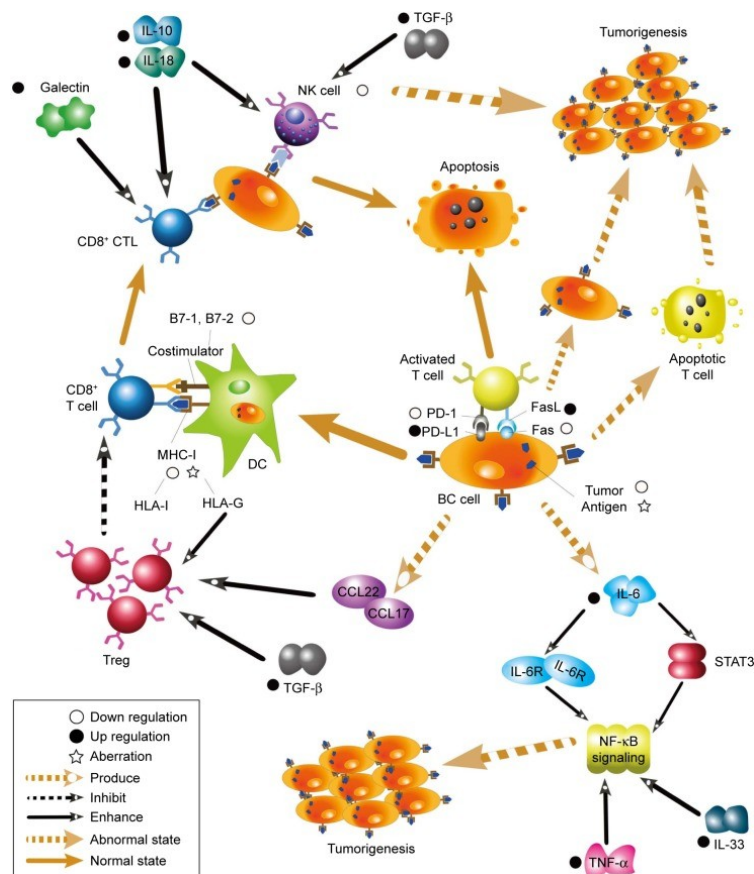


**Figure 9 | Mechanisms of immune evasion in breast cancer**

A summarized network of immune evasion mechanisms and their interactions. Adapted from Wang et al., 2017.

# 4. Epithelial-to-mesenchymal transition

A key element mediating tumor metastasis and invasion is the transitional state between the epithelial and mesenchymal phenotypes. The process is essential to development, stem cell behavior, wound healing, and cancer progression. The transition respects a conserved program with particular hallmarks and results in the downregulation of epithelial cells and the induction of mesenchymal cell characteristic[259]. Recent studies have shown a tight association between the EMT and invasiveness and resistance to apoptosis, chemotherapy, and radiation. Moreover, mesenchymal cells tend to have cancer stem-cell behavior and have an influence on TME components, possibly regulating anti-tumor immune editing[260].

## 4.1. Basic principles of the EMT

Plasticity in cellular organization is a hallmark of early embryonic developmental stages. The EMT was first observed by Elizabeth Hay in the 1980s in the primitive streak of chick embryos[261]. Cells expand their intracellular contact immediately after cleavage formation and create the epithelium, a polarized layer. Subsequently, cells develop apicobasal cell surface polarity, with actin microfilaments concentrated at the basolateral membranes and microtubules positioned at the basoapical axis positioning the cytoplasmic organelles. In epithelial cells, integrin receptors are localized on the basal domain, forming a basal lamina that interacts with the extracellular matrix, while the lateral domain comprises the junctional complexes, including E-cadherin[260].

The acquisition of the mesenchymal motile phenotype is characterized by the loss of their apico-basal polarity, epithelial cell-cell junction, and E-cadherin. Simultaneously, the cells acquire vimentin and N-cadherin, redistribute the actin cytoskeleton, and reprogram some gene expression, giving rise to the initiation of a front-rear polarity and migratory features[262]. The formation of mesenchymal cells is initiated during gastrulation,

an early phase in embryonic development when a single-layer blastula is reorganized into a multilayered structure called the gastrula. Mesenchymal endodermal and mesodermal cells detach from the epiblast (the epithelial layer) and ingress through the primitive streak[263]. Mesenchymal cells can convert back to the epithelial state, a reverse process called the mesenchymal-to-epithelial transition (MET), to establish paraxial and lateral mesodermal structures. The shifts between the EMT and the MET (crucial in some organogenesis such as heart development), gene expression, and non-transcriptional changes are regulated by TGF-β, canonical Wnt, and the RTK pathways[264].

Upon initiating the EMT, the epithelial cell-cell junctions, including E-cadherin, the tight junction, adherens junctions, desmosomes, and gap junctions such as connexins, are deconstructed and degraded. This process is associated with decreased claudin and occluding expression and the diffusion of zonula occludens 1 (ZO1). In addition, β-catenin and p120 catenin are protected from degradation and act only in transcription following E-cadherin degradation[265].

Apical-basal polarity is associated with three important polarity complexes linked to the cell junctions. Upon E-cadherin suppression, complexes are either repressed or inhibited from interaction with the membrane. Partitioning-defective proteins include PAR3, PAR6, and atypical protein kinase C (aPKC). Crumbs complexes, which are mainly associated with tight junctions and cortical actin, contain Crumbs, protein associated with Lin-7 1 (PALS1), and PALS1-associated tight junction protein (PATJ). The Scribble complexes associate with adherens junctions and comprise discs large (DLG) and lethal giant larvae (LGL). The repression of Crumbs and Scribble in the mesenchymal phenotype allows for directional motility[262].

## 4.2. EMT biomarkers

E-cadherin is a calcium-dependent cell-surface protein responsible for adhesion in epithelial cells through the cytoplasmic and extracellular domains. Its expression is a hallmark of the epithelial phenotype, and any suppression of its expression can lead to a mesenchymal phenotype. In BC cells, the loss of E-cadherin and the acquisition of N-cadherin are correlated with the acquisition of invasiveness and metastatic behavior, as well as a poor prognosis[266,267].

Vimentin is a hallmark of the mesenchymal invasive phenotype. It is an intermediate filament expressed at the site of cellular elongation and spikes. In BC cells, vimentin

expression is regulated independently by Smad-interacting protein 1 (SIP1) in epithelial cells[268].

In the BC basal phenotype, α-smooth muscle actin (α-SMA) is abundant in metastatic cells in comparison to non-metastatic one[269]. β-Catenin is a protein localized to the membrane of epithelial cells that translocates to the cytoplasm and the nucleus upon EMT induction. It is later responsible for promoting gene transcription. The expression of β-catenin is higher in invasive carcinomas than in DCISs. It has been shown that Wnt/β-catenin signaling is upregulated in invasive ductal carcinoma[270]. Discoidin domain receptor 2 (DDR2) is an abundant receptor for tyrosine kinase in BC. It stabilizes SNAIL and plays a role in adhesion to collagen in the extracellular matrix, promoting invasiveness[271].

Cancers can be classified based on their transcriptomic signatures, a method called EMT scoring. The score can help to semi-quantitatively assess the position of certain tumor types over a wide range of the EMT spectrum, with values ranging from −0.8 for the most epithelial phenotype to +0.6 for the most mesenchymal phenotype. As an example, melanomas and renal carcinomas have a majority of mesenchymal features while colon carcinomas show epithelial features. Others, such as BC, exhibit a wide range on the EMT spectrum. In general, tumor cell lines protect the initial EMT features from their original tumor. In BC, luminal and HER2/neu tumors exhibit an epithelial-like phenotype, whereas basal-like and claudin-low tumors are mesenchymal[272] (Figure 10).
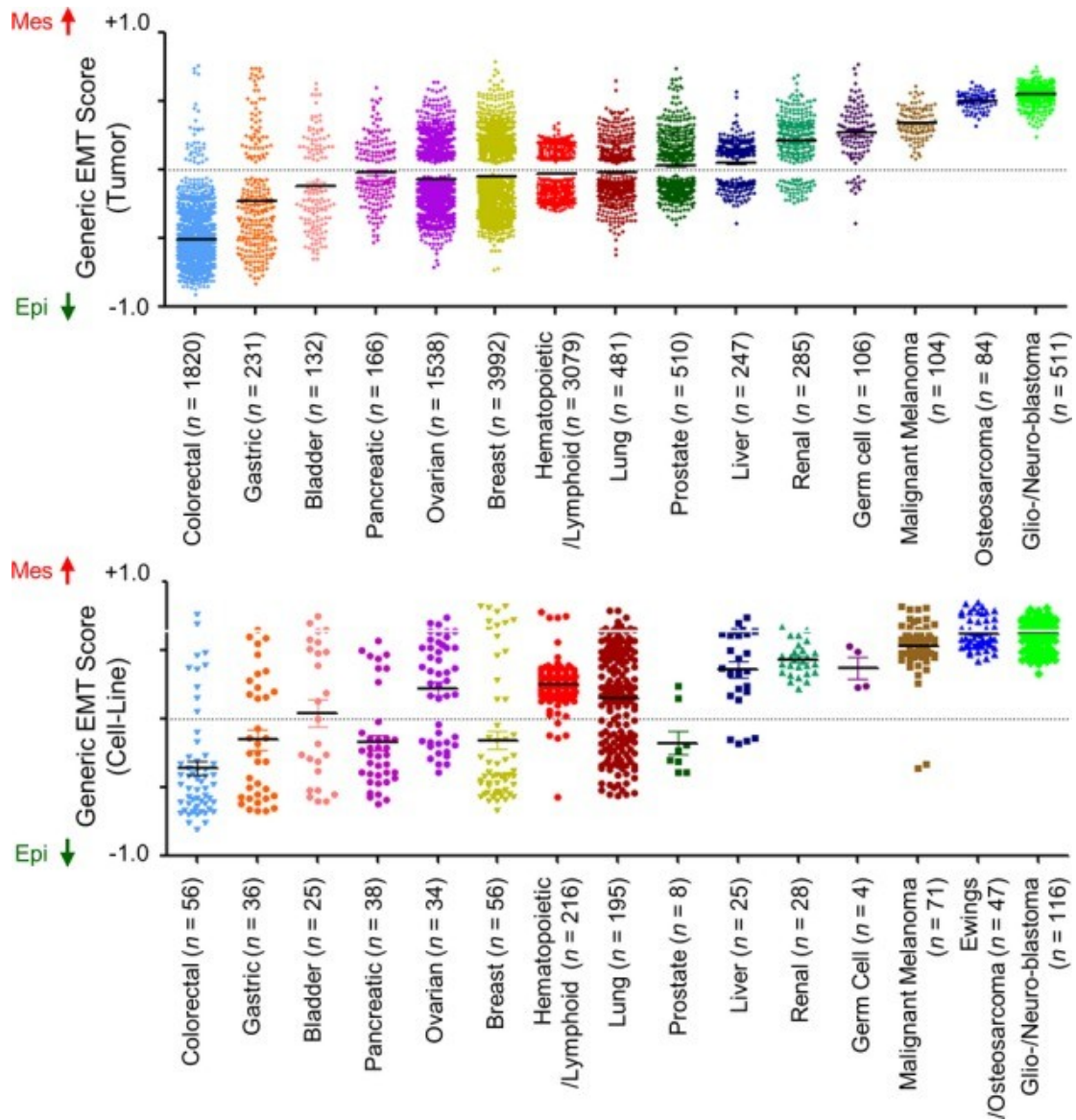
**Figure 10 | EMT scores in different cancers types**

Scatter plot of EMT scores (mean ± SEM;*y*-axis) of various cancers in clinical samples (upper panel) and cell lines (lower panel) sorted by cancer type and mean EMT score. EMT score nearer to +1.0 is more mesenchymal-like (Mes), whereas EMT score nearer to −1.0 is more epithelial-like (Epi). EMT scores of overlapping cell lines in Cancer Cell Line Encyclopedia (CCLE) and SANGER/COSMIC collections were averaged. Epithelial-mesenchymal transition spectrum quantification and its efficacy in deciphering survival and drug responses of cancer patients. Adapted from Zea Tan et al., 2014.

## 4.3. Cytoskeletal changes during the EMT

Cortical actin cytoskeleton reorganization is a key contributor to the EMT, guaranteeing dynamic cell motility. Mesenchymal cells are characterized by increased cell contractility and actin stress-fiber formation[273]. New actin-rich membranes, including lamellipodia (sheet-like membrane protrusions) and invadopodia (spike-like extensions), are formed to facilitate cell movement and act as sensory extensions. Invadopodia contribute a proteolytic function to extracellular-matrix degradation, thus aiding in invasion and migration. During the EMT, Rho GTPases regulate actin dynamics and negatively regulate the polarity and cell-cell junction complexes associated with polarity complexes. Rac1 and Cdc42 promote lamellipodia and filopodia formation, whereas RhoA supports actin stress-fiber formation. Rac1 promotes integrin clustering and microtubule polymerization at the leading edge of the cell[274] (Figure 11).
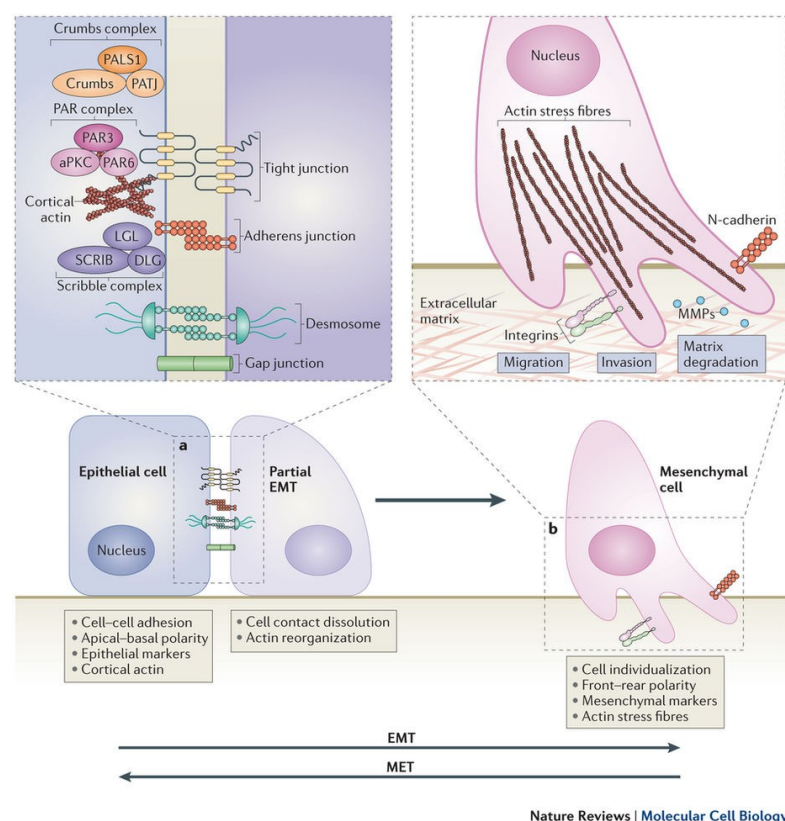


**Figure 11 | EMT process**

a) The first steps of EMT are the disassembly of epithelial cell–cell contacts that is, tight junctions, adherens junctions, desmosomes and gap junctions and the loss of cell polarity through the disruption of the Crumbs, PAR and Scribble complexes. The expression of epithelial genes is repressed, concomitantly with the activation of mesenchymal gene expression. b) Next, the epithelial actin architecture reorganizes, and cells acquire motility and invasive capacities by forming lamellipodia, filopodia and invadopodia, and by expressing matrix metalloproteinases

## 4.4. Gene expression and transcription factor regulation in EMT

The downregulation of E-cadherin and loss of the epithelial barrier function is controlled by the repression of genes encoding cell-junction proteins and the activation of genes generating mesenchymal proteins such as N-cadherin. The latter connects to the cytoskeleton and interacts with receptor tyrosine kinases (RTKs), comprising platelet-derived growth factor (PDGF) and fibroblast growth factor receptors (FGFRs). In mesenchymal cells, the overexpression of vimentin regulates the trafficking of organelles and membrane associated proteins, and it interacts with motor proteins that enable cell motility[275]. The main transcription factors involved in the EMT are SNAIL1/2, TWIST, and Zinc-finger E-box-binding 1 and 2. Other transcriptional factors such as Grainyhead-like-2 (GHL2), FOCX2, E47 (TFC3), KLF8, and PRRX1 are also implicated in inducing the EMT by targeting other genes and signaling pathways[276] (Figure 12).
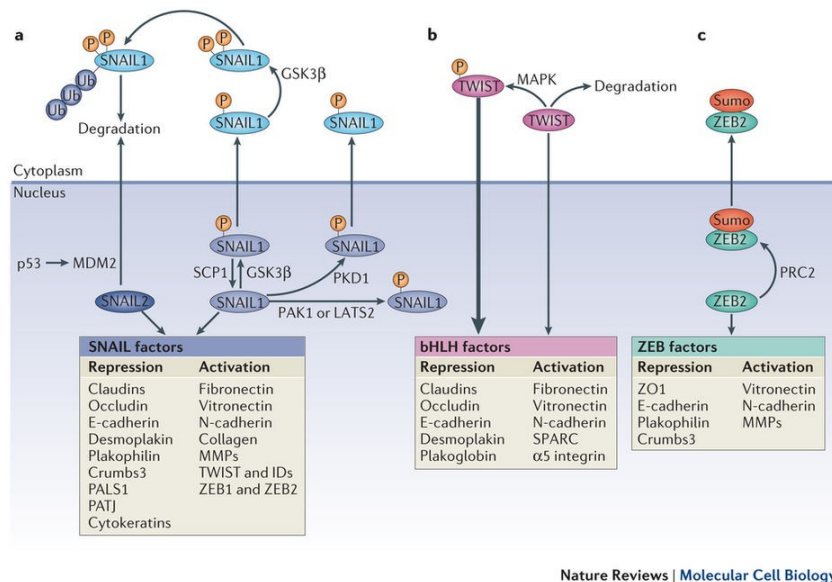


**Figure 12 | EMT transcription factors**

EMT is driven by SNAIL, ZEB and bHLH transcription factors that repress epithelial marker genes and activate genes associated with the mesenchymal phenotype. Post-translational modifications regulate their activities, subcellular localization and stability. a | GSK3β phosphorylates (P) SNAIL1 at two motifs; phosphorylation of the first motif facilitates the nuclear export of SNAIL1, and phosphorylation of the second motif enables the Ub-mediated degradation of SNAIL1. Phosphorylation of SNAIL1 by PKD1 also leads to its nuclear export. Conversely, phosphorylation of SNAIL1 by PAK1 or LATS2, or dephosphorylation of SNAIL1 by small C-terminal domain phosphatase1 (SCP1) promotes the nuclear retention of SNAIL1 and enhances its activity. SNAIL2 is degraded as a result of its p53-mediated recruitment to the p53–mouse double minute 2 (MDM2) complex. b | TWIST is phosphorylated by the MAPK p38, JNK and ERK, which protects it from degradation, and thus promotes its nuclear import and

functions. c | ZEB2 is sumoylated (Sumo) by Polycomb repressive complex 2 (PRC2) and subsequently exported from the nucleus, which reduces its activity as a transcription factor. Adapted from Lamouille et al., 2014.

### 4.4.1. SNAIL

SNAIL1, SNAIL2, and SNAIL3 (also termed SNAIL, SLUG, and SMUC, respectively) are the main transcription factors responsible for inducing the EMT by directly binding to the E-box DNA sequence in E-cadherin through their carboxy-terminal zinc-finger domains. Upon binding, SNAIL1 recruits polycomb-repressive complex 2 (PRC2). It contains the methyltransferase enhancer of zeste homologue 2 (EZH2); G9a, suppressor of variegation 3-9 homologue 1; the co-repressor SIN3A; histone deactylases 1, 2, and 3; and Lys-specific demethylase 1 (LSD1). All of these control histone repression, which is crucial to E-cadherin suppression, while the activation of another histone region contributes to the mesenchymal phenotype. The TGF-β and Wnt family proteins, Notch, and RTK-dependent growth factors activate SNAIL. The interaction of SNAILs is not limited to gene modification, as they also interact with other transcription factors such as SLAD3/4 complexes to cause the TGF-β-mediated repression of E-cadherin.

In addition, SNAIL1 phosphorylation at two Ser-rich motifs by glycogen synthase kinase-3β (GSK3β), p21 activated kinase 1 (PAK1), large tumor suppressor 2 (LATS2), or protein kinase D 1 (PKD1) inhibits its activity, while the Wnt, PI3K-AKT, Notch, and NF-κB pathways disturb GSK3β, thus enhancing SNAIL1 activity. For SNAIL2, p53 is responsible for its degradation and inhibiting the EMT. Blocking SNAIL2 leads to the inhibition and spread of of TNBC[277]. In BC cells, SNAIL promotes the EMT via the activation of nuclear ERK2. The overexpression of SNAIL in the epithelial MCF-7 BC cell line induces the EMT, increases cell migration, invasion, and tumorigenicity, and reduces cell adhesion.

### 4.4.2. bHLH

Homodimeric and heterodimeric basic helix-loop-helix (bHLH) transcription factors are a major group comprising E12, E47, TWIST1/2, and inhibitor of differentiation (ID). TWIST expression has a role similar to that of SNAIL in suppressing epithelial gene and E-cadherin expression and in activating mesenchymal gene and N-cadherin expression by the recruitment of SETD8, which mediates histone mono-methylation. TWIST represses E-cadherin and recruits B lymphoma Mo-MLV insertion region 1 homologue (BMI1), a component of PRC1. Interestingly, the hypoxic TME affects and activates TWIST via the

activation of HIF1α[278]. The stability of TWIST is regulated by its MAPK-dependent phosphorylation at Ser68[279].

### 4.4.3. ZEB

ZEB1/2-dependent repression involves recruitment of the co-repressor C terminal-binding protein (CTBP), binding to E-boxes, or recruitment of the SWI/SNF (switch/sucrose non-fermentable) chromatin remodeling protein BRG1. The post-sumoylation of ZEB2 by PRC2 can prevent its association with CTBP. ZEB1 has a dual effect, as it can switch to activating transcription factor if it interacts with the transcriptional co-activator p300/CBP-associated factor (PCAF). For the most part, ZEB expression tracks SNAIL and TWIST activation. Its expression is also activated by TGF-β and Wnt proteins and RAS-MAPK signaling[262,280]. An extensive network of microRNAs (miRs), especially miR-200 and miR-205, have been shown to stabilize the epithelial state and inhibit induction of the EMT by directly targeting ZEB1/2. The miR-200 is lost in invasive BC cells, and therefore ZEB1/2 is highly abundant[281]. MiR-106b-25 induces the EMT in BC cells by suppressing SMAD7 to increase TGF-β signaling[281].

In addition to the main transcription factors, several secondary factors are implicated. GRHL2 transcription factor sustains E-cadherin gene expression and protects the epithelial state from transforming to a mesenchymal one[282]. Forkhead box (FOX), GATA, and SRY box (SOX) are transcription factors that interact with SNAIL, TWIST, and ZEB to establish and stabilize the EMT.

The mesenchymal phenotype is induced by TGF-β through SMAD-mediated or non-SMAD-mediated signaling. TβRI and TβRII activate SMAD2 and 3 as well as SMAD4, which translocates to the nucleus to regulate transcription factors. SMAD also affects epithelial splicing-regulatory proteins and miRs that repress epithelial proteins. Non-SMAD-mediated signaling acts through the activation of PI3K/AKT/mammalian TOR complex (mTORC1) signaling. Additionally, TGF-β increases cell-cell junction dissociation and induces cytoskeletalchanges[256,283,284].

### 4.5. Mesenchymal cell resistance to T cells and NK cells

The EMT is defined as a tumor-related immune evasion and cancer cell intrinsic mechanism, as tumor cells undergo the transition to a mesenchymal phenotype not only to invade other sites, but also to resist the TME and therapies. The most well-established model for studying the correlation between the EMT and tumor immune evasion is the human mammary carcinoma model MCF-7. MCF-7 cell lines begin as epithelial cells

with an abundant expression of E-cadherin and no vimentin or N-cadherin expression. The EMT can be initiated in MCF-7 cells by inducing stable SNAIL expression or via prolonged exposure to TNF-α. The MCF-7 cell line's EMT score places it in the epithelial state, while the derivatives display a mesenchymal state. The resulting cells are mesenchymal, with high vimentin and E-cadherin expression and a total loss of E-cadherin. Additionally, the EMTed MCF-7 cells lose their cell-cell junction with a spindle-like shape and acquire the invasive phenotype[285-288].

Mesenchymal cell resistance to CTL-mediated cell lysis can engage many pathways. Akalay et al. showed that EMTed MCF-7 cell lines are resistant to CTL-mediated cell lysis. This resistance can be linked to the activation of autophagy[287] Interestingly, EMTed MCF-7 cells (cells after silencing WISP2, or Wnt-inducible signaling pathway protein 2) are similarly resistant to CTLs. The cross-talk between Wnt and TGF-β signaling promotes the reversion of CTL resistance in MCF-7-shWISP2 cells after treatment with TGF-β blockers[289]. Moreover, PD-L1 expression is high in MCF-7-derived cells compared to the parental cell line.

In the non-metastatic lung adenocarcinoma model IGR-Heu, a correlation has been observed between the hypoxic environment and the EMT spectrum. Remarkably, cells differed in their ability to shift to a mesenchymal phenotype under hypoxic conditions, and it was evident that the cells that underwent the EMT were more resistant to CTL-mediated cell lysis. The loss of E-cadherin in mesenchymal IGR-Heu explains the resistance, as CTL function relies on CD103 (αEβ7 integrin), an E-cadherin ligand[290,291].

Mesenchymal NSCLC tumor sub-clones show a significant resistance to NK cell-mediated cell lysis (compared with epithelial clones) due to defective IS signaling. A recent study suggested that high levels of the EMT-related factor Brachyury increases resistance to CTLs, NK cells, and lymphokine-activated killer cells. Nevertheless, SNAIL overexpression in colorectal cancer cells and the secretion of TGF-β made the cells more susceptible to NK cells due to an increase in the expression of MICA/B and ULBP1-3, NKG2D ligands[292].

## 4.6. EMT implication in resistance mechanisms

*In vitro* and *in vivo* studies showed that induction of the EMT is associated with stemness pathways and resistance to chemotherapy and radiotherapy. It has been established that the latter therapies can activate TGF-β, NF-κB, Wnt, FGF, and EGF/HER2 pathways, and thus stimulate EMT-transcription factors. From another aspect, miR-200/ZEB1 axis downregulation mediates the docetaxel resistance of prostate cancer[293]. MiR-21 has been implicated in the EMT and in trastuzumab and paxlitaxel or doxorubicin resistance in HER2^{+} BC cells[294,295]. Chemotherapy resistance occurs mainly through degradation of the drug by increasing the efflux of hydrophobic drugs regulated by the ATP-binding cassette (ABC). EMT cells have been shown to bind to the E-box in the ABC. Radiation therapy, as well as hypoxia, induces the generation of ROS that play a role in initiating the EMT[296].

TGF-β, the main inducer of the EMT, is known to have a negative effect on adaptive and innate immune cells. It can impair their maturation, differentiation, cytotoxicity, or ligand expression. In contrast, it also induces inhibitory Treg activation. Thus, TGF-β blockers can be a therapeutic strategy for immunotherapy, and they are now under clinical study[297]. Moreover, PD-L1 expression is related to the mesenchymal state via the miR-200/ZEB axis[298,299]. PD-L2, PD1, TIM3, LAG3, and CTLA-4 expression are also correlated with the EMT state[238]. SNAIL overexpression in mouse melanoma B16F10 cells induces an EMT associated with the impairment of DC maturation, less T-cell infiltration, and enhanced Treg suppressive functions. In an MMTV-PyMT mouse model for BC, SNAIL-expressing cells showed high Treg infiltration compared to control cells. The same results were obtained from a study on hepatocellular carcinoma wherein hypoxia-induced EMT cells had an immunosuppressive TME accompanied by defective T-cell proliferation and increased Treg-cell infiltration[300]. Altogether, these studies highlight the implication that the EMT process is involved in cancer-therapy resistance and immune editing[272]. Erlotinib, an EGFR inhibitor, and fulvestrant, an ER antagonist, may be efficient at improving the immune cell-mediated cell lysis of lung cancer cells by targeting mesenchymal cells[301].

# 5. Autophagy

Cancer cells respond to the hypoxic TME by activating autophagy to increase their anaerobic-dependent metabolism. Autophagy (also known as macroautophagy) is a highly conserved cytoplasmic degradation system and catabolic process. It is based on the formation of autophagosomes, the double-membrane vesicles responsible for surrounding cellular debris such as organelles and proteins. Autophagy has different cellular functions such as adaptation to starvation, protein and organelle degradation, cell death, anti-aging, development, and tumorsuppression[302].

The discovery of the autophagy process began in 1963 in Christian de Duve's group. Soon after, the anti-malarial drug chloroquine (CQ) proved to have anti-tumor activity. It took from then until 1998 to discover that CQ inhibits the autophagic process. Since then, a large number of findings have highlighted the biological functions of autophagy within healthy and aberrant cells. The Nobel prize for physiology and medicine in 2016 was awarded to Yoshinori Ohsumi for his contribution in shaping our knowledge of autophagy[303]. The autophagy process was known to be a key inhibitor for tumors, but studies have now shown that an increase in autophagic flux promotes tumor growth, resistance, and survival. The important question in cancer therapy is whether the activation or inhibition of autophagy should be the objective when targeting tumors. Understanding the implications of autophagy and related pathways in tumor cells has become a major area of interest for researchers in recent years.

## 5.1. Types of autophagy

Three different types of autophagy have been described thus far, including macroautophagy (here referred to as autophagy), microautophagy, and chaperone-mediated autophagy (CMA). Microautophagy is a process by which lysosomes degrade cytoplasmic components that enter through a metabolite transporter or a deformation in the lysosomal membrane. In contrast to both micro- and macro-autophagy, which non-specifically degrade cellular components, CMA is a specific autophagy in which the engulfed proteins are translocated to the lysosomal membrane via cytosolic chaperones[302]. The CMA process destroys proteins, transcription factors, glycolytic enzymes, and proteasome subunits. During starvation, CMA is responsible for oxidized-protein

elimination and amino-acid delivery. The cytosolic substrate includes the KFERQ-related motif, which is recognized by the heat shock cognate of Hsp70, a cytosolic chaperone. Lysosome-associated membrane protein 2A (LAMP-2A) translocates the complex throughout the lysosomal membrane[304] (Figure 13).

The next section will focus on and provide an overview of the main autophagic processes and signaling pathways in cancer and their implication for tumor evasion from the immune system.
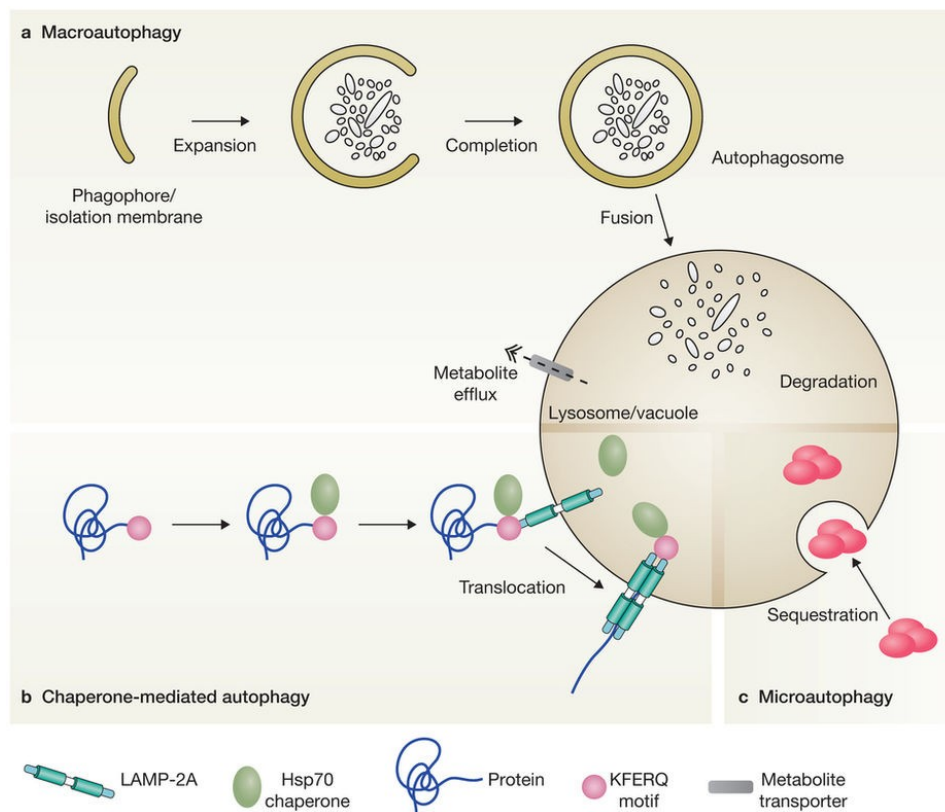


**Figure 13 | Types of autophagy**

a) Macroautophagy is characterized by the sequestration of structures targeted for destruction into double-membrane vesicles called autophagosomes. Complete autophagosomes first fuse with endosomes before finally exposing their content to the hydrolytic interior of lysosomes. The resulting metabolites are transported into the cytoplasm and used either for the synthesis of new macromolecules or as a source of energy. b) During chaperone-mediated autophagy, proteins carrying the pentapeptide KFERQ-like sequence are recognized by the Hsc70 chaperone, which then associates with the integral lysosome membrane protein LAMP-2A, triggering its oligomerization. This event leads the translocation of the bound protein into the lysosome interior through a process that requires Hsc70. c) Microautophagy entails the recruitment of

targeted components in proximity with the lysosomal membrane, which subsequently invaginates and pinches off. Adapted from Boya et al., 2013.

## 5.2. Functions of autophagy

Autophagy is considered a survival mechanism used by cells under specific conditions. A principal role of the autophagic process is its contribution to basal cellular and tissue homeostasis by the elimination of cytoplasmic contents, including proteins and organelles. The best evidence for this function is the accumulation of aberrant molecules such as ubiquitinated proteins and deformed organelles in autophagy-deficient neurons and hepatocytes. Autophagy is also implicated in lipophagy for regulating lipid metabolism[302]. Starvation-induced autophagy is an essential process to ensure cell survival. Blood glucose maintenance is a result of the anabolism and catabolism of amino acids released by liver autophagosomes. Moreover, autophagy-derived amino acids are a source of energy through the tricarboxylic acid cycle, as well as a substrate for protein synthesis[305] [306]. Furthermore, autophagy deficiency causes cardiac dysfunction and cardiomyopathy. Hypoxia-induced autophagy occurs in an ischemic-myocardium model[307].

The contribution of autophagy to protecting host cells is crucial, as autophagosomes can degrade intracellular bacteria and viruses. Autophagy is also implicated in the suppression of inflammation and downregulation of interferons and pro-inflammatory cytokines (e.g., IL-18)[308,309]. Furthermore, autophagosomes fuse with MHC class II loading compartments. The high expression of autophagy in MHC Class II-positive cells leads to the delivery of endogenous cytosolic proteins to MHC class II molecules and therefore contributes to CD4+ T-cell stimulation. Evidence for this function includes the fusion between ATG8/LC3 and influenza matrix protein 1, which leads to enhanced MHC class II presentation to CD4+ T cell[310].

Autophagosomes circulate randomly in the cytoplasm along microtubules, but their movement is influenced by the MTOC where lysosomes are concentrated. Subsequently, they fuse with the lysosomes to create the autophagolysosomes responsible for degrading their components. The process is controlled through intracellular signaling and extracellular induction and is divided into five distinct stages: vesicle initiation, vesicle nucleation, vesicle expansion, vesicle closure and fusion with lysosomes, and the degradation stage [302]. Autophagy-related genes (ATGs) control all these stages (Figure 14).

Diverse signals control the dynamics of the autophagic process and extra- or intracellular signaling initiates the first step of autophagosome formation. Cell starvation, hypoxia, and insulin/growth factor signals mediate a decrease in glucose transport, the end of mTOR-dependent inhibition, and Jun N-terminal kinase (JNK) activation. Energy loss can also induce autophagy by the activation of AMP kinase (AMPK). Calcium, ROS, cyclic AMP, inositol triphosphate, and calpain receptors control the process. Cell death can be associated with an increase in autophagosomes as death receptors such as TRAIL can induce autophagic cell death[302].

The first step in autophagosome formation is the constitution of the phagophore. Membrane nucleation and phagophore formation begin with activation of the ATG1 complex, which includes Unc-51-like kinase 1 or 2 (ULK1/2), ATG13, ATG101, ATG9A, and FIP200 (focal adhesion kinase (FAK)-family interacting protein of 200 kDa). Further, the phosphorylation of Beclin-1 by ULK1 supports the class III PI3K complex synthesis of PIP3 and facilitates its translocation to the membrane. The class III PI3K complex contains Vps34, ATG14, UV radiation resistance-associated gene protein (UVRAG or p63), and BECN1-regulated autophagy protein 1 (AMBRA1)[306].

In 1998, Beclin-1 (Bcl-2 interacting myosin-like coiled-coil protein; or ATG6), a member of the ATG family, was found to interact with the Bcl-2 protein. It is highly conserved in eukaryotes and implicated in additional cellular processes such as phagocytosis, trafficking, and the control of cytokinesis. Beclin-1 is a 60 kDa protein containing three important domains: the coiled-coil domain (CCD), the evolutionarily conserved domain (ECD), and a Bcl-2 homology domain[311]. The ECD is necessary for binding to the class III PIK3 complex. Together, CCD and BH3 form the large homo-oligomer responsible for the recruitment of ATGs. Bcl-2 can bind to the BH3 domain, and therefore constrains Beclin-1-dependent autophagy at the endoplasmic reticulum and mitochondria. Starvation acts to dissociate this interaction and activates Beclin-1 via Bcl-2 phosphorylation by JNK1[311-313].

Membrane elongation is controlled by two ubiquitination-like reactions. First, ATG7 and ATG10 conjugate ATG5 with ATG12. The membrane continues to expand due to the non-covalent conjugation of the ATG5-ATG12 complex with ATG16L1. The second reaction involves an association of the ATG8 family with the lipid phosphatidylethanolamine (PE). The ATG8 family comprises the microtubule associated protein 1A/1B- light chain 3 (LC3), gamma-aminobutyric acid receptor-associated protein (GABARAP), and GATE-16. Moreover, ATG4B (associated with ATG7 and ATG3)

conjugates cytoplasmic LC3I and PE to form lapidated LC3II, thus elongating the doubled membrane. Complete phagophore elongation results in the formation of a mature autophagosome[314]. Immediately after the autophagosome closes, the SNARE protein syntaxin 17 (STX17) is recruited to the LC3$^+$/ATG$^-$ membrane. The STX17$^+$ membrane then fuses with the lysosomes (LAMP1/2$^+$) to form the autophagolysosomes that degrade cargo components with hydrolases. The adaptor protein sequestosome 1/P62 is used as an autophagic-flux marker because it is degraded after vesicle recycling[314].

LC3 is a 17 kDa soluble protein abundant in mammalian tissues and cells. Upon LC3 conjugation with PE, LC3II is formed and localized on the inner and outer membrane of the autophagosomes. LC3II is often used as a marker to measure autophagic flux, as it remains associated with the autophagosomes until they fuse with lysosomes. It is the most used marker because the amount of LC3II represents the number of mature autophagososmes[315]. Nutrient starvation significantly increases the number of autophagosomes and correspondingly the quantity of LC3II. In some cases, an increased amount of LC3II could denote an inhibition of autophagy deprivation and autophagosome accumulation. Immunoblotting of LC3 results in LC3I and II bands. The LC3I band is not reliable for quantifying autophagy; comparing the amount of LC3II to a housekeeping protein is the best method. A decrease in the amount of p62 that binds to LC3 is a confirmation of autophagic flux as p62 gets degraded along with LC3. A precise quantification requires the addition of bafilomycin A, a lysosome inhibitor, or CQ, an inhibitor of fusion between the autophagosomes and lysosomes. A comparison between LC3II and p62 in the presence and absence of lysosome targeting provides the ideal representation of autophagic flux in a cell[313,316].
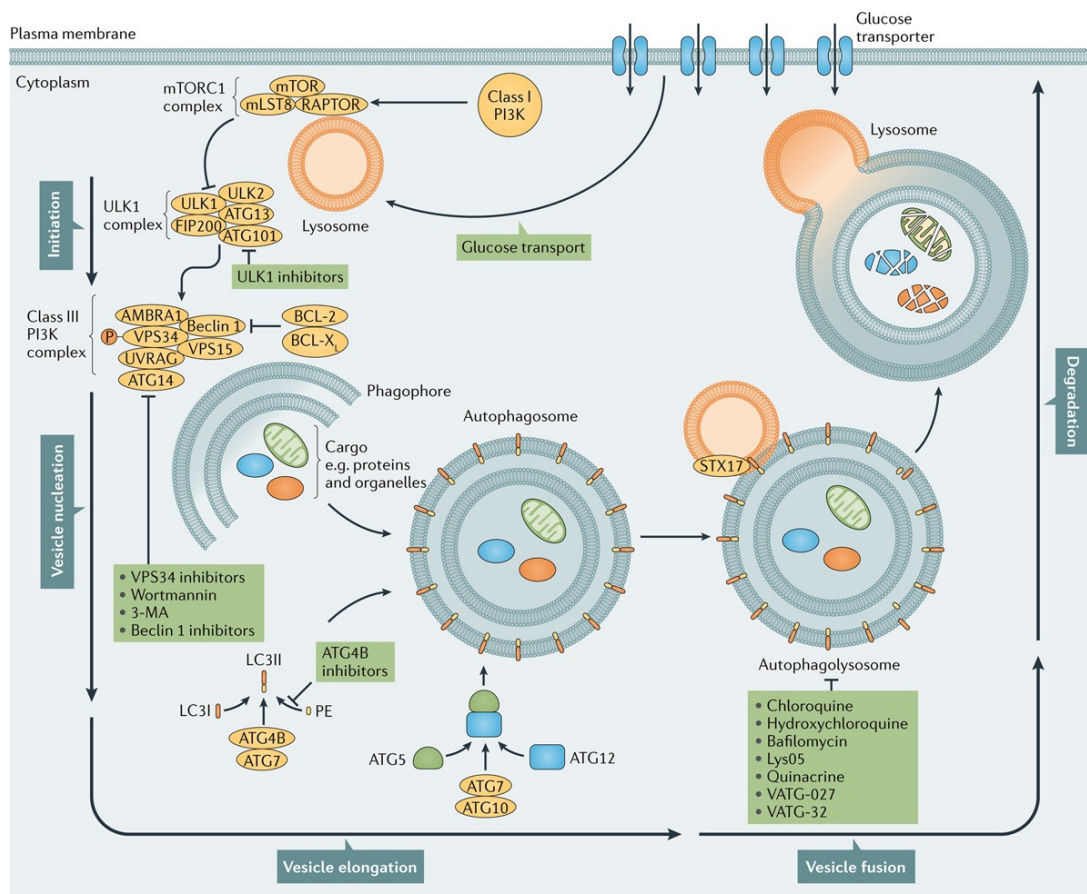
**Figure 14 | Stages of autophagy**

The process of autophagy is divided into five distinct stages: initiation, vesicle nucleation, vesicle elongation, vesicle fusion and cargo degradation. Adapted from Mulcahy Levy et al., 2017.

## 5.3. The autophagy link to the cytoskeleton

The interaction between autophagy and the cytoskeleton is still not well studied. Few reports describe the implication of the actin cytoskeleton in the biogenesis of autophagosomes from the ER or cargo transport. Actomyosin plays a role in integrating different cellular debris types into the growing cargo before detachment from the ER membrane[317]. The first evidence implicating the actin cytoskeleton in the autophagy process was the failure of autophagosome formation in cells treated with actin-disrupting drugs such as cytochalasin D and latrunculin B[318]. Other studies further established the colocalization of actin filaments and autophagy markers during the formation and transport of autophagosomes[319] (Figure 15).

The first actin element found to interfere with autophagosome formation was the nucleation factor ARP2/3. Pharmacological or genetic targeting of ARP2/3 produces decreased LC3-II and autophagosome levels and inhibits the formation of omegasomes,

an early structural stage of phagophors[320]. Furthermore, ARP2/3 is localized to the sides of autophagosomes at the points of actin comet tails, which are responsible for transporting autophagosomes after detachment from the ER[321]. ARP2/3-dependent actin filaments are important in phagophore formation, as are cofilin and CapZ[322]. Cortactin, which stabilizes actin branches formed by the ARP2/3 complex, is recruited to the autophagosome and lysosome fusion lysosomes[323].

Besides the evident role of ARP2/3, its activator also seems to play a crucial role in the autophagic process. The WAS protein family homologue (WASH) complex has been found to co-localize with phagosome markers, and its inhibition leads to autophagy being inhibited due to Beclin-1 suppression and defective ATG9 transportation[324]. The nucleation-promoting factors JMY (junction-mediating and regulatory protein) and WHAMM (WAS protein homolog associated with actin, Golgi membranes, and microtubules) are involved in the early stages of autophagosome formation and maturation[321].

The Rho-family GTPases control a wide variety of actin-related processes, but their precise role in autophagy is still not clear. RhoA has been shown to have a stimulatory effect on autophagosomes via the regulation of Rho-associated protein kinase (ROCK), while Rac depletion appears to enhance the autophagic pathway[325]. Recent data have shown that Cdc42 is as an important regulator of the autophagy process, as knocking it down produces reductions in LC3-I and LC3-II levels. These results suggest a crucial role for Cdc42 and its downstream proteins in the autophagic pathway.
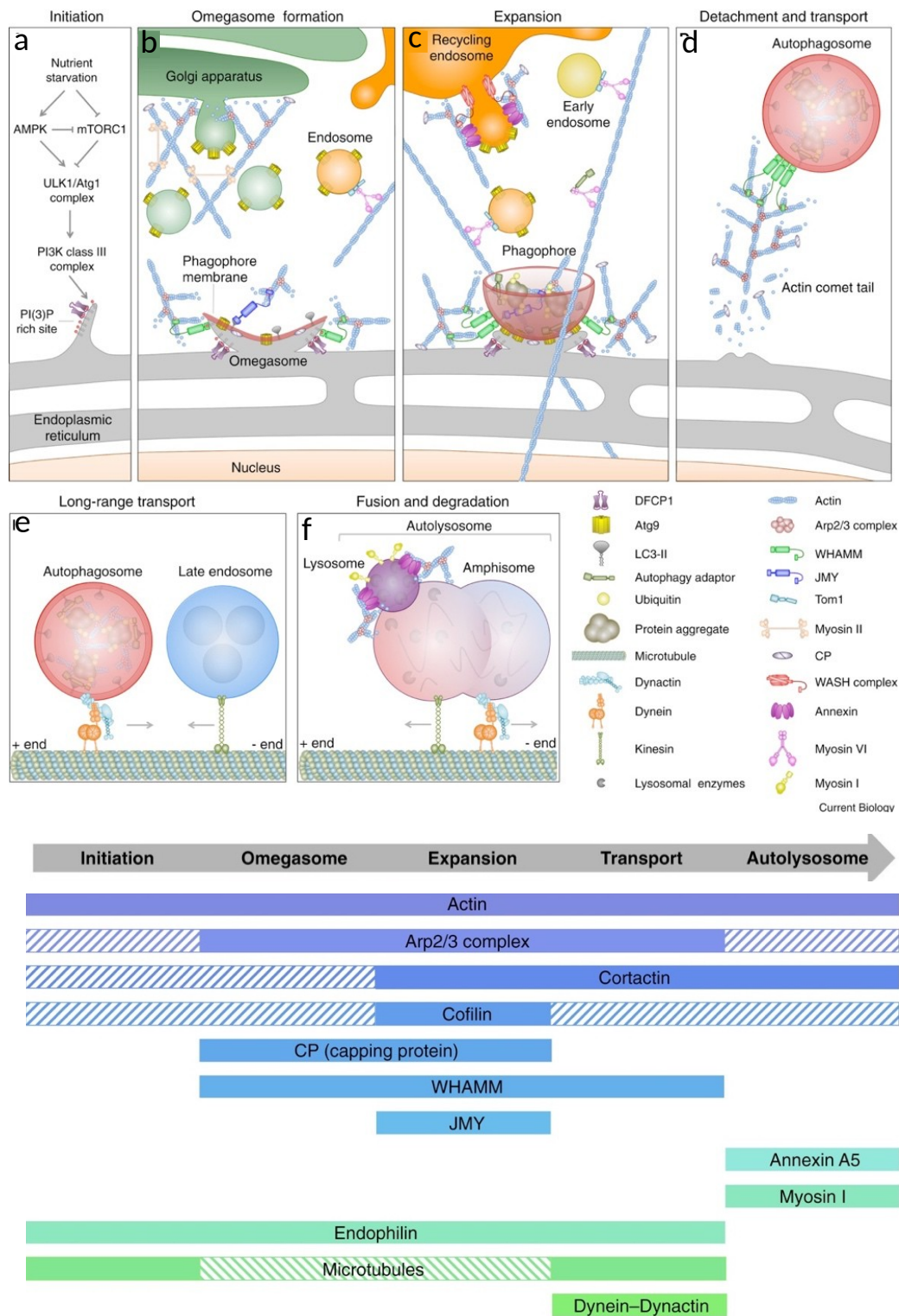
**Figure 15 | The cytoskeleton-autophagy connection**

Implication of the actin cytoskeleton in the overall autophagy process starting from (a) initiation, (b) omegasome formation, (c) expansion, (d-e) transport, and (f) ending with fusion with lysosomes and degradation.

Timeline showing the arrival and departure of cytoskeleton assembly factors. Solid bars indicate the timing of appearance of autophagy and cytoskeletal proteins during the various stages of autophagy (gray arrow). Striped bars indicate the predicted time of arrival based on the known functions of proteins for which direct evidence is still lacking. Adapted from Kast et al., 2017.

## 5.4. The role of autophagy in cancer immune evasion

Studies in recent years have focused on the implications of the autophagic process in various cancer types. However, the process can either inhibit or promote tumorigenesis, suggesting its role is context dependent. Some results have shown that autophagy has an important anti-tumor function and influences the initiation and progression of tumors[304]. In a large number of cases, patients with ovarian, breast, and prostate cancers with aggressive phenotypes have had monoallelic disruptions of BECN1 on chromosome 17q21. Indeed, many autophagy-associated protein deficiencies in mice are associated with tumorigenesis, while the deletion of Beclin 1 results in embryonic lethality[311]. Moreover, cytoplasmic LC3 has been found to be elevated in tumor tissues after chemotherapy.

It is, however, well established that autophagy is highly associated with the survival of tumor cells under stress related to hypoxia and inadequate angiogenesis. Tumor cells depend on autophagy due to deficiencies in the TME and the resulting increased metabolic demands. Remarkably, there is a logical association between autophagy and apoptosis given that one role of autophagy is in protecting cells from undergoing programmed cell death. In a recent study on BC cell lines, shRNAs targeting more than 100 autophagy regulators were applied to detect the level of survival and dependence on the autophagic process. The results showed that some cell lines experienced no global effects from inhibiting autophagy, while other cell lines were dependent on it. These outcomes were related to STAT3-mediated autophagy dependence[326].

Autophagy has been implicated in the resistance of several cancer types such as NSCLC, bladder, thyroid, melanoma, and BRAF-mutated central nervous system cancers. A recent study in B16 mouse-melanoma cells and the 4T1 human mammary carcinoma cell mouse model showed that T-cell responses to autophagy-competent and autophagy-deficient tumors (either genetic deletion of autophagy genes or CQ treatment) are similar[327]. Moreover, another study showed an enhanced immune response against tumors upon autophagy activation[328]. Countering the studies that showed no effect from autophagy inhibition, other studies have reported that autophagy inhibition resulted in an increase in immune anti-tumor activity and tumor regression in breast and melanoma cancer models in mice[288,329]. One struggle in targeting autophagy during tumor treatment is its non-specificity to tumor cells. General autophagy inhibition by gene deletion shows high toxicity due to the disruption to homeostasis and neuronal toxicity. However,

prolonged treatment with the lysosomal autophagy inhibitors CQ and HCQ have shown no serious adverse effects[330].

It has been established that targeting autophagy in tumor cells under hypoxia reestablishes CTL-mediated cell killing. Autophagy and HIF-$\alpha$ control induction and stabilize the STAT3-survival pathway [331]. Interestingly, hypoxia impairs BC cells' susceptibility to NK cell-mediated cell lysis by activating the autophagic process responsible for GzB degradation. Targeting Beclin 1 restores GzB levels in target cells and increases NK cell-mediated cell death[288].

Additionally, targeting Beclin 1 in melanoma cells inhibits their growth via activated NK-cell infiltration into the tumor. It has been established that autophagy-defective cells release CCL5 cytokines into the TME upon MAPK8/JNK-JUN/c-Jun signaling pathway activation. Increased CCL5 overexpression and release leads to the high NK-cell infiltration associated with overall survival in melanoma patients with high CCL5 level[332]. Overall, targeting autophagy in tumors promises to be a novel therapeutic strategy by enhancing the immune response, disrupting the immunosuppressive TME, and supporting anti-tumor therapies.

# 6. The actin cytoskeleton

Cellular functions, including cell division, migration, and shape, are regulated by a dynamic cytoskeleton. The three filament networks (actin, microtubules and intermediate filaments) that constitute the cellular skeleton are present in all types of cells, from plants to prokaryotes and eukaryotes. Contrary to older research that described a rigid cytoskeleton, recent decades have shown the cytoskeleton to be a dynamic structure with many essential biological functions. Along with its role in shaping the cell, the cytoskeleton participates in cell migration, division, intracellular trafficking, and many diverse processes.

Since the main goal of my PhD thesis is to reveal how actin cytoskeleton dynamics in tumor cells control immune evasion, this chapter will provide an overview of the actin cytoskeleton and its regulation.

## 6.1. A historical overview of actin

This section will highlight key breakthroughs made since the discovery of the actin protein. The story behind the discovery of actin begins in 1864 with the discovery of myosin by Wilhem Kuhne. Later, the British physiologist William Dobinson Halliburton discovered a new protein extracted from muscle cells and called it "myosin-ferment". This finding led to no further investigations until 1942, when Albert Szent-Gyorgyi and Bruno Ferenc Straub showed that myosin was composed of two proteins. The first protein, myosin A, has a low viscosity and is extracted after 20 min of exposing muscle tissue to a high salt concentration, while the second protein, myosin B, results from overnight extraction. The addition of ATP led to a reduction in the viscosity of myosin A, but not B, and to a shortening of the myosin B threads, but not those of myosin A. After purification, Straub identified the protein responsible for myosin fiber contraction and called it actin. He also showed that actin exists in two forms: globular actin (G-actin) and actin filament (AF). Moreover, adenosine 5′-triphosphate (ATP) was shown to be a functional part of G-actin that is hydrolyzed to adenosine 5′-diphosphate (ADP) when polymerized into filaments.

In 1954, two concurrent studies revealed that the force between actin and myosin is responsible for filament sliding and generating muscle fiber movement. Studies continued to uncover various elements of the cytoskeleton with the development of live imaging.

However, in 1969, a surprise awaited when actin was observed in cells other than muscle cells. Later, in 1974, Lazarides and Weber were the first to visualize the spatial arrangement of the actin cytoskeleton[333] (Figure 16).

Typical electron microscopy and immunofluorescence techniques prevented the observation of actin dynamics. It was the revolution in reactive fluorescent dyes that opened up the study of actin dynamics. In 1978, Taylor and Wang first saw the actin cytoskeleton *in vivo* after injecting 5′-iodoacetamido-fluorescein (IAF)-labeled actin into living cells[334]. Discoveries continued to uncover many specific actin components and functions such as focal adhesion, microtubule dynamics, and motor proteins. The first atomic model of AFs was produced by Holmes in 1990 [335]. By the early 1990s, signaling pathways governing the regulation of the actin cytoskeleton were discovered by Paterson. Rho GTPases were shown to be key components in the signal transduction connecting extracellular signals to the actin structures. Rho, Rac, and Cdc42 were shown to control cytoskeletal responses, and they are complicatedly inseparable as they guide one another.
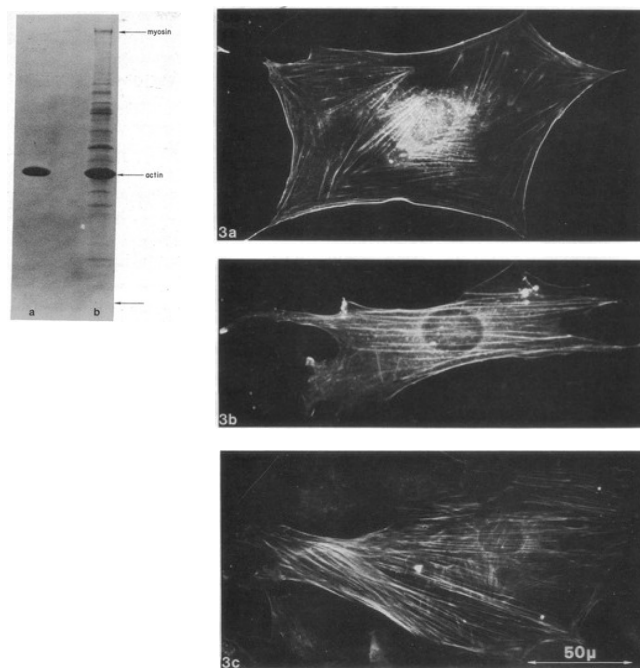


**Figure 16 | First visualization of actin**

SDS gel electrophoresis of actin. SDS polyacrylamide slab gel electrophoresis was performed in 12.5% slabs. a) Highly purified chicken muscle actin (10μg). b) A 30% ammonium sulfate cut of a low-salt extract from an ethanol powder of mouse fibroblasts (15μg). A small amount of myosin copurifies with actin under the extraction conditions used. The arrow at the bottom of the figure shows the dye front of the gel.
Indirect immunofluorescence of actin antibody with primary chick embryomyoblasts. The nuclear staining seen in this figure seems to be nonspecific. Purification of the antibody used in this experiment by 50%

ammonium sulfate fractionation removes the nuclear fluorescence. Adapted from Lazarides and Weber, 1974.

## 6.2. Structure of the actin molecule

The actin monomer is a 43 kDa globular protein with dimensions of 55 Å × 55 Å × 35 Å. It is the most abundant protein in most eukaryotic cells and the most conserved, with 90% identity between yeast, plants, and mammals. Studies in recent decades have also shown actin homologues in archae and bacteria (15% identity). Three main actin isoforms are described: the α-isoforms of cardiac, skeletal, and smooth muscles and the β- and γ-isoforms of muscle and non-muscle cells, respectively. Each isoform has a different function attributed to differences in a few amino acids at the N-terminus. α-Actin is implicated in contractile structures and functions, while β- and γ-actin provide mechanical support to maintain cell shape via actin polymerization in addition to their involvement in cell movement and intracellular transport.

Since the first atomic structure was revealed in 1990, eighty crystal structures have been reported for G-actin by co-crystallizing it with DNase I or profilin. An actin polypeptide is composed of 375 residues folded together into a flat protein. G-actin is composed of two primary domains (α and β-domains, also called the small and large domains) that are separated by two clefts. Four subdomains have been identified. Subdomains 1 and 3 are small and structurally related, whereas subdomains 2 and 4 are large and insert into subdomains 1 and 3, respectively. The upper cleft binds the nucleotide (ATP or ADP) and is associated with divalent cations ($Mg^{+2}$ or $Ca^{+2}$), while the lower cleft mediates contact between the subunits in a filament and is a major binding site for ADP. The strength of subunit interactions and the binding affinity of actin-binding proteins (ABPs) are controlled by nucleotide-dependent conformational changes, which essentially relies on interactions between the two clefts. Remarkably, monomeric actin exhibits different conformations when bound to ATP and ADP.

The actin cytoskeleton is composed of a network of assembled double-stranded AFs with different architectural types. The first organization is the cell cortex, a cross-linked network that creates a thin layer, which is important for cell shape and motility. Lamellipodia, localized at the front of the cell as branched and cross-linked networks, are implicated in cell motility and movement. Another structure is the aligned and parallel bundles of filopodia, which are thin protrusions at the front of the cell and important for directional cell migration and adhesion. The fourth architectural form is stress fibers,

composed of an anti-parallel contractile 3D network that is abundant throughout the body of the cell and provides force for many cellular processes (Figure 17).

Monomeric G-actin is gathered in a highly regulated process by numerous ABPs to form an AF. Each filament is approximately 7 to 10 nm long with a right-handed helical twist, with each twist composed of 13 subunits. Remarkably, the reconstruction of electron micrographs of frozen-hydrated filaments provided the best structure of an AF. G-actin differs from AFs by a relative rotation of the two major domains by about 20°. Additionally, the conformation of the DNase-I binding loop in S2 gives F-actin an open-loop conformation[336].
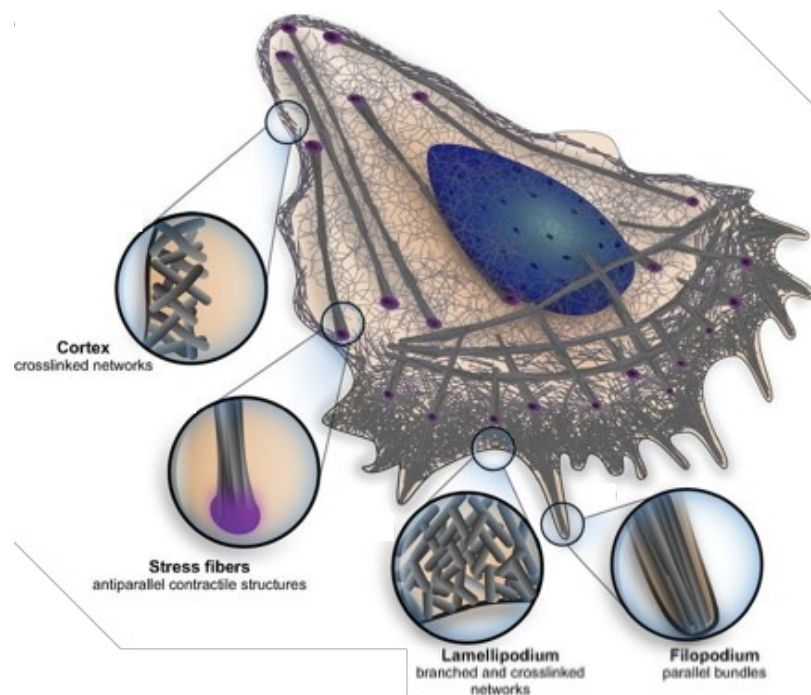


**Figure 17 | Overlay of actin architecture and mechanics in the moving cell**

Schematic representation of the cell with the different architectures indicated: the cell cortex; an example of a contractile fiber, the stress fiber; the lamellpodium; and filopodia. The zoom regions highlight architectural specificities of different regions of the cell. Blanchoin et al., 2014.

## 6.3. Principles of actin polymerization

Actin monomers continuously cycle through the process of polymerization and de-polymerization. The polymerization process happens spontaneously under physiological salt conditions (*in vitro*) in the presence of either monovalent or divalent cations. Importantly, the process relies strongly on the concentration of G-actin. Two steps shape the polymerization process: a rate-limiting step defined by the nucleation of short

oligomers and the elongation step. Polymerization begins with the formation of a dimer, and subsequently, the addition of a third monomer to form a trimer[335]. This association reaction is unstable and rapid; however, it becomes more stable with the addition of a forth monomer to produce a large oligomer. Remarkably, the concentration of dimers and trimers is low during the polymerization reaction[337].

Once trimers are formed, the elongation step begins. This involves the addition of ATP and $Mg^{+2}$-bound G-actin to both ends at different rates. The fast-growing end is the barbed- or plus-end, which usually grows 20-fold faster ($k = 11.6$ $\mu M^{-1} \cdot s^{-1}$) than the slow-growing end, which is called the pointed- or minus-end. As a function of their concentration, actin monomers can assemble at the barbed end and disassemble at the pointed end simultaneously in a dynamic steady state called AF treadmilling. Upon incorporation into a growing filament, ATP is hydrolyzed into ADP, and ADP-actin subunits and phosphate (Pi) are generated[336].

However, treadmilling is not the only key player in AF assembly. The elongation process involves two well-established tools, monomer-binding protein and capping proteins. Both mechanisms are effective in creating a vast pool of non-polymerized actin, whereas separately, none of these is qualified to provide the necessary number of monomers required to initiate the elongation step. Additionally, numerous severing and nucleating proteins are implicated in the branching and regulation of AFs[336] (Figure 18).
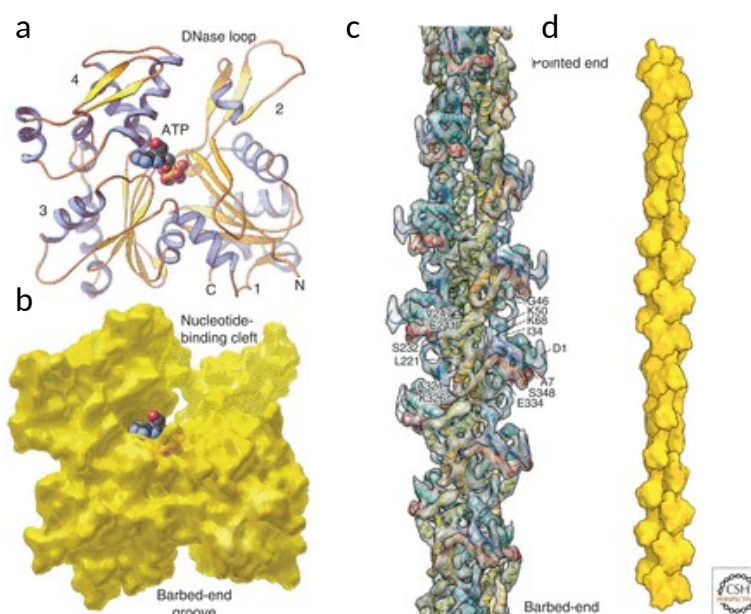


**Figure 18 | Structures of the actin molecule and AF**

a) Ribbon diagram of the actin molecule with space-filling ATP (protein data bank [PDB]: 1ATN). N, amino terminus; C, carboxyl terminus. Numbers 1, 2, 3, and 4 label the four subdomains. (b) Space-filling model of actin showing the nucleotide-binding cleft with ATP in situ and barbed-end groove. (c) Reconstruction of the AF from cryo-electron micrographs. The labels are single-letter abbreviations for selected amino acids. (d) Cartoon of the AF showing the position of the pointed and barbed ends. Adapted from Pollard and Earnshaw, 2007 and Fujii et al. 2010.

## 6.4. Actin binding proteins

It is well established that the dynamics of the cytoskeleton are governed by a vast array of ABPs. Actin filaments employ diverse mechanisms through ABPs to cope with the cellular condition, migration and invasion, and responding to intra- and extracellular signals. These proteins function to provide a large pool of actin monomers for the polymerization process. The ABPs are listed below and classified by their proper group function. Given the time and space, among the more than 100 ABPs, I will highlight the most effective proteins that regulate the cytoskeleton[338].

### 6.4.1. Monomer-binding proteins

Monomer-binding proteins are essential in regulating the actin monomer concentration within the cell. Under specific conditions and requirements, they either accelerate or prevent actin polymerization. Spontaneous actin assembly begins with one oligomer and depends on one critical concentration, that of the actin monomers[339].

Profilin is a small protein (~15 kDa) that is highly expressed in eukaryotes and abundant in the cytoplasm. It competes with thymosin-β4 in maintaining large amounts of non-polymerized actin. Several functions have been established for profilin. First, it promotes polymerization by transporting actin monomers to the barbed end[340]. This transport is mediated by binding to the actin nucleator formin at its proline-rich formin-homology 1 (FH1) domain, which leads to an increase in the elongation rate. Remarkably, profilin prevents the nucleation of new branches or the addition of new subunits to the pointed end by binding to ATP-G-actin. Moreover, profilin catalyzes nucleotide exchange by binding ATP to recently depolymerized monomers after ADP severance[341]. Thymosin-β4 is abundant in the cytoplasm and is a highly conserved polypeptide containing 43 amino acids with a high similarity to the WH2 domain. It not only sequesters actin monomers, but it is also a key player in determining the actin critical concentration by its formation of a complex with profilin and actin. It has a high affinity for Mg-ATP-actin, and therefore maintains the pool of non-polymerized actin monomers.

### 6.4.2. Nucleating proteins

Monomer-binding proteins can prevent AF polymerization. As a consequence, other mechanisms have evolved in cells to substitute for spontaneous actin assembly. Actin nucleator proteins are required at the initial step to promote the *de novo* polymerization of AF. Formin and actin-related protein 2/3 (ARP2/3) complex are the main classes of nucleating proteins in eukaryotes. As these proteins are of major concern in my study, this section will describe their structure, function, and regulations[342].

### 6.4.2.1. ARP2/3 and its related regulators

The first nucleating factor to be identified was the actin-related protein ARP2/3, which is a highly conserved large 220 kDa complex. ARP2/3 is composed of seven evolutionarily related subunits: ARP2, ARP3, and 5 isoforms of ARP complex component (ARPC1-5). Upon binding to the side of an existing AF, the complex functions to nucleate filaments and organize them into a Y-branched structure (~70°). The newly formed branch has a capped pointed-end and a polymerization-competent barbed-end. ARP2 and ARP3 are known to bind ATP, and this interaction is crucial for the activity of the complex. The hydrolysis of ATP leads to the detachment and release of the complex. It has been shown that ARP2 and ARP3 localize at the pointed-end of the new branch, while APRC2 and APRC4 associate with the parental filament. This interaction with the filament gives ARP2/3 its activity. Moreover, the phosphorylation of Thr and Tyr in ARP2 and interactions with nucleation-promoting factors (NPFs) are essential for a potent nucleation process (Figure 19).
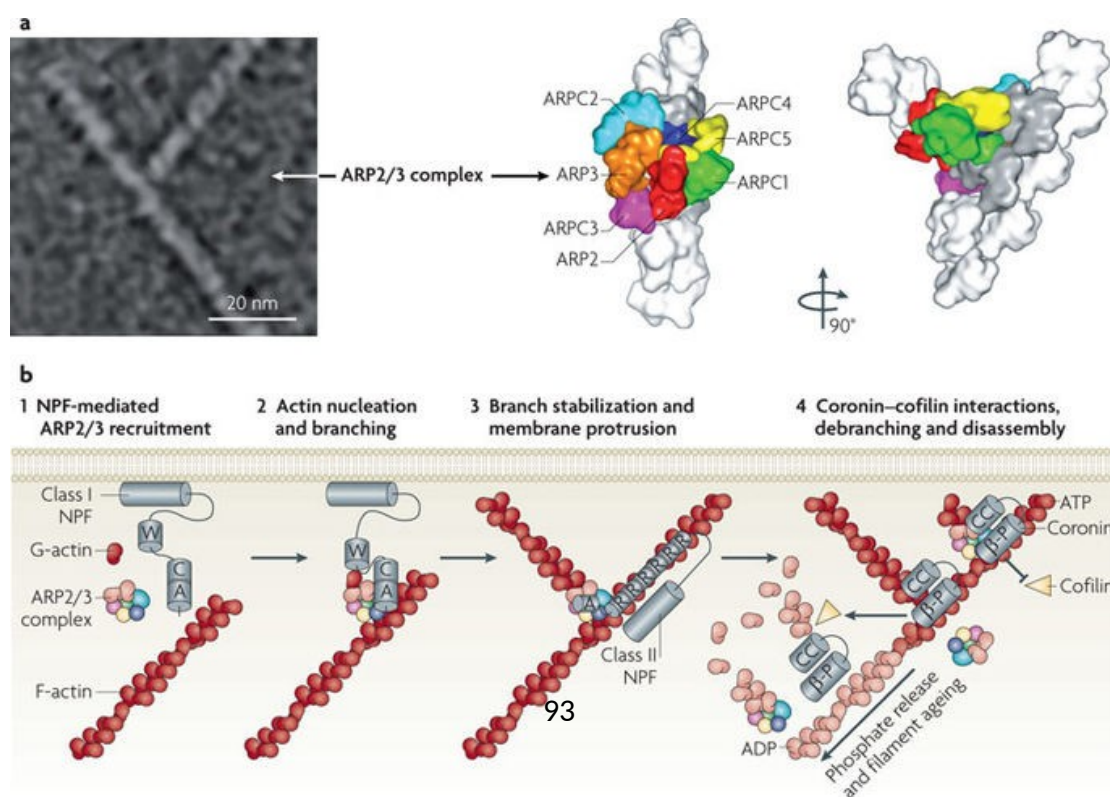
Nature Reviews | Molecular Cell Biology

**Figure 19 | ARP2/3 structure and function**

a) The morphology of a Y-branched actin filament and the actin-related protein 2/3 (ARP2/3) complex is shown in an electron micrograph and in structural models based on electron tomography. The ARP2/3 complex consists of ARP2 and ARP3 plus the additional subunits ARPC1–ARPC5. In this model, all seven subunits participate in binding to the existing filament and ARP2 and ARP3 act as the first two subunits of the nascent filament. b) ARP2/3 is recruited by the WCA domains of class I nucleation-promoting factors (NPFs) in proximity to cellular membranes (1). The collective activities of WASP homology 2 (WH2; W), connector (C) and acidic (A) segments serve the basic purpose of bringing ARP2/3 together with the first actin subunit in the new filament to generate a branch (2). ARP2/3 branch points can be stabilized by filamentous actin (F-actin)-binding class II NPFs, such as cortactin (3). Coronin family proteins interact with ARP2/3 and F-actin to prevent cofilin-mediated disassembly of newly formed filaments (4, top). Coronin can also replace ARP2/3 and synergize with cofilin to trigger debranching and disassembly of older ADP–actin filaments (4, middle). Disassembly of older branches can also occur spontaneously, following phosphate release from ARP2 and actin (4, bottom). Adapted from Campellone et al., 2010.

- ## Nucleation-promoting factors

Mammalian NPFs are classified into 2 classes. Class I includes Wiskott-Aldrich syndrome protein (WASP), neural-WASP (N-WASP), WASP-family verprolin-homologous protein (WAVE1-WAVE3), WASP and SCAR homologue (WASH), WASP homologue associated with actin, Golgi membranes, and microtubules (WHAMM), and junction-mediating regulatory protein (JMY). Class II contains hematopoietic lineage cell-specific protein 1 (HS1) and cortactin. NPFs activate ARP2/3 to interact with actin through the carboxy-terminal WCA domains, which include a WASP homology 1 and 2 (WH1 and 2) motif[343].

WASP is highly expressed in hematopoietic cells, while N-WASP is expressed in most cells. The deletion of both isoforms is crucial for embryonic survival and is implicated in neurological and cardiac diseases. ARP2/3-complex activation by N-WASP leads to a functional actin nucleation. The structure of WASP has been shown to have the WH1 motif in addition to CDC42/Rac-interactive binding (CRIB) and auto-inhibitory motifs[344].

WASP, the main regulator of ARP2/3, can be activated by the direct binding of small GTPases such as Cdc42 to the GTPase binding domain (GBD), which frees the WCA

domain. Additionally, proteins with the Src homology 2 and 3 (SH2 and SH3) domain can bind to the proline-rich domain (PRD) and activate N-WASP. Moreover, Tyr phosphorylation of the GBD can stabilize the activity of N-WASP. The structure of WASP has been shown to contain the WH1 motif in addition to CRIB and auto-inhibitory motifs. Interestingly, N-WASP has limited NPF activity due to inhibition of the GBD. This inhibition is enforced by WASP-interacting protein (WIP), a molecule that interacts with the WH1 motif.

Class II NPFs, including cortactin, have weaker activity than class I NPFs in activating ARP2/3 and the nucleation process. Interaction with class I NPFs occurs through t PRD and SH3 domains at the C terminal. Their structure has shown a lack of the WH2 domain, but a specific ARP2/3-binding domain is present at the N-terminal (Figure 20).
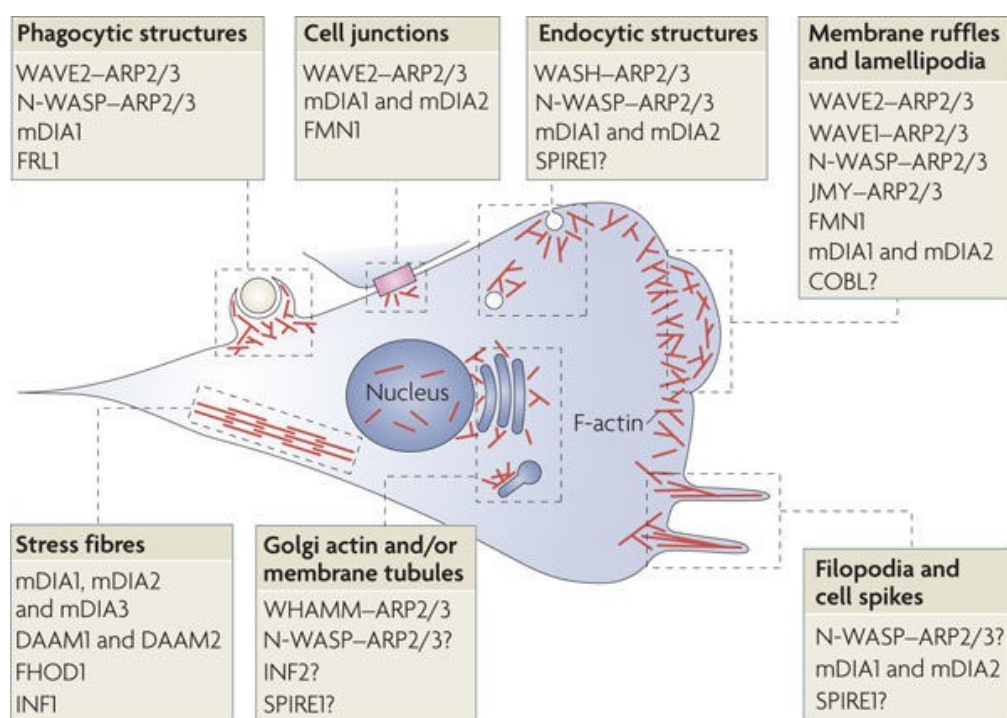
**Figure 20 | Nucleating protein function**

Filamentous actin (F-actin; red) is nucleated and organized into branched networks by the actin-related protein 2/3 (ARP2/3) complex and its nucleation-promoting factors or is generated in unbranched forms by formins and tandem WASP homology 2 (WH2) domain-containing nucleators. Functional roles for different nucleation factors in a generic mammalian cell are depicted during phagocytosis, cell junction assembly, endocytosis, membrane ruffling and lamellipodia dynamics, filopodia formation, Golgi and tubulovesicular membrane dynamics, and stress fibre formation. Question marks indicate that the precise role for the nucleation factor is unclear. Adapted from Campellone et al., 2010.

### 6.4.2.2. Formins

Formins are homodimeric proteins with formin-homology domains 1 and 2 (FH1 and 2) that bind to the barbed end of an AF. They have the role of nucleating and elongating unbranched actin complex and bundling new filaments. The formin family contains seven members that share FH domains[345]. When a formin protein encounters an actin subunit, the $\alpha$-helical linker of FH2 stretches, leading to it wrapping around the AF. The FH1 domain is enriched with proline-rich sequences that enable the formin protein to interact with profilin. Another important domain is the GBD. Due to the presence of the diaphanous auto-inhibitory domain (DAD) and the DAD-interacting domain (DID), formin functions can be auto-inhibited. Nevertheless, instead of using the WH2 domain, formins use the FH2 domain for interaction with AFs to promote elongation[346].

### 6.4.3. Severing and depolymerizing proteins

The actin-depolymerizing factor/cofilin family is an essential member of the ABPs implicated in the recycling of actin monomers. The family includes destrin and twinfilin as actin depolymerizing factors (ADF), cofilin-1 in non-muscle cells, and cofilin-2 in muscle tissues. Both cofilin-1 and ADF have similar functions in regulating AFs by binding and severing ADP subunits, leading to cytoskeleton turnover[347].

Destrin is a small globular 19 kDa protein that regulates the actin cytoskeleton by rapidly depolymerizing AFs in a stoichiometric manner. It is widely expressed in eukaryotes and has a 71% similarity to cofilin. Destrin can directly bind to a filament and remove an actin monomer, thereby dissociating the AF[348]. Cofilin-1, hereafter called cofilin, is a small 15 kDa protein that is highly expressed in eukaryotes. Cofilin severs AFs by binding to the barbed-end, which leads to creating free ends. ATP hydrolysis and Pi dissociation trigger cofilin to bind to the ADP-actin subunit[349]. It is well established that cofilin promotes actin assembly or disassembly depending on its concentration in the cytoplasm and the presence of other ABPs. Moreover, it can bind to actin monomers and inhibit nucleotide exchange[347].

In addition, the gelsolin family contains 8 members that act to sever AFs. The principal gelsolin member is a potent $Ca^{+2}$-dependent protein that acts mechanically by changing the actin conformation and weakening the non-covalent bonds between actin molecules. After rapidly binding to the actin subunit, gelsolin acts slowly to dissociate the filament and actin as it caps the disassembled part. The uncapping of these small filaments enriches the cytoplasm with numerous polymerization-competent ends[350].

### 6.4.4. Capping proteins

Eukaryote cells express proteins dedicated to capping the end of AFs and therefore inhibit continuous elongation. Their function is synchronized with profilin to ensure a limit on the number of polymerization-competent barbed ends. The capping process generally occurs in seconds and can last for 30 minutes. To end the capping process, polyphosphoinositides bind to the protein and inhibit its ability to form connections; V-1/ myotrophin is responsible for dissociating the capping proteins from the filament. Moreover, capping protein Arp2/3 myosin I linker (CARMIL) contains a capping protein interaction motif that regulates the activity of capping proteins.

Tropomodulin is the main capping protein oriented to specifically cap the pointed ends of AFs to block new subunit addition or loss. β-Actinin, CapZ, and Cap32/34 are also implicated in protecting the cytoskeleton from AF loss by binding to the barbed end., Some members of the gelsolin family also act as capping proteins.

### 6.4.5. Cross-linking and bundling proteins

An intact cytoskeleton is crucial for all processes that require spatial and temporal variation such as cell migration, invasion, division, and trafficking[351]. To meet these requirements, AFs are linked to each other to construct networks using actin cross-linking and bundling proteins[352]. One of the central functions of these proteins is to support the cytoplasm and cellular protrusions. Specialized and different polymorphisms can be obtained depending on the unique properties of the protein (e.g., its type and concentration) used to connect the network[353]. The importance of bundling proteins arises from their crucial role in the formation and function of actin structures such as lamellipodia, filopodia, stress fibers, and invadopodia. These organelles often contain more than one type of bundling protein, which coordinates cell dynamics. For instance, fascin, L-plastin, tensin, and α-actinin form the parallel bundles and orthogonal networks of stress fibers and lamellipodia. α-Actinin, talin, plectin, fimbrin, and vinculin form the protrusion's core. Dystophin is known to connect the cytoskeleton to the plasma membrane[351].

The 55 kDa fascin polypeptides are the most abundant bundling proteins in all cytoskeletal organelles. Fascin consists of four β-trefoil domains, including two major actin-binding sites on domains 1 and 4. It is well established that the expression of fascin

is upregulated in many invasive and metastatic cancers. Therefore, fascin has emerged as a potent marker for cancer prognosis and a target for many therapeutic drugs[354,355].

Another interesting member of the actin bundling proteins is L-plastin (also known as fimbrin). The expression of L-plastin was originally believed to only be in hematopoietic cells, but it was later shown that it is highly regulated in many types of cancer, and therefore, it is a vigorous marker for diagnosis[285]. The protein consists of two actin-binding domains that include two calponin-homology domains, and it is highly expressed in invadopodia and filopodia[356].

## 6.5. Rho GTPases in the actin cytoskeleton regulation

Various extracellular stimuli can induce changes in the actin cytoskeleton through the Rho-family of p21 GTPases and their downregulation proteins. Among the 20 discovered Rho GTPases, Rho, Rac, and Cdc42 are the key regulators of AF dynamics. The abnormal regulation of Rho GTPase activation affects all cellular processes, including motility, invasion, division, and tumorigenesis[357]. Upon stimulation, Rho GTPases regulate the polymerization and organization of AFs by binding to ABPs. This process is mediated by the cyclic interaction of GTPases with GTPase activating proteins (GAPs) and guanine-nucleotide-exchange factors (GEPs), which are responsible for cycling GTP hydrolysis. Guanine nucleotide-dissociation inhibitors (GDIs) act to sequester the activation of GTPases[358].

The implication of GTPases in actin cytoskeleton regulation was observed by Hall in 1993 after the injection of activated mutants of Rho GTPases into Swiss3T3 cells[359]. The first observations showed roles for RhoA in stress-fiber formation, Rac1 in forming lamellipodial protrusions, and Cdc42 in forming filopodial protrusions. All later studies have shown that the GTPases are tightly coupled and coordinate together to regulate the cytoskeleton through complex activation cascades[360].

The stimulation of tyrosine kinase receptors on PI3K produces PIP3, which is a regulator of GEF, a promoter of GTP-nucleotide exchange. The downstream targets of Rho GTPases consist primarily of formins, WASP, and kinases. Rho-associated coiled-coil kinase 1/2 (ROCK), p21-activated kinase (PAK), and mammalian diaphanous formin (mDia) are the major downstream effector molecules for Rho GTPases[359] (Figure 21).
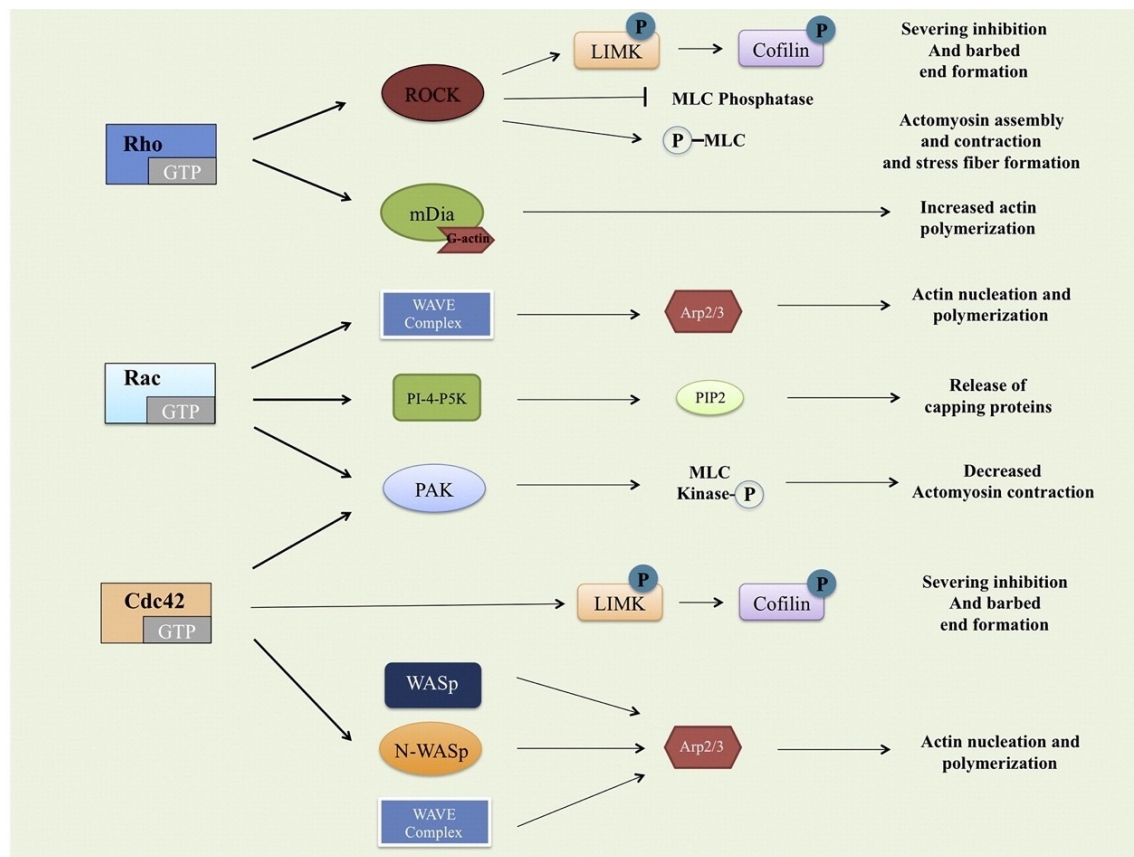
**Figure 21 | Rho GTPases and downstream effectors**

Downstream targets of Rho include the serine/threonine kinase ROCK which is mainly involved in the formation of stress fibers and focal adhesions. ROCK phosphorylates downstream myosin light chain (MLC) leading to actin–myosin contractility. At the same time, ROCK inhibits MLC dephosphorylation by inhibiting MLC phosphatases via their myosin binding subunit (MBS). The mammalian homolog of diaphanous (mDia) is another important Rho effector mediating actin nucleation. LIMK is also another downstream effector of Rho, which phosphorylates the actin severing protein cofilin inhibiting its severing activity and production of barbed ends. Downstream signaling of Cdc42 and Rac includes scaffold proteins belonging to the WASP/SCAR/WAVE family, key regulators of actin nucleation and polymerization. Active PAK phosphorylates MLCK thereby inactivating it and inhibiting MLC phosphorylation and contractility. PAK also phosphorylates and activates LIMK which potentially results in the phosphorylation of cofilin inhibiting its actin-severing function. Adapted from Hanna et al., 2013.

### 6.5.1. RhoA

RhoA is a ubiquitously expressed member of the Rho GTPase family with a crucial role in regulating the actin cytoskeleton and stress-fiber formation. GDIs maintain RhoA in an inactive GDP-bound state in the cytosol[361]. The dissociation of GDIs after activation leads to the translocation of RhoA to the plasma membrane, and hence, interaction with downstream molecules[362]. RhoA triggers ROCK-mediated actin cytoskeleton regulators such as myosin light-chain phosphatases, an important substrate for cell contractility. Moreover, ROCK activates LIM kinase (LIMK), which is responsible for ADF/cofilin phosphorylation and stimulation. Furthermore, RhoA is responsible for the activation of formin and its isoform mDia1, which is involved in cytoskeletal and microtubule rearrangement[363].

### 6.5.2. Rac1

Rac1 is an intracellular signal transducer implicated in the regulation of the actin cytoskeleton. It has been established that Rac1 plays an important role in lamellipodia induction and cell adhesion and migration. The downstream molecular signaling underlying actin regulation has also been well established. Rac1 is responsible for LIMK activation via PAK1. Additionally, Rac1 activates WAVE, whose structure lacks the GBD domain. This activation is mediated by binding to the adapter molecules IRSp53 and Abl. In addition, Rac1 regulates PI3K as well as the ERK pathway[364].

### 6.5.3. Cdc42

Cdc42 is a ubiquitously expressed small GTP-binding protein in the Rho family of GTPases. The role of Cdc42 in cells is crucial, and studies have shown that knocking out Cdc42 in mice causes embryonic death. The use of dominant-negative or constitutively active mutants showed the implications of Cdc42 in cellular processes despite the limitations such mutations place on other Rho GTPases[358]. The downstream effectors of Cdc42 are numerous (more than 20) and include actin proteins, kinases, and phospholipases. The most relevant pathways will be summarized. Cdc42 is the main and direct activator of the WASP family of proteins, including WASP, N-WASP, and WAVE, via binding to the CRIB motif. Cdc42 connects with the Toca (transducer of Cdc42-dependent actin assembly) families, enhancers of Arp2/3 activation. Additionally, Cdc42 stimulates LIMK-dependent cofilin activation and PAK[365].

The regulation of Cdc42 also affects the expression and activation other oncoproteins such as Ras and EGFR via PAK. Ras modifications lead to the initiation and progression of tumors by the activation of anti-apoptotic pathways such as Raf-MEK-ERK. It has also been established that the activation of Cdc42 is associated with the prevention of EGFR degradation and thus tumor cell progression. The regulation of IQGAP1 and 2 proteins and their binding with Cdc42 is an important pathway in tumors. The increased expression of both proteins tends to be oncogenic and related to metastasis[358,366]. Microinjecting constitutively active Cdc42 increases GTP-GDP cycling and hence, regulates the cytoskeleton and formation of filopodia. Some activating mutants lead to the induction of cellular transformation and foci formation. In the case of BC, Cdc42 deletion is key to the degradation of EGFR and consequently the reduction of cell growth and metastasis, whereas in melanoma and lung cancer, cdc42 overexpression serves as a prognosis marker[367,368].

Cdc42 represents a potent therapeutic target for many types of cancer. Due to the difficulties in blocking only one of the GTPases without affecting the whole process, inhibitors of the downstream effectors are used. ZCL278 acts against interactions between Cdc42 and the GEFs, while secramine blocks the recruitment of GDIs. Another potent molecule is CID2950007, which binds to the guanine nucleotide site on Cdc42, inhibiting the GTP-GDP cycle. Moreover, the PAK inhibitors PF-3758309 and FRAX597 have been used in many types of cancer models to block Cdc42 downstream pathway[369].

## 6.6. Actin cytoskeleton dynamics at the IS

Actin remodeling of the IS has been a focus of interest for many studies. Clarifying the actin filament and microtubule dynamics has led to a better understanding of the basics of immune cell-mediated cell lysis., Actin remodeling is a marker of immune cell activation in both T and NK cells and is a driver for cytotoxic granules[139]. The ISs of both T and NK cells show similarities in function and organization when considering the cytoskeletal rearrangement. This section will detail the AF dynamics[134].

WASP, WAVE, and HS1 are key regulators of ARP2/3, which is responsible for AF polymerization. WAVE is known to regulate actin polymerization in T cells, but it does not play a role in NK cells. Interestingly, the IL-2-dependent activation of WAVE can compensate for the absence of WASP in patients with Wiskott-Aldrich syndrome. This result would explain the cooperation between immune cells to induce a functional NK-cell lytic response. ARP2/3 complex activation can also be achieved by HS1, the hematopoietic homologue of cortactin. HS1 tends to cluster at the synaptic region where it is essential for connecting with LFA-1 signaling[370]. Interestingly, formin is implicated in the actin polymerization at T-cell synapses, but not in NK cells, where it functions only in assisting microtubule polarization[371,372].

As discussed in Section 2.1, MTOC polarizes to the leading-edge region upon target-cell recognition and adhesion. The MTOC and myosin IIA centered in the cSMAC are surrounded by protrusive actin polymerization in the dSMAC[161]. Actin remodeling at this stage is crucial for immune cell activation, as any disruption to the cytoskeleton leads to sequestering the activation state[156]. Remarkably, the pharmacological or genetic disruption of myosin IIA prevents TCR recruitment and activation. In T cells, AFs are responsible for TCR clustering at the IS. In NK cells, it is well established that the ligation of ICAM-1 on target cells and LFA-1 on NK cells initiates AF polymerization and accumulation[373]. At this stage, actin polymerization acts to maintain the LFA-1 clustering and thus ensures tight adhesion and a larger synapse diameter with the target[374]. A further ligation of 2B4 receptors participates in destabilizing LFA-1 and the actin connection, and thus NK-cell detachment[375].

The implication of actin at the synapse is not limited to adhesion receptor clustering, but also to activating and inhibitory receptor polarization. In T cells, the movement of activating receptors occurs in an actin and myosin IIA-dependent manner. Comparably, the NK-cell synapse shows a clustering of activating and inhibitory receptors (i.e.,

NKG2D and KIR2D) coupled to actin accumulation. Of note, NKG2D clustering at the IS has been observed to reduce KIR2D clusters in the same region[376].

As actin remodeling is a dynamic process, AFs undergo continual re-organization after the adhesion step. Actin hypodensity is observed in the same region where activation receptor clustering functions to clear the way for MTOC and lytic granules. This specific remodeling is governed by cofilin and coronin 1A, which promote the turnover of actin and ARP2/3[377,378]. At the termination stage, actin is remodeled to its basic state with no further secretion observed[379].

# PhD project objectives

An effective NK cell anti-tumor response relies mainly on the establishment of an active and functional IS. Although the dynamic and function of the actin cytoskeleton at the NK side of the synapse is well established, there is a gap of knowledge about the role of tumor actin cytoskeleton upon immune cell attack. The two objectives of my PhD Thesis were to:

(i)     characterize actin cytoskeleton organization and dynamics in breast cancer cells during NK cell attack.

(ii)     examine the role of the tumor cell actin cytoskeleton in the resistance to NK cell-mediated cell killing.

# Results

Most of the results obtained during my PhD were assembled into an article that was published in the journal of *Cancer Research*. In this article, we report, for the first time, actin cytoskeleton organization and dynamics in tumor cells during NK cell attack. In addition, we provide evidence that actin remodeling plays a central role in breast cancer cell escape from NK cell-mediated lysis. The article is provided as a main result section (1.2). The introduction and the discussion of the article are also provided in French to comply with the requirements from the University of Strasbourg (1.1 and 1.3, respectively). In follow-up studies, I investigated the mechanisms underlying actin-mediated immune evasion. The corresponding results are presented as classical result sections (2 to 4). This result chapter is followed by a general discussion and perspectives as well as complementary materials and methods.

## 1. Actin cytoskeleton remodeling drives breast cancer cell escape from natural killer-mediated cytotoxicity

### 1.1. Introduction to the article in French

**Note : Les références de cette introduction se trouvent dans l'article qui suit (1.2)**

Les cellules NKs sont des lymphocytes du système immunitaire inné qui possèdent une activité cytotoxique et contribuent à débarrasser l'organisme des cellules cancéreuses et des infections induites par des agents pathogènes. Contrairement aux cellules cytotoxiques du système immunitaire adaptatif, tels que les lymphocytes T cytotoxiques CD8$^+$, les cellules NKs tuent leurs cibles très rapidement et ne nécessitent pas une pré-activation par exposition préalable aux l'antigènes. Pour ces raisons, les cellules NKs sont fréquemment considérées comme une des premières lignes de défense contre le cancer. Les cellules NKs reconnaissent les cellules malignes en détectant une perte des molécules inhibitrices du complexe majeur d'histocompatibilité de classe I (CMH I) et/ou une surexpression de ligands activateurs induit par le stress, tels que les ligands du récepteur NKG2D comme ULBP1-6 et MICA/B. La balance entre les signaux inhibiteurs et activateurs déterminent en grande partie l'activation de la cytotoxicité des cellules NKs, même si des mécanismes complémentaires ont été décrits. Outre leur cytotoxicité directe et la production de cytokines pro-inflammatoires, les cellules NKs modulent l'activité d'autres cellules immunitaires et peut amorcer les cellules dendritiques pour activer les réponses anti-tumorales des lymphocytes T.

Si les cellules NKs ont une activité cytotoxique forte contre les cellules transformées, leur nombre dans les tumeurs solides est fréquemment faible. Afin de résoudre ce problème, le transfert de cellules NKs autologues ou allogéniques suivi de doses élevées d'IL-2 a été cliniquement évalué. Les deux approches thérapeutiques se sont avérées partiellement efficaces, mais n'ont pas réussi à induire une rémission durable. Les principaux obstacles à une efficacité clinique demeurent, notamment l'absence d'expansion des cellules NKs in vivo ainsi que les mécanismes immunosuppresseurs induits par les tumeurs. Avec l'avènement d'immunothérapies basées sur des cellules T autologues et approuvées par la FDA, l'intérêt de l'applicabilité des cellules NKs en immunothérapie contre le cancer a été réactivé. Des modifications génétiques similaires à celles employées pour générer des cellules T couplées à un récepteur antigénique chimérique(''CAR T cells''), pourraient être appliquées aux cellules NKs pour augmenter leur efficacité contre les tumeurs. Cependant, les mécanismes d'évasion insuits par les cellules cancéreuses et les microenvironnements tumoraux immunosuppresseurs demeurent des obstacles majeurs.

Après la reconnaissance des cellules tumorales, les cellules NKs vont suivre une série d'étapes spécifiques conduisant à la sécrétion orientée de granules lytiques préformés contenant des molécules cytotoxiques, tels que la perforine et la GzB. Un événement clé et précoce conduisant à la mort cellulaire des cellules tumorales est la formation d'une synapse immunologique entre les cellules immunitaires et leurs cibles, dont la fonction est de focaliser la sécrétion des granules lytiques vers les cellules cibles. La formation et l'activité de la synapse impliquent des réarrangements importants du cytosquelette d'actine dans les cellules NKs. Les premières étapes de la formation de la synapse sont associées à une accumulation importante de filaments d'actine, qui facilite la formation et la stabilisation de ''peripheral supramolecular activation clusters'' (pSMAC). Après réorganisation du cytosquelette, les granules lytiques convergent vers le centre organisateur des microtubules le long des microtubules. Par la suite, ces granules lytiques se polarisent vers la synapse. Les études d'imagerie à haute résolution ont démontré qu'un réseau dynamique d'actine est situé au centre de la synapse et que ce réseau contrôle la distribution de granules associés à la myosine IIA vers zones spécifiques de la membrane. Les deux principales classes de nucléateurs d'actine (le complexe ARP2/3 et formines) se sont avérées avoir des rôles critiques mais distincts au cours de la cytotoxicité médiée par les cellules NKs. Récemment, il a été montré que la coronine 1A a été impliquée dans la déconstruction du réseau d'actine corticale au niveau de la synapse, un processus

aboutissant à la création d'un espace où la sécrétion de granules se produit préférentiellement.

Par rapport aux les rôles bien établies du cytosquelette d'actine des cellules NKs pendant la reconnaissance et la destruction des cellules cibles, les configurations et fonctions de l'actine dans les cellules tumorales restent énigmatiques au cours de ces processus. Dans l'étude présente, nous démontrons de manière directe et pour la première fois que le cytosquelette d'actine des cellules tumorales joue un rôle clé dans la résistance à la lyse médiée par les cellules NKs.

## 1.2. Main article

# Actin cytoskeleton remodeling drives breast cancer cell escape from natural killer-mediated cytotoxicity

Cancer
Research

# Actin Cytoskeleton Remodeling Drives Breast Cancer Cell Escape from Natural Killer–Mediated Cytotoxicity

Antoun Al Absi[1,2], Hannah Wurzer[1,3], Coralie Guerin[4,5], Celine Hoffmann[1], Flora Moreau[1], Xianqing Mao[1], Joshua Brown-Clay[1], Rémi Petrolli[1], Carla Pou Casellas[1], Monika Dieterle[6], Jean-Paul Thiery[7,8], Salem Chouaib[7,9], Guy Berchem[1], Bassam Janji[1], and Clément Thomas[1]

## Abstract

Elucidation of the underlying molecular mechanisms of immune evasion in cancer is critical for the development of immunotherapies aimed to restore and stimulate effective antitumor immunity. Here, we evaluate the role of the actin cytoskeleton in breast cancer cell resistance to cytotoxic natural killer (NK) cells. A significant fraction of breast cancer cells responded to NK-cell attack via a surprisingly rapid and massive accumulation of F-actin near the immunologic synapse, a process we termed "actin response." Live-cell imaging provided direct evidence that the actin response is associated with tumor cell resistance to NK-cell–mediated cell death. High-throughput imaging flow cytometry analyses showed that breast cancer cell lines highly resistant to NK cells were significantly enriched in actin response-competent cells as compared with susceptible cell lines. The actin response was not associated with a defect in NK-cell activation but correlated with reduced intra-cellular levels of the cytotoxic protease granzyme B and a lower rate of apoptosis in target cells. Inhibition of the actin response by knocking down CDC42 or N-WASP led to a significant increase in granzyme B levels in target cells and was sufficient to convert resistant breast cancer cell lines into a highly susceptible phenotype. The actin response and its protective effects were fully recapitulated using donor-derived primary NK cells as effector cells. Together, these findings establish the pivotal role of actin remodeling in breast cancer cell resistance to NK-cell–mediated killing.

**Significance:** These findings establish the pivotal role of the actin cytoskeleton in driving breast cancer cell resistance to natural killer cells, a subset of cytotoxic lymphocytes with important roles in innate antitumor immunity. *Cancer Res; 78(19); 1–13. ©2018 AACR.*

## Introduction

Natural killer (NK) cells are lymphocytes of the innate immune system with cytotoxic activity that contributes to ridding the organism of pathogen-induced infections and cancer cells. Unlike other cytotoxic cells of the adaptive immune system, such as CD8^{+} cytotoxic T lymphocytes (CTL), NK cells kill their targets on a short time scale without requiring preactivation via prior antigen exposure. Accordingly, they are frequently referred to as the first line of defense against cancer (1). NK cells recognize malignant cells by sensing a loss of inhibitory MHC class I molecules (missing-self) and/or an overexpression of activating stress-induced ligands (altered-self), such as the NKG2D receptor ligands ULBP1-6 and MICA/B (2, 3). The balance between inhibitory and activating signals critically determines the activation of NK-cell–mediated cytotoxicity toward their targets, although some complementary mechanisms have also been described (4). In addition to Ca2^{+}-dependent exocytosis of cytotoxic enzymes (perforin and granzymes) leading to caspase-dependent and -independent apoptosis, NK cells can also promote slow, caspase-dependent, cancer cell death via the engagement of death receptors (e.g., Fas/CD95, DR4, and DR5) on target cells by their cognate ligands FasL and TRAIL (5). Besides their direct cytotoxicity and the production of proinflammatory cytokines, NK cells modulate the activity of other immune cells (6, 7) and can prime dendritic cells to activate antitumor-specific CTL responses (8, 9).

Although NK cells hold promising cytotoxic activity against transformed cells, their numbers in solid tumors are usually low. To overcome the poor infiltration, an autologous or allogeneic NK cell transfer followed by adjuvant high dose IL2 has been clinically evaluated (10–12). Both treatment regimens proved to be partially effective but failed to induce durable remissions. Major

[1]Laboratory of Experimental Cancer Research, Department of Oncology, Luxembourg Institute of Health, Luxembourg City, Luxembourg. [2]University of Strasbourg, Strasbourg, France. [3]Faculty of Science, Technology and Communication, University of Luxembourg, 2 avenue de l'Université, Esch-sur-Alzette, Luxembourg. [4]National Cytometry Platform, Department of Infection and Immunity, Luxembourg Institute of Health, Esch-sur-Alzette, Luxembourg. [5]Paris Descartes University, Paris, France. [6]NorLux Neuro-Oncology Laboratory, Department of Oncology, Luxembourg Institute of Health, Luxembourg City, Luxembourg. [7]INSERM UMR1186, Immunologie Intégrative des Tumeurs, Equipe Labellisée Ligue contre le Cancer, Institut Gustave Roussy, Villejuif, France. [8]Department of Biochemistry, Yong Loo Lin School of Medicine, National University of Singapore, Singapore; Institute of Molecular and Cell Biology, A-STAR, Singapore. [9]Thumbay Institute for Precision Medicine Gulf Medical University-Ajman-UAE.

**Note:** Supplementary data for this article are available at Cancer Research Online (http://cancerres.aacrjournals.org/).

H. Wurzer and C. Guerin contributed equally to this article.

**Corresponding Author:** Clément Thomas, Luxembourg Institute of Health (LIH), 84 Val Fleuri, 1526 Luxembourg, Luxembourg. Phone: 352-26-970-252; Fax: 352-26-970-390; E-mail: clement.thomas@lih.lu

AACR   OF1

113

bottlenecks to clinical efficacy remain, including lack of consistent in vivo NK-cell expansion and tumor-induced immunosuppressive mechanisms. With the advent of efficient and FDA-approved autologous T-cell immunotherapy, interest in exploring the applicability of NK cells for use in cancer immunotherapies has been reawakened (13). Genetic modification of NK cells, as demonstrated for CAR T cells, could help to circumvent challenges posed by the tolerance to self-cells, helping establish NK cells as potent effectors against malignancy (14, 15). However, evasion mechanisms mounted by cancer cells and immunosuppressive tumor microenvironments remain major hurdles (13, 16, 17).

Upon recognition of tumor cells, NK cells undergo a series of specific steps leading to directed secretion of preformed lytic granules containing cytotoxic mediators, such as perforin and granzyme B (GzB). An early and key event in NK-mediated cell death is the formation of an immunologic synapse (IS) between the immune cell and its target, the ultimate function of which is to focus lytic granule secretion toward the target cell. Both the formation and activity of the IS critically rely on actin cytoskeleton rearrangements in NK cells (18–22). The initial steps of IS formation are associated with a prominent accumulation of actin filaments (AF), which facilitates the formation and stabilization of the so-called peripheral supramolecular activation cluster SMAC (23). Following actin reorganization, lytic granules converge on the microtubule-organizing center (MTOC) along microtubules. These lytic granules, together with the MTOC, subsequently polarize within the IS (24). High-resolution imaging studies have demonstrated that a dynamic meshwork of fine AFs is located at the center of the IS and this meshwork controls the delivery of myosin IIA-associated granules to specific membrane areas (25–28). The two major classes of actin nucleators (the ARP2/3 complex and formins) were found to play critical but distinct roles during NK-cell–mediated cytotoxicity (19). Recently, coronin 1A was reported to promote deconstruction of the synaptic cortical actin network (29), a process resulting in permissive "clearances" where granule secretion preferentially occurs (25).

In striking contrast to the well-characterized roles of the cell actin cytoskeleton of NK cells during target cell recognition and killing, little is known about actin configurations and functions in target cells during these processes. In the present study, we address this gap and provide for the first time direct and compelling evidence of the pivotal role of the tumor cell actin cytoskeleton in resistance to NK-cell–mediated cell lysis.

## Materials and Methods

### Cell lines and cell culture conditions

The breast adenocarcinoma cell lines used as target cells in this study were purchased from ATCC and include MCF-7, MDA-MB-231, T47D, and Hs578T cells. Each of these cell lines was authenticated and checked for not being cross-contaminated through STR profiling analysis (Microsynth). All cell lines were maintained in DMEM high glucose with L-glutamine medium (Lonza). The NK-92MI cell line was purchased from ATCC and cultured in RPMI-1640 (Lonza) supplemented with 10% (v/v) fetal bovine serum (FBS, Life Technologies) and 10% (v/v) horse serum (ATCC). All other media were supplemented with 10% (v/v) FBS, 100 U/mL penicillin, and 0.1 mg/mL streptomycin (Sigma-Aldrich). Cell lines were cultured in a humidified atmosphere at 5% $CO_2$ and 37°C and routinely checked for Mycoplasma contamination using the MycoAlert Mycoplasma detection kit (Lonza).

### Isolation of human primary NK cells

Peripheral blood mononuclear cells (PBMC) were isolated from buffy coats provided by the Luxembourg Red Cross using Lymphoprep density gradient medium (StemCell). Briefly, samples were diluted 1:5 with PBS supplemented with 10% FBS. Thirty milliliters of diluted buffy coat was poured onto 15 mL of Lymphoprep medium in LeucoSep centrifuge tubes (Greiner Bio-One) and centrifuged for 30 minutes at $800 \times g$ in a swinging-bucket rotor with slow acceleration and no brake. The enriched PBMC fraction was harvested and washed twice with PBS containing 10% FBS. Remaining erythrocytes were lysed with 1× ACK lysis buffer for 5 minutes before NK-cell isolation using the MACS NK cell negative isolation kit (Miltenyi Biotec) according to the manufacturer's instructions. Human NK cells were cultured in RPMI medium (Lonza) supplemented with 10% (v/v) FBS, 10% (v/v) horse serum, 100 U/mL penicillin, and 0.1 mg/mL streptomycin, and 100 U/mL recombinant human IL2 (PeproTech).

### Cell transfection and pharmacologic treatments

MCF-7 cells were transfected with wild-type SNAIL and SNAIL-6SA (a constitutively active mutant of SNAIL) expression vectors. These vectors were obtained from Addgene (gift from Mien-Chie Hung; Addgene plasmids #16128 and #16221). Parental cells were transfected 48 hours prior to subsequent analyses using Lipofectamine 2000 transfection reagent (Thermo Fisher Scientific). The expression of recombinant SNAIL/SNAIL-6SA was confirmed by Western blotting. N-WASP and CDC42 knockdown was achieved by transfecting MCF-7 and MDA-MB-231 cell lines with N-WASP and CDC42 siRNAs (siWASP#1 5′-GGUUUUGUCGUAAUCCUCUAUU-3′, siWASP#2 5′-CCUUAAUGUAAUUUUACUUUA-3′, siCdc42#1 5′-CAGCAAUG-CAGACAUUUAAUU-3′, and siCdc42#2 5′-CGAUGGUGCUGUUG-GUAAAUU-3′). The nontargeting siCtrl was purchased from Qiagen. All cell lines were transfected 48 hours prior to each assay using DharmaFECT transfection reagent (GE Dharmacon), and knockdowns were confirmed by a Western blotting. The LifeAct-mEGFP-7 plasmid was obtained from Addgene (gift from Michael Davidson, Addgene plasmid #54610). The LifeAct-mEGFP fragment was subcloned into the lentiviral plasmid pCDH-EF1α-MCS-IRES-Puro (CD532A-2; System Biosciences) using the XbaI and BamHI restriction enzyme sites and NEBuilder HiFi DNA Assembly (NEB) to generate the pCDH-LifeAct-mEGFP expression plasmid used for lentiviral transduction. Transduced cells were selected with puromycin (0.5 μg/mL, Sigma-Aldrich).

In addition to SNAIL-induced epithelial-to-mesenchymal transition (EMT), MCF-7 cells were treated by either 5 ng/mL TGFβ (PeproTech) for 6 days or 10 ng/mL TNFα (BioLegend) for 3 days. Prior to TGFβ treatment, MCF-7 cells were starved for 24 hours (1% FBS).

For actin drug-based assays, target cells were treated with 0.5 μmol/L cytochalasin D or DMSO (Sigma; control) for 30 minutes and washed twice prior to presentation to NK cells.

### Imaging flow cytometry

For conjugate formation, NK cells were counted, stained with anti-human CD56-PE-Cy7 (BioLegend, clone: HCD56), and washed before the direct contact with LifeAct-mEGFP-target cells at an effector-to-target (E:T) ratio of 5:1. Cells were coincubated for 30 minutes prior to fixation with 2% paraformaldehyde

114

(Thermo Fisher Scientific) and permeabilized with 0.1% Triton X-100 (Sigma-Aldrich). Afterward, cells were washed twice with PBS and then stained with anti-human GzB monoclonal antibody-APC (Thermo Fisher Scientific, clone: GB12), anti-γ-tubulin antibody-PE (Santa Cruz, clone: D-10), and DAPI (0.3 μg/mL, Sigma-Aldrich) for 20 minutes. The Amnis brand ImageStreamX Mark II (EMD Millipore) imaging flow cytometer with five built-in lasers (405, 488, 561, 640, and 785 nm) was used for acquisition. Using INSPIRE (EMD Millipore), $2 \times 10^4$ events were collected per tube at 60× magnification on a low speed and high-sensitivity settings. Unstained, single-stained, and Fluorescence Minus One (FMO-) stained samples were collected for each experiment as controls. For better visualization of lytic granules, the extended depth of field was activated during the acquisition of GzB-containing samples. Ideas software (IDEAS 6.2.64.0, EMD Millipore) was used for data analysis. The gating strategy, masks, and features to analyze conjugates were created and applied. Features are used to calculate, analyze, and measure specific intensities in the cell while masks are designed to define a specific area of the cell where features could be applied. Masks can be established on the basis of the bright field or florescence image. The mask overlaying the synaptic region was created by Boolean logics of mEGFP-LifeAct and CD56-PeCy7, Dilate (mEGFP-LifeAct, 1) and Dilate (CD56-PE-Cy7,2). For actin response measurements, the mean fluorescence intensity (MFI) of mEGFP-LifeAct was calculated at the IS mask. To better calculate the intensity of the MTOC and improve the detection of γ-tubulin, the feature of Bright Detail Intensity R7 (BDI) was used. The software's BDI feature can compute the intensity of the bright spot that have radii smaller than 7 pixels. For GzB quantifications in target cells, the mask was defined on the mEGFP-LifeAct after subtracting the region of the immune synapse in order to exclude the intensity of GzB derived from NK cells. In order to assess apoptosis in target cells upon the contact with NK cells, the intensity of the signal of Annexin V–APC signal and DAPI was measured at the mask covering the mEGFP-LifeAct. The intensity of the Annexin V–PE was plotted versus the intensity of DAPI to distinguish between viable (Annexin V−, DAPI−), early apoptotic (Annexin V+, DAPI−), late apoptotic (Annexin V+, DAPI+), and necrotic cells (Annexin V−, DAPI+).

Target cell surface antigens were stained for 30 minutes prior incubation with NK cells, using the following antibodies: anti-human HLA-A, -B, -C-Brilliant Violet 605 (BioLegend; clone: W6/32), anti-human MICA/MICB-APC (BioLegend; clone: 6D4) and anti-human PD-L1-Brilliant Violet 605 (BioLegend; B7-H1, CD274) antibodies. The data were acquired on our imaging flow cytometer, and MFI values for each ligand were determined at the synaptic region using the above described IS mask.

Overall ligand expression at the cell membrane of control and N-WASP- and CDC42-depleted target cells was analyzed using a BD FACSAria II flow cytometer (BD Biosciences).

### Statistical analysis

The unpaired Student $t$ test in Microsoft Excel 2016 and GraphPad Prism was used to determine the statistical significance of the results obtained. For Annexin V experiment, a Z-score test for two population proportions was used to determine the statistical significance between samples. *, $P \leq 0.05$; **, $P \leq 0.01$ and ***, $P \leq 0.001$.

## Results

### Breast cancer cell resistance to NK-cell–mediated cell lysis is associated with a prominent "actin response"

To examine AF configurations in tumor cells during NK-cell attack, two breast adenocarcinoma cell lines were transduced with lentivirus to achieve stable expression of the actin reporter LifeAct-mEGFP (Fig. 1A; Supplementary Fig. S1A; ref. 30). The epithelial-like MCF-7 cell line (Supplementary Fig. S1B) was chosen for its high susceptibility to NK-cell–mediated lysis, whereas the mesenchymal-like MDA-MB-231 cell line was chosen for its highly resistant phenotype. As shown in Fig. 1B, MDA-MB-231 cells were almost three times less susceptible to NK-mediated lysis when compared with MCF7 cells. Only 13% of MDA-MB-231 cells were killed by NK-92MI cells at an E:T ratio of 5:1 after 4 hours, while 42% of MCF-7 cells were killed under the same conditions. A confocal microscopy analysis conducted 30 minutes after tumor cells were exposed to NK cells revealed that most NK-cell–conjugated MDA-MB-231 cells exhibited a massive accumulation of actin near the IS, hereinafter referred to as the "actin response" (Fig. 1C; Supplementary Movie S1). In contrast, this actin response was rarely observed in NK-cell–conjugated MCF-7 cells. Instead, most conjugated MCF-7 cells exhibited a rather homogeneous distribution of actin at their cortex (Fig. 1D; Supplementary Movie S2).

The actin response was induced remarkably fast, as evidenced by the many MDA-MB-231 cells showing synaptic actin accumulation, in as little as 2 minutes after presentation to NK cells. Target–effector cell conjugates were tracked over long periods of time using live-cell imaging, and time-lapse movies were assembled. In MDA-MB-231 cells, the actin response persisted throughout the whole duration of the interaction between the cancer and immune cells (Fig. 1E; Supplementary Movie S3).

After about 30 minutes, the NK cell detached without achieving lysis of its target, and the actin response in the escaped cancer cell rapidly ceased. As exemplified in Fig. 1E and Supplementary Movie S3, the escaped cells were still alive at the end of the recording (120 minutes; Fig. 1E; Supplementary Movie S3). In most MCF-7 cells, no actin response could be observed at any time during the interaction (Fig. 1F; Supplementary Movie S4). Multiple membrane blebs were detected at the target cell surface after 1 hour, indicating that the target cell entered apoptosis. A few minutes later, the target cell lysed, and the green fluorescence of the actin reporter disappeared.

Quantification of GFP fluorescence showed that, in MDA-MB-231 cells, the cortical region that included the IS contained on average about two times more F-actin as compared with the opposite side of the cell, whereas no statistically significant asymmetrical distribution of actin was found in MCF-7 cells ($n = 25$; Fig. 2A). Nevertheless, we noticed that a few MDA-MB-231 cells in conjugate with NK cells did not show the typical actin response; conversely, a number of MCF-7 cells accumulated F-actin at the IS. We accordingly assumed that each cell line comprised two cell subpopulations differing in their ability to remodel their actin cytoskeleton in response to NK-cell attack. To further characterize these subpopulations, we used high-throughput imaging flow cytometry and analyzed a large number of cell conjugates. Breast cancer cells were cocultured with NK cells for 30 minutes prior to fixation and permeabilization. Typically, $2 \times 10^4$ events were acquired on the imaging flow cytometer, and a gating strategy was applied to select in-focus, live, and interacting

115

Al Absi et al.
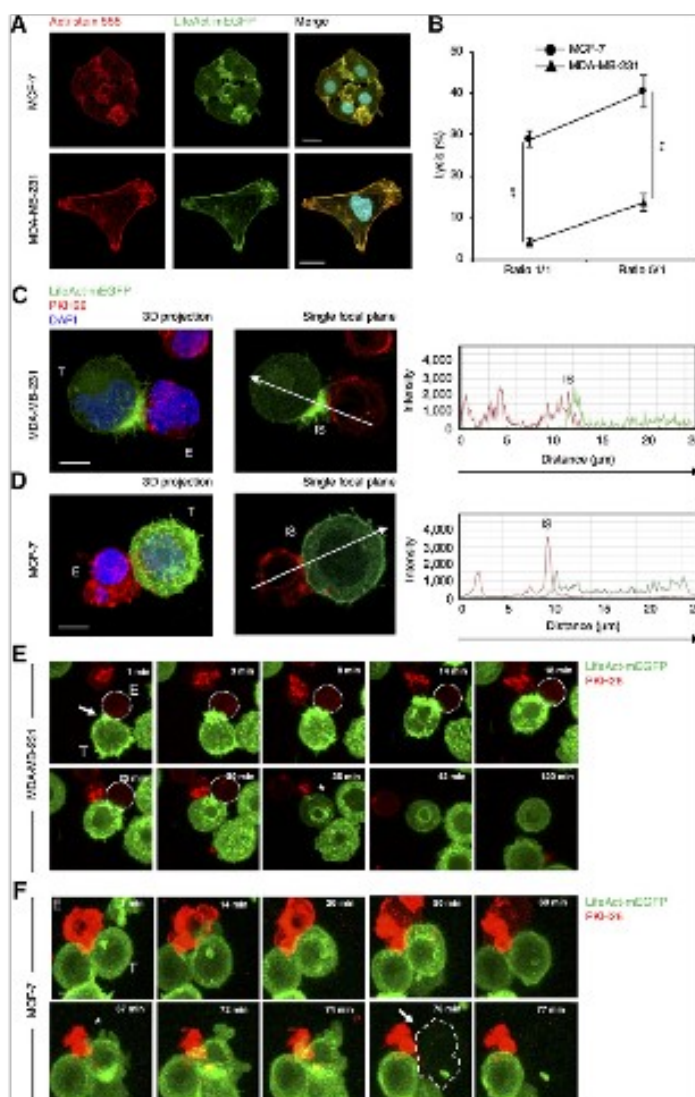


**Figure 1.**
Breast cancer cell line resistance to NK-cell-mediated cell death is associated with prominent F-actin accumulation near the immunologic synapse. **A,** Both MCF-7 and MDA-MB-231 cells were transduced to express the actin cytoskeleton reporter LifeAct-mEGFP (green). Stable cell lines were stained with Acti-stain 555 phalloidin (red) and DAPI (cyan). The yellow-orange signal in the merged images shows an extensive colocalization between the two actin probes. **B,** Cytotoxicity assays performed in three independent experiments with NK92MI cells (effectors) and MCF-7 or MDA-MB-231 cells (targets) at 1:1 and 5:1 effector:target ratios. The unpaired Student t test was applied to determine the statistical significance; **, P < 0.01. **C** and **D,** Confocal microscopy images showing the typical actin cytoskeleton organization in most MDA-MB-231 (**C**) and MCF-7 (**D**) target cells (green; T) in conjugation with PKH26-stained effector NK92MI cells (red; E). The charts on the right show the relative fluorescence intensities of LifeAct-mEGFP and PKH26 along the trajectories indicated on the corresponding confocal pictures. The region of the immunologic synapse is indicated by "IS." Note the spike in the fluorescent actin signal at the IS in MDA-MB-231 cells. Scale bars, 20 μm (**A**); 10 μm (**C** and **D**). Images are examples of at least 25 cells and three independent experiments. **E** and **F,** Time lapse imaging showing typical actin configurations over time in MDA-MB-231 (**E**) and MCF-7 (**F**) cells upon NK-cell attack. The arrow and the asterisk in **E** indicate the initiation of the actin response, and the detachment of the NK cell from its target and the subsequent cessation of the actin response in the escaped cancer cell, respectively. The asterisk and the arrow in **F** indicate the appearance of membrane blebs in the dying target cell and subsequent target cell lysis. Supplementary Movies S3 and S4 show the entire time-lapse movies (120 minutes) corresponding to **E** and **F,** respectively. Scale bars, 10 μm.

effector–target cell pairs (Fig. 2B). For analysis, a mask was manually generated using the IDEAS software to define the region of interest corresponding to the IS and its surrounding intracellular areas, hereinafter referred to as the "synaptic region" (Supplementary Fig. S1C). Such a mask was automatically applied to the data sets generated by imaging flow cytometry and confirmed to efficiently capture the actin response as exemplified in Fig. 2C.

For each cell line, the subpopulations of cells with or without an actin response were discriminated by comparing the relative intensity of LifeAct-mEGFP in the synaptic region and in the entire cell (Supplementary Fig. S1D). From three independent experiments, including a total of at least 500 conjugates, we calculated that 62% of MDA-MB-231 cells conjugated with NK cells exhibited an actin response, whereas the remaining 38% did
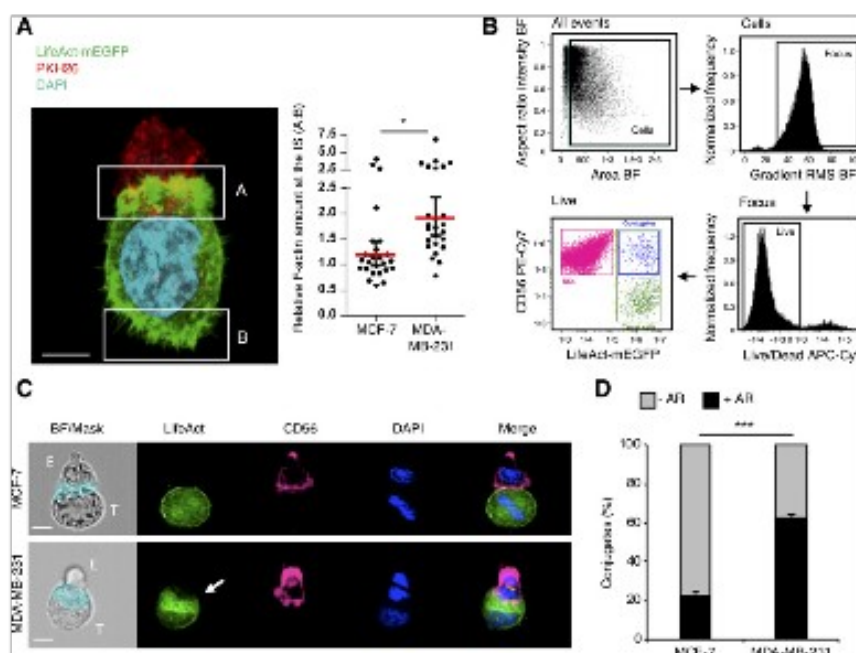
116

**Figure 2.**

Quantitative analysis of the actin response in susceptible and resistant breast cancer lines. **A,** Relative amounts of F-actin in tumor cells near the immunologic synapse. The left confocal image shows a typical conjugate between NK (red) and MDA-MB-231 (green) cells. The two white rectangles labeled A and B depict the regions of interest used for LifeAct-mEGFP fluorescence quantification. The right chart shows F-actin enrichment in the synaptic region of 25 MCF-7 and MDA-MB-231 cells conjugated with NK cells, as calculated by the ratio A:B. **B,** Gating strategy was used to identify NK-cell-target cell doublets using imaging flow cytometry. Cells were selected based on size, in order to exclude beads, by setting threshold values in a plot of area versus aspect ratio of events measured in the bright-field channel (top left). Focused events were then selected from a histogram plot of gradient root-mean-square of the bright-field channel (top right). Live cells were then selected for by setting threshold values for APC-Cy7 (Live/Dead) intensity (bottom right). Finally, the double-positive population (LifeAct-mEGFP for target cells and CD56-PeCy7 for NK cells) was selected as conjugates (bottom left). **C,** Typical examples of imaging flow cytometry panels obtained for conjugates between NK cells and MCF-7 cells (top row) or MDA-MB-231 cells (bottom row). The cyan area in the BF image depicts the mask applied to capture LifeAct signal near the immunologic synapse. Note the prominent actin response (arrow) in the MDA-MB-231 cell. **D,** Percentage of NK-cell-conjugated target cells with (black; +AR) and without (light gray; −AR) actin response in each cell line. Data are graphed as mean ± SE from three independent experiments including a total of 500 cell conjugates. The two-tailed unpaired Student $t$ test was applied to determine the statistical significance. ***, $P < 0.001$. Scale bars, 10 μm (**A**); 7 μm (**C**).

not (Fig. 2D). The opposite results were obtained for the MCF-7 cell line, in which only 22% of conjugated cells showed an actin response.

To extend the above data and further evaluate the relationship between tumor cell resistance to NK-mediated cell death and the actin response, we analyzed two additional breast cancer cell lines, the epithelial-like T47D cell line, and the mesenchymal-like Hs578T cell line (Supplementary Fig. S1B). As previously described, these cell lines were transduced to stably express LifeAct-mEGFP in order to image actin in target cells only, and to exclude any potential spillover effects from the actin cytoskeleton of NK cells (Supplementary Figs. S1A and S2A). Cytotoxic assays revealed that, similar to MDA-MB-231 cells, Hs578T cells were highly resistant to NK-cell lysis, displaying an NK-cell–mediated cytotoxicity of 13% at an ET ratio of 5:1 (Fig. 3A). In

addition, Hs578T cells were highly competent for the actin response, and more than 60% of conjugated tumor cells exhibited F-actin accumulation in the synaptic region (Fig. 3B; Supplementary Fig. S2B). In comparison, T47D cells were significantly more susceptible to NK-cell–induced lysis, and 36% displayed immune cell–mediated lysis at an ET ratio of 5:1 (Fig. 3A). These cells also exhibited a reduced ability to respond to NK-cell attack by an actin response (<30% of conjugated cells; Fig. 3B; Supplementary Fig. S2B). Interestingly, the amplitude of the actin response was relatively similar across cell lines with 30% to 45% of total cell F-actin accumulated at the synapse (Fig. 3C).

Taken together, our data reveal that a subpopulation of tumor cells responds to NK-cell attack by fast remodeling of their actin cytoskeleton, leading to a massive F-actin accumulation in the synaptic region. This is a process we termed the actin response.
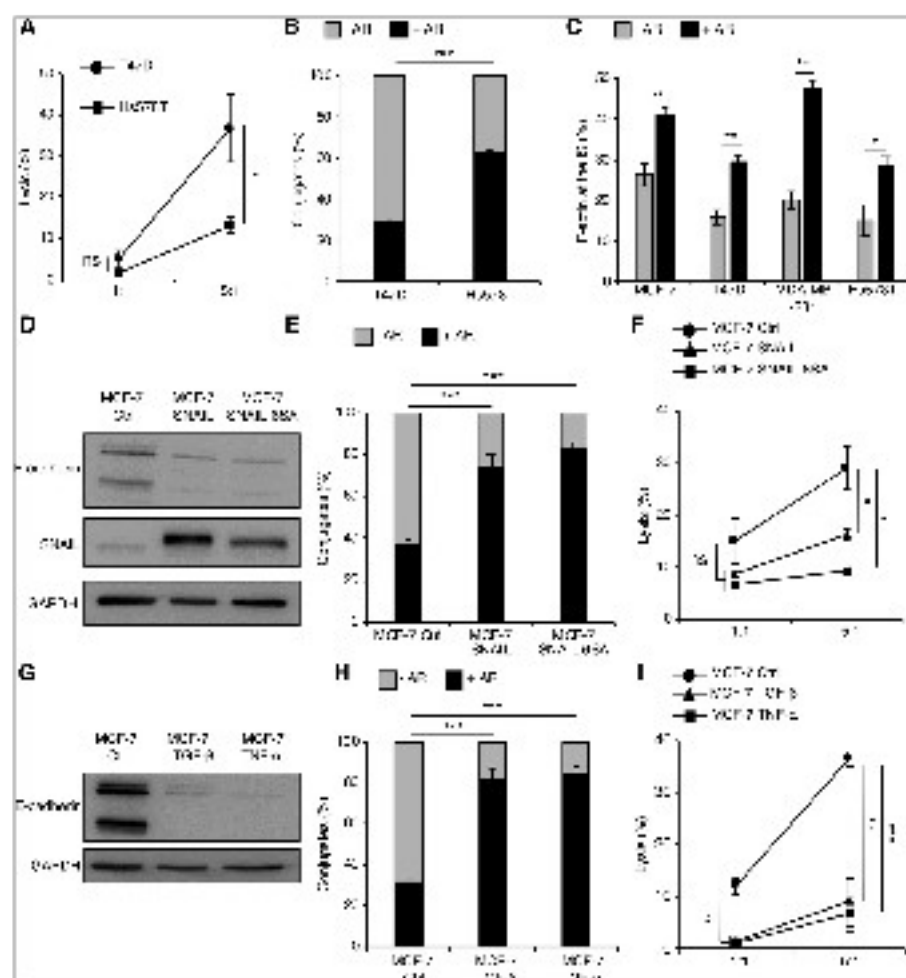
117

**Figure 3.**

The actin response is conserved among breast cancer cell lines and is enhanced by epithelial–mesenchymal transition. **A,** Cytotoxicity assays performed in three independent experiments with NK92MI cells (effectors) and T47D and Hs578T cells (targets) at 1:1 and 5:1 effector:target ratios. **B,** Percentage of NK-cell-conjugated target cells with (black; +AR) and without (light gray; −AR) actin response in T47D or Hs578T cell lines. Data are graphed as mean ± SE from three independent experiments including a total of 500 cell conjugates. **C,** Percentage of total cell F-actin in the synaptic region of target cells with (black; +AR) or without (light gray; −AR) actin response for different breast cancer cell lines. Data are shown as mean ± SE calculated from three independent experiments including a total of at least 500 cell conjugates. **D,** Western blot showing the expression of SNAIL and E-cadherin in transfected-only control MCF-7 cells (MCF-7 Ctrl), SNAIL-transfected MCF-7 cells (MCF-7 SNAIL), and SNAIL-6SA transfected MCF-7 cells (MCF-7 SNAIL-6SA). GAPDH was used as a loading control. **E,** Percentage of NK-cell-conjugated target cells with (black; +AR) and without (light gray; −AR) actin response in MCF-7 Ctrl, MCF-7 SNAIL, and MCF-7 SNAIL-6SA. **F,** Cytotoxicity assays performed in three independent experiments with NK92MI cells and either MCF-7 Ctrl, MCF-7 SNAIL, and MCF-7 SNAIL-6SA cells at 1:1 and 5:1 effector:target ratios. **G,** Western blot showing the expression of E-cadherin in mock-treated MCF-7 cells (MCF-7 Ctrl), TGFβ-treated (6 days, 5 ng/mL) MCF-7 cells (MCF-7 TGFβ) and TNFα-treated (3 days, 10 ng/mL) MCF-7 cells (MCF-7 TNFα). GAPDH was used as a loading control. **H,** Percentage of NK-cell-conjugated target cells with (black; +AR) and without (light gray; −AR) actin response in MCF-7 Ctrl, MCF-7 TGFβ, and MCF-7 TNFα. **I,** Cytotoxicity assays performed in three independent experiments with NK92MI cells and either MCF-7 Ctrl, MCF-7 TGFβ, or MCF-7 TNFα at 1:1 and 5:1 effector:target ratios. The two-tailed unpaired Student t test was applied to determine the statistical significance. $*$, $P < 0.05$; $**$, $P < 0.01$; $***$, $P < 0.001$.

118

Remarkably, this subpopulation was significantly larger in NK cell-resistant breast cancer cell lines than in more susceptible cell lines, suggesting that the actin response contributes to the resistant phenotype. In addition, our data point to a potential link between the EMT status of tumor cells and the actin response. Indeed, mesenchymal-like breast cancer cell lines, including MDA-MB-231 and Hs578T, proved to be significantly more competent for the actin response when compared with the epithelial-like ones, including MCF-7 and T47D (Figs. 2D and 3B; Supplementary Fig. S1B).

### EMT enhances the actin response frequency and breast cancer cell line resistance to NK-cell–mediated lysis

To further evaluate the relationship between EMT, actin response, and resistance to NK-cell lysis, EMT was experimentally induced in MCF-7 cells through transient expression of the wild-type EMT inducer SNAIL, or its degradation-resistant variant SNAIL-6SA variant. The mesenchymal transition of SNAIL- and SNAIL-6SA–expressing cell lines was evident by the adaption of a spindle-like morphology and reduced cell–cell contacts, as well as by the loss of E-cadherin (Fig. 3D). Both SNAIL- and SNAIL-6SA–overexpressing cells exhibited a robust increase (>2-fold) in the subpopulation of cells responding to NK-cell attack via synaptic F-actin accumulation as compared with control, transfected only, MCF-7 cells (Fig. 3E; Supplementary Fig. S2B). Consistent with its enhanced stability, SNAIL-6SA had a stronger effect than wild-type SNAIL, resulting in 82% and 74% of conjugated cells exhibiting an actin response, respectively (Fig. 3E). Forced expression of SNAIL or SNAIL-6SA also dramatically decreased MCF-7 cell susceptibility to NK-cell–mediated lysis. At an E:T ratio of 5:1, SNAIL- and SNAIL-6SA–expressing MCF-7 cells were 2- and 3-fold more resistant to NK-cell lysis when compared with the control cells, respectively (Fig. 3F).

In addition to SNAIL-induced EMT, we treated MCF-7 cells with either TGFβ or TNFα, and subsequently analyzed their competency for the actin response and their susceptibility to NK-cell–mediated cell lysis. Treatment efficacy was validated by E-cadherin downregulation and changes in cell morphology (Fig. 3G). Consistent with the above data, both treatments strongly increased the rate of actin response in MCF-7 cells as well as MCF-7 cell resistance to NK cells (Fig. 3H and I).

Together, our data indicate that the EMT status is a critical determinant of the capacity of breast cancer cells to remodel their actin cytoskeleton upon NK-cell attack, and to escape from NK-cell–mediated lysis.

### The actin response drives breast cancer cell resistance to NK-mediated cell lysis

We next aimed to evaluate the causal link between the actin response and breast cancer cell resistance to NK-cell–mediated lysis. First, we examined whether inhibition of synaptic F-actin accumulation affected breast cancer cell survival in cytotoxicity assays. Actin polymerization was impaired in target cells by knocking down either N-WASP (a key regulator of the ARP2/3 complex) or the Rho-subfamily small GTPase CDC42 (its upstream regulator; ref. 31). Resistant MDA-MB-231 and susceptible MCF-7 cell lines were transfected with small interfering RNA constructs (siRNAs) targeting N-WASP or CDC42 transcripts (siN-WASP and siCDC42, respectively). The two independent siRNAs used to target each transcript significantly decreased the corresponding protein expression levels in the two cell lines

(Fig. 4A). Imaging flow cytometry analysis showed that N-WASP- and CDC42 depletion reduced the subpopulation of actin response-competent cells in MDA-MB-231 cells by 2- to 3-fold (Fig. 4B). This inhibition of the actin response was associated with a significant increase in target cell susceptibility to NK-cell–mediated lysis, ranging from 50% to 150%. Conversely, N-WASP or CDC42 knockdown did not significantly affect the already reduced size of this subpopulation (around 20%) of MCF-7 cells that produce an actin response upon NK-cell attack (Fig. 4C), nor did it increase the susceptibility of MCF-7 cells to NK-cell lysis. The depletion of N-WASP or CDC42 was verified not to modify the overall expression of important ligands of NK-cell receptors at the target cell surface, including HLA-A, -B, -C, MICA/B, and program cell death-ligand 1 (PD-L1; Supplementary Fig. S3A–S3C), supporting our hypothesis that the increase of MDA-MB-231 cell susceptibility following N-WASP or CDC42 depletion is indeed the result of actin response inhibition.

We next quantified the extent of target cell apoptosis associated with the actin response. Briefly, target cells were incubated for 30 minutes with NK cells, labeled with Annexin V–APC and DAPI, and subsequently analyzed by imaging flow cytometry. For the analysis, a new mask was designed to capture Annexin V–APC and DAPI signals only in the LifeAct-mEGFP–expressing target cell from conjugates (Fig. 4D). For both MDA-MB-231 and MCF-7 cell lines, the number of apoptotic cells was considerably higher in the subpopulation of cells without an actin response when compared with the subpopulation of cells with an actin response. Consistent with the reduced subpopulation of actin response-competent cells in the MCF-7 cell line, this cell line contained a much higher total number of apoptotic cells when compared with the MDA-MB-231 cell line. Altogether, the above data provide further evidence that the actin response mediates breast cancer cell resistance to NK-cell–mediated lysis. The data also show that the inhibition of this process is sufficient to restore susceptibility in otherwise resistant breast cancer cells.

### The actin response is associated with changes in NK-cell receptor ligand density in the synaptic region of target cells

The possibility that the actin response was associated with local changes in the density of HLA-A, -B, -C, MICA/B, and PD-L1 on target cell surface was evaluated using imaging flow cytometry. Very interestingly, both HLA-A, -B, -C ligands and PD-L1 levels were increased (by 100% and 50%, respectively), while MICA/B ligands were modestly reduced (30%), at the synaptic region of MDA-MB-231 cells with an actin response as compared with MDA-MB-231 cells without an actin response (Supplementary Fig. S3D–S3F). Likewise, HLA-A, -B, -C ligands were significantly enriched at the synapse of MCF-7 cells with an actin response as compared with MCF-7 cells without an actin response (Supplementary Fig. S3D). However, synaptic MICA/B levels did not significantly differ in the two MCF-7 cells subpopulations (Supplementary Fig. S3E). PD-L1 was not amenable to quantification in the synaptic region of MCF-7 cells by imaging flow cytometry in our experimental setup. Together, these data suggest that the actin response increases inhibitory ligands, and possibly decreases activating ligands, at the synaptic region of target cells, respectively, which in turn may alter NK-cell function.

We then evaluated if the actin response was associated with a defect in NK-cell activation. To do so, we quantified MTOC polarization in NK cells conjugated with MCF-7 or MDA-MB-
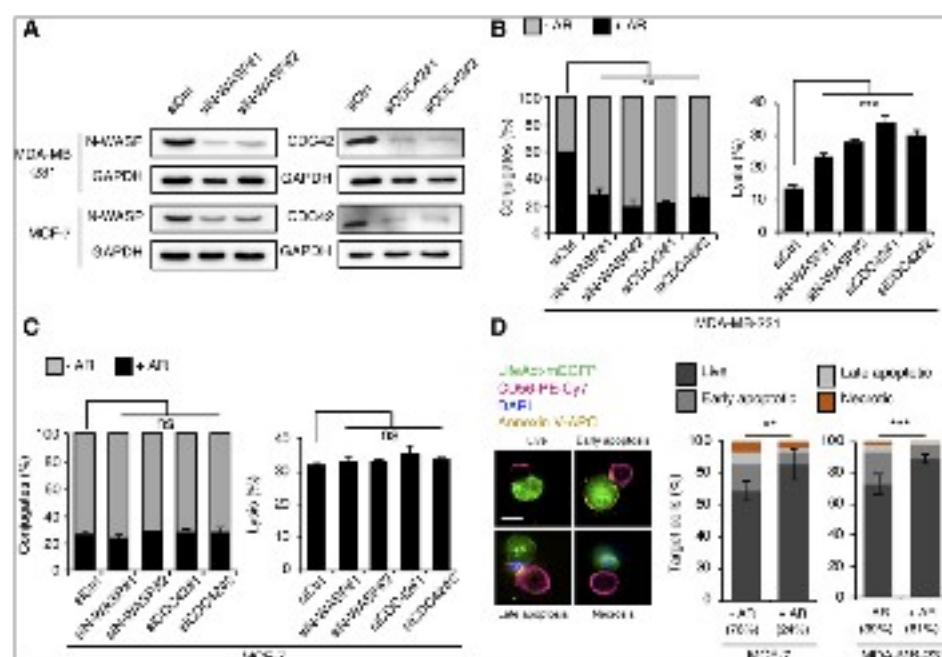
119

**Figure 4.**
Targeting the actin response increases tumor cell susceptibility to NK-cell-mediated cell lysis. **A,** MDA-MB-231 and MCF-7 cells were transfected with a control siRNA or different siRNAs targeting N-WASP or CDC42. Forty-eight hours after transfection, cells were lysed and levels of the specified proteins were analyzed by Western blotting. GAPDH was used as a loading control. The blots shown are representative of three independent experiments. **B and C,** Actin response frequency and cell susceptibility to NK-cell-induced lysis in N-WASP- and CDC42-deplete MDA-MB-231 and MCF-7 cells. Left, percentage of NK-cell-conjugated target cells with (black: +AR) and without (light gray: −AR) actin response in the indicated siRNA-transfected cell lines. Data are graphed as mean ± SE from three independent experiments including a total of 350 cell conjugates. Right, cytotoxicity assays performed in three independent experiments with NK92MI cells (effectors) and the indicated siRNA-transfected cell lines at 1:1 and 5:1 effector:target ratios. The two-tailed unpaired Student t test was used to determine statistical differences between the groups. **D,** MCF-7 and MDA-MB-231 cells were incubated with NK cells for 30 minutes and the percentage of unaffected (DAPI⁻; Annexin V⁻), early apoptotic (DAPI⁻; Annexin V⁺), late apoptotic (DAPI⁺; Annexin V⁺) and necrotic (DAPI⁺; Annexin V⁻) target cells conjugated with an NK cell was determined using imaging flow cytometry. Data are graphed as mean ± SE from three independent experiments including a total of 300 cell conjugates and in respect to the presence (+AR) or absence (−AR) of an actin response in target cells. The percentage of cells with or without an actin response is indicated below each bar of the chart. A Z-score test for two population proportions was used to determine the statistical significance between samples. Representative images of each possible type of cell conjugate are shown above the chart. Scale bar, 7 μm. Statistically significant differences are indicated by asterisks (**, P < 0.01; ***, P < 0.001; ns, nonsignificant).

231 cells. The two cell lines induced a similar overall polarization of the MTOC in NK cells (Fig. 5A). Moreover, MTOC polarization was not statistically different in NK cells conjugated with target cells with or without an actin response (Fig. 5B). In addition, MCF-7 and MDA-MB-231 cell lines induced similar NK-cell degranulation as evaluated by the degranulation marker lysosome-associated membrane protein-1 (LAMP-1)/CD107a (Fig. 5C; refs. 32, 33). However, these results do not totally rule out a role for the actin response in blocking NK-cell activation through modifying the ligand density at the synaptic region. Noticeably, NK92MI cells are a highly cytotoxic NK cell line lacking most of the killer inhibitory receptors (KIR) and, accordingly, are insensitive to an increase of HLA-A, -B, -C ligands (Supplementary Fig. S3D; refs. 34–36).

## The actin response reduces GzB levels in NK-cell-conjugated target cells

Following IS formation, NK cells directionally exocytose specialized secretory lysosomes containing cytotoxic proteins. Among these, the serine protease GzB is one of the central mediators of target cell death. We assessed the possibility that the actin response may alter GzB levels in target cells. First, we quantified GzB levels in NK-cell-conjugated target cells with or without an actin response using imaging flow cytometry. To exclude the bulk of GzB contained in effector cells and exclusively focus on the GzB fraction that is transferred to target cells, an appropriate mask was designed for data analysis (Fig. 5D). The poorly susceptible MDA-MB-231 cells were used as targets. We found that GzB levels were markedly reduced (by about 50%) in
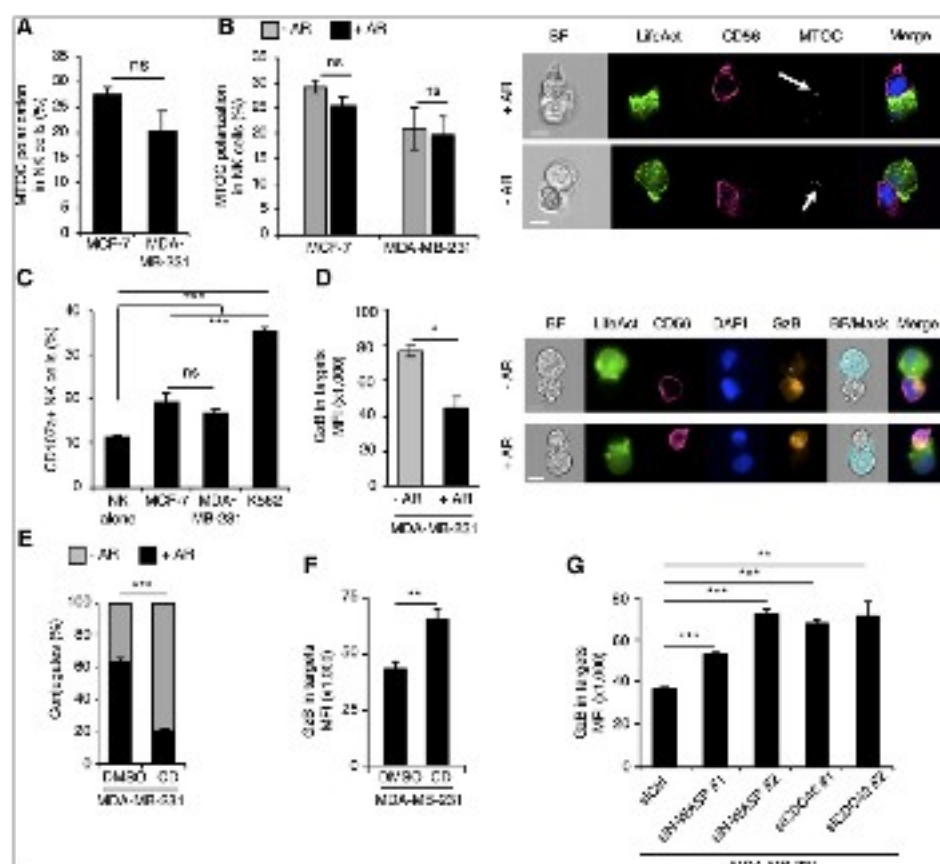
120

**Figure 5.**

The actin response is associated with significant decrease in GzB levels in target cells. **A,** Overall percentage of NK cells conjugated with MCF-7 or MDA-MB-231 cells exhibiting MTOC polarization toward the IS after 30 minutes of coincubation. Data are given as mean ± SE from three independent experiments including a total of 300 cell conjugates. **B,** Percentage of NK cells exhibiting MTOC polarization toward the IS in the presence (black; +AR) or absence (light gray; −AR) of actin response in the conjugated target cells. The panels on the right show examples of imaging flow cytometry images with polarized MTOC (arrows) in NK cells conjugated with MDA-MB-231 cells with (top; +AR) and without actin response (bottom; −AR). **C,** Percentage of CD107a-positive NK cells after 4 hours of coincubation with MCF-7 and MDA-MB-231 cell lines. NK cells without target cell were used as a negative control, while coincubation with K562 cells was used as a positive control. Data are given as mean ± SE from three independent experiments. **D,** GzB levels in NK-cell-conjugated MDA-MB-231 cells with (black; +AR) and without (light gray; −AR) actin response. Right, representative imaging flow cytometry images used for quantification. The light blue mask on the bright-field channel depicts the region of interest in which the GzB fluorescent signal was quantified. Note that NK-cell-contained GzB was totally excluded. Scale bars, 7 μm. **E,** Percentage of NK-cell-conjugated MDA-MB-231 cells with (black; +AR) and without (light gray; −AR) actin response after control (DMSO) and CD treatment. Data are given as mean ± SE from three independent experiments including a total of 300 cell conjugates. **F,** GzB levels in control (DMSO) and CD-pretreated MDA-MB-231 cells conjugated with NK cells. In all, about 200 conjugated target cells were scored. Data originate from three independent experiments and are expressed as MFI. **G,** MDA-MB-231 cells were transfected with a control siRNA or different siRNAs targeting N-WASP or CDC42. GzB levels in NK-cell-conjugated target cells were analyzed imaging flow cytometry. In all, about 350 conjugated target cells were scored. Data originate from three independent experiments and are expressed as MFI. The two-tailed unpaired Student t test was used to measure the statistical significance (*, $P < 0.05$; **, $P < 0.01$; ***, $P < 0.001$; ns, nonsignificant).

the cell subpopulation with an actin response compared with the cell subpopulation lacking an actin response. Next, we analyzed the effects of pharmacologic disruption of the actin response on GzB levels in target cells. The concentration of the actin-depolymerizing drug cytochalasin D (CD) and the treatment duration were optimized to disrupt most filamentous actin in

121

MDA-MB-231 cells, without compromising cell viability (Supplementary Fig. S4A and S4B). In addition, CD was carefully washed out prior to target cell incubation with NK cells in order not to impair their function, leaving a reduced, but sufficient, time window for analysis before substantial actin cytoskeleton recovery (Supplementary Fig. S4C). As shown in Fig. 5E, CD treatment strongly reduced the subpopulation of actin response–competent target cells by 3-fold. Along with this effect, CD treatment significantly increased the overall average level of GzB in conjugated target cells, indicating that the actin response was causally linked to GzB level reduction (Fig. 5F). To rule out any potential effect of residual amounts of CD on NK-cell activity, we also quantified GzB levels in target cells in which the actin response was genetically impaired via N-WASP or CDC42 knockdown (see Fig. 4). Consistent with the above data, N-WASP and CDC42 depletion significantly increased the overall average level of GzB in target cells by about 2-fold (Fig. 5G). Stratifying the data according to the presence or absence of an actin response revealed that the fraction of cells that resisted F-actin disruption and responded to NK attack by synaptic actin accumulation maintained reduced levels of GzB (Supplementary Fig. S5). Collectively, our data indicate that the actin response protects target cells from lysis by limiting GzB accumulation.

### The actin response is similarly induced by donor-derived NK-cell–mediated lysis

We asked whether the protection of breast cancer cells by the actin response was restricted to cytotoxicity induced by the NK-92MI cell line used in this study. To address this question, primary NK cells were isolated from buffy coats of five human donors by negative selection (>99% purity; Supplementary Fig. S6), and they were used in the subsequent analyses as effector cells. First, we evaluated primary NK-cell cytotoxicity against the MCF-7 and MDA-MB-231 cell lines (Fig. 6A). As expected, donor-derived NK cells exhibited reduced cytotoxic activity compared with the highly cytotoxic NK-92MI cell line, and only modest target cell killing (1%–10%) was achieved at an E:T ratio of 1:1. However, significant target cell death (5%–33%) was induced at an E:T ratio of 5:1, confirming that isolated primary NK cells were functional. Despite interindividual variability in the cytotoxic potential, NK cells from all five donors more effectively killed MCF-7 cells when compared with MDA-MB-231 cells. Consistent with our previous data, confocal microscopy revealed that a majority of MDA-MB-231 cells conjugated with primary NK cells exhibited an actin response (Fig. 6B), whereas most MCF-7 cells did not. Quantitative analysis using imaging flow cytometry analyses established that the actin response was at least twice as frequent in MDA-MB-231 cells (60%–76%) as compared with MCF-7 cells (26%–37%; Fig. 6C). In addition, for each of the combinations of the five sources of primary NK cells and the two target cell lines, we found significantly lower GzB levels in target cells exhibiting an actin response when compared with those without an actin response (Fig. 6D and E). In conclusion, the actin response and its protective effects were fully recapitulated using donor-derived primary NK cells as effector cells.

### Discussion

Tumor escape from cytotoxic immune cells is a major hurdle for achieving efficacious immunotherapies. Here, we demonstrate a critical role for the actin cytoskeleton in driving breast cancer cell resistance to NK-cell–mediated lysis. Using high-throughput imaging flow cytometry, we found that common tumor cell lines contain two subpopulations of cells differing in their capacity to respond to NK-cell attack via fast and prominent accumulation of AFs near the IS. Remarkably, the rate of the "actin response" in a given cell line is inversely correlated with the overall susceptibility of this cell line to NK-cell–mediated lysis. Live-cell imaging provided direct evidence that tumor cells exhibiting an actin response survive NK-cell attack and remain alive after immune cell detachment, while tumor cells without an actin response are efficiently lysed. Accordingly, apoptosis in NK-cell–conjugated target cells is markedly reduced in the actin response–competent cell subpopulation. Moreover, inhibition of the actin response is sufficient to convert the initially resistant MDA-MB-231 cell line into a highly susceptible phenotype. Altogether, these findings demonstrate a causal relationship between the actin response and resistance to NK cells.

The actin response is a remarkably fast and localized process that takes place almost immediately after physical contact between the target and effector cells. Tracking individual cell conjugates over time revealed that the actin response lasts throughout the entire period of interaction and rapidly stops after effector cell detachment. This suggests a model in which a signal from the IS is transmitted to the proximal tumor cell cortex where it induces sustained actin polymerization. Although the upstream components of the signaling pathway remain to be identified, the robust inhibition of the actin response induced by N-WASP or CDC42 knockdown suggests that the ARP2/3 complex is a key downstream effector responsible for the burst of actin polymerization following NK-cell attack. The role of N-WASP and CDC42 in driving ARP2/3 complex-dependent actin polymerization at the membrane has been extensively documented (37, 38). Notably, CDC42 is a key regulator of membrane protrusions (such as filopodia) and polarity (39, 40). Consistent with this, the actin response is associated with spike-like projections (Fig. 1C and E). Similar to filopodia or invadopodia, actin nucleators of the formin family (41) and AF crosslinking proteins, such as fascin (42) or CSRP2 (43), are likely to be required for the extension of actin response-associated protrusions.

From a functional standpoint, the actin response was associated with a significant reduction in GzB levels in target cells. Moreover, inhibiting the actin response through pharmacologic impairment of actin dynamics or genetic ablation of CDC42 or N-WASP restored high GzB levels in target cells. Interestingly, our data show that the actin response is associated with modifications in the density of NK-cell receptor ligands in the region of the synapse. Most noticeably, both MCF-7 cells and MDA-MB-231 cells with an actin response exhibited a significant increase (+100%) of HLA-A, -B, -C inhibitory ligands at the synapse as compared with the respective cells without an actin response. Such modifications provide a mechanistic insight into how the actin response mediates target cell resistance to NK-cell–mediated lysis. However, we found no association between the actin response and abnormal MTOC polarization or degranulation activity in the effector cells. These results can be explained by the lack of expression of most KIR receptors in the NK cell line (NK92MI) used in our study, which renders this cell line insensitive to HLA-A, -B, -C inhibitory ligands (34–36). Consequently, the decrease in GzB levels observed in target cells with an actin response must originate from an additional mechanism, e.g., actin response-mediated obstruction of GzB

122
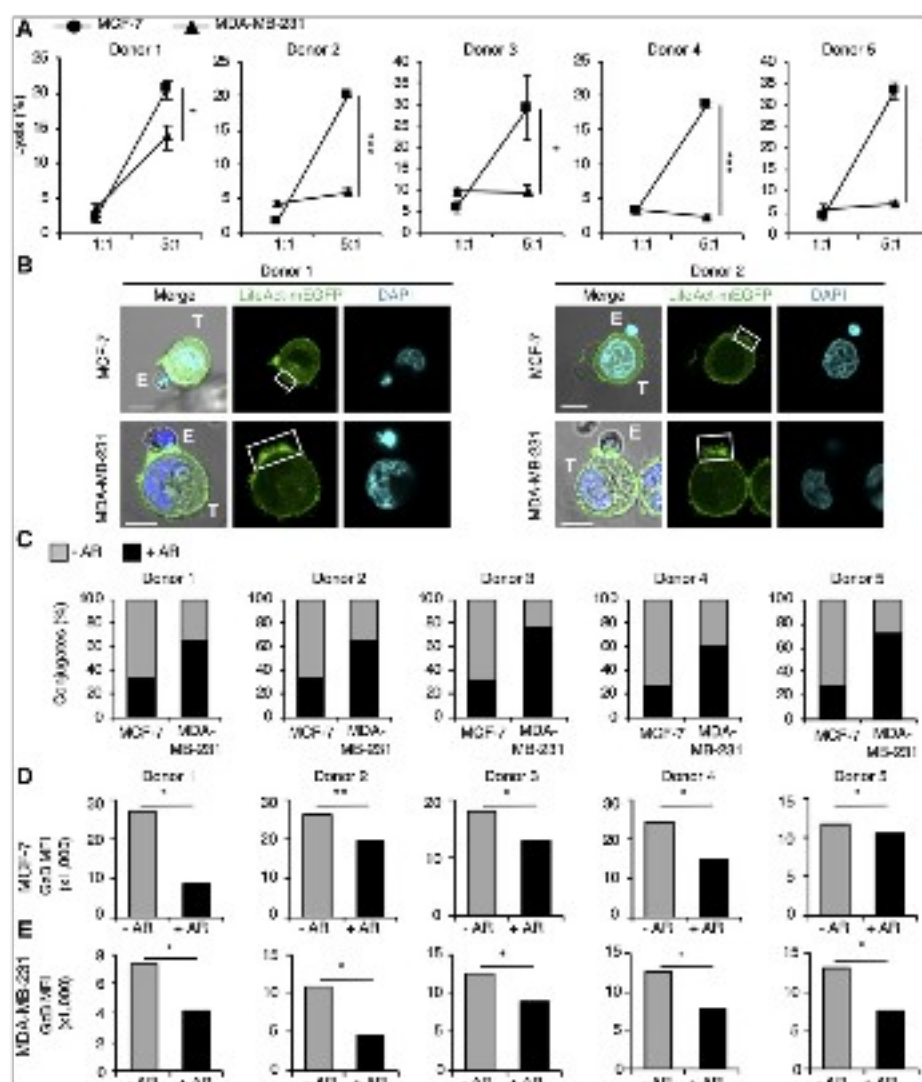
**Figure 6.**
The actin response is induced by human donor NK cells. **A,** Cytotoxicity assays performed in triplicates using NK cells isolated from five healthy donors on MCF-7 and MDA-MB-231 cells (targets) at 1:1 and 5:1 effector:target ratios. **B,** Representative confocal microscopy images showing the typical actin cytoskeleton organization in most MCF-7 (top) and MDA-MB-231 (bottom) target cells (green; T) in conjugation with primary NK cells (E) isolated from two donors. The white rectangles indicate the position of the synaptic region. Scale bar, 10 μm. **C,** Percentage of NK-cell-conjugated target cells with (black; +AR) and without (light gray; −AR) actin response in each cell line and for each donor. In all, about 300 conjugated target cells were scored. **D** and **E,** Gzβ levels in NK-cell-conjugated MCF-7 (**D**) and MDA-MB-231 (**E**) target cells with (black; +AR) and without (light gray; −AR) actin response. At least 200 conjugated target cells were scored for each cell line and each donor. Data are expressed as MFI. The two-tailed unpaired Student t test was used to determine statistical significance (*, $P < 0.05$; **, $P < 0.01$; ***, $P < 0.001$).

123

uptake into target cells or actin response-mediated GzB degradation inside target cells.

In this regard, we recently reported that autophagy promotes NK-cell–derived GzB degradation in hypoxic MCF-7 cells, thereby reducing target cell susceptibility to NK-cell–mediated lysis (44, 45). In keeping with this, inhibition of autophagy in target cells improves tumor elimination by NK cells in *in vivo* mouse models of breast cancer and melanoma (45). Considering the multiple and critical roles of the actin cytoskeleton during various steps of autophagy (46), follow-up studies should elucidate the link between the actin response and autophagy-mediated GzB degradation in tumor cells.

There is mounting evidence that EMT promotes tumor cells' escape from cytotoxic immune cells, such as CTL- and NK cells (47–50). In support of this, our data show that the mesenchymal-like breast cancer cell lines have a much higher capacity to generate an actin response as compared with epithelial-like breast cancer cell lines. Furthermore, both genetic (SNAIL or SNAIL-6A overexpression) and pharmacologic (TGFβ or TNFα treatment) induction of EMT increases tumor cell competency for the actin response and resistance to NK-cell–mediated cell death. During EMT, extensive actin cytoskeleton remodeling is required to drive morphologic and functional adaptations, such as the acquisition of migratory and invasive properties (51). Thus, EMT-associated cytoskeletal changes likely confer tumor cells with an increased capacity to undergo rapid actin remodeling in response to immune attack.

An intriguing finding of our study is that breast cancer cell lines contain two main subpopulations of cells differing in their capacity to mobilize the actin cytoskeleton in response to NK cell attack and to survive this attack. A direct and important implication of this previously unknown facet of intra-cancer cell line heterogeneity is that the apparently high susceptibility of a given cell line, such as MCF-7, may actually mask the existence of a minor subpopulation of immune-resistant (and actin response-competent) cells. This knowledge should be taken into consideration in cytotoxicity assay-based studies, and efforts should be made to target the actin response–competent cell subpopulation. The characterization of the signaling pathway(s) controlling the actin response and the identification of druggable molecular targets to impair this process are promising future directions. These efforts might help sensitize intrinsically resistant cancer cells to immune cell–mediated cytotoxicity and improve the efficacy of immunotherapies.

## Disclosure of Potential Conflicts of Interest

## Authors' Contributions

Conception and design: A. Al Absi, B. Janji, C. Thomas
Development of methodology: A. Al Absi, C. Guerin
Acquisition of data (provided animals, acquired and managed patients, provided facilities, etc.): A. Al Absi, H. Wurzer, C. Guerin, C. Hoffmann, F. Moreau, X. Mao, J. Brown-Clay, R. Petrolli, C. Pou Casellas
Analysis and interpretation of data (e.g., statistical analysis, biostatistics, computational analysis): A. Al Absi, C. Guerin, C. Hoffmann, J.-P. Thiery, G. Berchem, C. Thomas
Writing, review, and/or revision of the manuscript: A. Al Absi, H. Wurzer, J. Brown-Clay, J.-P. Thiery, S. Chouaib, G. Berchem, B. Janji, C. Thomas
Administrative, technical, or material support (i.e., reporting or organizing data, constructing databases): M. Dieterle
Study supervision: A. Al Absi, B. Janji, C. Thomas

## Acknowledgments

## References

1. Smyth MJ, Hayakawa Y, Takeda K, Yagita H. New aspects of natural-killer-cell surveillance and therapy of cancer. Nat Rev Cancer 2002; 2:850–61.
2. Vivier E, Ugolini S, Blaise D, Chabannon C, Brossay L. Targeting natural killer cells and natural killer T cells in cancer. Nat Rev Immunol 2012; 12:239–52.
3. Malmberg KJ, Carlsten M, Björklund A, Sohlberg E, Bryceson YT, Ljunggren HG. Natural killer cell-mediated immunosurveillance of human cancer. Semin Immunol 2017;31:20–9.
4. Long EO, Kim HS, Liu D, Peterson ME, Rajagopalan S. Controlling natural killer cell responses: integration of signals for activation and inhibition. Annu Rev Immunol 2013;31:227–58.
5. Smyth MJ, Cretney E, Kelly JM, Westwood JA, Street SE, Yagita H, et al. Activation of NK cell cytotoxicity. Mol Immunol 2005;42:501–10.
6. Vivier E, Tomasello E, Baratin M, Walzer T, Ugolini S. Functions of natural killer cells. Nat Immunol 2008;9:503–10.
7. Moretta A, Marcenaro E, Sivori S, Della Chiesa M, Vitale M, Moretta L. Early liaisons between cells of the innate immune system in inflamed peripheral tissues. Trends Immunol 2005;26:668–75.
8. Mocikat R, Braumüller H, Gumy A, Egeter O, Ziegler H, Reusch U, et al. Natural killer cells activated by MHC class I(low) targets prime

dendritic cells to induce protective CD8 T cell responses. Immunity 2003;19:561–9.
9. Walzer T, Dalod M, Vivier E, Zitvogel L. Natural killer cell-dendritic cell crosstalk in the initiation of immune responses. Expert Opin Biol Ther 2005;5Suppl 1:S49–59.
10. Rosenberg SA, Lotze MT, Muul LM, Leitman S, Chang AE, Ettinghausen SE, et al. Observations on the systemic administration of autologous lympho-kine-activated killer cells and recombinant interleukin-2 to patients with metastatic cancer. N Engl J Med 1985;313:1485–92.
11. Miller JS, Soignier Y, Panoskaltsis-Mortari A, McNearney SA, Yun GH, Fautsch SK, et al. Successful adoptive transfer and in vivo expansion of human haploidentical NK cells in patients with cancer. Blood 2005; 105:3051–7.
12. Geller MA, Cooley S, Judson PL, Ghebre R, Carson LF, Argenta PA, et al. A phase II study of allogeneic natural killer cell therapy to treat patients with recurrent ovarian and breast cancer. Cytotherapy 2011;13:98–107.
13. Guillerey C, Huntington ND, Smyth MJ. Targeting natural killer cells in cancer immunotherapy. Nat Immunol 2016;17:1025–36.
14. Carlsten M, Childs RW. Genetic Manipulation of NK Cells for Cancer Immunotherapy: Techniques and Clinical Implications. Front Immunol 2015;6:266.

124

15. Burga RA, Nguyen T, Zulovich J, Madonna S, Ylisastigui L, Fernandes R, et al. Improving efficacy of cancer immunotherapy by genetic modification of natural killer cells. Cytotherapy 2016;18:1410–21.
16. Marcus A, Gowen BG, Thompson TW, Iannello A, Ardolino M, Deng W, et al. Recognition of tumors by the innate immune system and natural killer cells. Adv Immunol 2014;122:91–128.
17. Hanahan D, Weinberg RA. Hallmarks of cancer: the next generation. Cell 2011;144:646–74.
18. Katz P, Zaytoun AM, Lee JH Jr. Mechanisms of human cell-mediated cytotoxicity. III. Dependence of natural killing on microtubule and micro-filament integrity. J Immunol 1982;129:2816–25.
19. Butler B, Cooper JA. Distinct roles for the actin nucleators Arp2/3 and hDia1 during NK-mediated cytotoxicity. Curr Biol 2009;19:1886–96.
20. Orange JS, Roy-Ghanta S, Mace EM, Maru S, Rak GD, Sanborn KB, et al. IL-2 induces a WAVE2-dependent pathway for actin reorganization that enables WASp-independent human NK cell function. J Clin Invest 2011;121:1535–48.
21. Brown AC, Dobbie IM, Alakoskela JM, Davis I, Davis DM. Super-resolution imaging of remodeled synaptic actin reveals different synergies between NK cell receptors and integrins. Blood 2012;120:3729–40.
22. Mace EM, Dongre P, Hsu HT, Sinha P, James AM, Mann SS, et al. Cell biological steps and checkpoints in accessing NK cell cytotoxicity. Immunol Cell Biol 2014;92:245–55.
23. Orange JS, Harris KE, Andzelm MM, Valter MM, Geha RS, Strominger JL. The mature activating natural killer cell immunologic synapse is formed in distinct stages. Proc Natl Acad Sci USA 2003;100:14151–6.
24. Mentlik AN, Sanborn KB, Holzbaur EL, Orange JS. Rapid lytic granule convergence to the MTOC in natural killer cells is dependent on dynein but not cytolytic commitment. Mol Biol Cell 2010;21:2241–56.
25. Rak GD, Mace EM, Banerjee PP, Svitkina T, Orange JS. Natural killer cell lytic granule secretion occurs through a pervasive actin network at the immune synapse. PLoS Biol 2011;9:e1001151.
26. Mace EM, Orange JS. Dual channel STED nanoscopy of lytic granules on actin filaments in natural killer cells. Commun Integr Biol 2012;5:184–6.
27. Mace EM, Wu WW, Ho T, Mann SS, Hsu HT, Orange JS. NK cell lytic granules are highly motile at the immunological synapse and require F-actin for post-degranulation persistence. J Immunol 2012;189:4870–80.
28. Sanborn KB, Rak GD, Maru SY, Demers K, Difeo A, Martignetti JA, et al. Myosin IIA associates with NK cell lytic granules to enable their interaction with F-actin and function at the immunological synapse. J Immunol 2009;182:6969–84.
29. Mace EM, Orange JS. Lytic immune synapse function requires filamentous actin deconstruction by Coronin 1A. Proc Natl Acad Sci USA 2014;111:6708–13.
30. Riedl J, Crevenna AH, Kessenbrock K, Yu JH, Neukirchen D, Bista M, et al. Lifeact: a versatile marker to visualize F-actin. Nat Methods 2008;5:605–7.
31. Prehoda KE, Scott JA, Mullins RD, Lim WA. Integration of multiple signals through cooperative regulation of the N-WASP-Arp2/3 complex. Science 2000;290:801–6.
32. Alter G, Malenfant JM, Altfeld M. CD107a as a functional marker for the identification of natural killer cell activity. J Immunol Methods 2004;294:15–22.
33. Krzewski K, Gil-Krzewska A, Nguyen V, Peruzzi G, Coligan JE. LAMP1/CD107a is required for efficient perforin delivery to lytic granules and NK-cell cytotoxicity. Blood 2013;121:4672–83.
34. Tam YK, Maki G, Miyagawa B, Hennemann B, Tonn T, Klingemann HG. Characterization of genetically altered, interleukin 2-independent natural killer cell lines suitable for adoptive cellular immunotherapy. Hum Gene Ther 1999;10:1359–73.
35. Maki G, Klingemann HG, Martinson JA, Tam YK. Factors regulating the cytotoxic activity of the human natural killer cell line, NK-92. J Hematother Stem Cell Res 2001;10:369–83.
36. Klingemann H, Boissel L, Toneguzzo F. Natural killer cells for immuno-therapy - advantages of the NK-92 cell line over blood NK cells. Front Immunol 2016;7:91.
37. Castellano F, Montcourrier P, Guillemot JC, Gouin E, Machesky L, Cossart P, et al. Inducible recruitment of Cdc42 or WASP to a cell-surface receptor triggers actin polymerization and filopodium formation. Curr Biol 1999;9:351–60.
38. Rohatgi R, Ma L, Miki H, Lopez M, Kirchhausen T, Takenawa T, et al. The interaction between N-WASP and the Arp2/3 complex links Cdc42-dependent signals to actin assembly. Cell 1999;97:221–31.
39. Nobes CD, Hall A. Rho, rac, and cdc42 GTPases regulate the assembly of multimolecular focal complexes associated with actin stress fibers, lamellipodia, and filopodia. Cell 1995;81:53–62.
40. Kozma R, Ahmed S, Best A, Lim L. The Ras-related protein Cdc42Hs and bradykinin promote formation of peripheral actin microspikes and filopodia in Swiss 3T3 fibroblasts. Mol Cell Biol 1995;15:1942–52.
41. Schirenbeck A, Bretschneider T, Arasada R, Schleicher M, Faix J. The Diaphanous-related formin dDia2 is required for the formation and maintenance of filopodia. Nat Cell Biol 2005;7:619–25.
42. Vignjevic D, Kojima S, Aratyn Y, Danciu O, Svitkina T, Borisy GG. Role of fascin in filopodial protrusion. J Cell Biol 2006;174:863–75.
43. Hoffmann C, Mao X, Dieterle M, Moreau F, Al Absi A, Steinmetz A, et al. CRP2, a new invadopodia actin bundling factor critically promotes breast cancer cell invasion and metastasis. Oncotarget 2016;7:13688–705.
44. Viry E, Noman MZ, Arakelian T, Lequeux A, Chouaib S, Berchem G, et al. Hijacker of the antitumor immune response: autophagy is showing its worst facet. Front Oncol 2016;6:246.
45. Baginska J, Viry E, Berchem G, Poli A, Noman MZ, van Moer K, et al. Granzyme B degradation by autophagy decreases tumor cell susceptibility to natural killer-mediated lysis under hypoxia. Proc Natl Acad Sci USA 2013;110:17450–5.
46. Kast DJ, Dominguez R. The Cytoskeleton-Autophagy Connection. Curr Biol 2017;27:R318–26.
47. Akalay I, Janji B, Hasmim M, Noman MZ, André F, De Cremoux P, et al. Epithelial-to-mesenchymal transition and autophagy induction in breast carcinoma promote escape from T-cell-mediated lysis. Cancer Res 2013;73:2418–27.
48. Terry S, Buart S, Tan TZ, Gros G, Noman MZ, Lorens JB, et al. Acquisition of tumor cell phenotypic diversity along the EMT spectrum under hypoxic pressure: consequences on susceptibility to cell-mediated cytotoxicity. Oncoimmunology 2017;6:e1271858.
49. Terry S, Savagner P, Ortiz-Cuaran S, Mahjoubi L, Saintigny P, Thiery JP, et al. New insights into the role of EMT in tumor immune escape. Mol Oncol 2017;11:824–46.
50. Akalay I, Tan TZ, Kumar P, Janji B, Mami-Chouaib F, Charpy C, et al. Targeting WNT1-inducible signaling pathway protein 2 alters human breast cancer cell susceptibility to specific lysis through regulation of KLF-4 and miR-7 expression. Oncogene 2015;34:2261–71.
51. Yilmaz M, Christofori G. EMT, the cytoskeleton, and cancer cell invasion. Cancer Metastasis Rev 2009;28:15–33.

125

# Cancer Research

AAC-R  American Association
for Cancer Research

# Actin Cytoskeleton Remodeling Drives Breast Cancer Cell Escape from Natural Killer- Mediated Cytotoxicity

Antoun Al Absi, Hannah Wurzer, Coralie Guerin, et al.

| | |
|---|---|
| **Updated version** | Access the most recent version of this article at:<br>doi:10.1158/0008-5472.CAN-18-0441 |
| **Supplementary Material** | Access the most recent supplemental material at:<br>http://cancerres.aacrjournals.org/content/suppl/2018/08/08/0008-5472.CAN-18-0441.DC1 |

| | |
|---|---|
| **E-mail alerts** | Sign up to receive free email-alerts related to this article or journal. |
| **Reprints and Subscriptions** | To order reprints of this article or to subscribe to the journal, contact the AACR Publications Department at pubs@aacr.org. |
| **Permissions** | To request permission to re-use all or part of this article, use this link<br>http://cancerres.aacrjournals.org/content/early/2018/09/19/0008-5472.CAN-18-0441 .<br>Click on "Request Permissions" which will take you to the Copyright Clearance Center's (CCC)<br>Rightslink site. |

**A**

| | MCF-7 | T47D | MDA-MB-231 | Hs578T |

LifeAct-mEGFP

Actin

**B**

E-cadherin

Vimentin

GAPDH

**C**

LifeAct-mGEFP · CD56 · DAPI · BF/Mask · Merge

**D**

NK cell-MCF-7 cell doublets

| | Count | Percentage |
|---|---|---|
| Total doublets | 365 | 100 |
| - AR | 285 | 78 |
| + AR | 80 | 22 |

NK cell-MDA-MB-231 cell doublets

| | Event | Percentage |
|---|---|---|
| Total doublets | 182 | 100 |
| - AR | 50 | 27,5 |
| + AR | 132 | 72,5 |
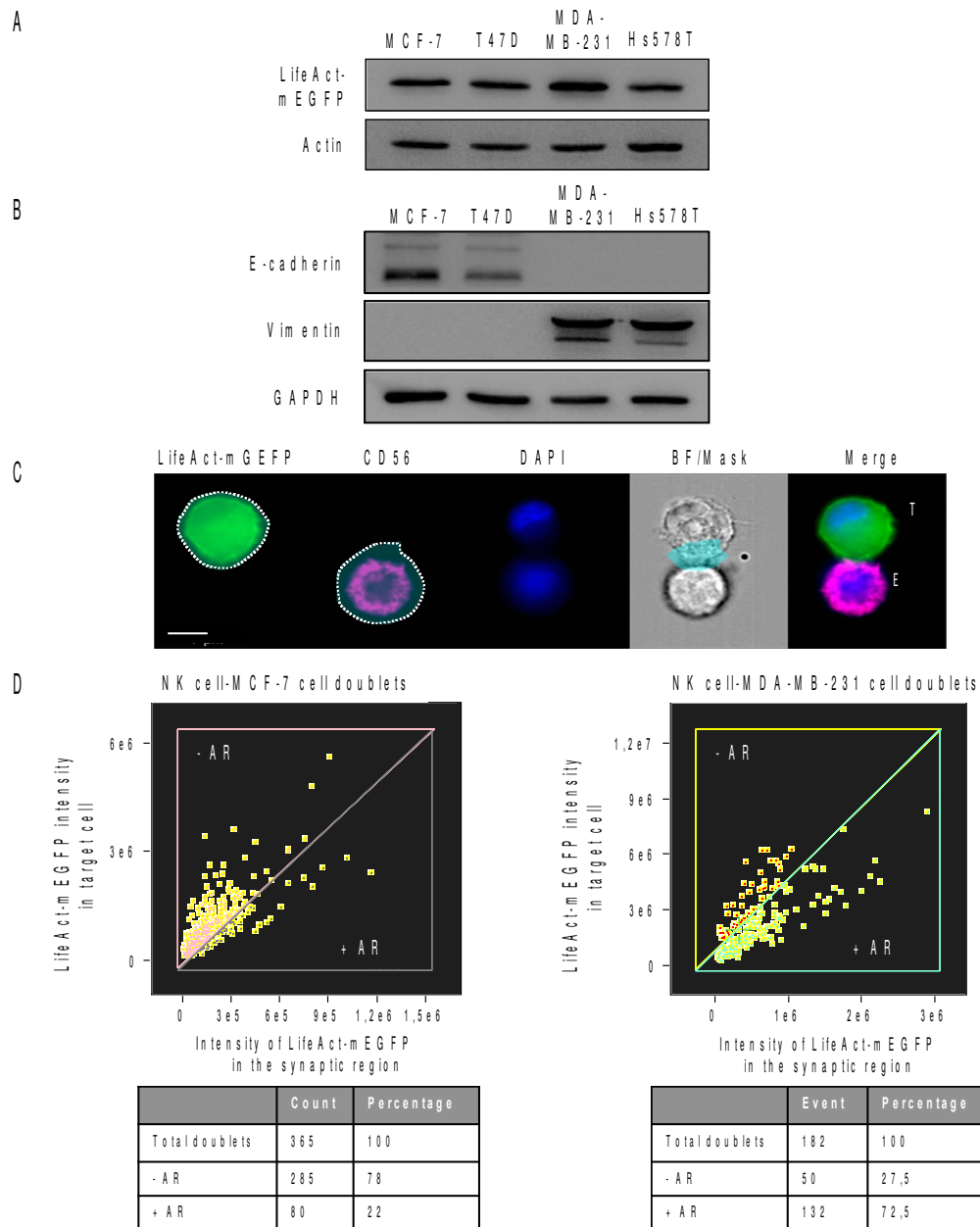
**Fig. S1. Expression of LifeAct-mEGFP, E-cadherin and vimentin in the breast cancer cell lines used in this study and quantification of the actin response using imaging flow cytometry. (A)** Breast cancer cell lines were transduced with lentivirus to stably express the actin reporter LifeAct-mEGFP. Cells were subsequently subjected to western blot analysis to evaluate LifeAct-mEGFP expression level. Actin was used as a loading control. **(B)** Expression of the epithelial marker E-cadherin and the mesenchymal marker vimentin in MCF-7, T47D, MDA-MB-231 and Hs578T breast cancer cell lines as evaluated by western blot. GAPDH was used as a loading control. **(C)** Representative images showing the masks (dark blue and dotted lines) generated by the IDEAS software and applied to the target (T) and effector (E) cells to capture the synaptic region and the actin response. The synaptic region (light blue mask on the bright field channel) is defined as the overlapping area between the target cell mask (LifeAct-mEGFP) and the NK cell mask (CD56-PE-Cy7). Scale bar, 7 ∝m. **(D)** Method to determine the percentage of target cells with (+AR) and without (-AR) an actin response. An example is given for both MCF-7 and MDA-MB-231 cell lines. LifeAct-mEGFP intensity in the synaptic region was plotted against LifeAct-mEGFP intensity in the whole target cell. The cells with enriched F-actin in the synaptic region were scored as positive for the actin response.
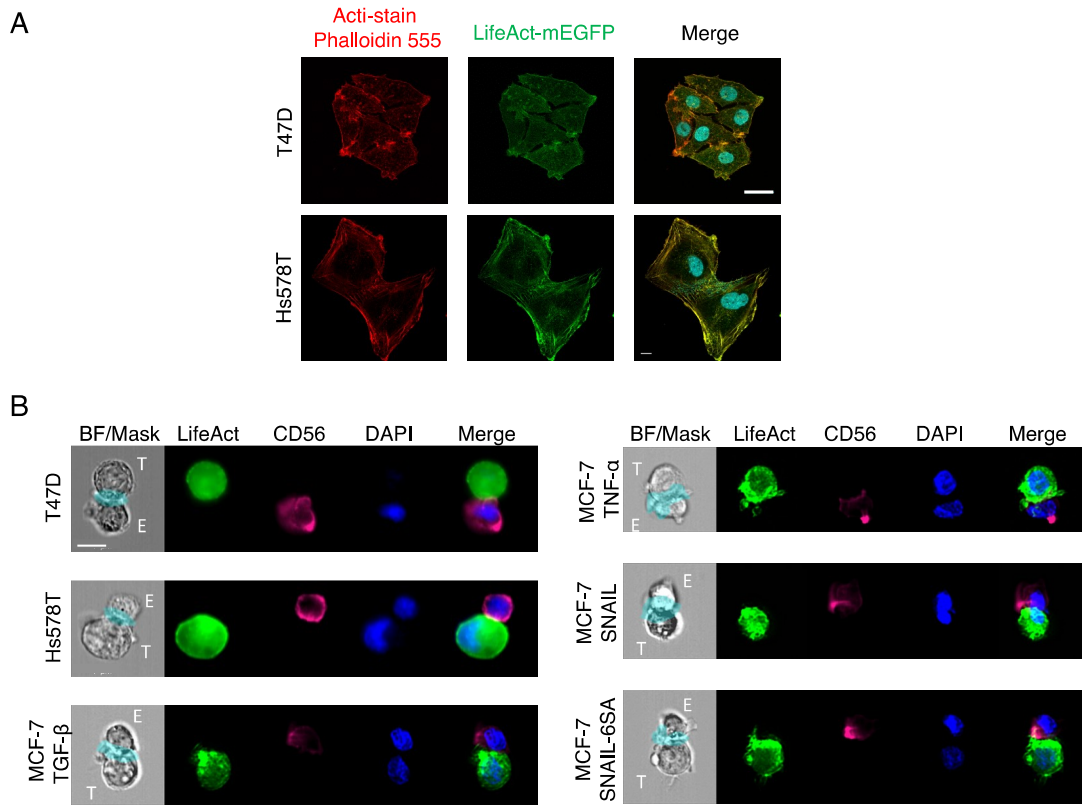
**Fig. S2. Actin response in LifeAct-expressing breast cancer cells as visualized by imaging flow cytometry.**
**(A)** Confocal microscopy images showing the effectiveness and localization of LifeAct-mEGFP transduction in T-47D and Hs578T breast cancer cells. Cells were stained with Acti-stain 555 Phalloidin (red) and DAPI (cyan). The yellow-orange signal in merge images shows extensive co-localization between LifeAct-mEGFP and the actin probe. Scale bar, 20 μm. The corresponding data for MCF-7 and MDA-MB-231 cells are presented in Fig. 1A. **(B)** Representative imaging flow cytometry panels used to quantify the actin response in T-47D and Hs578T, and in MCF-7 cells treated with TGF-β or TNF-α or transfected with SNAIL expressing vectors. An example is given for each breast cancer cell line used in this study. Only the situation ('actin response' or 'no actin response') observed in most cells of each cell line is illustrated. Scale bar, 7 μm.

128
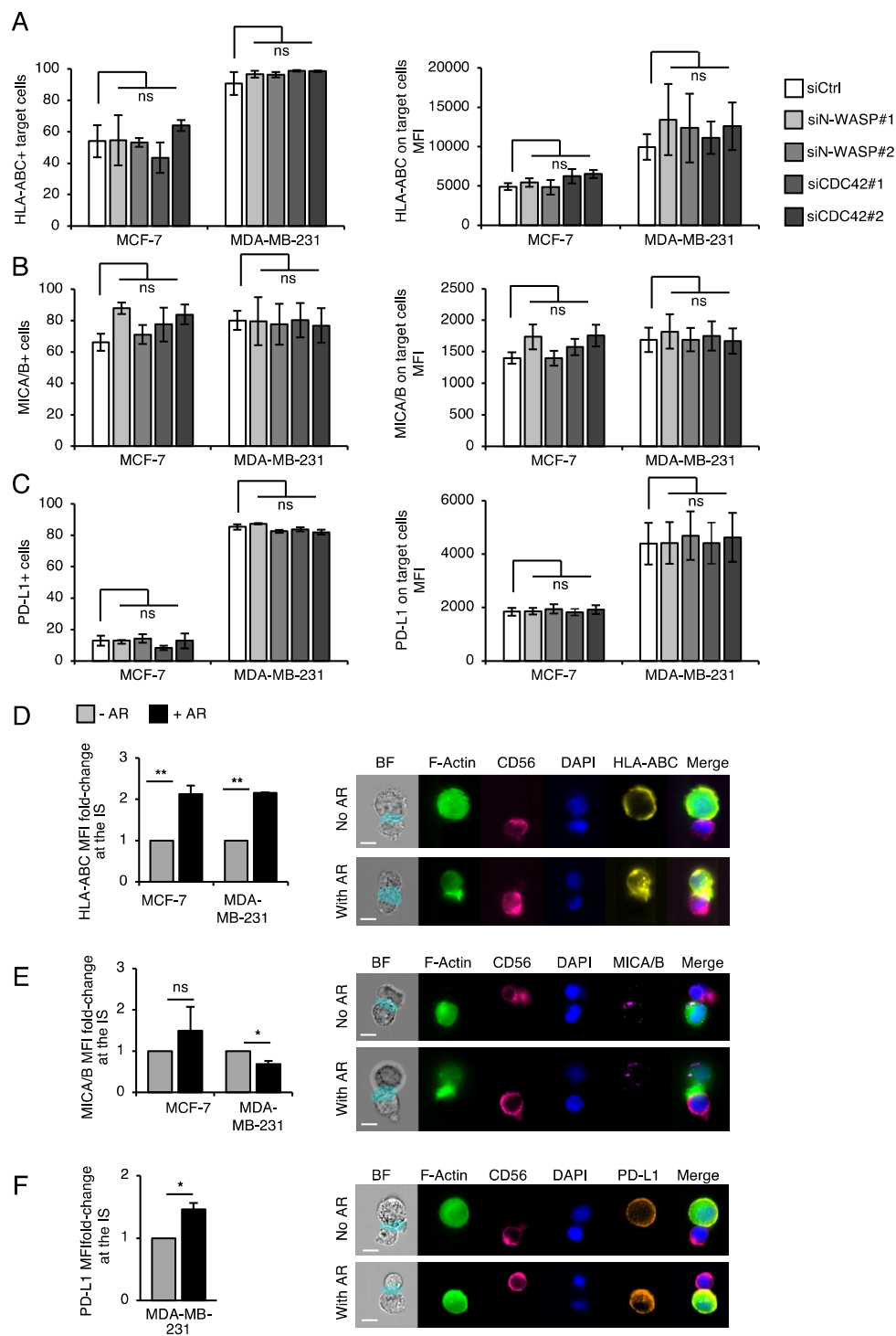
**Fig. S3. Relative expression of HLA-A, -B, -C, MICA/B and PD-L1 ligands on MCF-7 and MDA-MB-231 cells. (A-C)** Percentage of cells positive for (left panels) and relative expression of (right panels) HLA-A, -B, -C (A), MICA/B (B) and PD-L1 (C) at the surface of MCF-7 and MDA-MB-231 cells 48 hours after N-WASP or CDC42 siRNA transfection. Data originate from three independent experiments and are expressed as percentage of positive cells and as average MFI values. **(D-F)** Relative expression of ligands at the synaptic region of MCF-7 and MDA-MB-231 cells with an actin response (black, +AR) or without an actin response (light grey, -AR; set to 1) as evaluated by imaging flow cytometry. The right panels show typical examples of imaging flow cytometry images obtained from conjugates between NK92MI cells and MDA-MB-231 cells. Data originate from three independent experiments and are expressed as FMI fold changes and relative to target cells without an actin response (set to 1). Scale bar, 7 $\mu$m. The two-tailed unpaired Student's $t$-test was used to measure the statistical significance. * denote $p < 0.05$; ** $p < 0.01$; ns: non-significant.

A    B    C

Acti-stain 555 Phalloidin
DAPI

+ DMSO, 30 min    + CD (0.5 µM), 30 min    + CD (0.5 µM), 30 min
+ Wash
+ Recovery, 60 min
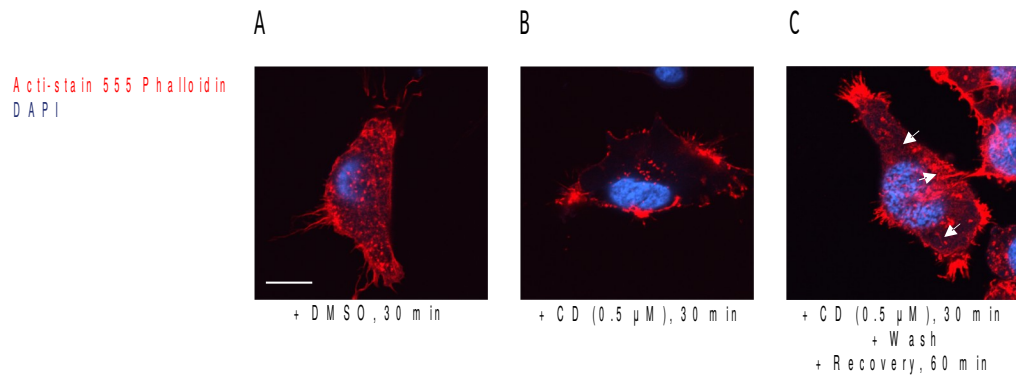
**Fig. S4. Cytochalasin D-mediated depolymerization of the actin cytoskeleton in breast cancer cells.** Cytochalasin D (CD) treatment (concentration and duration) was optimized to efficiently promote F-actin disruption in target cells without affecting cell viability. Only MDA-MB-231 cells are shown here. **(A-C)** Typical actin cytoskeleton organization in control, DMSO-treated, cells (A), CD-treated cells (B), and CD-treated cells after 1 hour recovery (C). Arrows indicate the reappearance of F-actin based structures. Scale bar, 10 ∝m.
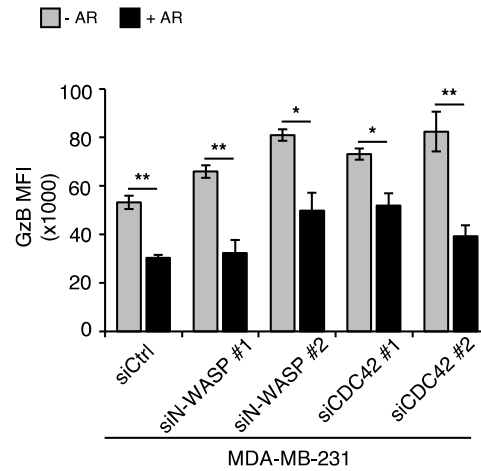
**Fig. S5. GzB levels in MDA-MB-231 cells with and without actin response after N-WASP- and CDC42-depletion.** MDA-MB-231 cells were transfected with a control siRNA or different siRNAs targeting N-WASP or CDC42. GzB levels in NK cell-conjugated target cells were quantified using imaging flow cytometry and the results were stratified by whether (black, +AR) or not (light grey, -AR) the target cells generated an actin response. At least 200 conjugated target cells were scored for each siRNA condition. Data originate from three independent experiments and are expressed as mean fluorescence intensities (MFI). The two-tailed unpaired Student's $t$-test was used to determine statistical significance (* $p < 0.05$, ** $p < 0.01$).
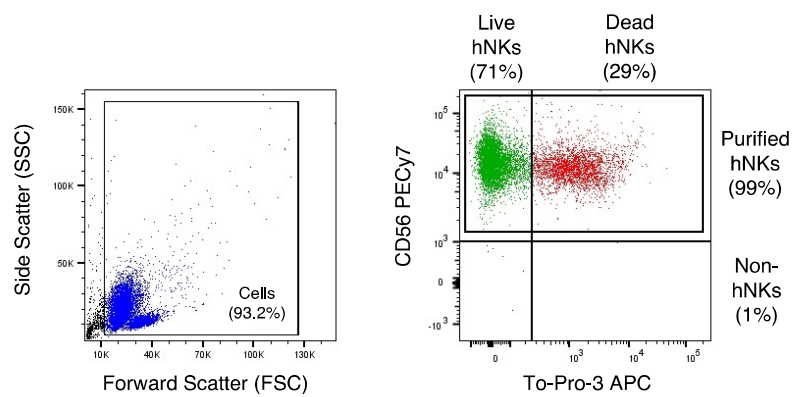
**Fig. S6 │ Purity and viability of primary NK cells isolated from healthy donors.** Primary NK cells were isolated from enriched PBMC fractions via negative selection as indicated in the 'Materials and Methods' section. The purity and viability of isolated primary NK cells used in this study was checked via flow cytometry using the NK cell surface molecular marker CD56 and TO-PRO-3 staining, respectively. The primary NK cells isolated from donor 1 are shown as a representative example.

**Supplementary Materials and Methods**

**Western blot analysis**

Protein extracts were isolated in RIPA lysis buffer (Millipore) supplemented with a protease and phosphatase inhibitor mixture (Roche). The Bradford protein assay was used to determine the protein concentration (5000006; Bio-Rad). Next, 30 µg of protein lysate was separated by SDS-PAGE on a 12% SDS agarose gel and transferred to a PVDF membrane (Millipore). Membranes were immunoblotted with monoclonal rabbit anti-N-WASP (#4848, Cell Signaling), polyclonal rabbit anti-CDC42 (#2462, Cell Signaling), monoclonal mouse anti-E-cadherin (#610182, BD biosciences), monoclonal mouse anti-vimentin (#SC-6260), monoclonal rabbit anti-GAPDH (#5174S, Cell Signaling), polyclonal rabbit anti-actin (#A2066, SIGMA), polyclonal rabbit anti-SNAI1 (#sc-28199, Santa Cruz), or polyclonal rabbit anti-GFP (#A11122, Invitrogen) antibodies overnight. Membranes were washed and incubated with HRP-conjugated goat anti-rabbit IgG. Protein bands were detected using the SuperSignal™ West Femto Chemiluminescent Substrate (Thermo Scientific) and visualized by ImageQuant LAS 4000 (GE Healthcare Life Science).

**Cell labelling and confocal microscopy**

For the conjugate formation assay, NK-92MI cells were counted, re-suspended and stained with PKH26 dye (PKH26 red fluorescent cell linker kit, Sigma-Aldrich) for 5 minutes at room temperature. NK-92MI cells were washed twice with RPMI medium containing FBS and horse serum and subsequently incubated with 1 x $10^5$ target cells (E:T ratio of 2:1) per 200 µl of medium. Conjugates were plated on poly-L-lysine-coated chambered coverslips (µ-Slide 8 Well, Ibidi) for 45 minutes prior to fixation with 2% paraformaldehyde (PFA, Thermo Fisher Scientific) for 10 minutes. Cells were washed with PBS, permeabilized with 0.1% Triton X-100 (Sigma-Aldrich), and counterstained with DAPI (0.3 µg/ml, Sigma-Aldrich). For target cell staining, 1 x $10^5$ target cells were seeded into chambered coverslips. The next day, cells were washed twice, fixed with 4% PFA, permeabilized with 0.1% Triton X-100 and immunostained with anti-vimentin (Santa Cruz) or anti-E-cadherin (BD biosciences) primary antibodies, followed by secondary goat anti-mouse Alexa Fluor 488 antibodies for detection. For AF visualisation, cells were co-stained with Acti-stain 488 Phalloidin (Cytoskeleton) and DAPI. For assays with cytochalasin D, cells were stained with Acti-stain 555 Phalloidin (Cytoskeleton). For live-cell imaging, target cells were seeded into chambered coverslips (Ibidi) at a concentration of 1 x $10^5$ cells per well. Slides were mounted within a temperature-controlled chamber maintained at 37° C under a constant atmosphere of 5% $CO_2$. NK cells were labelled with the PKH26 Fluorescent Cell

linker (Red) for 5 minutes at RT and washed three times. At the beginning of recording, $2 \times 10^5$ NK cells were added to each slide. Images of conjugates were acquired on a laser scanning confocal microscope (LSM880 FastAiry, Carl Zeiss) with an oil immersion Plan-Apochromat 63x objective. 3D projections and time lapse movies were assembled using Zen imaging software (ZEISS) and NIH ImageJ software(49), respectively.

## Actin quantification

For each cell line, 25 conjugates from three independent experiments were analyzed for actin cytoskeleton accumulation. To quantify actin filament enrichment at the target side of the IS, the target cell image was divided into two equal regions of interest (one at the synapse and one at the opposite side). Florescence intensity of LifeAct-mEGFP was measured using the ROI tool of ImageJ software. Results were reported as the fold increase in the intensity of LifeAct-mEGFP at the synaptic region divided by the same intensity at the distal region.

## Cytotoxicity analysis

Target cells expressing LifeAct-mEGFP were incubated with effector cells at an E:T ratio of 1:1 or 5:1 for 4 hours at 37° C. Before analysis, TO-PRO®-3 (Invitrogen) was added to assess the percentage of death target and then samples were immediately analyzed by flow cytometry (FACSCanto; BD Biosciences).

## Degranulation assay

NK-92MI cells were incubated for 4 hours at 37°C alone or with LifeAct-mEGFP-expressing target cells (5:1). NK cells incubated without target cells were used as a negative control. The NK cell-susceptible K-562 cell line (kindly provided by the NORLUX Neuro-Oncology Laboratory from LIH; ATCC) was used as a positive control for the assay. To block intracellular protein transport and CD107 degradation, monensin-containing GolgiStop reagent (BD Biosciences) was added to samples after 1 hour of incubation at a concentration of 6 µg/ml. Two hours later, cells were stained with anti-human CD107a-APC (BD bioscience, clone: H4A3) and samples were immediately analyzed by flow cytometry (FACSCanto; BD Biosciences).

## 1.3. Discussion of the article in French

L'échappement tumoral aux cellules immunitaires cytotoxiques est un obstacle majeur à de nombreuses immunothérapies. Dans cette étude, nous démontrons le rôle critique du cytosquelette d'actine dans la mise en place de la résistance des cellules du cancer du sein à la lyse induite par les cellules NKs. Grâce à l'utilisation de la cytométrie de flux en image à haut débit, nous avons trouvé que les lignées cellulaires tumorales communes contiennent deux sous-populations de cellules différant par leur capacité à répondre à l'attaque des cellules NKs via une accumulation forte et rapide d'actine filamenteuse dans la région de la synapse. De façon Remarquable, le taux de ''réponse actine'' dans une lignée cellulaire donnée est inversement corrélé avec la susceptibilité globale de cette lignée cellulaire à la lyse induite par les cellules NKs. L'imagerie en temps réel de cellules vivantes a démontré de manière directe que les cellules tumorales présentant une réponse actine survivent à l'attaque des cellules NKs et restent en vie après la séparation des conjugués, tandis que les cellules tumorales sans réponse actine sont efficacement lysées. Ces observations sont en accord avec nos analyses indiquant que le taux d'apoptose dans les cellules cibles conjuguées aux cellules NKs est considérablement réduit dans la sous-population cellulaire compétente pour la réponse actine. De plus, l'inhibition de la réponse actine suffi à convertir les lignées cellulaires résistantes, telles que 1001 et MDA-MB-231, en un phénotype hautement susceptible. Au total, ces résultats établissent un lien de causalité entre la réponse d'actine et la résistance aux cellules NKs.

La réponse d'actine est un processus remarquablement rapide et localisé qui a lieu presque immédiatement après le contact physique entre les cellules cibles et les cellules effectrices. Le suivi des conjugués cellulaires individuels au cours du temps a révélé que la réponse actine dure pendant toute la durée de l'interaction et s'arrête rapidement après le détachement de la cellule effectrice. Ceci suggère un modèle dans lequel un signal de la synapse est transmis vers le cortex des cellules tumorales où il induit une polymérisation active et continue d'actine. Bien que les composants en amont de la voie de signalisation restent à identifier, l'inhibition robuste de la réponse actine induite par le knockdown de N-WASP ou de Cdc42 suggère que le complexe ARP2/3 est un effecteur clé responsable de la polymérisation de l'actine suite à l'attaque des cellules NKs. Le rôle de N-WASP et de Cdc42 dans la polymérisation de l'actine dépendante du complexe ARP2/3 à la membrane a été largement documenté. Notamment, Cdc42 est un régulateur clé des

projections membranaires (comme les filopodes) et de la polarité cellulaire. Il est intéressant de noter que la réponse actine est associée à des projections membranaires de type filopodes. Comme dans les filopodes, les nucléateurs d'actine de la famille des formines et des protéines de bundling, telles que la fascin, sont probablement nécessaires pour l'extension des projections membranaires associées à la réponse d'actine.

D'un point de vue fonctionnel, la réponse actine est associée à une réduction significative des niveaux de GzB dans les cellules cibles. De plus, l'inhibition pharmacologique ou génétiques (ablation de Cdc42 ou N-WASP) de la réponse actine restaure des niveaux élevés de GzB dans les cellules cibles. En revanche, nous n'avons trouvé aucune association entre la réponse d'actine et une polarisation anormale du MTOC ou le processus de dé-granulation au niveau des cellules effectrices. Ceci sugère un mécanisme où la réponse actine obstrue la pénétration du GzB dans les cellules cibles et/ou facilite la dégradation du GzB à l'intérieur des cellules cibles plutôt qu'un mécanisme où la réponse actine inhibe l'activation des cellules NKs. À cet égard, nous avons récemment rapporté que l'autophagie favorise la dégradation du GzB dérivée des cellules NKs dans les cellules MCF-7 hypoxiques, réduisant ainsi la sensibilité des cellules cibles à la lyse induite par les cellules NKs. Dans le même sens, l'inhibition de l'autophagie dans les cellules cibles améliore l'élimination des tumeurs par les cellules NKs dans des modèles murins in vivo de BC et de mélanome. Considérant les rôles multiples et critiques du cytosquelette d'actine dans les différentes étapes de l'autophagie, les études futures devront élucider le lien entre la réponse d'actine et la dégradation de GzB par l'autophagie dans les cellules tumorales.

Le rôle de l'EMT dans l'évasion des cellules tumorales aux cellules immunitaires cytotoxiques, telles que les cellules T et NKs est de plus en plus reconnu. Nos résultats indiquent que les lignées cellulaires de type mésenchymal ont une capacité largement supérieure aux lignées de type épithelial à générer une réponse actin. En outre, une EMT expérimentale augmente à la fois la compétence des cellules tumorales à la réponse actine et la résistance à la lyse induite par les cellules NKs. Au cours de l'EMT, de vastes modifications du cytosquelette d'actine sont nécessaires pour conduire les adaptations morphologiques et fonctionnelles, telles que l'acquisition de propriétés migratrices et invasives. Ainsi, les changements de propriétés du cytosquelette d'actine (organisation, dynamique) qui accompagne le processus de l'EMT confèrent probablement aux cellules tumorales une capacité accrue à mobiliser rapidement leur actine en réponse à une attaque immunitaire.

Une observation intrigante de notre étude est que les lignées cellulaires du cancer du sein contiennent deux sous-populations de cellules différant par leur capacité à mobiliser le cytosquelette d'actine en réponse à l'attaque des cellules NKs et de survivre à cette attaque. Une implication directe et importante de cette nouvelle facette de l'hétérogénéité intra-lignée tumorale est que la susceptibilité apparemment élevée d'une lignée donnée, telle que MCF-7, peut en réalité masquer l'existence d'une sous-population mineure de cellules immuno-résistantes (et compétentes pour la réponse d'actine). Cette information devrait être prise en compte dans des études basées sur des analyses de cytotoxicité *in vitro*, et les efforts de recherche devraient se concentrés sur la sous-population cellulaire compètent pour la réponse d'actine. La caractérisation des voies de signalisation qui contrôle la réponse actine et l'identification de cibles moléculaires pour altérer ce processus sont des axes de recherche prometteurs. Les résultats pourraient contribuer au développement de nouvelles stratégies visant à accroitre la susceptibilité des cellules tumorales aux cellulaires immunitaires et à améliorer l'efficacité des immunothérapies.

## 2. The actin response facilitates autophagy-mediated degradation of Granzyme B in tumor cells (results and discussion)

In the article presented in section 1.2 of the results, we provide evidence that the actin response is associated with, and is actually required for, GzB level reduction in resistant target cells. Very interestingly, autophagy was recently proposed to promote NK cell-derived GzB degradation in hypoxic MCF-7 cells, and thereby reduce target cell susceptibility to NK cell-mediated lysis[288,409]. In keeping with this, inhibition of autophagy in target cells improves tumor elimination by NK cells in *in vivo* mouse models of BC and melanoma[303]. Considering the multiple and critical roles of the actin cytoskeleton in autophagy[317], I decided to investigate the link between the actin response and autophagy-mediated GzB degradation in tumor cells. The section below directly follows-up the article presented in section 1.2 and addresses the mechanism by which the actin response leads to a decrease in GzB levels in resistant breast cancer cells. The results and discussion have been merged and there is no separate discussion section.

### 2.1. Inhibition of autophagy reverts breast cancer cell resistance to NK cell-mediated cell lysis

First, we examined if autophagy is implicated in the resistance of normoxic breast cancer cells to NK cell-mediated cell death. To do so, MCF-7, 1001 and MBA-MB-231 cells were transfected with 2 different siRNAs targeting Beclin-1 transcripts. Beclin-1 is a key regulator of autophagy that is required for autophagic vesicle formation[302]. Beclin-1 knockdown has been previously shown to effectively inhibit autophagy in various types of cells, including cancer cells[303,313]. As shown in figure 22, western blot analysis confirmed that Beclin-1 was significantly knocked down in the three breast cancer cell lines after the transfection with the two siRNAs. We then analyzed the susceptibility of autophagy-deficient breast cancer cells to NK cell-mediated cell lysis after 4 hours incubation with NK-92MI effector cells at an effector-to-target ratio (E:T) 5:1. Cytotoxic assays revealed that the two highly resistant cell lines 1001 and MDA-MD-231 became significantly (2 to 3 times) more susceptible to NK cell-mediated lysis upon Beclin-1 knockdown. These data support that autophagy is an important mediator of breast cancer cell resistance to NK cell-mediated lysis under normoxia. In contrast, the highly

susceptible phenotype of the MCF-7 cell line was not significantly modified by Beclin-1 depletion. This result is consistent with the low basal level of autophagy reported in MCF-7 cells cultured in standard, normoxic, conditions [410]
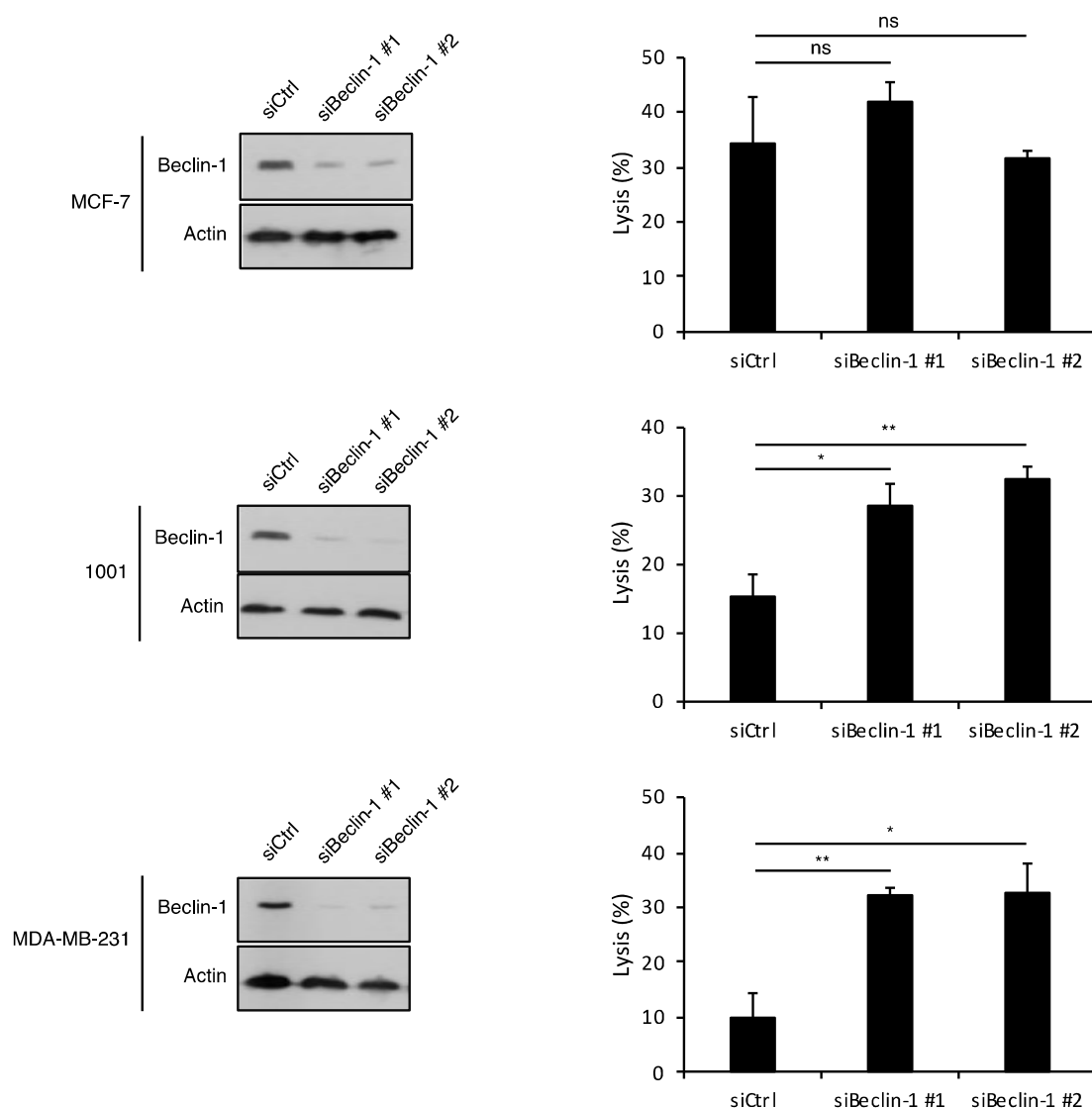


**Figure 22 | Beclin-1 knockdown reverts breast cancer cell resistant to NK cell-mediated cell lysis**

MCF-7, 1001 and MDA-MB-231 cell lines were transfected with control siRNA (siCtrl) or two different siRNAs targeting Beclin-1 (siBeclin-1 #1 and #2). Western blots (left panels) are representatives of three independent experiments and show the significant knockdown of Beclin-1 48 hours after cell line transfection. Actin is shown as a loading control. Cytotoxicity assays (right panels) were performed in triplicates with NK92MI cell as effectors at an E:T ratio 5:1. The two-tailed unpaired Student's t-test was applied to determine the statistical significance. * denotes $p < 0.05$; ** $p < 0.01$; ns: non-significant.

## 2.2. Autophagy promotes Granzyme B degradation in resistant breast cancer cells

As previously stated, autophagy was reported to promote NK cell-derived GzB degradation in hypoxic MCF-7 cells[288,409]. We hypothesized that autophagy may have a similar function in normoxic resistant breast cancer cells. To test such a hypothesis, we quantified GzB levels in control and Beclin-1-depleted MCF-7, 1001 and MDA-MB-231 cells. Target cells were incubated for 30 min with NK-92MI cells prior fixation, permeabilization and staining. Imaging flow cytometry was used to quantify GzB levels in NK cell-conjugated target cells exclusively. Our results show that Beclin-1 depletion significantly increases (by up to two times) GzB levels in both 1001 and MDA-MB-231 cell lines (Figure 23 b and c). In contrast, Beclin-1 knockdown had no effect on GzB levels in MCF-7 cells (Figure 23 a). Together these results are highly consistent with the effects of Beclin-1 depletion on tumor cell susceptibility to NK cell-mediated lysis (Figure 22). In addition, they extend the previous findings on hypoxia [288,409] and generalize autophagy-mediated GzB degradation as a general resistance mechanism against NK cell-mediated cell death. This also raises the possibility that hypoxia may increase tumour cell competency for the actin response. Although this remains speculative, it would be consistent with the fact that hypoxia is potent inducer of EMT[411] and that EMT, in turn, strongly increases the actin response rate in breast cancer cells (see Figure 3 from the article, p.129). If this turns to be right (experimental work in progress), then our data would provide a mechanistic insight into how hypoxia promotes autophagy-mediated GzB degradation (see below).

a

b

c
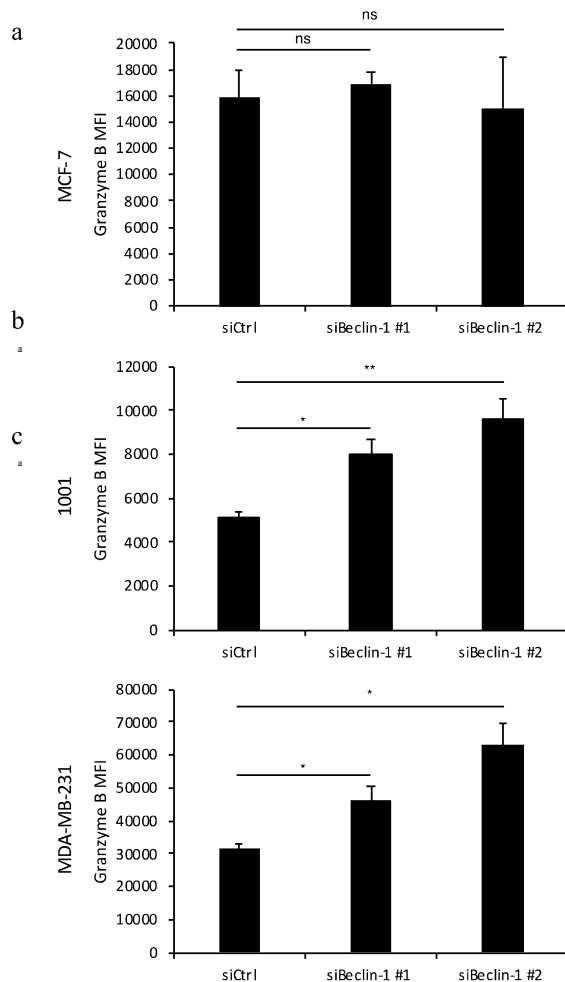
**Figure 1 | Granzyme B levels in Beclin-depleted and control breast cancer cells**

GzB levels in control (siCtrl) and Beclin-1-depleted (siBeclin-1 #1 and #2) MCF-7 (a), 1001 (b) and MDA-MB-231 (c) cells conjugated to NK cells were quantified by imaging flow cytometry. In all, about 300 target cells were measured for each condition from three independent experiments. The results are presented as mean florescence intensity (MFI) of GzB in target cells. The two-tailed unpaired Student's t-test was applied to determine the statistical significance. * denotes $p < 0.05$; ** $p < 0.01$; ns: non-significant.

## 2.3. The actin response drives autophagosome polarization toward the synaptic region (preliminary results)

The actin cytoskeleton plays central roles in intracellular trafficking by promoting the formation and transport of various types of vesicles[336]. Furthermore, evidence has emerged over the recent years that actin polymerization is critically required for the formation and transport of autophagosomes[317]. To investigate the possible link between the actin response and autophagosomes in the resistance of breast cancer cells to NK cell-mediated cell death, we analyzed autophagosome distribution in NK cell-conjugated breast cancer cells with respect to the presence or absence of an actin response. To do so, we used the autophagosomal marker LC3, imaging flow cytometry and specific masks and features in the IDEAS software for analysis. The peak mask allowed us to distinguish between cells with unspecific diffuse signal versus specific and highly localized LC3

143

puncta. The BDI R7 feature was used as it computes the intensity of bright spots at the selected region of interest that are less than 7 pixels in radius. In addition to LC3 intensity-based measurements, the spot count feature was used as a complementary method as it was shown to be a potent tool to assess the activation of autophagy[316](Figure 24).
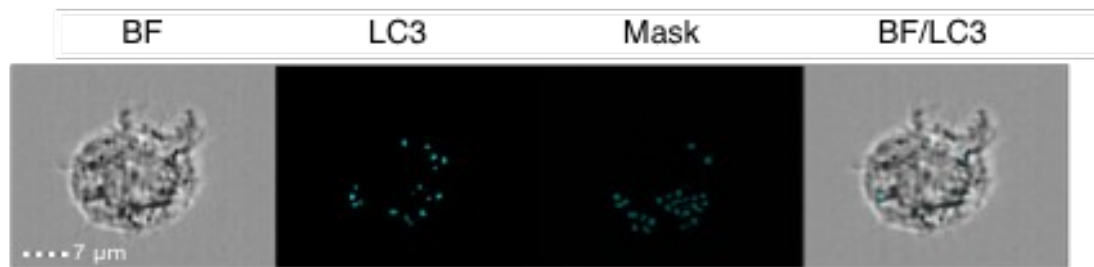


**Figure 23 | LC3 staining in breast cancer cells and the Peak mask**

Representative panel of the Peak mask generated in the IDEAS software for LC3 puncta detection. The light blue dots represent LC3 puncta in an MCF-7 cell. Scale bar, 7 μm.

MCF-7, 1001 and MDA-MB-231 cells were incubated with NK-92MI effector cells for 30 min prior to LC3 staining and analysis at the imaging flow cytometer. For each cell line, the quantity of autophagosomes in the synaptic region of target cells was compared in the subpopulations of cells with and without actin response (Figure 25a). The results obtained by the BDI and spot count quantification approaches were highly consistent (Figure 25 b and c). With all cell lines, we found that autophagosomes were significantly enriched (about 2-fold) in the synaptic region of target cells exhibiting an actin response as compared to that of target cells without actin response. We calculated that the percentage of total cancer cell autophagosomes at the synaptic region increased from < 15% in cells without actin response to > 30% in cells with an actin response. This suggests that the actin response drives autophagosome accumulation near the synapse in the cancer target cells. Such accumulation presumably increases the autophagic capacity locally, resulting in facilitated NK cell-derived GzB degradation and cancer target cell survival. Although this requires further confirmation, our preliminary data suggest that there is no difference in autophagosome quantity in target cells with and without actin response (data not shown). We accordingly propose that the actin response drives autophagosome recruitment toward the synaptic region rather than autophagosome

formation. Nevertheless, future work should better characterize the rate of autophagosome formation in chloroquine-treated cells[412].
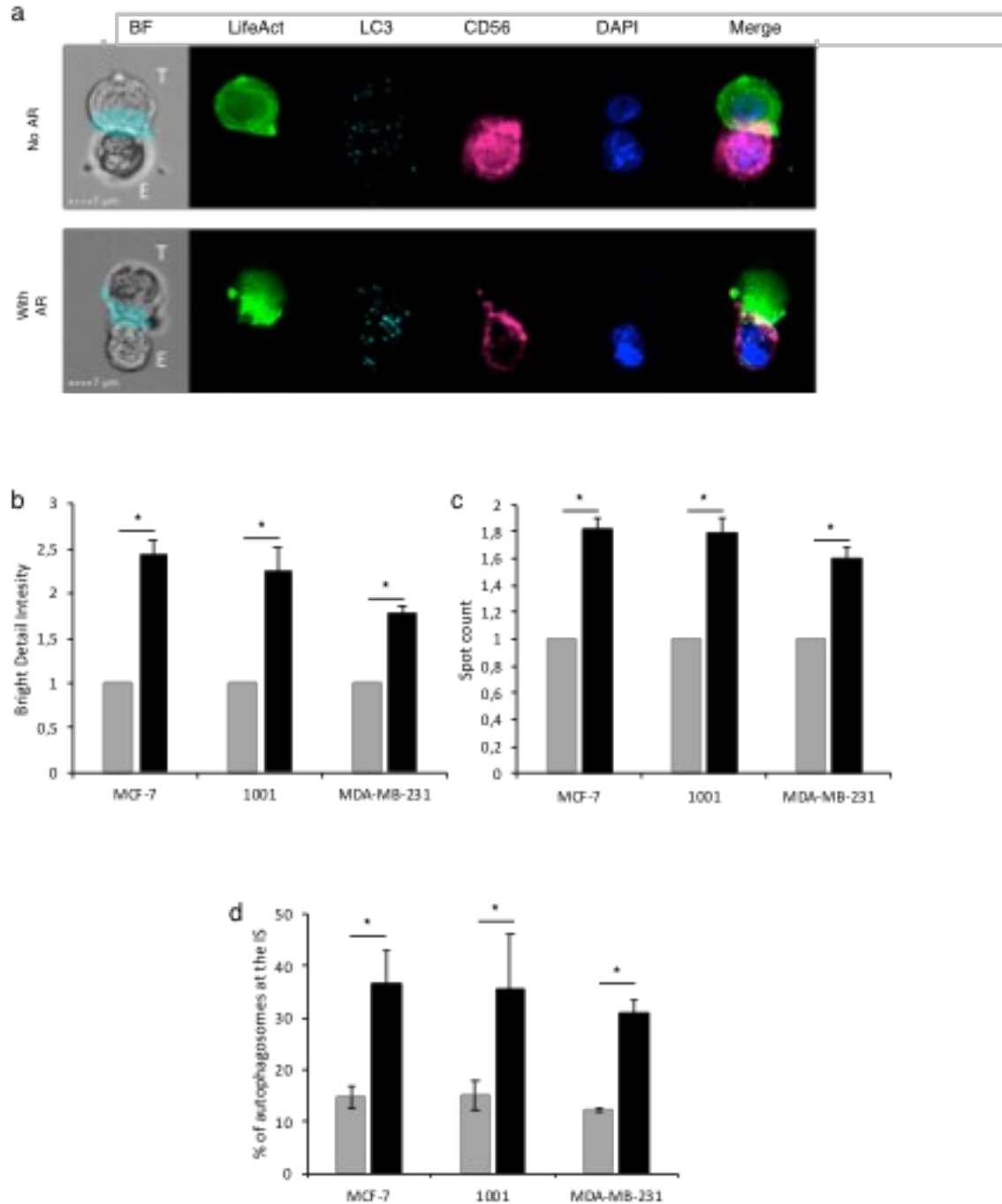
**Figure 24 | The actin response is associated with autophagosome polarization towards the synaptic region in target cells**

a) Representative panels obtained by imaging flow cytometry showing autophagosome distribution in MDA-MB-231 cells without (no AR, upper panels) and with (with AR, lower panels). The cyan area in the right field image depicts the mask applied to capture the synaptic region in the target cell. Scale bar, 7 μm. b) and c) relative autophagosome concentration at the synaptic region of MCF-7, 1001 and MDA-MB-231 cells with (+AR) or without (-AR; set to 1) actin response as evaluated by the BDI (b) and spot count (c) approaches. d) Percentage of total cancer cell autophagosomes in the synaptic region of MCF-7, 1001 and MDA-MB-231 cells with (+AR) or without AR (-AR), as calculated by the BDI approach. Data are graphed as mean ± SE from three independent experiments including a total of 300 conjugates. The two-tailed unpaired Student's t-test was applied to determine the statistical significance. * denotes $p < 0.05$.

The above data were validated using primary NK cells isolated from five healthy donors (Fig. 26). Both the BDI and spot count quantification approaches confirmed a higher level of autophagosome in the synaptic region of NK cell-conjugated 1001 cells exhibiting an actin response, as compared to that of target cells without actin response.
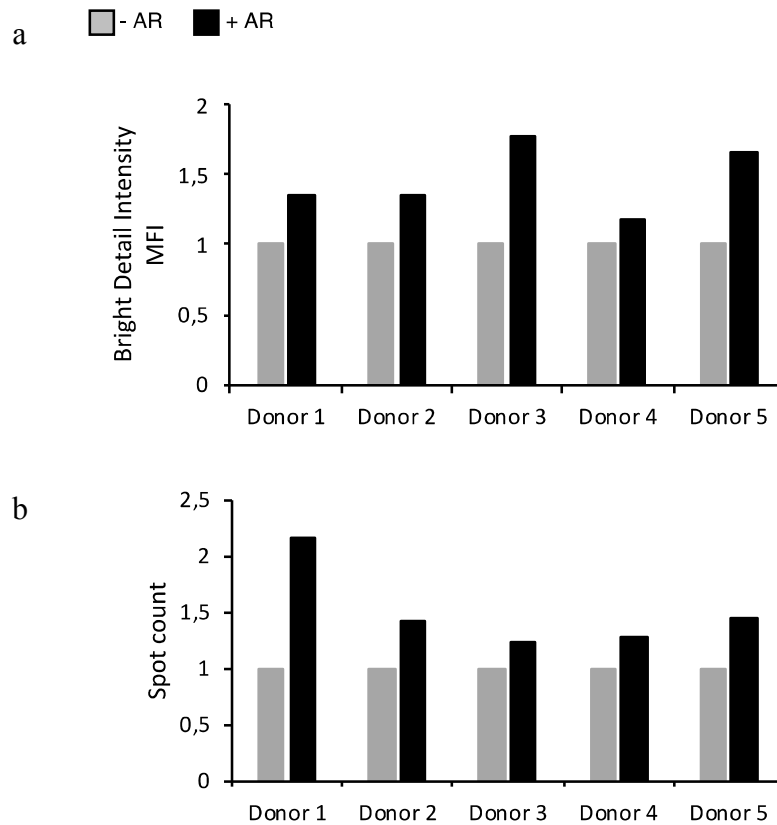


**Figure 25 | Relative autophagosome concentration at the synaptic region of 1001 cells challenged by primary NK cells**

Primary NK cells were isolated from five healthy donors, activated with IL-2 (100u/ml) and incubated with 1001 cells for 30 minutes. The BDI (a) and spot count (b) approaches were used to quantify LC3 at the synaptic region of at least 200 conjugates without (-AR, light grey) or with (+AR, black) actin response. Data are expressed relative to synaptic LC3 levels in cancer cells without actin response (set to 1).

# 3. Preliminary data regarding the mechanism underlying actin response initiation (results and discussion)

This last result section presents some preliminary data regarding the mechanism(s) by which the actin response is induced in breast cancer cells, with a focus on NK cell adhesion to its target and NK cell activation.

## 3.1. NK cell adhesion and activation in actin response initiation

A critical question that remains to be answered is: what is (are) the signal(s) triggering actin response initiation in competent cancer cells? We hypothesized that either effector cell adhesion or effector cell activation could be key event in directing actin response initiation in the target cell. To evaluate such possibility, we analyzed the effects of pharmacological blocking of the adhesion molecule ICAM-1[416] and of MICA/B, a highly polymorphic ligand of the NK cell activating receptor[53]. We conducted these analyses on MDA-MB-231 cells since they contain a large subpopulation of cells competent for the actin response.

First, target cells were incubated for one hour with purified mouse anti-human ICAM-1 (CD54) antibodies prior to washing and presentation to NK cells. Control cells were similarly treated using purified mouse IgG1, κ Isotype. As expected, blocking ICAM-1 reduced the number of conjugates (by about 32%) between MDA-MB-231 cells and NK cells (Figure 23a). Accordingly, it also decreased the overall cell line susceptibility to NK cell-mediated cell death in cytotoxic assays (Figure 23b). However, within the cell-cell conjugates that still formed upon ICAM-1 blocking, the rate of actin response was unchanged as compared to the control cells (Figure 23 c). This suggests that, although the adhesion molecule ICAM-1 is critical for conjugate formation (and accordingly efficient target lysis), it is not specifically involved in actin response induction.

Second, MDA-MB-231 cells were treated with purified mouse anti-human MICA/B antibodies or control mouse IgG2a, κ Isotype. As shown in Figure 23d, blocking of the activating ligand resulted in a statistically-significant increase of target cell resistance to NK cell-mediated lysis. Very interestingly, we found that MICA/B antibodies induced a significant reduction of the rate of actin response in conjugated target cells. This result suggests that NK cell activation is a prerequisite for the induction of the actin response in competent tumor cells. In other terms, the actin response would be triggered by a signaling pathway downstream of NK cell activation.
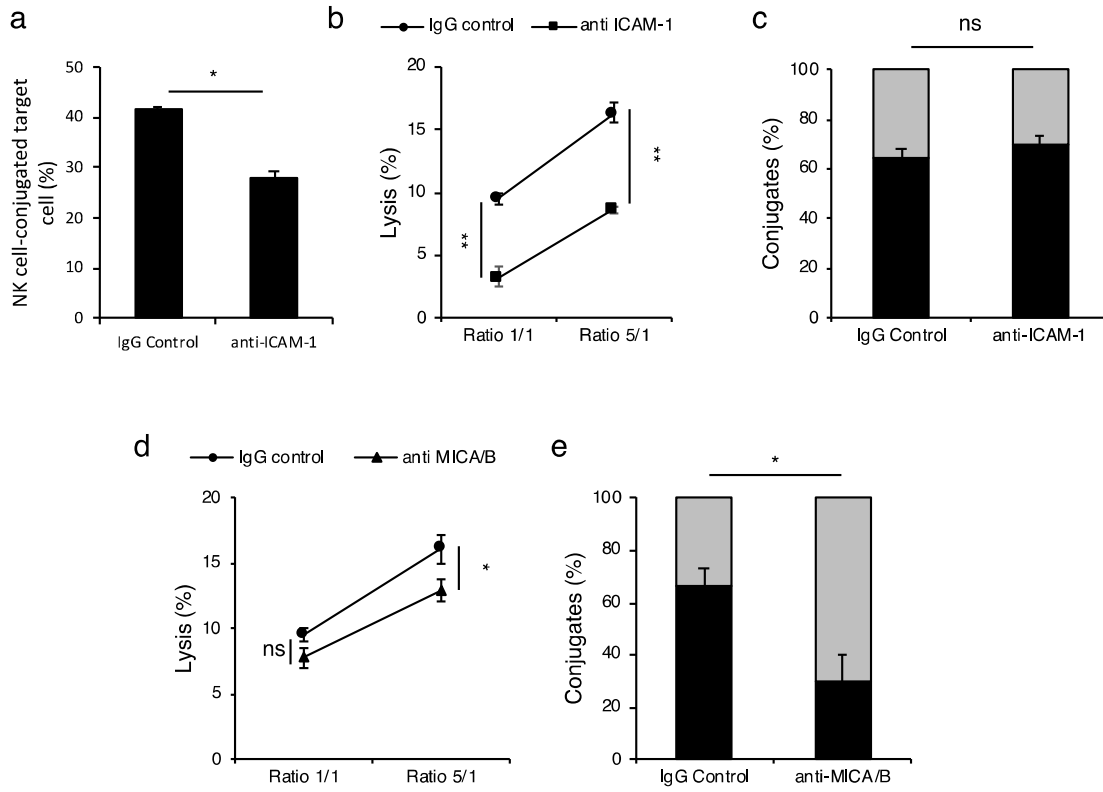
**Figure 26 | Effects of ICAM-1 and MICA/B blocking on the actin response**

MDA-MB-231 cells were treated with anti-ICAM-1 antibodies or an IgG1 control for 1-hour prior their presentation to NK92MI cells. (a) Percentage of target cells conjugated by NK cells. (b and d) Cytotoxicity assays performed with NK92MI cells and MDA-MB-231 treated with either anti-ICAM-1 antibodies (b), anti-MICA/B antibodies (d) or IgG1 controls at 1:1 and 5:1 effector:target ratios. (c-e) Percentage of NK cell-conjugated MDA-MB-231 cells with (black, +AR) and without (light grey, -AR) actin response after treatment with anti-ICAM-1, anti-MICA/B or IgG control antibodies. Data originate from three independent experiments. The two-tailed unpaired Student's *t*-test was used to measure the statistical significance. * denote $p < 0.05$; ** $p < 0.01$; ns: non-significant.

# Supplementary materials and methods

Most of the materials and methods related to my studies was included in the article in Cancer Research (Result section 1.2) The materials and methods related to the supplementary result sections are given below.

**Beclin-1 knockdown**

Beclin-1 was knocked-down transfecting MCF-7, 1001 and MDA-MB-231 cell lines with two different Beclin-1 targeting siRNAs (siBeclin-1 #1 5'-CGACUUGUUCCUUACGGAATT-3', and siBeclin-1 #2 5'-GGUCUAAGACGUCCAACAATT-'3) for 48 hours. Non-targeting control siRNAs (siCtrl) were purchased from Qiagen. Beclin-1 depletion was confirmed by Western blotting using rabbit anti-Beclin-1 antibody (Cell Signaling; clone: D40C5) and secondary HRP-conjugated goat anti-rabbit IgGs.

**Blocking antibodies**

The blocking antibodies used in this study were purchased from Biolegend and include: LEAF™ Purified anti-human CD54 antibody (clone: HA58); LEAF™ Purified Mouse IgG1 (clone: MOPC-21); LEAF™ Purified anti-human MICA/MICB antibody (clone: 6D4) and LEAF™ Purified Mouse IgG2a (clone: MG2a-53). Target cells were blocked with 4 μg of antibody per million cells in 100 μl of medium for 1 hour. Cells were washed twice prior to presentation to NK92MI effector cells.

**Imaging flow cytometry**

For autophagosome detection, target cells were presented to effector cells and stained with anti-human LC3-PE antibodies (Cell Signaling; clone: D11) for 30 min. The Peak mask was selected to identify the most brilliant LC3-PE puncta. Then, Boolean logics of mEGFP-LifeAct and CD56-PeCy7 with the Peak LC3-PE was created to select only LC3 spots at the synaptic region. The Bright Detail Intensity (BDI) R7 feature was applied on the LC3-PE Peak mask at the synaptic region. Using the same mask, the feature Spot Count was applied to determine the number of LC3 spots at the synaptic region. BDI R7

and Spot Count features were applied on the mask of mEGFP-LifeAct to measure LC3 in whole target cell.

**Statistical analysis**

The unpaired Student's *t-test* in Microsoft Excel 2016 was used to determine the statistical significance of the results obtained. For fold-change results, a Student's *t*-test used on the logarithmic values to determine the statistical significance between samples. * $p \leq 0.05$ and ** $p \leq 0.01$. ns: non-significant.

# Synthetic model for actin response-mediated breast cancer resistance to NK cells and perspectives

Based on our findings we propose the following 4-step-model for actin-response-mediated breast cancer resistance to NK cells (Figure. 31). The section below presents and discusses the model in detail and highlights important perspectives to my PhD work.

During **step 1**, the effector cells recognize and adheres to its target. Physical contact between the two cells appears to be necessary but not sufficient to drive the actin response. During **step 2**, the NK cell cytotoxicity is activated following the recognition of upregulated activating ligands and/or deficient self-molecules on the target cell surface. Our preliminary data indicate that blocking activating ligands, such as MICA/B, significantly lowers the rate of actin response observed upon NK cell attack, suggesting that NK cell activation generates a feedback signal towards the target cell that is responsible for actin response initiation. Such mechanism might serve as a safeguard against unnecessary induction of the actin response upon contact with non-killer cells. Although the signaling molecules involved in actin response initiation remain to be identified, our data support that they converge towards Cdc42 and N-WASP, two key regulators of the ARP2/3 actin nucleation machinery[368]. During **step 3**, the massive accumulation of F-actin in the synaptic region of the target cell mediates (at least) two processes leading to cancer cell immune resistance. **In process 1**, the actin response induces a significant reduction in NK cell-derived GzB levels within the target cells. We assume that the quantity of GzB in target cells exhibiting an actin response is kept below the critical threshold required for effective apoptosis. Our mechanistic investigations show that the actin response promotes autophagosome accumulation near immunological synapse. This presumably locally increases autophagy at the main site of GzB entry, and thereby facilitates GzB degradation. Although actin polymerization plays several central roles in autophagosome biogenesis and transport[318], our preliminary data support that the actin response induces polarization of pre-existing autophagosomes towards the synaptic region without modifying the overall quantify of autophagosome in the target cell. The exact mechanism by which the actin response mediates autophagosome recruitment at the synapse should be investigated. **In process 2**, the actin response stimulates the recruitment of inhibitory ligands, such as HLA-A, -B, -C in the synaptic region. This process is likely to alter "long term" signaling towards the effector cell and may turn the lytic synapse into an inhibitory synapse[417]. Although the mechanism underlying actin-dependent recruitment is unknown it is tempting to draw a parallel with the actin cytoskeleton-dependent recruitment of activation receptors in the NK cell[44,140,418]. A limitation of our work is that the NK92MI cells we use as effector cells do not express

156

inhibitory KIRs[419]. It is thus conceivable that the actin response may have even higher protective effects when target cells are attacked by KIR-expressing NK cells. During **step 4**, the NK cell detaches from the surviving target. Remarkably, the actin response rapidly stops after effector cell detachment, supporting the idea that a signal from the NK cell is transmitted to the proximal tumour cell cortex where it induces sustained actin polymerization.

**Step 1**

Recognition and adhesion
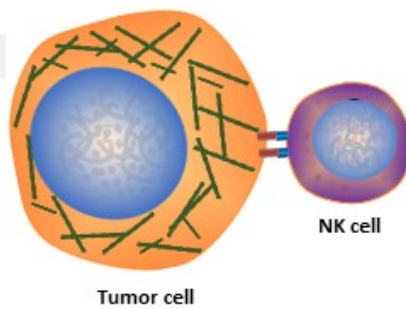
NK cell

Tumor cell

**Step 2**

NK cell activation and actin response initiation

IS

N-WASP

Cdc42

ARP2/3

Actin polymerization
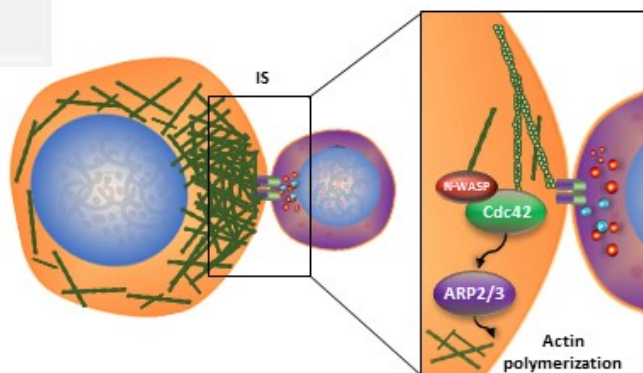
**Step 3 - process 1**

Autophagosome polarization
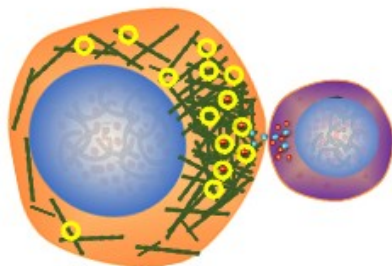
**Step 3 - process 2**

Inhibitory/activation ligand re-distribution

HLA-A,B,C clustering

MICA/B exclusion
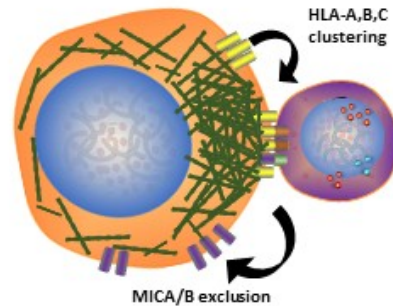
**Step 4**

NK cell detachment, actin depolymerisation and tumor cell escape

Autophagosome    LFA-1    KIRs    NKG2D    GzB    Cdc42    N-WASP

ICAM-1    HLA-A,B,C    MICA/B    Perforin    ARP2/3    Actin filaments
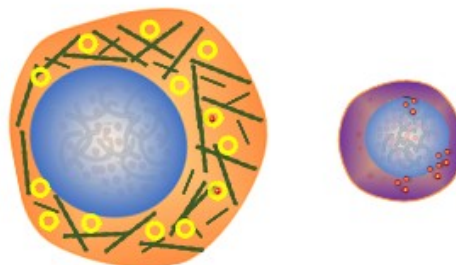
**Figure 27 | Model for actin response-mediated breast cancer cell resistance to NK cells**

Step1: the NK cell recognizes and adheres to the target tumor cell. Step 2: the NK cell is activated and this is, in turn, generates a feedback signal towards the target cell directing local and sustained actin polymerization. Downstream components of the related signaling pathway likely involve CDC42 activation and subsequent N-WASP-mediated induction of the ARP2/3 complex. Step3: The massive accumulation of F-actin in the synaptic region of the target cell drives two important processes. First, it drives autophagosomes recruitment at the synaptic region, and thereby facilitates autophagy-mediated GzB degradation (process 1). Second, it increases inhibitory ligand density (and possibly, decreases activating ligand density) at the synaptic region, leading to a shift of the balance of inhibitory/activating signals and attenuation/inhibition of NK cell cytolytic activity (process 2). Step 4: The NK cell detaches from the surviving tumor cell, the feedback signal directing actin polymerization stops, and the actin response rapidly dissipates upon actin filament depolymerization and, possibly, severing.

An important finding of my work is that all the BC cell lines we examined contain two cell subpopulations differing in their capacity to generate an AR in response to NK attack and to survive this attack. A direct implication of this novel layer of intra-cancer cell line heterogeneity is that the apparent (overall) high susceptibility exhibited by some cell lines, such as MCF-7, actually masks the existence of a minor, AR-competent and highly resistant, cell subpopulation. We hypothesize that a similar cell subpopulation exists in tumors and contributes to cancer progression, metastasis and relapse. Future work should examine this hypothesis. First, highly infiltrated clinical breast tumor specimens can be searched for the presence of synaptic actin accumulation using electron microscopy. In addition, a relevant (syngeneic and immunocompetent) mouse model should be used to confirm the role of the AR in tumor immune evasion *in vivo*, and to provide a rationale for targeting this process as a therapeutic approach to improve the anti-tumor immune response. In that attempt, we already verified inter species conservation of the actin response in mouse 4T1 cells modified to stably express LifeAct-mEGFP.

Another important question to be evaluated in follow-up studies is the possibility that other cytotoxic immune cells, such as CTLs, also induce an actin response in breast cancer cells. Although the mechanism of CTL activation differs from that of NK cells, both types of immune cells induce cancer cell death through highly similar mechanisms, including the secretion of cytotoxic molecules, such as GzB[373]. It is accordingly conceivable that the actin response protects cancer cells against different types of cytotoxic cells.

Our in vitro data indicate that Cdc42 is an effective point of intervention to block the actin response and its protective effects against NK cells. However, from a clinical

standpoint, direct targeting of Rho GTPase, such as Cdc42, has proven to be challenging[366-369,420]. Although direct small-molecule inhibitors of Cdc42 have been developed and found to have anti-tumor activity in preclinical studies[369,421], none of those has been clinically approved or entered clinical trials to our best knowledge. Importantly, Cdc42 has been reported to have critical roles in NK cell-mediated lysis[422,423]. Accordingly, the use of direct inhibitors of Cdc42 to inhibit cancer cell immune resistance can be expected to simultaneously harm NK cell activity. Thus, the translation of our findings into clinical applications requires the identification of clinically relevant targets. For instance, some of Cdc42 upstream or downstream effectors may exhibit much higher specificity to the AR as compared to Cdc42 itself, which regulates multiple cellular pathways. The clinical efficacy of inhibitors of Cdc42 downstream effectors, such as p21 Activated Kinases (PAKs) is currently evaluated, and there are various additional druggable kinases further downstream of Cdc42 signalling and PAKs[424]. Follow-up studies should characterize the molecular signalling pathways involved in the actin response and identify clinically relevant targets to interfere with this process. Considering the that the actin response is a highly dynamic process, changes in gene expression are unlikely involved in actin response initiation. Such rapid cytoskeletal remodeling presumably involves posttranslational modifications like phosphorylation, a key component of the signaling pathways controlling actin dynamics [425-427]. We thus plan to conduct phosphoproteomic analyses aimed to identify proteins whose phosphorylation status is modified during the actin response.

# Contributions to articles

# Article 1

**Hypoxia promotes breast cancer cell invasion through HIF-1α-mediated up-regulation of the invadopodial actin bundling protein CSRP2.**

Xianqing Mao, Celine Hoffmann, Joshua Brown-Clay, Flora Moreau, <u>Antoun Al Absi</u>, Hannah Wurzer, Barbara Soussa, Fernando Schmitt, Guy Berchem, Bassam Janji and Clément Thomas. *Scientific Reports*. 2018.

# SCIENTIFIC REPORTS

# Hypoxia promotes breast cancer cell invasion through HIF-1α-mediated up-regulation of the invadopodial actin bundling protein CSRP2

Céline Hoffmann[1], Xianqing Mao[1], Joshua Brown-Clay[1], Flora Moreau[1], Antoun Al Absi[1], Hannah Wurzer[1,2], Barbara Sousa[3], Fernando Schmitt[3], Guy Berchem[1], Bassam Janji[1] & Clément Thomas[1]

Hypoxia is a common feature of solid tumours that promotes invasion and metastatic dissemination. Invadopodia are actin-rich membrane protrusions that direct extracellular matrix proteolysis and facilitate tumour cell invasion. Here, we show that CSRP2, an invadopodial actin bundling protein, is upregulated by hypoxia in various breast cancer cell lines, as well as in pre-clinical and clinical breast tumour specimens. We functionally characterized two hypoxia responsive elements within the proximal promoter of CSRP2 gene which are targeted by hypoxia-inducible factor-1 (HIF-1) and required for promoter transactivation in response to hypoxia. Remarkably, CSRP2 knockdown significantly inhibits hypoxia-stimulated invadopodium formation, ECM degradation and invasion in MDA-MB-231 cells, while CSRP2 forced expression was sufficient to enhance the invasive capacity of HIF-1α-depleted cells under hypoxia. In MCF-7 cells, CSRP2 upregulation was required for hypoxia-induced formation of invadopodium precursors that were unable to promote ECM degradation. Collectively, our data support that CSRP2 is a novel and direct cytoskeletal target of HIF-1 which facilitates hypoxia-induced breast cancer cell invasion by promoting invadopodia formation.

Metastasis, i.e. the spread of tumour cells from the primary tumour and subsequent colonization of distant organs, is the most life-threatening aspect of cancer[1]. The hypoxic tumour microenvironment is a potent driver of tumour aggressiveness and metastasis, and is highly associated with poor clinical outcomes in various cancers[2–4]. A fundamental process underlying the pro-metastatic effect of hypoxia is the stimulation of tumour cell invasive capabilities. At the subcellular level, hypoxia has recently been reported to promote the formation of actin-rich membrane protrusions, termed invadopodia[5]. Invadopodia facilitate tumour cell invasion through dense extracellular matrix (ECM) by recruiting transmembrane and secreted metalloproteinases (MMPs) that catalyze ECM component degradation, and creating pores through which mesenchymal tumour cells can migrate[6,7]. Both *ex vivo* and *in vivo* studies have provided direct evidence of the critical roles of invadopodia during key steps of the metastatic cascade, such as basement membrane breaching, intravasation and extravasation[8–12]. In addition, it has been suggested that invadopodia may contribute to other important aspects of disease progression, such as tumour growth and angiogenesis[13,14], further increasing interest in their potential as therapeutic targets.

Invadopodium biogenesis largely relies on cytoskeletal rearrangements orchestrated by a combination of lamellipodial and filopodial actin machineries[15–18]. A critical step of invadopodium initiation is the assembly of an actin core by the ARP2/3 complex and its associated regulators, such as N-WASP and cortactin. Invadopodium

[1]Laboratory of Experimental Cancer Research, 84 Val Fleuri, L-1526, Luxembourg, Luxembourg. [2]Faculaty of Science, Technology and Communication, University of Luxembourg, 2 avenue de l'Université, L-4365, Esch-sur-Alzette, Luxembourg. [3]IPATIMUP- Institute of Molecular Pathology and Immunology of the University of Porto, Medical Faculty of Porto University, Rua Julio Amaral de Carvalho 45, 4200-135, Porto, Portugal. Céline Hoffmann and Xianqing Mao contributed equally to this work. Correspondence and requests for materials should be addressed to C.T. (email: Clement.thomas@lih.lu)

166

elongation is promoted by the expansion of the actin core in both branched networks and unbranched bundles. At the tip of invadopodia, actin bundles presumably potentiate the protrusive force generated by actin polymerization, whereas the dendritic actin network progressively expands to fill and stabilize upstream regions[16,18]. The actin cytoskeleton proteins and upstream signalling pathways involved in invadopodium biogenesis have been characterized to a great extent[7]. However, our understanding of how important components of the tumour microenvironment, such as hypoxia, shape the invasive behavior of tumour cells remains fragmented[5,7].

Cysteine-rich protein 2 (CSRP2) is a short (21 kDa) two LIM domain-containing protein, which is upregulated in invasive breast cancer cells, and localizes along the protrusive actin core of invadopodium[19]. Similar to its relatives CSRP1 and CSRP3/muscle LIM protein[20,21], CSRP2 crosslinks actin filaments in stable bundles, suggesting that it contributes to the assembly and/or maintenance of the invadopodium actin backbone[19]. Accordingly, CSRP2 knockdown significantly inhibits invadopodium formation in aggressive breast cancer cells, as well as MMP secretion and 3D matrix invasion. It also strongly reduces tumour cell dissemination in two mouse models of breast cancer metastasis. The clinical relevance of these findings to human breast cancer disease is supported by microarray data identifying *CSRP2* in a cluster of 14 upregulated genes characteristic of the highly aggressive basal-like breast carcinoma subtype[22]. In addition, among basal-like tumour patients, those with high CSRP2 expression exhibit an increased risk for developing metastasis. In the present study, we show that hypoxia upregulates CSRP2 in different breast cancer cell lines, and that such upregulation results from HIF-1-mediated transactivation of the CSRP2 promoter. We provide evidence that CSRP2 depletion strongly reduces the ability of hypoxia to enhance invadopodia formation, ECM degradation and invasion in highly invasive breast carcinoma cell lines, such as MDA-MB-231 and mouse 4T1. In weakly invasive, epithelial-like, MCF-7 cells, hypoxia-induced CSRP2 expression was required for the formation of invadopodium precursors, which were unable to promote ECM digestion due to the lack of MT1-MMP expression. Finally, we found that CSRP2 up-regulation correlates with hypoxic regions in both pre-clinical and clinical breast tumour specimens, and is associated with poor prognosis in breast cancer patients. Overall, our data point to an important role for CSRP2 in facilitating the pro-invasive and -metastatic effects of hypoxia in breast cancer.

## Results

### Hypoxia promotes HIF-1 dependent CSRP2 up-regulation in breast cancer cells.
The hypoxic tumour microenvironment is a critical promoter of breast cancer progression and metastasis[3,23]. We assessed the effects of hypoxia on the expression of the pro-invasive and -metastatic invadopodial protein CSRP2 in four breast cancer cell lines, including luminal/epithelial-like MCF-7 and T47D ($ER^+$, $PR^+$), and mesenchymal-like MDA-MB-231 and Hs578T ($ER^-$, $PR^-$, $HER2^-$, claudin-low). In agreement with our previous report[19], CSRP2 was absent or only weakly expressed in epithelial-like cells under normoxia, whereas it was expressed at significant levels in mesenchymal-like cells (Fig. 1A and B). Exposing cells to hypoxia (0.1% $pO_2$) for 24 hours induced a significant up-regulation of CSRP2 in all four cell lines (Fig. 1A). Indeed, CSRP2 protein levels increased by about ten times in epithelial-like cells and by about five times in mesenchymal-like cells, as compared to the respective normoxic controls. At 48 hours of hypoxia, high CSRP2 protein expression was maintained in all cell lines (Fig. 1B). To extend these data, *CSRP2* transcript levels were analysed in normoxic and hypoxic conditions using real-time qRT-PCR. In the four breast cancer cell lines, hypoxia induced a significant and sustained elevation of *CSRP2* transcripts (Fig. 1C and D), suggesting that CSRP2 levels were regulated at the transcriptional level.

Tumour cells respond to hypoxic stress by an activation of HIFs, which drive the transcription of target genes through binding to cis-regulatory elements, termed hypoxia responsive elements (HREs)[24]. Accumulating evidence indicates that HIF-1 functions as a master regulator of the hypoxic response in breast cancer[2,23]. To evaluate the role of HIF-1 in hypoxia-induced CSRP2 expression, its oxygen-regulated subunit (HIF-1$\alpha$) was depleted in MCF-7 cells prior exposure to hypoxia. HIF-1$\alpha$ knockdown significantly inhibited hypoxia-induced CSRP2 up-regulation at both protein and mRNA levels (Fig. 2A,C and D). Similar results were obtained by knocking down HIF-1$\alpha$ in MDA-MB-231 cells (Fig. 2B,E and F), supporting that the gene encoding CSRP2 is a novel, and direct downstream target of HIF-1.

### HIF-1$\alpha$ drives CSRP2 transcription by direct binding to HRE motifs.
The consensus core HRE sequence 5′-[A/G]CGT-3′ was initially characterized based on the comparison of various known HIF target genes[25]. Later on, flanking nucleotides were demonstrated to contribute additional information to the likelihood of HIF-1 transactivation[26]. *In silico* analysis using the weight matrix-based program *Alggen PROMO*[27], identified two high-confidence HREs (HRE1 and HRE2) in the proximal promoter region of *CSRP2*, while manual scanning found two additional lower confidence core HRE sequences further upstream (Fig. 2G).

To validate HIF-1$\alpha$ binding to these two putative HREs, we conducted ChIP analyses, using HIF-1$\alpha$ specific antibody (Fig. 2H). Results revealed that HIF-1$\alpha$ significantly binds to both HREs, even under normoxic conditions. Additionally, there was a dramatic and significant increase (>12 fold) in HIF-1$\alpha$ occupancy at these sites under hypoxia (Fig. 2H–J).

To study the transactivation of *CSRP2* by HIF-1$\alpha$, the nucleotides $-1,920$ to $+103$ relative to the transcription start site were cloned into a luciferase reporter vector. MCF-7 cells were chosen to conduct the reporter assays as they express low levels of CSRP2 and HIF-1$\alpha$ under normoxic conditions (Fig. 2A). As shown in Fig. 2K, hypoxia induced a significant increase in luciferase activity as compared to normoxia. A *VEGFA* promoter luciferase reporter was used as a positive control of hypoxia-induced gene transcription. Confirming the ChIP results, mutation of HRE1 decreased the hypoxic induction of transcriptional activity at the *CSRP2* promoter, while mutation of HRE2 reduced this induction to an insignificant amount ($p = 0.1237$). These results suggest that the HRE2 sequence is the major motif responsible for hypoxia-dependent induction of *CSRP2* expression, while HRE1 may also contribute to a lesser extent.
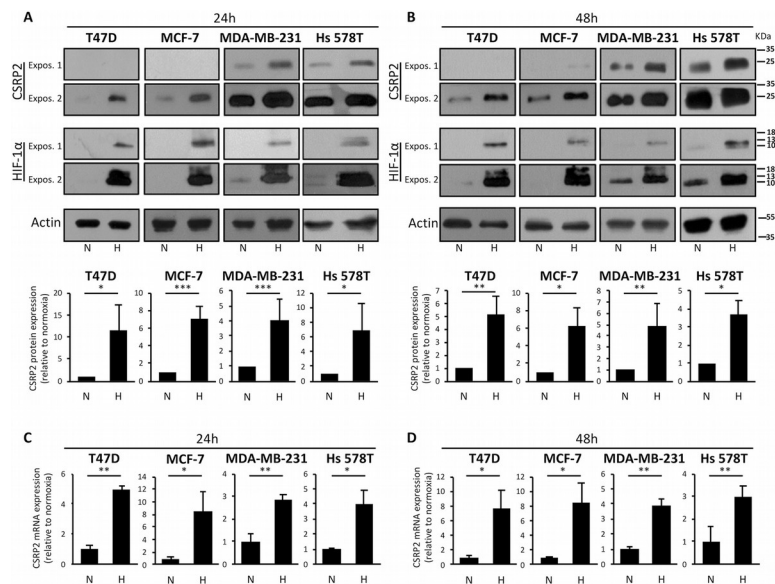
167

**Figure 1.** Hypoxia upregulates CSRP2 protein and transcript levels in human breast cancer cells. (**A,B**) Western blot analysis of CSRP2 and HIF-1α protein levels in epithelial (T47D, MCF-7) and mesenchymal (MDA-MB-231, HS-578T) human breast cancer cells cultured for 24 h (**A**) or 48 h (**B**) in normoxic (N) or hypoxic (H) conditions. Short and long exposures for CSRP2 and HIF-1α blots are shown to better appreciate the differences between the cell lines ("Expos. 1" and "2", respectively). After quantification, protein levels were normalized to β-actin levels and CSRP2 protein levels in hypoxia were expressed as fold of normoxic control (set to 1). The lower charts indicate the mean ± s.e. calculated from at least 4 independent experiments. (**C,D**) qRT-PCR analysis of CSRP2 transcript levels in the same four cell lines after 24 h (**C**) or 48 h (**D**) incubation in normoxic (N) or hypoxic (H) conditions. Results are expressed as CSRP2 transcript levels in hypoxia relative to normoxic control (set to 1). Shown are the mean ± s.e. calculated from 3 (**C**) and 4 (**D**) independent experiments. *p < 0.05; **p < 0.01; ***p < 0.001.

To further confirm that the *CSRP2* promoter is transactivated by HIF-1α, constitutively stable HIF-1α was co-transfected into MCF-7 cells along with the luciferase reporter plasmids. Again, a *VEGFA* promoter luciferase reporter construct was used as a positive control of HIF-1α transcriptional activity. As shown in Fig. 2L, HIF-1α induced a significant transactivation of the *CSRP2* promoter, supporting its role in hypoxia-promoted *CSRP2* expression.

Taken together, ChIP and luciferase reporter experiments show that hypoxia induces binding of the HIF-1α transcription factor to the *CSRP2* promoter, primarily at the HRE2 site, and subsequent induction of *CSRP2* expression.

**CSRP2 mediates hypoxia-stimulated invadopodium formation.** The role of CSRP2 in hypoxia-stimulated invadopodium formation and activity was investigated in both a highly invasive cell line with significant basal levels of CSRP2 (MDA-MB-231), and a weakly invasive cell line with low basal expression of CSRP2 (MCF-7). First, fluorescent gelatin degradation assays were conducted with MDA-MB-231 cells following transfection with control scrambled siRNAs (siCtr) or CSRP2 targeting siRNAs (siCSRP2 #1 and #2; Fig. 3A). As illustrated in Figs 3B and S1, hypoxia promoted invadopodia-mediated ECM degradation in siCtr-transfected cells, as shown by a significant overall increase in the density of dark punctate in the fluorescent matrix background. Quantitative analyses revealed that the percentage cells associated with local ECM degradation (% of active cells) increased from about 50% in normoxia to about 70% in hypoxia (Fig. 3C, left panel). Even more remarkably, hypoxia induced a 5-fold increase in the average surface of matrix degradation per cell (degradation index; Fig. 3C, right panel).

Consistent with these data, siCtr-transfected MDA-MB-231 cells exhibited a higher number of mature invadopodia (as defined by F-actin and cortactin co-labelled dots overlapping with areas of gelatin clearing) and were significantly more invasive in hypoxia as compared to normoxia (Fig. 3D and E, respectively). CSRP2 knock-down inhibited the stimulatory effects of hypoxia and decreased the percentage of active cells, the degradation

168
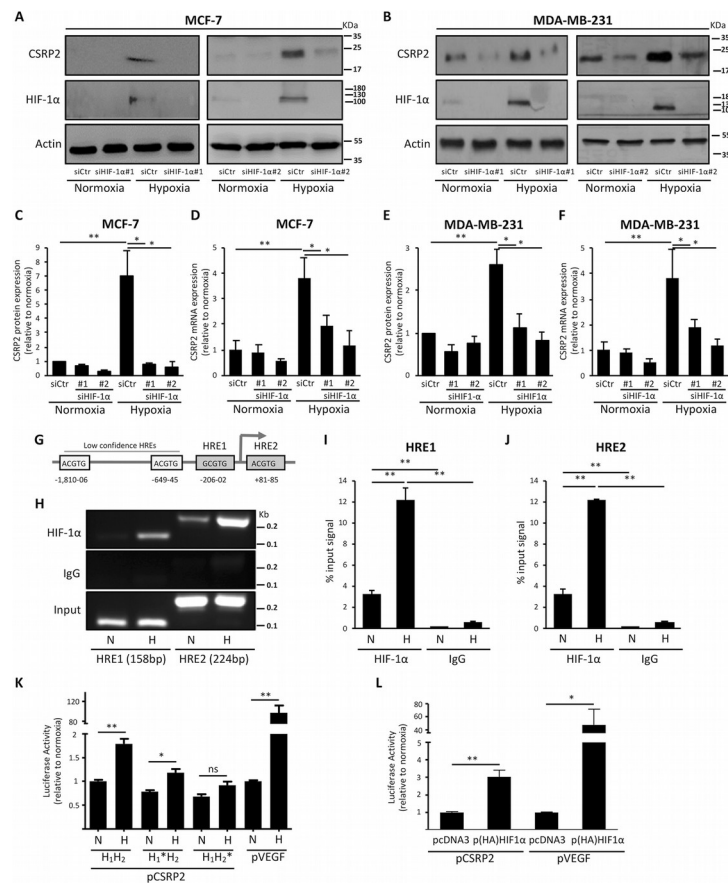
**Figure 2.** HIF-1α regulates CSRP2 promoter activity. (**A,B**) Western blot analysis of CSRP2 and HIF-1α protein levels in MCF-7 (**A**) and MDA-MB-231 (**B**) breast cancer cells incubated in normoxia or hypoxia and transfected with control siRNAs (siCtr) or two different HIF-1α targeting siRNAs (siHIF-1α#1 and #2). (**C,E**) After quantification, protein levels were normalized to β-actin levels and CSRP2 and HIF-1α protein levels were expressed relative to siCtr-transfected normoxic control (set to 1). Shown are the mean ± s.e. calculated from four (**C**) and five (**E**) independent experiments. (**D,F**) qRT-PCR analysis of CSRP2 transcript levels in the same cell lines and culture conditions. Results are expressed as CSRP2 transcript levels in hypoxia relative to siCtr-transfected normoxic control (set to 1). Shown are the mean ± s.e. calculated from three (**D**) and four (**F**) independent experiments. (**G**) A schematic representation of the putative HREs identified in the proximal promoter of CSRP2. The position (relative to the transcriptional start site; TSS) of low and high confidence HREs is indicated. (**H**) ChiP analysis for HIF-1α recruitment to CSRP2 promoter regions containing HRE1 and HRE2 in MCF-7 cells cultured in normoxic (N) or hypoxic (H) conditions. (**I,J**) Quantification of ChiP data for HRE1 (G) and HRE2 (H) from three independent experiments. Data are expressed as percentage of PCR product signal obtained for chromatin fragments immunoprecipitated with HIF-1α antibodies or IgG (non-specific binding control) relative to the corresponding input signal. (**K**) Luciferase reporter assays to evaluate the normoxic and hypoxic activity of a wild type CSRP2 promoter with intact HRE1 and HRE2 (H1H2) and two variants with point mutations in HRE1 (H1*H2) or HRE2 (H1H2*) in MCF-7 cells. VEGF promoter was used as a positive control. Data are expressed as mean of luciferase signal ± s.e. in hypoxia relative to normoxic control (set to 1; n = 3 independent experiments). (**L**) Luciferase assays for the wild type CSRP2 promoter in MCF-7 cells transfected with a control empty plasmid (pcDNA3) or HIF-1α expressing plasmid (p(HA) HIF-1α). Data are expressed as mean of luciferase signal ± s.e. in hypoxia relative to normoxic control (set to 1; independent experiments). *p < 0.05; **p < 0.01.

169
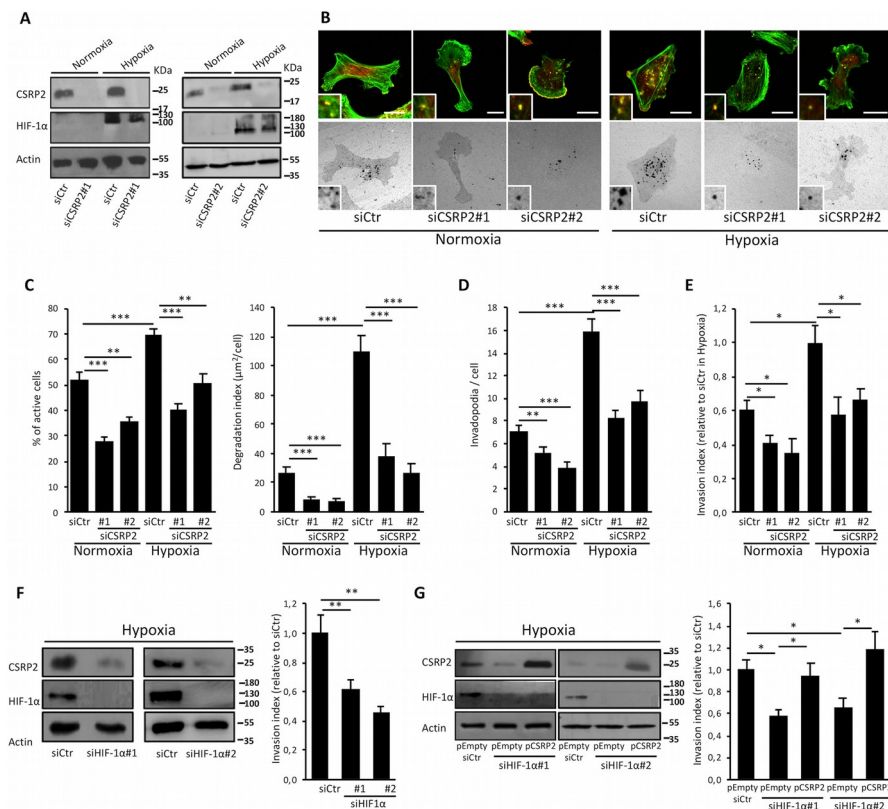
**Figure 3.** Hypoxia-dependent stimulation of MDA-MB-231 cell invasive potential is mediated by CSRP2. (**A**) Western blot analysis of CSRP2 and HIF-1α protein levels in MDA-MB-231 cells transfected with non-targeting (siCtr) or 2 different CSRP2-targeting (siCSRP2#1 and 2) siRNAs and cultured under normoxia or hypoxia. (**B**) Gelatin degradation assay. Control and CSRP2 depleted cells were plated on Oregon Green 488-labelled gelatin-coated coverslips for 16 hours, fixed and stained for actin (green) and cortactin (red, upper panels). (**C,D**) Quantitative analyses corresponding to experiments shown in (**B**) with actively ECM degrading cells as expressed as percentage of the total cell population (**C**) left panel), degradation index (average of degraded matrix per cell; (**C**) right panel) and the number of mature invadopodia per cell (F-actin and cortactin co-labelled puncta overlapping with areas of gelatin clearing; **D**). The data originate from at least three independent experiments (n ≥ 60 cells). (**E**) Transwell invasion assay. Invading control and CSRP2 depleted cells in normoxia and hypoxia at 24 h were quantified via MTT staining. Results were expressed relatively to the invasion of siCtr-transfected hypoxic cells (set to 1). The data originate from 3 independent experiments. (**F**) Transwell invasion assay with hypoxic MDA-MB-231 cells transfected with control (siCtr) or HIF-1α (siHIF-1α#1 and #2) targeting siRNAs. CSPR2 and HIF-1α protein levels were analysed by western blot (left panel). The data originate from 6 independent experiments. (**G**) Similar transwell invasion assay as in (**F**) with MDA-MB-231 cells that were further transfected with an empty pCDNA3.1 expression plasmid (pEmpty) or a CSRP2 overexpression vector (pCSRP2). Results were expressed relatively to the invasion of siCtr and pEmpty co-transfected cells (set to 1). The data originate from 6 independent experiments. Bars = 15 μm. *p < 0.05; **p < 0.01, ***p < 0.001.

index and the number of invadopodia per cell to values similar to those obtained for control cells in normoxia (Figs 3B–D and S1). In addition, CSRP2 knockdown inhibited tumour cell invasion under hypoxia with an almost similar magnitude as HIF-1α knockdown (Fig. 3E and F). In contrast, CSRP2 depletion did not significantly modify the MDA-MB-231 cell migration under normoxia or hypoxia, supporting that CSRP2 has a specific function in invasion (Fig. S2). Remarkably, CSRP2 forced expression was sufficient to increases the invasiveness of

HIF-1α depleted MDA-MB-231 cells under hypoxia (Fig. 3G). In agreement with our previous report[19], CSRP2 knockdown also repressed invadopodia-mediated matrix degradation and invasion under normoxia (Fig. 3B–E). Collectively, these data suggest that hypoxia promotes invadopodia-mediated breast cancer cell invasion by upregulating CSRP2, a basic component of the invadopodial actin cytoskeleton machinery. To strengthen this conclusion, we validated the role of CSRP2 in facilitating hypoxia-stimulated invadopodia formation, ECM degradation and cell invasion in another invasive breast cancer cell line, namely the mouse 4T1 cell line (Fig. S3).

Contrary to MDA-MB-231 and 4T1 cells, MCF-7 cells failed to promote localized gelatin degradation under both normoxia and hypoxia (Fig. 4A). This lack of activity was consistent with the fact that MCF-7 cells did not express membrane type-1 MMP (MT1-MMP; Fig. 4B), a membrane-tethered MMP required for proteolytic activity[28,29]. However, hypoxia promoted cortactin relocalization to actin puncta, whose appearance and localization at the ventral side of tumour cells were reminiscent of invadopodia (Fig. 4A). Similar ventral actin/cortactin puncta were induced by hypoxia when MCF-7 cells were plated on non-denatured collagen (Fig. S4). To further examined the nature of these structures, we used two additional invadopodium markers, namely N-WASP and Tks5[30]. Both effectively labelled the actin/cortactin puncta that formed under hypoxia (Fig. 4F and G), which were accordingly termed invadopodium precursors. As shown in Fig. 4H, CSRP2 was also recruited to hypoxia-induced invadopodium precursors, suggesting it is required for, or possibly mediates, their formation. To assess this possibility, the number of invadopodium precursors was determined in MCF-7 cells that were transfected with control or CSRP2-targeting siRNAs prior to incubation in normoxic or hypoxic conditions. Under normoxia, both siCtr- and siCSRP2-transfected cells exhibited about two invadopodium precursors on average (Fig. 4C and D). Hypoxia increased invadopodium precursors density in control cells by almost 9-fold, with an average of 17 invadopodium precursors per cell. Interestingly, this effect was associated with a significant increase in the secretion of pro-MMP-2 and pro-MMP-9, suggesting that, although proteolytically inactive, these invadopodium precursors are mature enough for MMP secretion (Fig. 4E). CSRP2 knockdown significantly lowered the number of hypoxia-induced invadopodium precursors, with about eight precursors per cell on average (Fig. 4C and D). Accordingly, it also inhibited hypoxia-promoted secretion of proMMP-2 and proMMP-9 (Fig. 4E). Thus, although MCF-7 cells lack MT1-MMP expression and matrix degrading activity, they assemble invadopodium precursors in response to hypoxia in a CSRP2 dependent manner.

Collectively our data indicate that CSRP2 an important mediator of hypoxia-stimulated invadopodium formation in breast cancer cells.

### CSRP2 is upregulated in hypoxic, HIF-1α-positive regions of human breast cancer cell line xenografts.
To validate that CSRP2 is up-regulated by intratumoral hypoxia, MCF-7 and MDA-MB-231 cells were orthotopically injected in the mammary fat pad of immunodeficient mice, and the resulting primary tumours were collected for immunofluorescence analyses. As shown in Fig. 5A, CSRP2 was strongly upregulated in hypoxic, pimonidazole-stained, regions of both MCF-7- and MDA-MB-231-cell derived tumours. In addition, tumour sections were co-labelled for CSRP2 and HIF-1α (Fig. 5B). Strong CSRP2 signals were very frequently associated with HIF-1α positive regions in both MCF-7 and MDA-MB-231 tumour xenografts. Pixel intensity correlation analyses confirmed a strong correlation between CSRP2 and HIF-1α expression in all tumour sections analysed, with Pearson coefficient values ranging from 0.50 to 0.85 for MCF-7 cell-derived tumours, and from 0.63 to 0.86 for MDA-MB-231 cell-derived tumours (n = 22 and 21, respectively; Fig. S5). These data provide compelling evidence that CSRP2 expression is not only stimulated by experimental hypoxia produced in low-oxygen incubators, but is also induced by *in vivo* tumour hypoxia.

### Clinical significance of hypoxia-induced CSRP2 expression in breast cancer.
We next assessed the co-expression of *CSRP2* and metastasis-effector genes reported to be regulated by HIF in patient tumours[31]. This analysis was conducted using a publicly available gene expression database of a large cohort of breast cancer patients (n = 1,215). We found that *CSRP2* expression positively correlates with the expression of 21 out of 25 genes for which the expression data is available (p < 0.01; Table 1). Correlation coefficient values >0.3 were obtained for 9 of these 21 genes, and correlation coefficient values >0.5 were obtained for 2 genes, *LOXL4* (r = 0.54; p = 1.5e-92) and *MET* (r = 0.50; p = 1.5e-79).

To more directly evaluate CSRP2 up-regulation in hypoxic areas of human breast tumours, we conducted immunohistochemical analyses of clinical breast cancer specimens. Looking for hints of a hypoxic expression profile, we found that CSRP2 was frequently upregulated in or near the centre of tumour nests, a presumably highly hypoxic region (Fig. 5C). Next, we analysed and compared CSRP2 and HIF-1α protein expression in 48 triple negative breast cancer tissue array samples, and the results were scored by a pathologist (Table S1). 14/48 (>30%) cases showed weak to obvious HIF-1α expression, of which 11 (>78%) were also positive for CSRP2. Rank analysis confirmed a statistically significant correlation between CSRP2 and HIF-1α protein levels in clinical samples with a correlation coefficient value of 0.42 (p = 0.0027). In addition, CSRP2 and HIF-1α exhibited partially overlapping distribution in successive tumour sections (Fig. 5D). As previously reported[19], CSRP2 staining was also frequently observed in inflammatory/immune cells. Such staining likely account for the lower, yet significant, correlation obtained for clinical samples as compared to mouse xenografts.

To evaluate the clinical relevance of our findings, the prognostic value of CSRP2 in breast cancer was evaluated by Kaplan Meier analysis using transcriptomics data sets including 1402 breast cancer patients[32]. High *CSRP2* mRNA expression was significantly associated with reduced overall survival for breast cancer patients. The best cut off between low and high *CSRP2* expression to discriminate the subgroups with different outcomes was determined to be the upper quartile (HR = 1.6, logrank P = 0.00011; Fig. 5E). Upper quartile survival, i.e. time beyond which 75% of the patients are expected to survive, for patients with low and high *CSRP2* expression was 118.8 and 64.8 months, respectively. Stratifying patients according to upper tertile or median *CSRP2* expression values established weaker, yet significant, association between *CSRP2* expression and overall survival
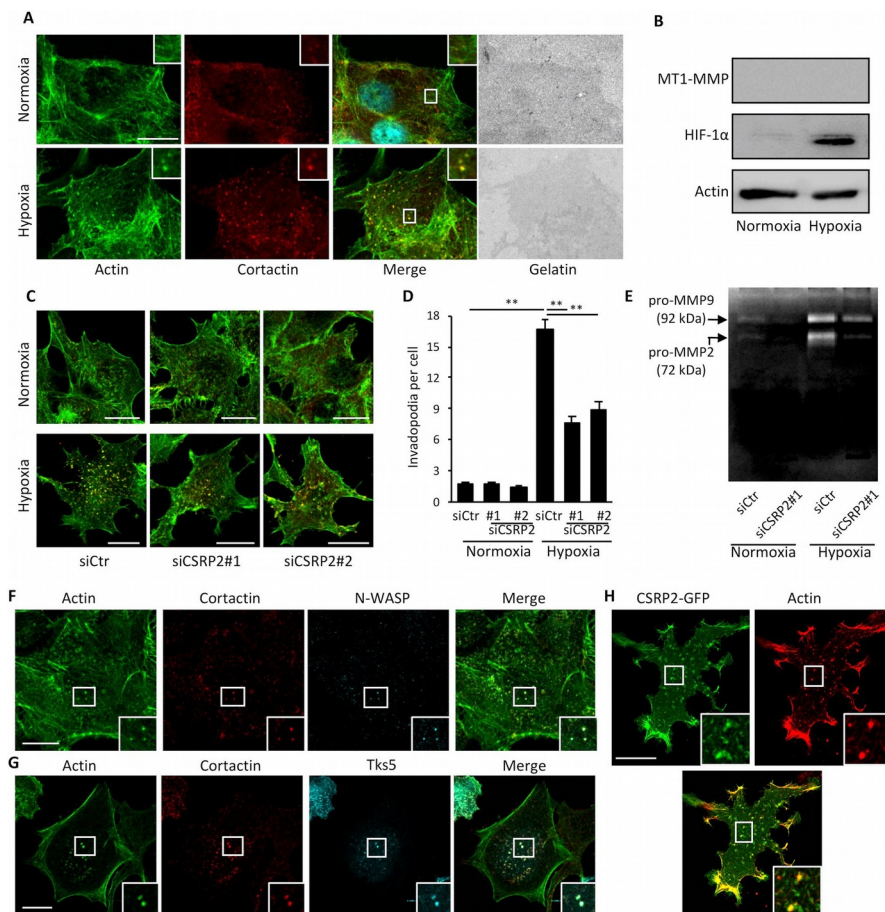
**Figure 4.** Hypoxia-induced invadopodium precursors formation in MCF-7 cells requires CSRP2 upregulation. (**A**) Gelatin degradation assay showing that normoxic (upper panels) and hypoxic (lower panels) MCF-7 cells do not promote (Oregon Green 488-labelled) gelatin degradation after 48 h. After fixation, MCF-7 cells were stained for actin (in green) and cortactin (in red), and imaged using confocal microscopy. (**B**) Western blot analysis of the MT1-MMP and HIF-1α protein levels in normoxic and hypoxic MCF-7 cells. (**C**) MCF-7 cells were transfected with non-targeting or 2 different CSRP2 siRNAs (siCSRP2#1 and 2), cultured under normoxic or hypoxic conditions, and invadopodium precursors were detected by actin (green) and cortactin (red) co-labelling. (**D**) Quantitative analysis of invadopodium precursor density in MCF-7 cells as in (**C**). The data originate from 3 independent experiments (n = 60). (**E**) Gelatin zymography assay conducted with the conditioned media collected from MCF-7 cells cultured as in (**C,D**). The zymogram is representative of three independent experiments. Similar data were obtained with siCSRP2#2. (**F,G**) Hypoxic MCF-7 cells were labelled for actin (green), cortactin (red) and either N-WASP (immunolabelling, **F**) or Tks5 (Tks5-GFP, **G**). (**H**) CSRP2-GFP co-localizes with actin (red) at invadopodium precursors in hypoxic MCF-7 cells. The insets show magnification of invadopodium precursors. Bars = 15 μm; *p < 0.05; **p < 0.01.

(HR = 1.49, logrank P = 0.00056, and HR = 1.28, log-rank p = 0.025, respectively; Fig. S6). In addition to overall survival, CSRP2 overexpression significantly correlated with shorter distant metastasis- and relapse- free survival (p = 0.015 and 1.9e-07, respectively; Fig. 5F and G). Comparison of *CSRP2* expression in different breast cancer subtypes revealed that *CSRP2* expression is an order of magnitude higher in the basal subtype, compared to the other subtypes and, accordingly, is a stronger predictor of distant metastasis-free survival (Fig. S7).

172
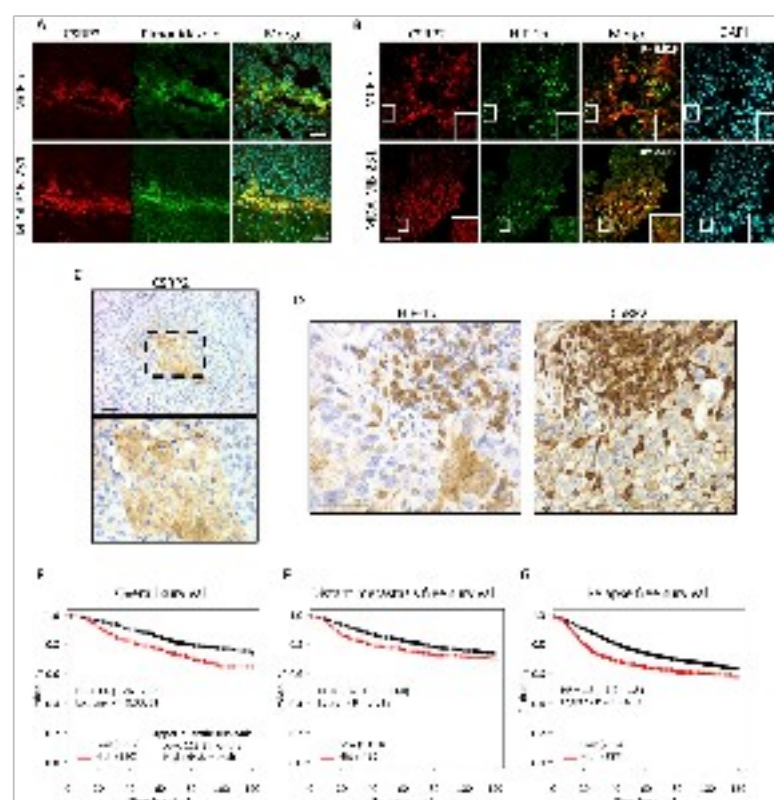
**Figure 5.** CSRP2 co-localises with HIF-1α in tumour xenografts and human breast cancer sections, and is significantly associated with worse outcomes in breast cancer patients. (A,B) MCF-7 or MDA-MB-231 murine tumour xenografts were sectioned, stained with pimonidazole and immunolabelled for CSRP2 and/or HIF-1α. A correlation coefficient for co-localization of CSRP2 and HIF-1α is indicated in (B). These results are representative of at least 21 tumour sections originating from 4 animals for each type of xenograft (Fig. S5). (C) Immunohistochemistry showing typical CSRP2 upregulation at the centre of a tumour nest (box) in a lymph node of metastatic breast cancer. (D) Representative example of serial tissue sections of a triple negative breast tumour stained for HIF-1α and CSRP2 using immunohistochemistry. From the 48-sample TMA, a correlation coefficient value of 0.42 was calculated by Spearman Rank analysis (p = 0.0027; Table S1). (E–G) Kaplan-Meier survival analyses in relation to CSRP2 expression (affy ID 207030s_at) in breast carcinoma using overall (E) distant metastasis free (F) or relapse free (G) survival as an endpoint. The patient samples, hazard ratio with 95% confidence interval, and p value (Logrank test) are displayed on each chart. Upper quartile survival for patients with low and high CSRP2 expression is indicated in (F). Bars = 50 μm.

---

Taken all together, our data suggest that tumour hypoxia promotes CSRP2 overexpression, exacerbating the clinical outcome of breast cancer patients by enhancing tumour cell invasion and subsequent spread to distant tissues.

## Discussion

Both experimental and clinical studies have provided evidence that the hypoxic tumour microenvironment is an important risk factor for distant metastasis in breast cancer[3]. Here, we identified a novel mechanism by which hypoxia promotes mesenchymal invasion in breast cancer cells through the upregulation of CSRP2, a structural component of the actin cytoskeleton machinery involved in invadopodium formation[19]. Our functional investigations revealed that CSRP2 knockdown in MDA-MB-231 cells inhibits hypoxia-stimulated invadopodia formation and ECM degradation. Accordingly, it also significantly suppressed the stimulatory effect of

| Gene | Correlation coefficient | p-value |
|---|---|---|
| LOXL4 | 0.539 | 1.5E-92 |
| MET | 0.505 | 1.5E-79 |
| COX2/PTGS2 | 0.468 | 3.9E-67 |
| SNAIL1/SNAI1 | 0.427 | 5.0E-55 |
| TWIST1 | 0.388 | 5.7E-45 |
| ANGPTL4 | 0.385 | 2.9E-44 |
| L1CAM | 0.347 | 1.3E-35 |
| LOX | 0.331 | 1.9E-32 |
| PLAUR | 0.328 | 5.9E-32 |
| MMP2 | 0.303 | 2.8E-27 |
| LOXL2 | 0.3 | 1.3E-26 |
| PLOD2 | 0.283 | 7.4E-24 |
| PGF | 0.274 | 2.7E-22 |
| ANGPT2 | 0.263 | 1.1E-20 |
| SDF-1/CXCL12 | 0.255 | 1.7E-19 |
| CXCR4 | 0.248 | 1.8E-18 |
| MMP14 | 0.242 | 1.3E-17 |
| CXCR3 | 0.18 | 2.6E-10 |
| AMF/GPI | 0.118 | 3.7E-05 |
| P4HA2 | 0.097 | 6.9E-04 |
| VEGFA | 0.093 | 1.2E-03 |

**Table 1.** Co-expression of *CSRP2* with a manually curated set of hypoxia-induced, pro-metastatic, breast cancer genes. A manually formulated set of 26 genes consistently and directly found to be induced by HIF-1α, as well as being drivers of invasion and/or metastasis of breast cancer cells, was analysed for co-expression with *CSRP2* in the large TCGA dataset of gene expression in invasive, human breast cancers (n = 1,215). R values were calculated using Pearson's correlation or Spearman's rho for those genes with a normal distribution or otherwise, respectively, and the R value was used to calculate a p-value given the *n* of the sample set.

hypoxia on MDA-MB-231 cell invasiveness. Conversely, forced CSRP2 expression in HIF-1α-depleted hypoxic MDA-MB-231 cells was sufficient to increase cell invasion to an extent similar as in control hypoxic cells. Together these data support that CSRP2 is not only required for hypoxia-stimulated invasion, but contributes to drive this process.

Contrary to MDA-MB-231 cells, MCF-7 cells were unable to carry out localized gelatin matrix degradation under normoxia or hypoxia. In keeping with this, our western blot analyses revealed that both normoxic and hypoxic MCF-7 cells do not express MT1-MMP, a membrane anchored MMP which is critically required for tumour cell proteolytic activity[28,29]. Although proteolytically inactive, MCF-7 cells responded to hypoxia by assembling invadopodium precursors characterized by the re localization of cortactin, N-WASP and Tks5 to actin accumulations at the ventral cell membrane. This finding is highly consistent with a previous report showing that MT1-MMP depletion in MDA-MB-231 cells strongly inhibits gelatin matrix degradation but only modestly alters the onset of invadopodium formation[29]. In tumour cells, soluble MMP secretion is facilitated at invadopodia[33]. Thus, the increased secretion of MMP-2 and MMP-9 that is associated with the formation of invadopodium precursors in hypoxic MCF-7 cells (Fig. 4E) represents another piece of evidence of the nature of these structures. Consistent with the fact that MT1-MMP catalyses MMP-2 activation by cleavage of its pro-domain[34], and that MMP-2 contributes to MMP-9 activation[35,36], mostly inactive, high-molecular weight, forms of MMP-2 and MMP-9 were detected in our serum-free gelatin zymography assays.

Since invadopodium assembly and activity seems to be decoupled in hypoxic MCF-7 cells, this cell line turned out to be an appropriate experimental model to further characterize the mechanism by which CSRP2 mediates hypoxia-stimulated invasion. Indeed, our quantitative data show that CSRP2 knockdown significantly reduced the number of invadopodium precursors induced by hypoxia in MCF-7 cells, validating the structural role of CSPR2 in invadopodium assembly we previously suggested[19].

Our mechanistic investigations revealed that the proximal promoter of CSRP2 can be activated by either hypoxic culture conditions or HIF-1α overexpression, and that it contains two HREs (HRE1 and 2) able to promote HIF-1 recruitment. Although both HREs were found to contribute to hypoxia-induced transactivation of *CSRP2* promoter, our data luciferase reporter assays suggest that HRE2 has a predominant role over HRE1. Consistent with ChIP and luciferase reporter data, CSRP2 and HIF-1α protein levels were significantly correlated in both pre-clinical and patient tumour specimens, supporting that tumour hypoxia is an important determinant of CSRP2 up-regulation in breast cancer. The four breast cancer cell lines we analyzed responded to experimental hypoxia by increasing CSRP2 mRNA and protein expression. As previously reported[19], invasive cells (MDA-MB-231 and Hs578T) exhibited significant basal CSRP2 levels under normoxia while weakly invasive cells (T47D and MCF7) did not. We noticed that invasive cells frequently exhibited detectable amounts of HIF-1α under normoxia (as evaluated by western blot, Fig. 1A and B). Normoxic stabilization of HIF-1α and activation of HIF-1 signalling in triple negative breast cancer cells, such as MDA-MB-231 cells, was recently shown to be

regulated by a long noncoding RNA, namely *LINK-A*[37]. This pathway may account, at least to some extent, for normoxic expression of CSRP2 in triple negative breast cancer cells, which in turn contributes to maintain a constitutive invasive phenotype[19]. The significant basal expression level of CSRP2 in invasive normoxic cells (Fig. 1) is not contradictory with the role of CSRP2 in mediating the pro-invasive effects of hypoxia, and shows that hypoxia operates in breast cancer cells by up-regulating an actin regulatory protein that is also required for normoxic invasion. Other hypoxia-invadopodia axes were identified in cancer of different origins, such as melanoma, fibrosarcoma, and head and neck cells[38–41]. To our best knowledge, our report is the first example where hypoxia promotes cancer cell invasion by direct, HIF1-mediated, targeting of a basic structural cytoskeletal component of invadopodia.

A recent study has provided evidence that pancreatic ductal adenocarcinoma (PDAC) invasion and metastasis are promoted by HIF-1 dependent upregulation of another actin bundling protein, namely fascin[42]. Although the effects of fascin overexpression on PDAC cell invadopodium formation were not specifically evaluated, fascin has been shown to be a critical invadopodial component in prostate cancer and breast cancer cells[16,43,44]. Noticeably, fascin and CSRP2 knockdown achieves comparable reduction in ECM degradation and 3-D invasion in invasive breast cancer cells[16,19,43], suggesting a functional interaction/redundancy between these two actin bundling proteins. Remarkably, fascin ranks first in the most highly correlated genes to *CSRP2* in invasive breast cancer tumours (publicly available TCGA data at the cBioPortal for Cancer Genomics, http://www.cbioportal.org), raising the possibility that hypoxia and HIF-1 coordinate CSRP2 and fascin upregulation to promote invadopodium assembly/stabilization and invasion.

The clinical significance of our findings is further supported by transcritomic-associated survival analysis indicating that CSRP2 overexpression is associated with significantly shorter overall, metastasis- and relapse-free survival. Besides its role in breast cancer, CSRP2 was recently identified as a downstream target of *H19*, the long non-coding RNA with the strongest association with colorectal cancer patient survival[45]. Patients with high CSRP2 expression in colorectal tumours, display significantly shorter overall survival, and combined analysis of *H19* with *CSRP2* appears to be a powerful prognostic factor for overall survival. Another recent clinical study established a significant association between CSRP2 expression and B-cell acute lymphoblastic leukemia (ALL) relapse, and proposed CSRP2 as a prognostic marker for B-cell ALL patients with normal cytogenetics[46]. Functional analyses suggest that CSRP2 promotes B-cell ALL cell proliferation, migration, and drug resistance. Because hypoxia is a common feature of the bone marrow microenvironment that promotes HIF-dependent blood cancer progression and resistance to therapy[47], our data call for evaluation of hypoxia-regulated CSRP2 expression in blood cancers. Although the specific functions of CSRP2 in breast cancer, colorectal cancer and B-cell ALL may differ, these studies all point to the deleterious clinical consequence of CSRP2 overexpression.

Collectively, our data indicate that hypoxia exerts a direct control on invadopodium-mediated tumour cell invasion through HIF-1-mediated upregulation of the actin-bundling protein CSRP2 and provide a new mechanistic basis for the pro-metastatic effects of tumour hypoxia in breast cancer.

## Methods

**Cell lines.** MCF-7 cells were purchased from ATCC. MDA-MB-231, Hs578T, T47D and 4T1 cells were available at the Luxembourg Institute of Health. These cell lines were regularly tested for mycoplasma contamination and cultured in complete growth medium following ATCC recommendations. A standard tissue culture incubator was used for a normoxic culture conditions (21% $O_2$; 5% $CO_2$). For hypoxic treatment, cells were placed in a hypoxia work station (Invivo2 400, Ruskinn) for 24 hours or 48 hours, calibrated to maintain a hypoxic atmosphere of 0.1% $O_2$ and 5% $CO_2$ by continuous flow of nitrogen. The CSRP2-depleted 4T1 and corresponding control cell lines by lentiviral transduction. CRP2 knockdown was achieved by pGIPZ lentiviral shRNAs (clone ID: V3LMM_417823 from GE Dharmacon, gene set RMM4532). A non-silencing shRNAs (RHS4346, sh-; GE Dharmacon) was used as a control. Lentivirus production was achieved by co-transfecting lentiviral pGIPZ shRNAs with packaging and envelope plasmids in HEK293T cells using Xtreme transfection reagent (Roche). 4T1 cells were infected with virus, and transduced cells were selected with 0.5 μg/ml puromycin (Sigma-Aldrich).

**Western blot analysis.** Total protein extracts from cells was prepared in RIPA lysis buffer (Millipore) supplemented with protease and phosphatase inhibitor mixture (Roche). The extracts were subjected to Western blot using antibodies directed against CSRP2 (HPA045617, Sigma), Actin (A2066, Sigma), HIF-1α (610959, BD biosciences), and MT1-MMP (ab51074, Abcam). Protein bands were detected using Western Lightning Ultra (Perkin Elmer) and visualized with CL-Xposure film (Thermo Scientific). Protein levels were quantified using ImageJ (NIH, Bethesda, USA).

**siRNA transfection.** CSRP2 knockdown was achieved by transfection of 10 nM of 2 different predesigned siRNAs directed against human CSRP2 (siCSRP2#1, SI04283727, target sequence 5′-ACAGTGGCAATTCACGATGAA-3′ and siCSRP2#2, SI04251863, target sequence 5′-ACAGGCCTACAACAAATCCAA-3′; QIAGEN) using DharmaFECT™ transfection reagent (GE Dharmacon) and following manufacturer's instructions. HIF-1α knockdown was achieved using 2 different predesigned, functionally verified, siRNAs directed against human HIF-1α (siHIF1#1, SI02664053, targeted sequence 5′-AGGAAGAACTATGAACATAAA-3′, Qiagen and siHIF1#2, targeted sequence 5′-TACGTTGTGAGTGGTATTATT; Eurogentec), while non-targeting siRNAs were used as a control (Eurogentec). Freshly transfected cells were incubated 24 h under normoxia prior subsequent treatment or analysis.

**Quantitative RT-PCR.** Total RNA was isolated using the miRCURY RNA Isolation Kit (Exiqon) following the manufacturer's instructions. Purified RNA was reverse transcribed to cDNA using the Reverse Transcriptase Core kit (Eurogentec). Quantitative real-time PCR reactions were performed using SYBR Green I (Qiagen) on an Applied Biosystems ViiA 7 Real-Time PCR System (Thermo Fisher Scientific). The primers used were

175

5′-GATCTCGGACTCCCTGGAC-3′ (forward) and 5′-TCCCCAGACAGGCATTTT-3′ (reverse) for CSRP2 and 5′-TGTCCTGAATGTGGTCACCTGA-3′ (forward) and 5′-CTGCAGTCTCCTTGCACACCT-3′ (reverse) for mitochondrial ribosomal protein L32 (MRPL32). To calculate the relative abundance of the mRNA transcripts, the $\Delta\Delta$Ct method was used, with MRPL32 used as a reference mRNA. The Y-axis reflects fold change in gene expression.

**Chromatin immunoprecipitation assay.** MCF-7 cells were grown in 15 cm plates. Once the cells had reached 70% confluence, they were subjected to 24 hours of normoxia or hypoxia, as indicated. Chromatin was isolated and sheared using the Bioruptor Pico sonicator (Diagenode), with 10 cycles of 30 seconds on at high power, followed by 30 seconds off. Sheared chromatin was used for ChIP, with anti-HIF-1A$\alpha$ (ChIP grade, Active Motif, 39665) or negative control antibodies, with the ChIP-IT Express kit (Active Motif), according to the manufacturer's protocol. Pulled-down chromatin was then purified using the Chromatin IP DNA Purification Kit (Active Motif) and RT-PCR was performed using the following primer pairs: 5′-AAGTCCCTCTCCAAGTCC-3′ (forward) and 5′-CCACCAGGAGACAAAAGG-3′ (reverse) for HRE1, and 5′-TGCCTTTTGTCTCCTGGTG-3′ and 5′-ATGGGGATGTCGGAGGAGA-3′ (forward) for HRE2.

**Luciferase reporter assay.** Genomic DNA was purified from MCF-7 cells, using the AllPrep DNA/RNA/Protein Mini Kit (Qiagen). A region corresponding to $-1,920$ to $+103$ bp relative to the transcription start site of the human *CSRP2* gene was PCR amplified using the primers 5′-GATCACGCGTCAGGGACAGACAGCAGAAACA-3′ (forward) and 5′-GATCAGATCTTTGAGTCGGAGGCGGGAGCACGTAC-3′ (reverse), and inserted into the *MluI-BglII* multiple cloning site of the pGL3-Promoter vector (Promega). The HRE1 and HRE2 sites were mutated using overlapping PCR strategy and the following primer pairs: 5′-GAGGGAGCGGTCCCGGGAGCTGGGAAG-3′ (forward) and 5′-CGCCCGGCATCTTCCCAGCTCCCGG-3′ (reverse) for HRE1*, and 5′-CTAGCTCCGCCTGCGGTAGCTGCTCC-3′ (forward) and 5′-CTCACTTGAGTCGGAGGCGGGAGCAGCTACCGC-3′ (reverse) for HRE2*. The VEGF promoter luciferase reporter plasmid was provided by Dr. Amato J. Giaccia (Standford University school of Medicine, CA, USA). Briefly, $7 \times 10^4$ cells were seeded in each well of a 24-well plate. Six hours after plating, cells were transfected with the promoter luciferase reporter constructs, pGL4.73 [hRluc/SV40] vector (which contains the Renilla luciferase sequence downstream of the SV40 promotor), and, where indicated, a constitutively stable mutant HIF-1$\alpha$ expression vector (Addgene ref #52636), using Turbofect (Thermo Fisher Scientific), according to the manufacturer's protocol. Immediately after transfection, the plates were placed in either a normoxic or hypoxic incubator, as indicated. Twenty four hours after transfection, firefly and Renilla luciferase activities were measured using the Dual-Luciferase Reporter assay kit (Promega) and the ratio of firefly/Renilla luciferase was determined.

**Cell invasion and migration assays.** CSRP2- or HIF-1-depleted cells and control cells were incubated for 24 hours in hypoxia or normoxia. Fifty thousand cells were subsequently transferred onto 8.0 μm-pore transwell inserts (Greiner) in serum free DMEM, as previously described[19]. For invasion assays, transwell inserts were pre-coated with 100 μl of EHS matrix (330 μg/ml in serum-free DMEM) and incubated for 1 hour at 37 °C to allow polymerization. For migration assays, transwell inserts were pre-coated with collagen (100 μg/ml, collagen I, Millipore). The wells were filled with DMEM supplemented to 10% FBS as a chemoattractant. After 18 hours (MDA-MB-231 cell migration), 24 hours (MDA-MB-231 cell invasion) or 48 hours (4T1 cell invasion) incubation in hypoxia or normoxia, the total number of cells and the number of invasive cells were evaluated by MTT, and the percentage of invasion was calculated and normalized to siCtr-transfected normoxic cells (set to 1). For some specific assays, cells were co- transfected with HIF-1A targeting siRNAs and a plasmid allowing CSRP2 overexpression. The latter plasmid was generated by inserting CSRP2 coding sequence into the XhoI-BamHI cloning site of modified pCDNA 3.1- (Invitrogen) including a terminal HA tag. The primers used to PCR amplify CSRP2 coding sequence were 5′-GATCCTCGAGATGCCTGTCTGGGGAGGTGG-3′ (forward) and 5′-GATCAGGATCCCGCTGGGCATGAACAAGAGCCC-3′ (reverse). An empty pCDNA 3.1- was used as a control.

**Gelatinase zymography assays.** Four hundred thousand MCF-7 cells were plated in each well of a six-well plate. Six hours later, they were transfected with either control or CSRP2-targeting siRNAs. Twenty-four hours later, cells were washed with PBS, incubated with serum-free DMEM, and the plates were incubated in normoxic or hypoxic conditions for 32 hours. The conditioned media was collected and concentrated using Amicon Ultra Centrifugal Filters, 30 kDa cut-off (Merck Millipore, 803024), from an initial volume of two ml to a final volume of 22 μl. The conditioned media was then subjected to gelatinase zymography analysis. Briefly, the conditioned media was mixed with 4x sample buffer (0.25 Tris/HCl pH 6.8, 40% glycerol, 8% SDS and 0.1% bromophenol blue) and resolved on a 10% SDS-polyacrylamide gel containing 0.01% porcine gelatin (Sigma, G-8150). The MMPs were then renatured by soaking the gel in renaturing buffer (2.5% Triton in dH$_2$O) for 30 minutes. The gels were then washed several times with dH$_2$O and incubated for 30 minutes with developing buffer (0.05 M Tris-HCl pH 7.8, 0.2 M NaCl, 0.005 CaCl$_2$, and 0.02% Brij-35). The buffer was then poured out, fresh buffer added and the gel was incubated overnight at 37 C. The following day, the gels were visualized with Coomassie blue staining.

**Fluorescent gelatin degradation assays.** Fluorescent gelatin slides were prepared similarly as described in Artym *et al.*[29]. In brief, 16-mm coverslips were coated with poly-L-Lysine (25 μg/ml, 20 minutes at room temperature) and crosslinked with glutaraldehyde (0.5%, 15 minutes at room temperature). After extensive PBS washing, coverslips were inverted on a 60 μl drop of 0.2% gelatin solution containing a mix of 1:20 Oregon green 488-labelled gelatin (Molecular Probes) and unlabeled porcine gelatin (Sigma). After a 15-minute incubation, and 3 washes, coverslips were sterilized with 70% ethanol for 30 minutes and subsequently incubated with complete medium for 30 minutes. MDA-MB-231 cells were pre-incubated for 32 hours in hypoxia or normoxia before they

176

were transferred onto gelatin-coated coverslips for a 16-hour incubation period in the same culture conditions. A low-density seeding was used to avoid cell clustering and facilitate the analysis. MCF-7 and 4T1 cells were directly loaded onto gelatin-coated coverslips and incubated for 48 hours in hypoxia or normoxia. Then, tumour cells were fixed and stained for actin and cortactin (see "Confocal microscopy and cell imaging" subsection). Active cells were defined as cells with dark dots (corresponding to fluorescent gelatin-cleared areas) underneath actin-cortactin co-labelled invadopodia. Digested gelatin areas were quantified with the threshold tool in ImageJ software, and an average degradation index (degraded matrix area per cell) was calculated.

**Confocal microscopy and cell imaging.** Imaging was performed on a laser scanning confocal microscope (LSM880 FastAiry, Carl Zeiss) equipped with a x63/1.4 numerical aperture (NA) oil immersion Plan-Apochromat objective for cell imaging or a x40/1.3 oil immersion Plan-Apochromat for tumour slice imaging. All pictures were acquired with multitrack configuration with a confocal optical slice set at 1 µm thickness. MDA-MB-231, 4T1 and MCF-7 cells were plated on gelatin-coated coverslips (see "Fluorescent gelatin degradation assays" subsection) for 16 hours or 48 hours. MCF-7 cells were also plated on collagen-coated coverslips (100 µg/ml, collagen I, Millipore) for 48 hours. Pre-fixation was performed in 3.5% PFA and 0.3% Triton X-100 in PEM (100 mM PiPES, pH6.9, 1 mM EGTA and 1 mM $MgCl_2$) for 3 minutes whereas fixation was performed in PFA 3.5% in PEM for 20 minutes. Cortactin and N-WASP were immunodetected using mouse monoclonal antibodies (clone 4F11, Millipore) and rabbit monoclonal antibodies (clone 30D10, Cell Signalling), respectively. The actin cytoskeleton was labelled using Acti-stain 488 or 555 or 670 (Cytoskeleton) phalloidin depending on the experimental conditions. To facilitate evaluation, actin cytoskeleton was always depicted in green regardless of the type of staining used. Before confocal microscopy imaging, coverslips were mounted in Fluoromount medium (Sigma). In some experiments, MCF-7 cells were transfected using Lipofectamine 2000 (Thermo Fisher Scientific) with a construct coding for GFP-fused Tks5 (Tks5-GFP; kind gift from Dr. Sara A. Courtneidge, Portland, USA) or a construct coding for GFP-fused CSRP2 (CSRP2-GFP). The latter was obtained by inserting the CSRP2 coding sequence into the pEGFP-N1 plasmid vector *via* XhoI and BamHI restriction sites. After 48 hours in hypoxic conditions, MCF7 cells expressing CSRP2-GFP were incubated 4 hours with live cell imaging actin probe (siR-Actin 1 µM, Cytoskeleton) before observation under the microscope in hypoxic conditions (5% $CO_2$ and 0.1% $O_2$).

***In vivo* xenograft assays and immunofluorescent staining.** Animal work was conducted in accordance with the national and international regulations. The protocols were reviewed and approved by the animal welfare body of LIH (protocol LECR-2016-07), and received an authorization from the Ministry of Agriculture and Ministry of Higher Education and Research. Five million of MCF-7 or MDA-MB-231 tumour cells in 50 µl matrigel diluted 1:1 in PBS were subcutaneously implanted into the mammary fat pad of NOD *scid* gamma (NSG; NOD.Cg-Prkdc[scid] Il2rg[tm1WjI]/SzJ), 8-week-old female mice (Charles River). Primary tumour dimensions (length, width and height) were periodically measured using calipers and the tumour volume was calculated according to the formula: ½ × L × W × H. When tumours reached a size of approximately 200 mm³, they were harvested and flash frozen in isopentane.

The tumours were sectioned with a cryostat (Leica SM1850 UV) in 120 µm thick sections and fixed in 4% paraformaldehyde for 15 min. Then sections were permeabilized for 15 min in 0.1% Triton followed by 3 baths in 0.1% NaBH4. HIF-1α and CSRP2 were immunolocalized using mouse monoclonal (610959, BD Biosciences) and rabbit polyclonal antibodies (HPA045617, Sigma), respectively. For correlation analyses, sections were fixed in acetone:chloroform (1:1) for 5 min at −20 °C, which results in a better preservation of CSRP2. HIF-1 and CSRP2 co-localization was estimated by calculating Pearson's coefficient values using the JACoP plugin from ImageJ software[48]. Twenty-one and 22 sections originating from 4 independent MCF-7 and MDA-MB-231 xenograft tumours, respectively, were used for calculations. Scattered plots were generated using the Zen 2.1. software of the confocal microscope (LSM880 FastAiry, Carl Zeiss). Staining of tumour hypoxic regions was achieved using The Hydroxyprobe™-1 Plus Kit (Hydroxyprobe hpi, Burlington, MA, USA). Mice were injected intraperitoneally with a pimonidazole HCL solution at a dosage of 60 mg/kg body weight 30 minutes prior sacrifice. FITC-conjugated IgG1 mouse monoclonal antibody from the same Kit was used for immunofluorescence staining.

**Immunohistochemistry.** Human triple negative breast cancer tissue arrays (BRC964) including 48 cases were purchased from Pantomics, Inc. (Richmond, CA, USA). Immunohistochemical staining was performed as previously described[19] using rabbit polyclonal antibodies against human CSRP2 (HPA045617, Sigma-Aldrich; 1/250) and rabbit monoclonal antibodies against HIF-1α (EP118; Epitomics). Rabbit anti-cytokeratin and normal rabbit serum were used as positive and negative controls. The results were semi-quantitatively scored by a pathologist as followed: 0: no signal, 0.5: insufficient signal, 1: weak signal, 2: moderate signal, and 3: strong signal. Values below 1 were considered as negative. For statistical analyses, an intensity index was calculated by multiplying the intensity score by the percentage of positive cells. Intensity index values were used to rank all the samples for Spearman rank correlation test.

**Statistical analysis.** All numerical data are shown as mean ± SEM. Error bars represent standard errors. Statistical significance was determined by Spearman rank correlation test for the *in vivo* immunohistochemical results, paired two-tailed Student's t distribution test for transwell cell invasion assay, and unpaired two-tailed Student's t test for the other analyses. For the analysis of the active cell population on gelatin, p values were calculated from the Z-score for 2 population proportion. P values < 0.05 were considered statistically significant.

The expression analysis of HIF-1α target genes and of *CSRP2* in human breast cancer here is wholly based upon data generated by the TCGA Research network: http://cancergenome.nih.gov/. The TCGA breast cancer gene expression data was downloaded from the UCSC Cancer Genome Browser. Normality of the distribution of expression values for each gene was assessed using the D'Agostino-Pearson omnibus test. *CSRP2* expression was normally

177

distributed, so for genes that had a normal expression distribution, a Pearson's correlation coefficient was calculated. For genes that were not normally distributed, a Spearman's rank correlation coefficient was calculated. These values were then used to calculate a p-value, given the $n$ of the sample size (1,215 in this case). To compare *CSRP2* across different breast cancer subtypes, one-way ANOVA was used to confirm that the groups were statistically significantly different and two-tailed t-tests were performed to compare the groups in a pair-wise fashion.

Kaplan-Meier survival plots, hazard ratio with 95% confidence intervals and log-rank p values were generated using the Kaplan-Meier Plotter tool[32] to test for associations between CSRP2 expression (Affy probe 207030s_at), and overall-, metastasis- and relapse-free survival in breast cancer patients. Gene expression data and survival information were downloaded from GEO, EGA and TCGA. Only Affymetrix HG-U133A, HG-U133 Plus 2.0 and HG-U133A 2.0 arrays were included. Biased arrays were excluded and redundant samples were removed.

## References

1. Steeg, P. S. Targeting metastasis. *Nat Rev Cancer* **16**, 201–218, https://doi.org/10.1038/nrc.2016.25 (2016).
2. Gilkes, D. M., Semenza, G. L. & Wirtz, D. Hypoxia and the extracellular matrix: drivers of tumour metastasis. *Nat Rev Cancer* **14**, 430–439, https://doi.org/10.1038/nrc3726 (2014).
3. Semenza, G. L. The hypoxic tumor microenvironment: A driving force for breast cancer progression. *Biochim Biophys Acta* **1863**, 382–391, https://doi.org/10.1016/j.bbamcr.2015.05.036 (2016).
4. Rankin, E. B. & Giaccia, A. J. Hypoxic control of metastasis. *Science* **352**, 175–180, https://doi.org/10.1126/science.aaf4405 (2016).
5. Gould, C. M. & Courtneidge, S. A. Regulation of invadopodia by the tumor microenvironment. *Cell Adh Migr* **8**, 226–235 (2014).
6. Linder, S. The matrix corroded: podosomes and invadopodia in extracellular matrix degradation. *Trends in cell biology* **17**, 107–117, https://doi.org/10.1016/j.tcb.2007.01.002 (2007).
7. Eddy, R. J., Weidmann, M. D., Sharma, V. P. & Condeelis, J. S. Tumor Cell Invadopodia: Invasive Protrusions that Orchestrate Metastasis. *Trends in cell biology*, https://doi.org/10.1016/j.tcb.2017.03.003 (2017).
8. Leong, H. S. *et al.* Invadopodia are required for cancer cell extravasation and are a therapeutic target for metastasis. *Cell reports* **8**, 1558–1570, https://doi.org/10.1016/j.celrep.2014.07.050 (2014).
9. Stoletov, K. & Lewis, J. D. Invadopodia: a new therapeutic target to block cancer metastasis. *Expert Rev Anticancer Ther* **15**, 733–735, https://doi.org/10.1586/14737140.2015.1058711 (2015).
10. Tokui, N. *et al.* Extravasation during bladder cancer metastasis requires cortactinmediated invadopodia formation. *Mol Med Rep* **9**, 1142–1146, https://doi.org/10.3892/mmr.2014.1965 (2014).
11. Gligorijevic, B. *et al.* N-WASP-mediated invadopodium formation is involved in intravasation and lung metastasis of mammary tumors. *Journal of cell science* **125**, 724–734, https://doi.org/10.1242/jcs.092726 (2012).
12. Gligorijevic, B., Bergman, A. & Condeelis, J. Multiparametric classification links tumor microenvironments with tumor cell phenotype. *Plos Biol* **12**, e1001995, https://doi.org/10.1371/journal.pbio.1001995 (2014).
13. Blouw, B. *et al.* The invadopodia scaffold protein Tks5 is required for the growth of human breast cancer cells *in vitro* and *in vivo*. *Plos One* **10**, e0121003, https://doi.org/10.1371/journal.pone.0121003 (2015).
14. Hotary, K. B. *et al.* Membrane type I matrix metalloproteinase usurps tumor growth control imposed by the three-dimensional extracellular matrix. *Cell* **114**, 33–45 (2003).
15. Albiges-Rizo, C., Destaing, O., Fourcade, B., Planus, E. & Block, M. R. Actin machinery and mechanosensitivity in invadopodia, podosomes and focal adhesions. *Journal of cell science* **122**, 3037–3049, https://doi.org/10.1242/jcs.052704 (2009).
16. Schoumacher, M., Goldman, R. D., Louvard, D. & Vignjevic, D. M. Actin, microtubules, and vimentin intermediate filaments cooperate for elongation of invadopodia. *The Journal of cell biology* **189**, 541–556, https://doi.org/10.1083/jcb.200909113 (2010).
17. Yamaguchi, H. & Condeelis, J. Regulation of the actin cytoskeleton in cancer cell migration and invasion. *Biochim Biophys Acta* **1773**, 642–652, https://doi.org/10.1016/j.bbamcr.2006.07.001 (2007).
18. Linder, S., Wiesner, C. & Himmel, M. Degrading devices: invadosomes in proteolytic cell invasion. *Annual review of cell and developmental biology* **27**, 185–211, https://doi.org/10.1146/annurev-cellbio-092910-154216 (2011).
19. Hoffmann, C. *et al.* CRP2, a new invadopodia actin bundling factor critically promotes breast cancer cell invasion and metastasis. *Oncotarget* **7**, 13688–13705, https://doi.org/10.18632/oncotarget.7327 (2016).
20. Hoffmann, C. *et al.* Human Muscle LIM Protein Dimerizes along the Actin Cytoskeleton and Cross-Links Actin Filaments. *Molecular and cellular biology* **34**, 3053–3065, https://doi.org/10.1128/MCB.00651-14 (2014).
21. Tran, T. C., Singleton, C., Fraley, T. S. & Greenwood, J. A. Cysteine-rich protein 1 (CRP1) regulates actin filament bundling. *BMC Cell Biol* **6**, 45 (2005).
22. Hu, Z. *et al.* The molecular portraits of breast tumors are conserved across microarray platforms. *BMC Genomics* **7**, 96, https://doi.org/10.1186/1471-2164-7-96 (2006).
23. Liu, Z. J., Semenza, G. L. & Zhang, H. F. Hypoxia-inducible factor 1 and breast cancer metastasis. *J Zhejiang Univ Sci B* **16**, 32–43, https://doi.org/10.1631/jzus.B1400221 (2015).
24. Semenza, G. L. Hypoxia-inducible factors: mediators of cancer progression and targets for cancer therapy. *Trends Pharmacol Sci* **33**, 207–214, https://doi.org/10.1016/j.tips.2012.01.005 (2012).
25. Semenza, G. L. *et al.* Hypoxia response elements in the aldolase A, enolase 1, and lactate dehydrogenase A gene promoters contain essential binding sites for hypoxia-inducible factor 1. *J Biol Chem* **271**, 32529–32537 (1996).
26. Wenger, R. H., Stiehl, D. P. & Camenisch, G. Integration of oxygen signaling at the consensus HRE. *Sci Stke* **2005**, re12, https://doi.org/10.1126/stke.3062005re12 (2005).
27. Messeguer, X. *et al.* PROMO: detection of known transcription regulatory elements using species-tailored searches. *Bioinformatics* **18**, 333–334 (2002).
28. Munoz-Najar, U. M., Neurath, K. M., Vumbaca, F. & Claffey, K. P. Hypoxia stimulates breast carcinoma cell invasion through MT1-MMP and MMP-2 activation. *Oncogene* **25**, 2379–2392, https://doi.org/10.1038/sj.onc.1209273 (2006).
29. Artym, V. V., Zhang, Y., Seillier-Moiseiwitsch, F., Yamada, K. M. & Mueller, S. C. Dynamic interactions of cortactin and membrane type 1 matrix metalloproteinase at invadopodia: defining the stages of invadopodia formation and function. *Cancer research* **66**, 3034–3043, https://doi.org/10.1158/0008-5472.CAN-05-2177 (2006).
30. Sharma, V. P. *et al.* Tks5 and SHIP2 regulate invadopodium maturation, but not initiation, in breast carcinoma cells. *Curr Biol* **23**, 2079–2089, https://doi.org/10.1016/j.cub.2013.08.044 (2013).
31. Gilkes, D. M. & Semenza, G. L. Role of hypoxia-inducible factors in breast cancer metastasis. *Future Oncol* **9**, 1623–1636, https://doi.org/10.2217/fon.13.92 (2013).
32. Gyorffy, B. *et al.* An online survival analysis tool to rapidly assess the effect of 22,277 genes on breast cancer prognosis using microarray data of 1,809 patients. *Breast cancer research and treatment* **123**, 725–731, https://doi.org/10.1007/s10549-009-0674-9 (2010).
33. Jacob, A. & Prekeris, R. The regulation of MMP targeting to invadopodia during cancer metastasis. *Front Cell Dev Biol* **3**, 4, https://doi.org/10.3389/fcell.2015.00004 (2015).

178

34. Nishida, Y. *et al.* Activation of matrix metalloproteinase-2 (MMP-2) by membrane type 1 matrix metalloproteinase through an artificial receptor for proMMP-2 generates active MMP-2. *Cancer research* **68**, 9096–9104, https://doi.org/10.1158/0008-5472.CAN-08-2522 (2008).
35. Toth, M., Chvyrkova, I., Bernardo, M. M., Hernandez-Barrantes, S. & Fridman, R. Pro-MMP-9 activation by the MT1-MMP/MMP-2 axis and MMP-3: role of TIMP-2 and plasma membranes. *Biochem Biophys Res Commun* **308**, 386–395 (2003).
36. Li, Z., Takino, T., Endo, Y. & Sato, H. Activation of MMP-9 by membrane type-1 MMP/MMP-2 axis stimulates tumor metastasis. *Cancer Sci* **108**, 347–353, https://doi.org/10.1111/cas.13134 (2017).
37. Lin, A. *et al.* The LINK-A lncRNA activates normoxic HIF1alpha signalling in triple-negative breast cancer. *Nat Cell Biol* **18**, 213–224, https://doi.org/10.1038/ncb3295 (2016).
38. Hanna, S. C. *et al.* HIF1alpha and HIF2alpha independently activate SRC to promote melanoma metastases. *J Clin Invest* **123**, 2078–2093, https://doi.org/10.1172/JCI66715 (2013).
39. Diaz, B., Yuen, A., Iizuka, S., Higashiyama, S. & Courtneidge, S. A. Notch increases the shedding of HB-EGF by ADAM12 to potentiate invadopodia formation in hypoxia. *The Journal of cell biology* **201**, 279–292, https://doi.org/10.1083/jcb.201209151 (2013).
40. Arsenault, D., Brochu-Gaudreau, K., Charbonneau, M. & Dubois, C. M. HDAC6 deacetylase activity is required for hypoxia-induced invadopodia formation and cell invasion. *Plos One* **8**, e55529, https://doi.org/10.1371/journal.pone.0055529 (2013).
41. Lucien, F., Brochu-Gaudreau, K., Arsenault, D., Harper, K. & Dubois, C. M. Hypoxia-induced invadopodia formation involves activation of NHE-1 by the p90 ribosomal S6 kinase (p90RSK). *Plos One* **6**, e28851, https://doi.org/10.1371/journal.pone.0028851 (2011).
42. Zhao, X. *et al.* Hypoxia-inducible factor-1 promotes pancreatic ductal adenocarcinoma invasion and metastasis by activating transcription of the actin-bundling protein fascin. *Cancer research* **74**, 2455–2464, https://doi.org/10.1158/0008-5472.CAN-13-3009 (2014).
43. Li, A. *et al.* The actin-bundling protein fascin stabilizes actin in invadopodia and potentiates protrusive invasion. *Curr Biol* **20**, 339–345, https://doi.org/10.1016/j.cub.2009.12.035 (2010).
44. Van Audenhove, I. *et al.* Stratifying fascin and cortactin function in invadopodium formation using inhibitory nanobodies and targeted subcellular delocalization. *FASEB journal: official publication of the Federation of American Societies for Experimental Biology* **28**, 1805–1818, https://doi.org/10.1096/fj.13-242537 (2014).
45. Ohtsuka, M. *et al.* H19 Noncoding RNA, an Independent Prognostic Factor, Regulates Essential Rb-E2F and CDK8-beta-Catenin Signaling in Colorectal Cancer. *EBioMedicine* **13**, 113–124, https://doi.org/10.1016/j.ebiom.2016.10.026 (2016).
46. Wang, S. J. *et al.* Cysteine and glycine-rich protein 2 (CSRP2) transcript levels correlate with leukemia relapse and leukemia-free survival in adults with B-cell acute lymphoblastic leukemia and normal cytogenetics. *Oncotarget*, https://doi.org/10.18632/oncotarget.16416 (2017).
47. Schito, L., Rey, S. & Konopleva, M. Integration of hypoxic HIF-alpha signaling in blood cancers. *Oncogene*, https://doi.org/10.1038/onc.2017.119 (2017).
48. Bolte, S. & Cordelieres, F. P. A guided tour into subcellular colocalization analysis in light microscopy. *J Microsc* **224**, 213–232, https://doi.org/10.1111/j.1365-2818.2006.01706.x (2006).

## Acknowledgements

## Author Contributions

C.T. conceived and designed the overall study with input from X.M. and C.H. C.H. and X.M. performed most of the experiments with technical assistance from F.M. J.B.C. and H.W. conducted luciferase reporter and gel zymography analyses. A.A.A. conducted ChIP experiments. F.S. and B.S. provided significant support for immunohistochemistry analyses. G.B. and B.J. provided technical support and conceptual advice. C.T. and X.M. wrote the manuscript. All authors read and approved the final manuscript.

## Additional Information

**Supplementary information** accompanies this paper at https://doi.org/10.1038/s41598-018-28637-x.

**Competing Interests:** The authors declare no competing interests.

**Publisher's note:** Springer Nature remains neutral with regard to jurisdictional claims in published maps and institutional affiliations.

179

**Fig S1. CSRP2 knockdown inhibits hypoxia promoted invadopodia-mediated ECM degradation MDA-MB-231.** Fluorescent gelatin degradation assay in normoxic or hypoxic conditions. Random pictures from one experiment with control (siCtr) and CSRP2-depleted (siCRP2#2) cells plated on Oregon Green 488-labelled gelatin-coated coverslips for 16 hours, fixed and stained for the actin cytoskeleton (red) and the nucleus. These are examples of pictures used for the quantitative analyses shown in Fig. 3C.
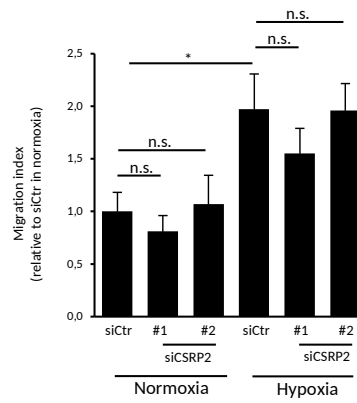
**Fig. S2. CSRP2 is not required for MDA-MB-231 cell migration under normoxia or hypoxia.** Transwell migration assay with normoxic or hypoxic MDA-MB-231 cells transfected with control (siCtr) or two different CSRP2-targeting siRNAs (siCSRP2 #1 and 2). Cells were plated on collagen-coated transwell for 18h and quantified via MTT staining. Results were expressed relatively to the migration of siCtr-transfected normoxic cells (set to 1). The data originate from 3 independent experiments. *p < 0.05.
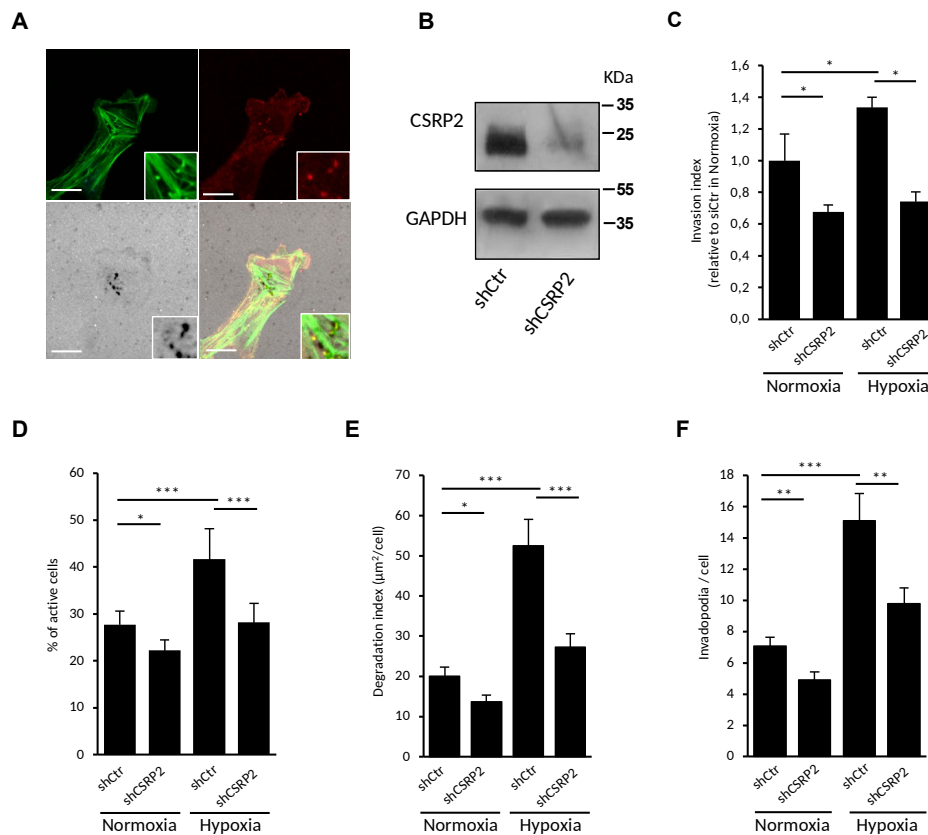
**Fig. S3. CSRP2 is required for hypoxia-stimulated invadopodia formation, ECM degradation and cell invasion in mouse 4T1 cells.** (**A**) Gelatin degradation assay showing that mouse 4T1 cells form mature invadopodia. Cells were plated on Oregon Green 488-labelled gelatin-coated coverslips for 48 hours, fixed and stained for actin and cortactin to visualize invadopodia (insets). (**B**) Western blot showing CSRP2 protein levels in 4T1 cell lines transduced to stably express a control, non-targeting, shRNA (shCtr) or a CSRP2 transcript-targeting shRNA (shCSRP2). (**C**) Transwell invasion assay. Invading control and CSRP2-depleted 4T1 cells in normoxia and hypoxia at 48 h were quantified via MTT staining. Results were expressed relatively to the invasion of expressing normoxic cells (set to 1). The data originate from 3 independent experiments. (**D**) Actively ECM degrading cells as expressed as percentage of the total cell population. (**E**) Degradation index corresponding to the average of degraded matrix per cell. (**F**) Number of mature invadopodia per cell (as defined by the number F-actin and cortactin co-labelled puncta overlapping with areas of gelatin clearing). The data originate from at least three independent experiments (n ≥ 60 cells). Bars = 15 μm. *p < 0.05; **p < 0.01, ***p < 0.001.
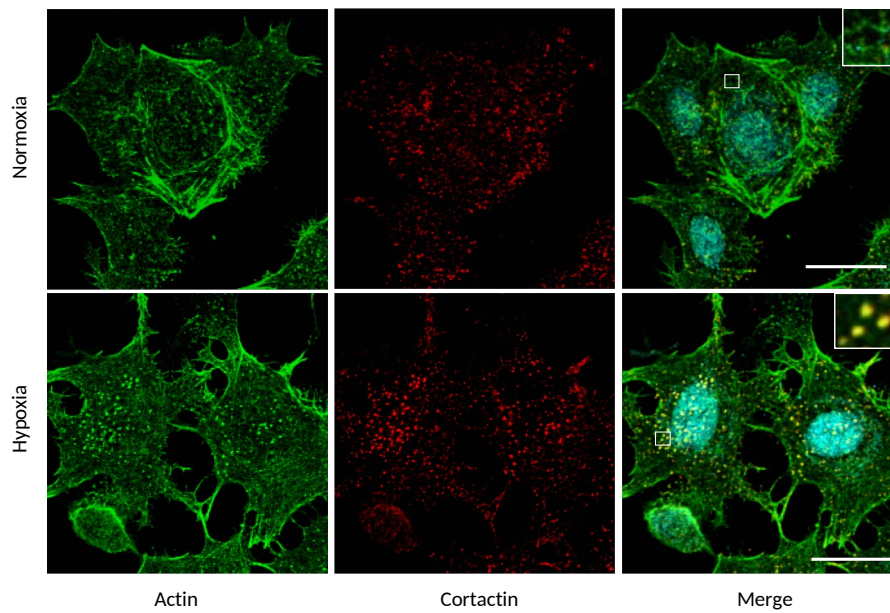
**Fig. S4. Hypoxia-induced invadopodium precursors in MCF-7 plated on non-denatured collagen.** MCF-7 cells were plated on collagen I-coated slides and incubated for 24 hours in normoxic or hypoxic conditions. After fixation, MCF-7 cells were stained for actin (in green) and cortactin (in red), and imaged using confocal microscopy. The inset shows that only hypoxia induces cortactin relocalization to ventral actin puncta. Bars = 15 µm.

**A**



**B**

MCF7

| | | |
|---|---|---|
| Mouse 1 | Tumor section 1 | 0.721 |
| | Tumor section 2 | 0.581 |
| | Tumor section 3 | 0.726 |
| | Tumor section 4 | 0.751 |
| | Tumor section 5 | 0.813 |
| Mouse 2 | Tumor section 1 | 0.737 |
| | Tumor section 2 | 0.798 |
| | Tumor section 3 | 0.729 |
| | Tumor section 4 | 0.74 |
| | Tumor section 5 | 0.719 |
| Mouse 3 | Tumor section 1 | 0.808 |
| | Tumor section 2 | 0.792 |
| | Tumor section 3 | 0.846 |
| | Tumor section 4 | 0.747 |
| | Tumor section 5 | 0.769 |
| Mouse 4 | Tumor section 1 | 0.5 |
| | Tumor section 2 | 0.765 |
| | Tumor section 3 | 0.738 |
| | Tumor section 4 | 0.771 |
| | Tumor section 5 | 0.703 |
| | Tumor section 6 | 0.584 |
| | Tumor section 7 | 0.801 |
| | average | 0.73+/-0.08 |
| | p-value | 6.80E-05 |

**C**

MDA-MB-231

| | | |
|---|---|---|
| Mouse 1 | Tumor section 1 | 0.787 |
| | Tumor section 2 | 0.717 |
| | Tumor section 3 | 0.691 |
| | Tumor section 4 | 0.747 |
| | Tumor section 5 | 0.726 |
| Mouse 2 | Tumor section 1 | 0.744 |
| | Tumor section 2 | 0.806 |
| | Tumor section 3 | 0.691 |
| | Tumor section 4 | 0.627 |
| | Tumor section 5 | 0.756 |
| Mouse 3 | Tumor section 1 | 0.709 |
| | Tumor section 2 | 0.701 |
| | Tumor section 3 | 0.738 |
| | Tumor section 4 | 0.723 |
| | Tumor section 5 | 0.695 |
| Mouse 4 | Tumor section 1 | 0.731 |
| | Tumor section 2 | 0.824 |
| | Tumor section 3 | 0.821 |
| | Tumor section 4 | 0.776 |
| | Tumor section 5 | 0.802 |
| | Tumor section 6 | 0.859 |
| | average | 0.75+/-0.15 |
| | p-value | 6.67E-05 |

**Fig. S5. CSRP2 and HIF-1α protein levels are highly correlated in MCF-7 and MDA-MB-231 tumour xenografts.** (**A**) Example of scattered plots showing pixel intensity for CSRP2 versus HIF-1α signals in an MCF-7 tumour section. (**B and C**) Tables showing the correlation coefficients for CSRP2 and HIF-1α protein levels (extracted from scattered plots) in 22 MCF-7 (B) and 21 MDA-MB-231 (C) tumour xenograft sections. The sections originating from the same tumour were taken from distant sites. An average correlation coefficient value and a corresponding p value are given below each table.

**A**

Overall survival

HR = 1.49 (1.18 - 1.86)
logrank P = 0.00056

— Low (939)
— High (463)

**B**

Overall survival

HR = 1.28 (1.03 - 1.6)
Log-rank P = 0.025

— Low (702)
— High (700)
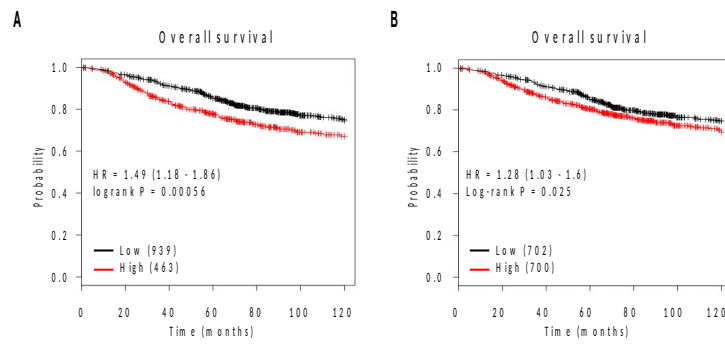
**Fig. S6. Kaplan-Meier survival analyses in relation to CSRP2 expression (affy ID 207030s_at) in breast carcinoma using overall survival as an endpoint.** Patients were stratified according to the upper (A) or median (B) CSRP2 expression values. The patient samples, hazard ratio with 95% confidence interval, and p value (Logrank test) are displayed on each chart.

**A**

CSRP2 expression in
human breast cancers

**B**

Distant metastasis-free survival
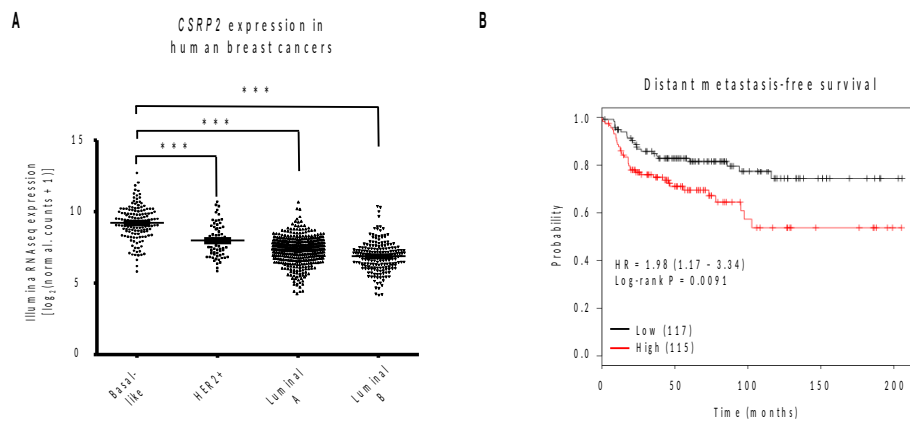
**Fig. S7.** ***CSRP2*** **levels are elevated and is a stronger predictor of distant metastasis-free survival in basal subtype human breast cancers. (A)** *CSRP2* gene expression data for the large TCGA invasive, human breast cancer data set (n = 1,215) was compared across the different breast cancer subtypes and found to be an order of magnitude higher in the basal subtype. (**B**) Kaplan-Meier survival analysis was performed; patients were stratified according to the median *CSRP2* expression value and distant metastasis-free survival was used as an endpoint. The patient samples, hazard ratio with 95% confidence interval, and *p* value (log-rank test) are displayed on the chart. *** denotes a p-value less than 0.001.

# Article 2

## CRP2, a new invadopodia actin bundling factor critically promotes breast cancer cell invasion and metastasis.

Hoffmann C, Mao X, Dieterle M, Moreau F, <u>Al Absi A</u>, Steinmetz A, Oudin A, Berchem G, Janji B and Thomas C. *Oncotarget*. 2016.

# CRP2, a new invadopodia actin bundling factor critically promotes breast cancer cell invasion and metastasis

Céline Hoffmann[1,*], Xianqing Mao[1,*], Monika Dieterle[1,2], Flora Moreau[1], Antoun Al Absi[1], André Steinmetz[3], Anaïs Oudin[2], Guy Berchem[1], Bassam Janji[1] and Clément Thomas[1]

[1] Laboratory of Experimental Cancer Research, Department of Oncology, Luxembourg Institute of Health, 84 Val, Fleuri, Luxembourg, Luxembourg

[2] NorLux Neuro-Oncology Laboratory, Department of Oncology, Luxembourg Institute of Health, 84 Val, Fleuri, Luxembourg, Luxembourg

[3] Department of Oncology, Luxembourg Institute of Health, 84 Val, Fleuri, Luxembourg, Luxembourg

[*] These authors have contributed equally to this work

Correspondence to: Clément Thomas, email: clement.thomas@lih.lu

## ABSTRACT

A critical process underlying cancer metastasis is the acquisition by tumor cells of an invasive phenotype. At the subcellular level, invasion is facilitated by actin-rich protrusions termed invadopodia, which direct extracellular matrix (ECM) degradation. Here, we report the identification of a new cytoskeletal component of breast cancer cell invadopodia, namely cysteine-rich protein 2 (CRP2). We found that CRP2 was not or only weakly expressed in epithelial breast cancer cells whereas it was up-regulated in mesenchymal/invasive breast cancer cells. In addition, high expression of the CRP2 encoding gene *CSRP2* was associated with significantly increased risk of metastasis in basal-like breast cancer patients. CRP2 knockdown significantly reduced the invasive potential of aggressive breast cancer cells, whereas it did not impair 2D cell migration. In keeping with this, CRP2-depleted breast cancer cells exhibited a reduced capacity to promote ECM degradation, and to secrete and express MMP-9, a matrix metalloproteinase repeatedly associated with cancer progression and metastasis. In turn, ectopic expression of CRP2 in weakly invasive cells was sufficient to stimulate cell invasion. Both GFP-fused and endogenous CRP2 localized to the extended actin core of invadopodia, a structure primarily made of actin bundles. Purified recombinant CRP2 autonomously crosslinked actin filaments into thick bundles, suggesting that CRP2 contributes to the formation/maintenance of the actin core. Finally, CRP2 depletion significantly reduced the incidence of lung metastatic lesions in two xenograft mouse models of breast cancer. Collectively, our data identify CRP2 as a new cytoskeletal component of invadopodia that critically promotes breast cancer cell invasion and metastasis.

## INTRODUCTION

Metastasis is the primary cause of death from cancer and is a major hurdle for cancer treatment [1]. A critical step of the metastatic cascade is the acquisition by carcinoma cells of the ability to remodel the extracellular matrix (ECM) and migrate through the stromal environment and tissue barriers. At the subcellular level, such ability is associated with actin-rich membrane protrusions termed invadopodia, which recruit and drive the local secretion of matrix metalloproteinases (MMPs) able to promote ECM degradation [2, 3]. Invadopodia were initially described on the basal surface of cultured cancer and v-Src transformed cells in the 80's [4]. However, their relevance in cancer progression and potential as therapeutic targets have only recently been recognized [5-7]. For instance, a recent intravital imaging-based study has provided direct and compelling

evidence of the key role played by invadopodia during the extravasation of human breast cancer cells in mouse models [6]. Although initially promising, MMP inhibitors failed in the clinic, mostly due to high toxicity [8], and new molecular targets to inhibit invadopodia formation and/or activity are required.

Invadopodia comprise a protrusive actin-dense core and a surrounding region enriched in signaling and adhesion proteins [3, 9]. In the core, actin filaments (AFs) are cross-linked in thick bundles, which presumably focus actin polymerization-promoted force for protrusive activity, and stabilize invadopodia over long periods to optimize ECM degradation [9-12]. Consistent with such important roles for actin core bundles, the invasive and metastatic potential of tumor cells was considerably reduced by inhibiting the expression or activity of fascin, an invadopodia-enriched actin-bundling factor [9, 10, 12-14]. Although T-fimbrin, another AF crosslinking protein, was also detected in invadopodia, its knockdown only had minimal effects on invadopodia biogenesis and activity [9], suggesting that fascin is the major actin bundling factor in invadopodia.

Cysteine-rich proteins (CRPs) define an evolutionary-conserved subfamily of short (21 kDa) LIM domain proteins characterized by two LIM domains [15, 16]. The three vertebrates CRPs (CRP1-3) exhibit a dual cytoplasmic and nuclear localization, and are preferentially expressed in muscle tissues [17]. In the nucleus, CRPs can interact with transcription factors, such as MyoD, SRF and GATA family proteins, to facilitate smooth (CRP1 and CRP2) or striated muscle (CRP3) differentiation [18, 19]. In the cytoplasm, they decorate filamentous actin structures and bind to cytoskeletal proteins, such as α-actinin and zyxin [17]. However, their exact functions in this compartment remain unclear. Missense mutations in human CRP3 have been associated with dilated and hypertrophic cardiomyopathy [20-22], and CRP3 ablation in transgenic mice promotes disruption of cardiac cytoarchitecture organization, cardiomyopathy and heart failure [23, 24]. We recently provided evidence that CRP3 binds to filamentous actin and self-associates to assemble AFs into bundles, suggesting that it has a direct structural role in cytoarchitecture maintenance [25]. Others reported that CRP1 localizes to neuron filopodia and critically regulates filopodia formation and dendritic growth by a mechanism involving AF crosslinking [26, 27]. Here, we show that CRP2 is an autonomous actin bundling protein whose expression is up-regulated in highly invasive breast cancer cells, and that accumulates along and within the actin core of mature invadopodia. In addition, we provide evidence that this previously overlooked cytoskeletal component of invadopodia promotes breast cancer cell invasiveness and metastasis, and we discuss its potential as a therapeutic target.

# RESULTS

## CRP2 is up-regulated in aggressive breast cancer tumors and cell lines

A microarray-based analysis identified the CRP2 encoding gene, *CSRP2*, in a cluster of 14 genes whose high expression is characteristic of basal-like breast carcinoma [28], a breast cancer subtype associated with poor prognosis. To further evaluate the prognostic value of *CSRP2*, we conducted *in silico* survival analyses using publicly available gene expression datasets with well-defined patient clinical follow-up [29]. Kaplan-Meier and logrank tests revealed that, within the basal-like subtype, breast cancer patients with higher expression of *CSRP2* in the primary tumor exhibit significantly reduced metastasis-free survival as compared to patients with lower expression of *CSRP2* (Figure 1A; HR = 1.98, $P$ = 0.01). In parallel, immunohistochemical analyses revealed that of the 48 invasive breast cancer cases analyzed, 17 (35.4%) were negative, 27 (56.3%) showed weak to moderate staining and 4 (8.3%) exhibited strong staining (Figure 1D). Some residual normal cells were also labeled but they usually exhibited weaker staining as compared to the tumor cells in the same tissue sample (Figure 1E). Interestingly, inflammatory cells also exhibited strong staining (data not shown). To assess the possibility that CRP2 expression was associated with the intrinsic invasive/metastatic potential of breast tumor cells, we compared CRP2 protein levels in a range of well-characterized human cell lines. As shown in Figure 1B, only low levels of CRP2 protein were detected in non- or poorly metastatic, epithelial, breast cancer cells [30], including SKBR3, T-47D, MCF-7 and BT474 cells. In contrast, CRP2 protein levels were considerably higher in highly metastatic, mesenchymal, breast cancer cells, including MDA-MB-231 and Hs548T cells. We analyzed two additional cell lines derived from MCF-7 cells that underwent an epithelial-to-mesenchymal transition (EMT) following either prolonged TNF treatment (1001 cells [31]), or expression of constitutively active Snail (SNAI1-S6A cells [32]). As shown in Figure 1C, both 1001 and SNAI1-S6A cells exhibited a substantial increase in CRP2 protein as compared to the parental epithelial MCF-7 cells. Together the above data suggest that CRP2 up-regulation is associated with the mesenchymal/invasive breast cancer cell phenotype and an increased risk of metastasis in patients.

## CRP2 localizes to breast cancer cell invadopodia

To get an insight into the role of CRP2 in breast cancer cells, CRP2 was fused to GFP and expressed in highly metastatic, Basal-like, MDA-MB-231-luc-

190

D3H2LN cells [33] (hereafter referred to as MDA-MB-231-luc cells). As shown in Figure 2A-2E, CRP2-GFP extensively decorated actin stress fibers. In addition, it co-localized with actin (Figure 2B) and cortactin (Figure 2C), a critical invadopodia protein [34], in invadopodia actively engaged in matrix degradation (Figure 2D). In contrast with other LIM proteins, such as paxillin and Hic-5, which accumulate in a ring surrounding punctate degraded areas [35], CRP2-GFP localized in the invadopodia core overlying the areas of gelatin degradation (Figure 2E). To refine CRP2 localization, we used a chemoinvasion assay in which invadopodia can elongate over long distances through 1-μm-diameter pores in response to growth factors [9]. Projection along the z-axis of confocal sections revealed that CRP2-GFP decorates the whole length of extended actin cores (Figure 2F-2I, and Supplementary Movie 1). Noticeably, such a distribution was highly similar to that previously reported for fascin [9], suggesting functional interaction or redundancy

between both CRP2 and fascin in invadopodia. To extend our analysis, the endogenous CRP2 protein was detected in MDA-MB-231-luc cells, as well as in another invasive breast cancer cell line, namely Hs578T. According to the above GFP fusion data, endogenous CRP2 accumulated within the invadopodia actin core in both cell types (Supplementary Figure 1 and Supplementary Figure2A, respectively). Finally, CRP2-GFP was localized in MDA-MB-231-luc cells embedded in a 3D matrix [36, 37], a condition that better mimics the tumor microenvironment. It was previously reported that, in 3D Matrigel, MDA-MB-231-luc cells adopt an elongated shape, develop cell-matrix adhesions [38] and invade by reshaping the surrounding matrix in a protease dependent manner [37]. As shown in Figure 2J-2L, CRP2-GFP accumulated in actin- and cortactin-enriched areas located at the cell leading edge, in extending pseudopodia, supporting the idea that CRP2 contributes to the mesenchymal mode of invasion in breast cancer cells.
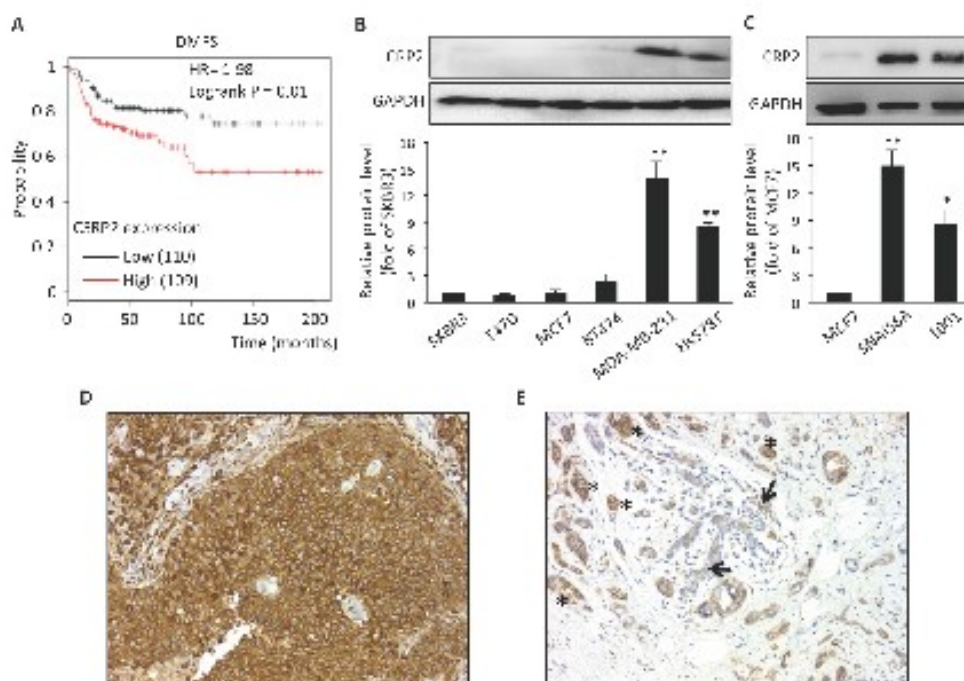


Figure 1: CRP2 up-regulation is associated with a significantly higher risk of metastasis in basal-like breast cancer patients, and correlates with the mesenchymal phenotype in human breast cancer cell lines. A. Kaplan-Meier survival analyses in relation to *CSRP2* expression (affy ID 207030_s_at) in breast carcinoma from the basal subtype using distant metastasis free survival as an endpoint. The patient samples, hazard ratio with 95% confidence interval, and *p* value (Logrank test) are displayed on the chart. B. and C. CRP2 protein level in human breast cancer cell lines (B) and in MCF7-derived cells which underwent EMT through the expression of a constitutively active version of Snail (SNAIL S6A) or prolonged TNF treatment (1001; C). Relative CRP2 expression (lower panels) are calculated from at least three independent experiments and expressed as fold of CRP2 protein level in SKBR3 (B) or MCF7 cells (C). D. and E. Immunohistochemical staining of CRP2 in two cases of invasive ductal carcinoma showing strong staining in tumor cells (D), and faint staining in residual normal breast tissue (arrows; strongly stained tumor cells are indicated by asterisks; (E), respectively (magnification: 200x). Error bars denote standard error. Significant levels: *: $p < 0.05$ and **: $p < 0.001$ (unpaired, two-tailed *t*-test).

## CRP2 is an autonomous actin-bundling protein

Recently, both CRP1 and CRP3, as well as several plant CRP-like proteins, were reported to regulate actin cytoskeleton organization and dynamics [16, 25, 26, 39-41]. The importance of actin bundling for invadopodia biogenesis and activity (9) prompted us to evaluate the ability of CPR2 to remodel AF networks. To do so, AFs were co-polymerized with recombinant CRP2, and the resulting structures were analyzed by real-time total internal reflection fluorescence (TIRF) microscopy. In a control experiment conducted in the absence of CRP2, actin polymerization generated a randomly organized meshwork of fine AFs (Figure 3A). In contrast, in the presence of CRP2, AFs organized in a reticulated network of thick and long actin bundles (Figure 3B). The formation and growth of CRP2-promoted bundles resulted from the fusion of preexisting AFs or fine bundles, and elongation of individual AFs within bundles (Figure 3E and 3F, respectively; Supplementary Movies 2 and 3). By tracking the fast-growing end of bundled AFs, we established that CRP2 has weak intrinsic selectivity for AF polarity and mostly assembles actin bundles of mixed polarity (Figure 3E, 3F and 3G). To extend these data, we analyzed the cytoskeletal modifications potentially induced by CRP2 overexpression in MDA-MB-231 cells. For practical reasons, we focused on actin stress fibers as these structures are easily amenable to quantitative analyses. As shown in Figure 3C, the stress fibers of CRP2-GFP expressing cells appeared considerably thicker than those of control cells expressing GFP alone. The extent of actin bundling in both cell lines was quantified as previously described in Hoffmann et al. [25]. From three independent experiments, including about 200 optical sections, we calculated an average skewness value (a reliable indicator of actin bundling) of $1.43 \pm 0.04$ and $1.83 \pm 0.04$ for GFP control cells and CRP2-GFP expressing cells, respectively (Figure 3D). In conclusion, our data demonstrate that CRP2 exhibits actin bundling activity in both in vitro reconstitution assays and breast cancer cells.

## CRP2 critically regulates breast cancer cell invasion

To further characterize the function of CRP2 in breast cancer cells, a series of in vitro functional assays were conducted with two MDA-MB-231-luc-derived cell lines expressing independent CRP2-targeting shRNAs (shCRP2a and shCRP2b), and one control cell line expressing a non-targeting control shRNA (sh-; Figure 4A). Both shCRP2a and shCRP2b cells exhibited significantly reduced CRP2 protein levels as compared to sh- cells (Figure 4A), and were checked for the absence of any CRP1 or CRP3 up-regulation, which could compensate for CRP2 knockdown (Supplementary

Figure 3). Both MTT and [³H]Thymidine incorporation assays revealed that CRP2 knockdown did not affect the proliferation rate of MDA-MB-231-luc cell monolayer cultures (Figure 4B and 4C, respectively). Three-dimensional (3D) spheroids were successfully obtained from both control (sh-) and CRP2-depleted cells, and expanded as compact spheres in 10% Engelbreth-Holm-Swarm (EHS) matrix (Figure 4D). However, CRP2 knockdown significantly reduced 3D spheroid growth. Indeed, after 6 days of culture, sh- spheroids exhibited an average volume of $0.237 \pm 0.006$ mm³ whereas shCRP2a and shCRP2b only reached $0.167 \pm 0.008$ and $0.141 \pm 0.005$ mm³, respectively (Figure 4D, right chart). The migratory potential of each cell line was then evaluated in both 2D and 3D conditions. In 2D scratch wound assays, nearly identical closure curves were obtained for sh-, shCRP2a and shCRP2b cells, indicating that CRP2 depletion does not alter 2D cell migration (Figure 4E). This result was confirmed by the similar average migration velocities ($\sim 0.5$ µm/min⁻¹) that were calculated for each cell line by tracking single cells migrating towards FBS in collagen-coated µ-Slide Chemotaxis³ᴰ chambers (Ibidi; Figure 4F). In contrast, 3D scratch wound assays revealed that CRP2 knockdown significantly reduces the ability of MDA-MB-231-luc cells to invade into a 3D collagen matrix (Figure 4G). In these conditions, gap closure after 72h for shCRP2a and shCRP2b cells was reduced by about 30% and 40% as compared to control sh- cells, respectively. In addition, single cell tracking analyses showed that CRP2 depletion reduces by about 50% the average velocity of collagen invading cells (Figure 4H). To strengthen these data, transwell invasion assays were performed with MDA-MB-231-luc cells treated with control or CRP2 siRNA. As shown in Figure 4I, transient CRP2 knockdown inhibited the invasion potential of MDA-MB-231-luc cells by about 50%. Finally, the pro-invasive function of CRP2 was validated in Hs578T cells (Supplementary Figure 2B-2D). Indeed, both transwell invasion and single cell tracking analyses showed that CRP2 depletion significantly reduced Hs578T cell invasion.

The possibility that CRP2 up-regulation can promote breast cancer cell invasion in weakly invasive cells was tested in gain-of-function analyses using MCF-7 epithelial cells, which only contain very low levels of CRP2 protein (Figure 1B and 1C). We established a stable MFC-7 cell line in which CRP2 protein expression was about 10 times higher than in control MCF-7 cells (Figure 5A). Remarkably, CRP2 overexpression increased MCF-7 cell invasion by a factor 2.5 in transwell invasion assays (Figure 5B). Together our data provide clear evidence that CRP2 critically regulates breast cancer cell invasion whereas it is not required for 2D cell migration.
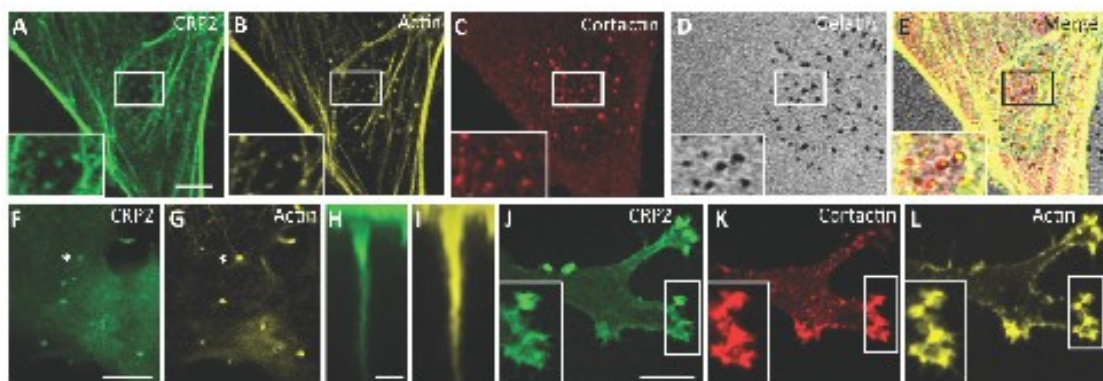
**Figure 2: CRP2 localizes to active invadopodia.** A.-D. CRP2-GFP localizes to actively degrading invadopodia. Cells were grown on Cy3-conjugated gelatin-coated coverslips (D) for 6 h and CRP2-GFP A. was co-localized with actin (B) and cortactin (C). E. Merge of (A-D) F.-I. CRP2-GFP (F) and (H) and actin (G) and (I) co-localize in elongated invadopodia. F. and G. correspond to a focal plane located at 1.4 μm underneath the ventral cell surface, whereas (F) and I show projections along the z axis (35 confocal slices) of the entire invadopodium labeled by an asterisk in (F) and (G) J.- L. CRP2-GFP (J), cortactin (K) and actin (L) in MDA-MB-231-luc cells invading a 3D EHS matrix. The image corresponds to a projection of 17 confocal slices. Bars = 5 μm (A-G), 1 μm (H) and (I), 10 μm (J-L).
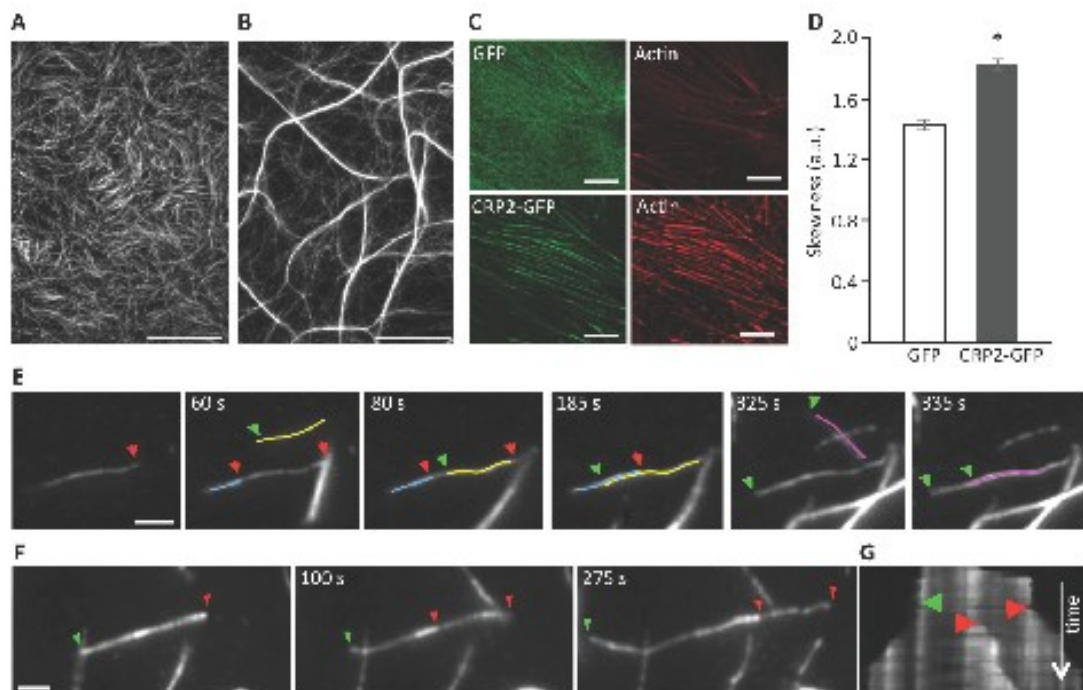


**Figure 3: CRP2 promotes actin bundling in *in vitro* reconstituted assays and in breast cancer cells.** A. and B. Actin filaments (1 μM) polymerized alone (A) or in the presence of recombinant CRP2 (3 μM; B). C. Typical examples of ROI (13 x 13 μm) used for skewness measurements in Acti-stain 555 phalloidin-stained MDA-MB-231-luc cells expressing GFP alone or CRP2-GFP. D. Skewness average calculated from three independent experiments, including 200 optical sections as in (C). Error bars denote standard error. Significant level: *: $p < 0.001$. E. and F. Selection of images from Supplementary Movies 2 and 3 (real-time time TIRF microscopy) showing CRP2-induced crosslinking of actin filaments (E) and actin filaments elongation inside a bundle (E) and (F). In both cases 1 μM actin was copolymerized with 3 μM CRP2. Green and red arrows point to fast growing barbed ends of filaments elongating toward the left and right, respectively. For better readability some actin filaments were highlighted in color. G. Kymograph corresponding to (F) and Supplementary Movie 3, showing that CRP2 assembles bundles of mixed polarity. Bars = 20 μm (A and B), 10 μm C., 2 μm (E and F).

193
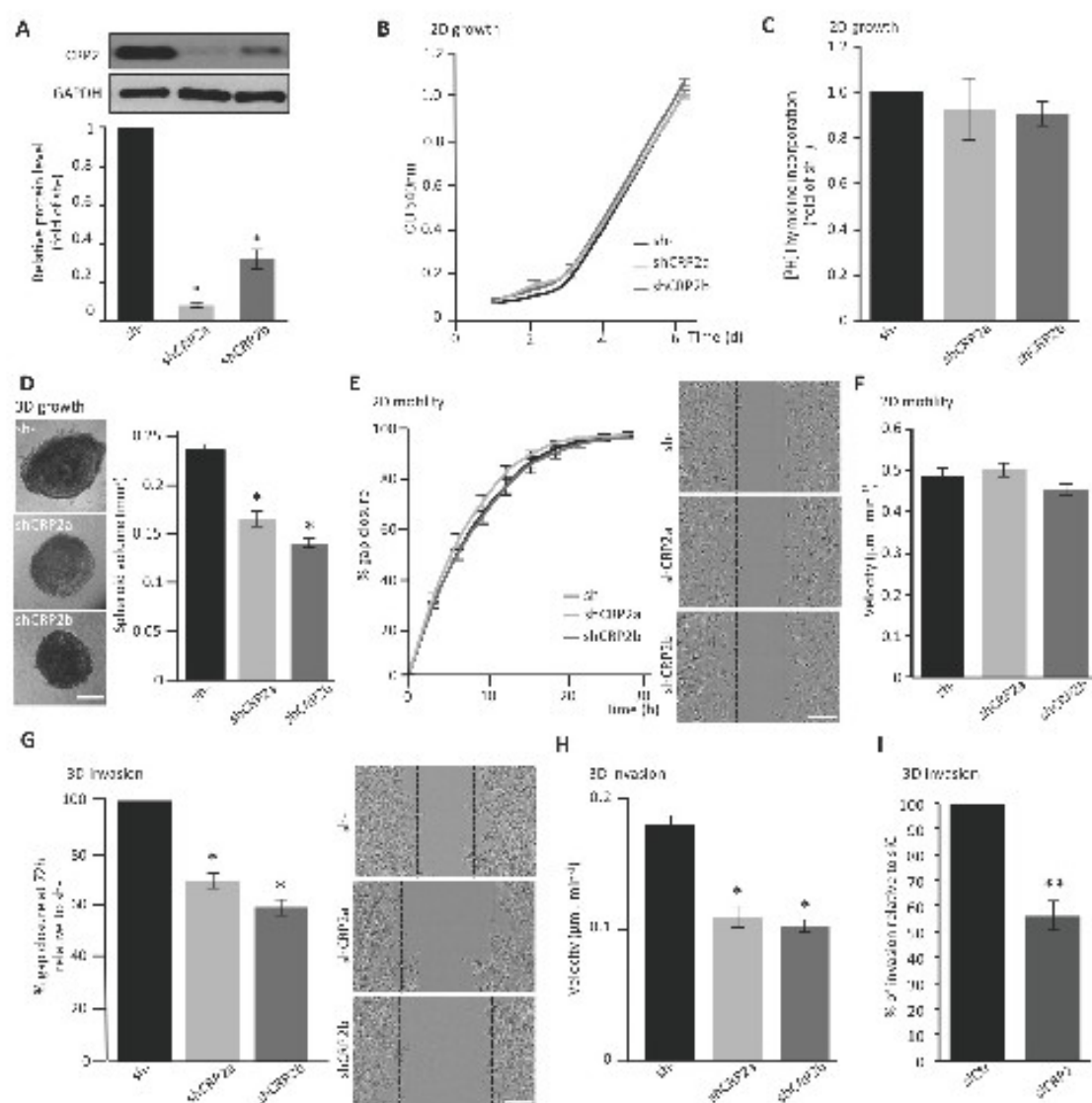
**Figure 4: CRP2 contributes to breast cancer cell invasion. A.** CRP2 protein level in MDA-MB-231-luc cell lines stably expressing two independent shRNAs targeting CRP2 transcripts (shCRP2a and shCRP2b) or a control, non-targeting, shRNA (sh-). Average expression values (lower panel) in shCRP2a and b cell lines were calculated from three independent western blot analyses and expressed as fold of CRP2 protein in sh- cells. **B.** Proliferation rate of sh-, and shCRP2a and b cell lines as assessed by MTT assay. **C.** Proliferation rate as assessed by [³H]Thymidine incorporation. The data are expressed as fold of [³H]Thymidine incorporation in control sh- cells. Unpaired two-tailed, $t$-test revealed no statistical difference in the proliferation rate of the three cell lines. **D.** 3D cell spheroid proliferation assay. The right chart indicate the average spheroid volume at 6 days of culture ($n = 25$). **E.** 2D scratch wound assay (on 2D collagen matrix surface). Gap closure was analyzed using the automated image acquisition and processing system IncuCyte (Essen BioScience). The right image panel show typical gap closure at 6h for each cell line. **F.** Velocity of 2D migrating cells. For each cell line, at least 150 cells migrating on collagen-coated μ-Slide Chemotaxis³ᴰ chambers (Ibidi) were tracked over 2 days, and an average velocity was calculated. **G.** 3D scratch wound assay. After wounding, cells were embedded in a 3D collagen matrix. Results were normalized to sh- and are expressed as percentage of gap closure after 72h. The right image panel show typical gap closure at 72 h for each cell line. **H.** Velocity of invading cells. For each cell line, at least 150 cells embedded in a 3D collagen matrix were tracked over 2 days and an average velocity was calculated. **I.** Transwell assay performed with MDA-MB-231-luc cells transfected with control (siCtr) or CRP2 specific (siCRP2) siRNA. Invading cells at 24 h were quantified by MTT assay, and the results were normalized to siCtr cells (set at 100%). All the data originate from at least three independent experiments. Error bars denote standard error. Significant levels: *: $p < 0.001$, **: $p < 0.05$. Bars = 300 μm (D) and 150 μm (E and G).

194

## CRP2 knockdown inhibits extracellular matrix degradation and MMP-9 expression

A hallmark of invading mesenchymal cells is their capacity to remodel/degrade the ECM and clear paths through challenging physical barriers, such epithelial and vascular basement membranes. Here, we assessed whether CRP2 knockdown can alter the ability of MDA-MB-231-luc tumor cells to promote ECM degradation. As shown in Figure 6A, control sh- MDA-MB-231-luc cells efficiently promoted fluorescent gelatin degradation as indicated by dark spots in the bright fluorescent matrix background. About 70% of the cell population was active and a degradation index of $34.2 \pm 2.2 \ \mu m^2$ of degraded matrix per cell was calculated (Figure 6C and 6D, respectively). The depletion of CRP2 significantly reduced both parameters with only 49% and 46% of active cells and degradation indexes of $18.3 \pm 2.1$ and $16.5 \pm 1.5 \ \mu m^2$/cell for shCRP2a and shCRP2b, respectively (Figure 6A, 6C and 6D). As shown in Figure 6B-6D, the rescue of CRP2 expression in shCRP2a cells (Supplementary Figure 4) restored matrix degrading activity to a similar level as in control cells, further confirming that the above effects were due to CRP2 knockdown.

Extracellular matrix degradation is primarily mediated by metalloproteinases (MMPs) that are secreted at sites of invadopodia. We thus aimed at evaluating the contribution of CRP2 to MMP secretion in MDA-MB-231-luc cells. Among secreted MMPs, the gelatinases

MMP-2 and MMP-9 are of particular interest as they can hydrolyze major ECM components, such as gelatin and type IV collagen [42], and were repeatedly associated with breast cancer progression [43-45]. Previous studies established that MDA-MB-231 secrete low basal levels of MMP-2 and MMP-9 (i.e. when cultured in serum free media) and respond to phorbol 12-myristate 13-acetate (PMA) by secreting MMP-9 [46]. Using gelatin zymography analyses, we confirmed that MDA-MB-231-luc cells secrete no or very low basal levels of MMP-9 and MMP-2, and this was not modified by knocking down CRP2 expression (Figure 7A and 7B). As expected, PMA induced MMP-9 secretion (under its 92 kDa pro-form). Remarkably, CRP2 knockdown significantly compromised MMP-9 secretion. Expression analyses revealed that PMA induced MMP-9 expression at both protein and mRNA levels (Figure 7C and 7D), and that this process was abrogated in CRP2-depleted cells. Thus, the reduced MMP-9 secretion observed in CRP2 depleted cells was mostly due to the inhibition of MMP-9 expression. As shown in Supplementary Figure 5, these data were validated in Hs578T breast cancer cells, demonstrating that the role of CRP2 in MMP-9 expression/secretion is not restricted to the MDA-MB-231 cell lineage.

## CRP2 knockdown inhibits metastatic colonization

Based on our data, we predict that CRP2 should significantly contribute to breast cancer metastasis. To test
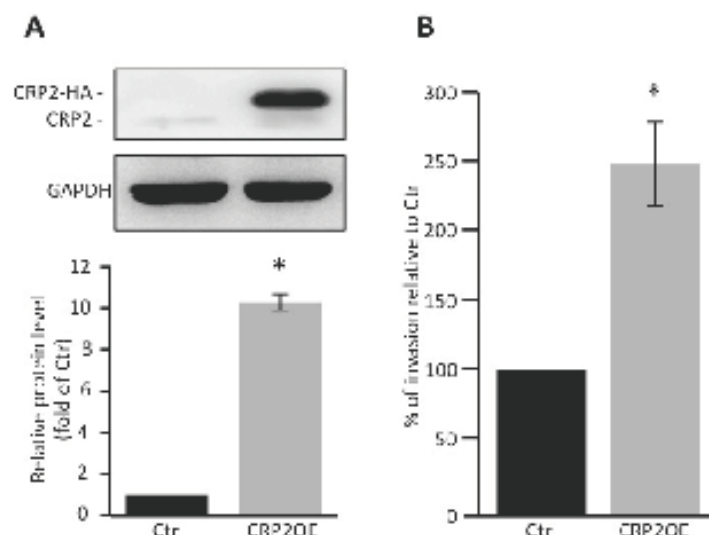


**Figure 5: CRP2 overexpression promotes MCF-7 cell invasion.** A. CRP2 protein level in MCF-7 cell lines stably expressing CRP2-HA (CRP2OE) or a control empty vector (Ctr). Average total CRP2 expression (lower panel) are calculated from three independent western blot analyses and are expressed as fold of endogenous CRP2 protein in Ctr cells. B. Transwell invasion assay. Invading cells at 48 h were quantified by MTT assay, and the results were normalized to Ctr cells (set at 100%). The data originate from 5 independent experiments. Error bars denote standard error. Significant levels: *: $p < 0.005$.

195

this assumption, CRP2-depleted (shCRP2a) and control (sh-) MDA-MB-231-luc cells (Figure 4A) were injected into the tail vein of athymic nu/nu female mice. Lung implantation of tumor cells was immediately controlled after tail vein injection by bioluminescence imaging (Figure 8A). After 5 weeks, lungs were excised and the

number of GFP positive metastatic colonies was analyzed. As illustrated in Figure 8B, lesions were dramatically reduced in lungs from mice injected with CRP2-depleted tumor cells as compared to lungs from control mice. Quantitative analyses revealed that the median number of metastatic colonies was 8 and 53 for shCRP2a lungs and
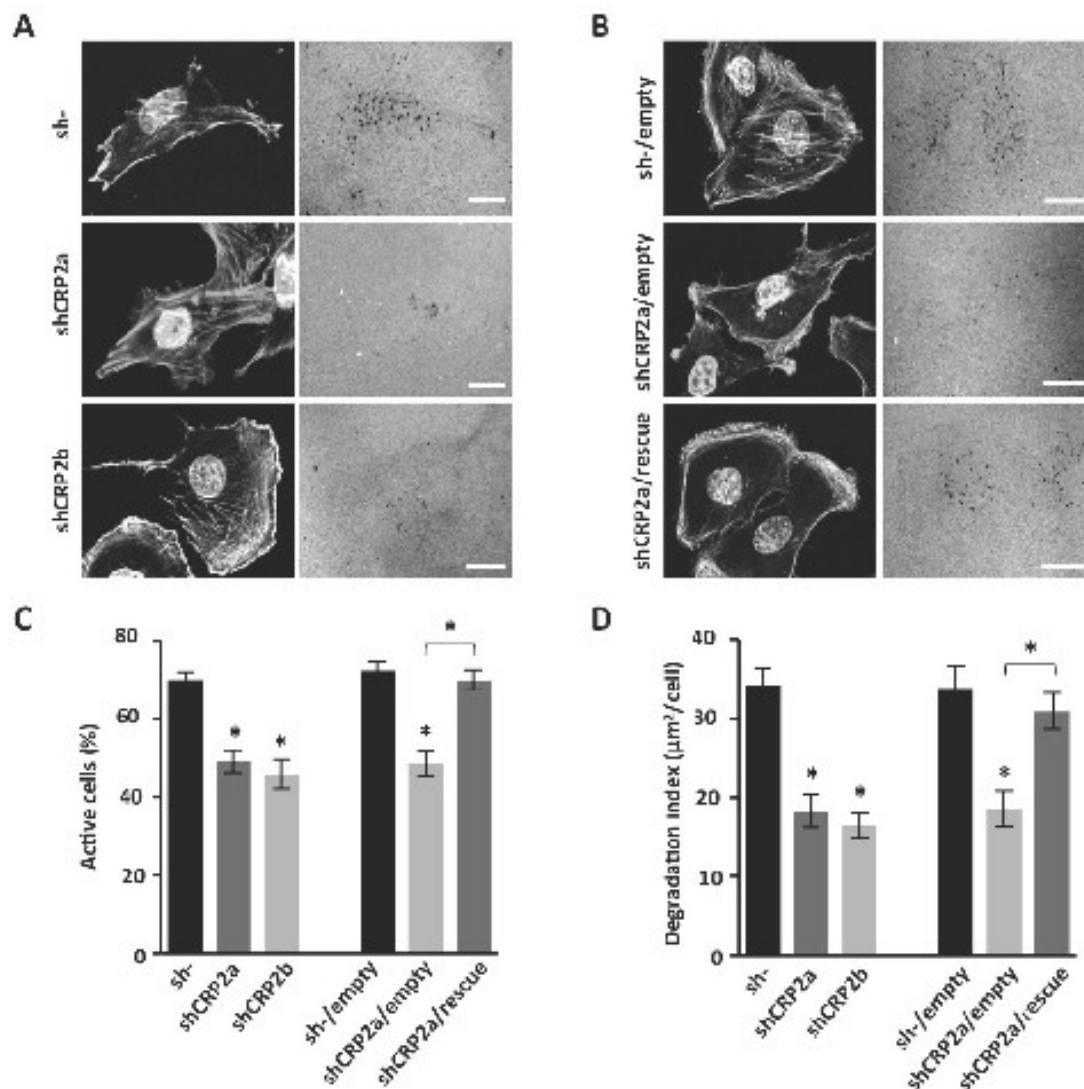


Figure 6: CRP2 is required for ECM degradation. A. Gelatin degradation assay. Control sh- and shCRP2a and shCRP2b cells were plated on Cy3-conjugated gelatin for 18 h, fixed and stained with DAPI and Acti-stain™ 670 phalloidin (left panels). Gelatin degraded areas appear as dark punctuate in the fluorescent background (right panels). B. Same as A for an shCRP2a-derived cell line in which CRP2 expression was restored by expressing an shRNA-resistant CRP2 coding sequence (shCRP2a/rescue), and related controls, i.e. sh- and shCRP2a cells lines transduced with an empty vector (sh-/empty and shCRP2a/empty, respectively; see also Supplementary Figure 4). C. and D. Quantitative analyses corresponding to the experiments shown in (A) and (B) Actively ECM degrading cells were scored and expressed as percentage of the total cell population (C). A degradation index corresponding to the ratio of degraded gelatin surface per cell was calculated (D). The data originate from at least three independent experiments (n ≥70 cells). Error bars denote standard error. Significant levels: *: $p < 0.0001$. Bars = 20 μm.

sh- lungs, respectively (Figure 8C; $p < 0.05$). Moreover, out of a total of 8 mice injected with sh- cells, one mouse exhibited extensively necrotized lungs (Figure 8D) and three developed macro-metastases at other sites than lungs, including hind legs, the brain and the liver, respectively (Figure 8E-8G). In striking contrast, none of the 9 mice injected with shCRP2a cells exhibited any sign of metastatic lesions in other tissues than lungs.

Since the above experimental metastasis model based on tumor cell intravascular injection does not recapitulate the early steps of the metastatic cascade, e.g. extravasation, we further examined CRP2 pro-metastatic

activity in a spontaneous metastasis model. Here, CRP2-depleted and control MDA-MB-231-luc cells were injected in the mammary fat pad of NOD *scid* gamma (NSG) mice. The size of primary tumors was measured using calipers. As shown in Figure 8H and 8I, CRP2 knockdown had no significant effect on primary tumor growth. In contrast, the number of metastatic lesions to the lungs was significantly reduced ( > 50%) in CRP2-depleted tumor bearing mice as compared to control mice (Figure 8J and 8K). These data are in good agreement with the established pro-invasive role of CRP2 and confirm that CRP2 promotes breast cancer metastasis.
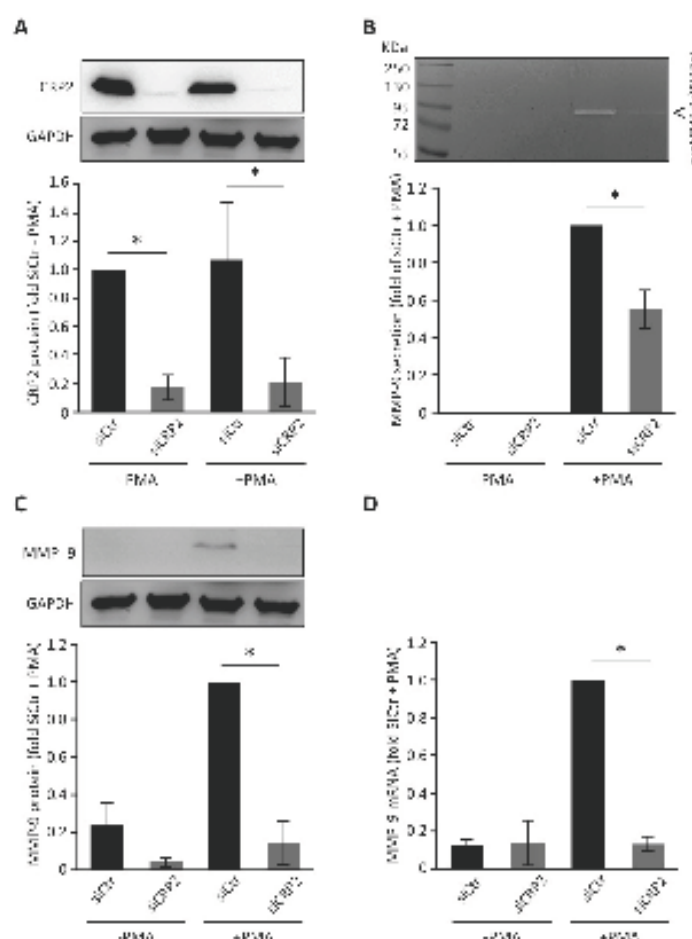


Figure 7: CRP2 regulates MMP-9 expression in MDA-MB-231-luc cells. A. CRP2 protein level in MDA-MB-231-luc cells transfected with a control siRNA (siCtr) or a CRP2 targeting siRNA (siCRP2). Forty hours after transfection, cells weretreated with or without PMA (100 ng/ml) in serum-free DMEM for 24 h. Average expression values (lower panel) were expressed as fold of CRP2 protein in untreated (-PMA) control siCtr cells which was set to 1. B. Gelatin zymography assays. The medium of the cell cultures described in A. was collected and assessed for its content in secreted pro-MMP-9. The results were expressed as fold of pro-MMP-9 secretion in PMA-treated control siCtr cells which was set to1. C. and D. Expression levels of cytosolic MMP-9 protein (C) and MMP-9 mRNA (D) in the cell cultures described in A. as assessed by western blot and real-time qPCR analyses, respectively. The results were expressed as fold of pro-MMP-9 expression in PMA-treated control siCtr cells which was set to 1. The data originate from at least 3 independent experiments. Error bars denote standard error. Significant levels: *: $p < 0.01$.
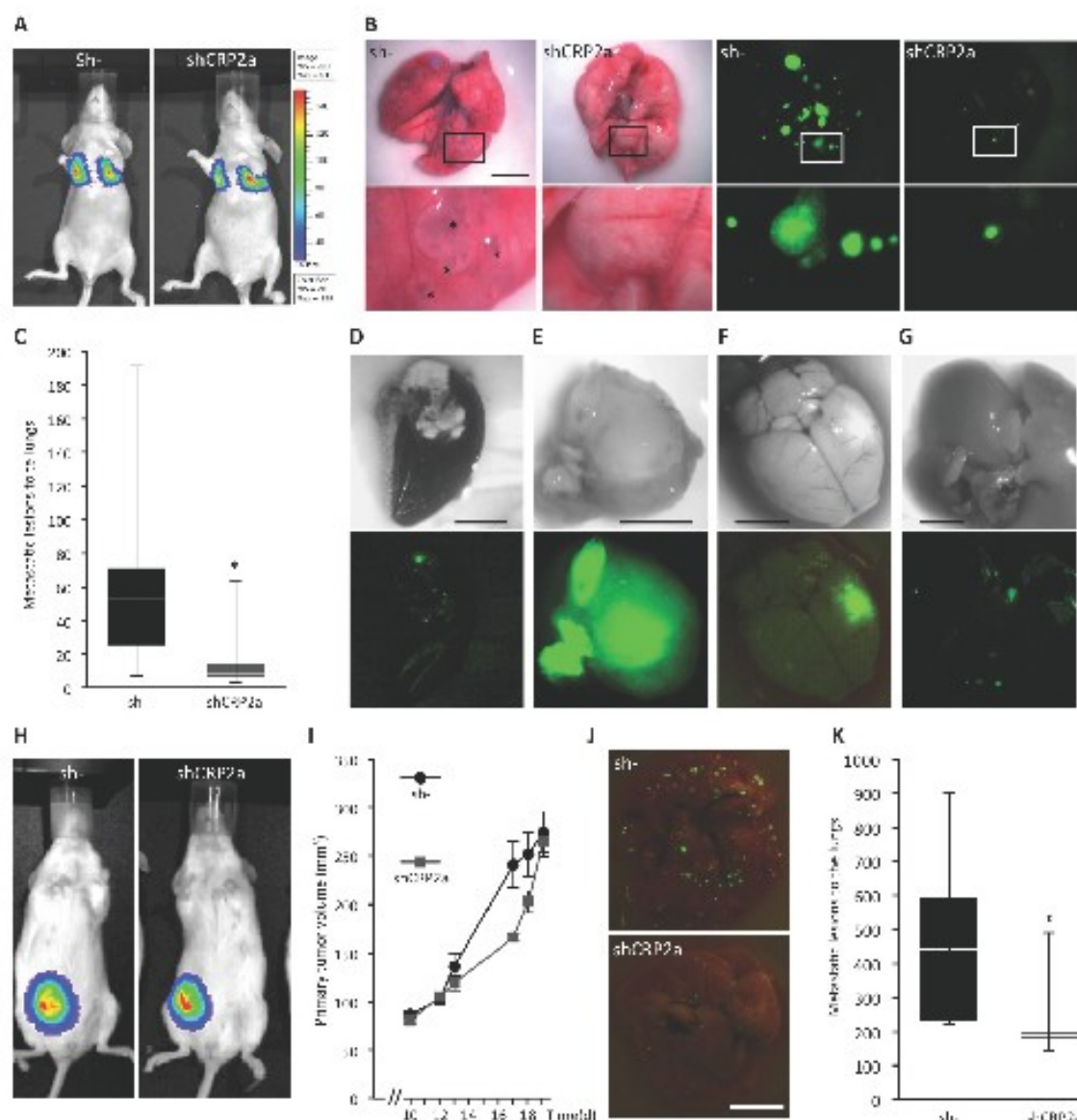
**Figure 8: CRP2 promotes breast cancer metastasis. A.** Implantation of control (sh-) and CRP2-depleted (shCRP2a) MDA-MB-231-Luc cells ($1 \times 10^6$) to the lungs of athymic nu/nu female mice was immediately controlled by bioluminescence imaging after tail vein injection. **B.** Typical lung metastatic lesions observed after 5 weeks with white light (four left panels) and fluorescence microscopy to detect GFP (cell transduction marker; four right panels). Lower panels are magnifications corresponding to the above white rectangles. Asterisks indicate some extended metastatic lesions. **C.** Number of lung metastatic lesions in sh- and shCRP2a xenograft mice ($n = 8$ and 9, respectively). Data are presented as standard box plots with whiskers from minimum to maximum values. **D.** Extensively necrotized lung of one sh- mouse. **E.-G.** Metastases at other sites than lungs observed in sh- mice, including a hind leg (E; the image corresponds to the excised tumor), the brain (F) and the liver (G). The lower panels show the corresponding GFP (cell transduction marker) signals. **H.-K.** Orthotopic tumor model. Control (sh-) and CRP2-depleted (shCRP2a) MDA-MB-231-Luc cells ($5 \times 10^5$) were implanted in a mammary fat pad of NOD *scid* gamma mice ($n = 5$ and 6, respectively). **H.** Bioluminescence imaging showing typical and similar signals at the primary tumor site in sh- and shCRP2a xenograft mice (19 days after tumor cell implantation). **I.** Primary tumor volume. **J. and K.** Typical lung metastases (J) and number of lung metastatic lesions (K) 20 days after tumor cell implantation. Error bars denote standard error. Significant levels: *: $p < 0.05$. Bars = 5 mm.

198

# DISCUSSION

The present study provides evidence that CRP2 is a new actin bundling factor that localizes in breast cancer cell invadopodia and plays a critical role in invadopodia-mediated ECM degradation, cell invasion and metastasis. Although this is the first report of the presence of CRP2 in invadopodia, a proteomic study has recently identified CRP1 (which shares about 80% amino acid identity with CRP2) as a new component of podosomes [47], which are invadopodia-like organelles that promote ECM degradation in normal motile cells [3]. The distribution of CRP2 within invadopodia and its intrinsic actin-bundling activity strongly suggest that it directs the assembly of the actin bundles running inside and along the whole length of invadopodia. Contrary to T-fimbrin which was reported to be dispensable for invadopodia formation and activity (as evaluated by the degree of matrix degradation) in breast cancer cells [9], CRP2 knockdown decreased the degradation index by about 50% (Figure 4D), a value remarkably similar to the one reported for fascin depletion [9]. Thus, in the context of breast cancer, CRP2 and fascin might have similar importance in invadopodia function. However, they are unlikely to function as fully redundant, exchangeable, actin bundling factors. They considerably differ in their domain organization and 3-D architecture, and in the mechanism by which they promote actin bundling. Fascin functions as a monomer with two majors actin-binding sites [48, 49]. In contrast, we recently established that CRP3, which shares the same overall domain organization with CRP2 and CRP1, dimerizes along the actin cytoskeleton of muscle cells, and that its C-terminal LIM domain functions as an actin-binding module whereas its N-terminal domain promotes dimerization [25]. Thus, CRP2 actin-bundling activity likely involves protein dimerization. Nuclear magnetic resonance-based studies have shown that the > 50 amino acid-long linker region connecting the two LIM domains of CRP2 is mostly unfolded and highly flexible, providing each LIM domain motional freedom and independent spatial orientation [50]. Such an overall conformational plasticity contrasts with the more compact folding of fascin consisting in two double β-trefoil domain lobes (each containing one actin-binding site) hold together by a polar interface [13, 51]. The structural specificities of CRP2 and fascin likely account for their respective selectivity for AF polarity. Indeed, whereas CRP2 can crosslink AFs in both parallel and antiparallel orientations (Figure 5), fascin, whose folding restricts movements between its actin-binding domains, exclusively assembles tightly packed unipolar bundles [25, 49]. Although direct evidence is lacking, invadopodia are thought to contain unipolar bundles with their fast growing, barbed, ends oriented towards the tip. In this context, the structural flexibility of CRP2 and its low selectivity for AF polarity likely allow it to cooperate with fascin to assemble/stabilize unipolar bundles in breast cancer cell invadopodia. Nevertheless, the existence of a mixed polarity bundle population cannot be ruled out.

How is CRP2 expression regulated in breast cancer cell remains to be explored. However, the striking association between CRP2 up-regulation and the mesenchymal phenotype in breast cancer cell lines suggests that CRP2 is part of the EMT process whose role in tumor cell invasion and metastasis is increasingly recognized [52]. Interestingly, in vascular smooth muscle cells, CRP2 expression is driven by TGF-β [53], a potent inducer of EMT in cancer cells [54]. In this context it is worth mentioning that Hic-5, a four LIM domain-containing protein, was shown to be a key mediator of TGF-β-induced EMT, invadopodia formation and cell invasion [35]. Noticeably, ectopic expression of Hic-5 in epithelial, non-invasive, breast MCF-10A cells is sufficient to promote invadopodia formation and ECM degradation, suggesting that Hic-5 can recruit other key invadopodia components, and/or activate signaling pathways driving invadopodia formation. Remarkably, in fibroblasts, CRP2 and Hic-5 physically interact and co-regulate cell contractibility in response to mechanical stress [55]. Thus, a seducing scenario that awaits further examination is that Hic-5 and CRP2 also interact at invadopodia and contribute to invadopodia response to mechanical cues. Although Hic-5 localizes to the outer ring of invadopodia [35] whereas CRP2 localizes at the actin core, Hic-5 might recruit CRP2 during the early phase of invadopodia formation, following which CRP2 would translocate to and bundle nascent AFs. TGF-β, which was also reported to induce fascin expression in breast cancer cells, would thus coordinate up-regulation of key cytoskeletal proteins for invadopodia formation.

Targeting invadopodia represents an attractive alternative to MMP inhibitor-based strategies, which so far failed in clinical trials due to the lack of inhibitor specificity and unacceptable sides effects [56]. In this context, CRP2 emerges as a new potential therapeutic target to treat metastatic breast cancers. Importantly, mice lacking CRP2 are viable, fertile and only exhibit subtle alteration of cardiac ultrastructure [57]. It is thus conceivable that targeting CRP2 in patients would only cause minor side effects. Recently, small molecules impairing fascin bundling activity were shown to inhibit metastasis in breast cancer models with no toxicity in mice [13, 14], highlighting that the actin cytoskeleton, and more particularly actin bundlers, are realistic targets for anti-metastasis therapy. Our results call for the development of optimized strategies aimed at co-targeting fascin and CRP2. In support of this idea, the depletion of either fascin or CRP2 is not sufficient to fully abolish invadopodia-mediated ECM degradation *in vitro* ([9] and Figure 4, respectively). CRP2-based therapy might also turn out being an alternative to anti-fascin molecules in case they fail in clinic trials or to overcome resistance issues.

199

## MATERIALS AND METHODS

### Cell lines and cell culture

MCF-7 and MDA-MB-231-luc-D3H2LN (MDA-MB-231 luc) cells were purchased from ATCC and Perkin Elmer, respectively. The other cell lines used in this study including, MDA-MB-231, T47D, BT474 and SKBR3 cells were collected from cell line collections available at the Luxembourg Institute of Health or University of Luxembourg (kind gifts from Elisabeth Reckinger-Schaffner, Life Sciences Research Unit). MCF-7-derived 1001 and SNAIL 6SA cells were kindly provided by Dr. Bassam Janji (Luxembourg Institute of Health and University) with the permission of the respective inventors (see Acknowledgements). MCF-7-snail 6SA were maintained in DMEM:F12 (1:1; Lonza) supplemented with 1mM Sodium Pyruvate (Lonza) and 500 µg/ml G418 (Sigma-Aldrich). MCF-7, MDA-MB-231, MDA-MB-231-luc and 1001 cells were maintained in DMEM high glucose with L-glutamine medium (Lonza). The other cells were cultured in complete growth medium following ATCC recommendations. All the media were supplemented with 10% (v/v) fetal bovine serum (FBS, Life Technologies), 100 U/ml penicillin and 0.1 mg/ml streptomycin (Sigma-Aldrich). Cells were grown in a humidified atmosphere at 5% $CO_2$ and 37°C. For MMP-9 induction and gelatinase zymography analyses, cells were incubated in serum-free medium and treated with PMA (100 ng/ml, Sigma-Aldrich) for 24 h. The conditioned media from PMA-treated and control cells were centrifuged at 4°C for 10 min at 300 x g and the supernatants were collected for subsequent analyses.

### CRP2 knockdown and ectopic expression

CRP2 knockdown was achieved by two pGIPZ lentiviral shRNAs (clone ID: V3HS_327411 and V3HS_327407, designated as shCRP2a and b). A non-silencing shRNAs (RHS4346, sh-; GE Dharmacon) was used as a control. For rescue experiments, the shCRP2a recognition site in the coding sequence of CRP2 was mutated (silent mutations) by overlapping PCR and the resulting CRP2mut_shCRP2a fragment was inserted into pcDNA3.1 (-) HA via BamHI an XhoI. The CRP2mut_shCRP2a-HA fragment was then PCR amplified and inserted into pCDH-EF1-MCS-IRES-Neo (hereafter referred to as pCDH, SBI, Systems Bioscience) via XbaI and NotI to generate the "shCRP2a/rescue" plasmid. For transwell, MMP-9 zymography, chemotaxis and MMP-9-expression analyses, CRP2 knockdown was achieved by transfecting MDA-MB-231-luc or Hs578T cells with CRP2 specific siRNAs (siCRP2; target sequence: 5'-TTGGATTTGTTGTAGGCCTGT-3'; Eurogentec)

using DharmaFECT™ transfection reagent (GE Dharmacon). A non-targeting siRNA (siCtr; Eurogentec) was used as a control. Transfected cells were kept 48 h in culture prior subsequent analyses, and CRP2 knockdown was confirmed by western blot. For stable expression of CRP2-GFP and GFP (control) under control of the CMV promoter in MDA-MB-231-luc cells, the insert present in the lentiviral expression plasmid "L134" (kindly provided by Dr. Birke Bartosch; INSERM, Lyon, France) was replaced with eGFP amplified from the pEGFP-N1 expression vector (Clontech). The CRP2 coding sequence (clone ID: BC000992) was subsequently inserted in N-terminal of eGFP via XhoI and BamHI restriction sites to generate the "L134_CRP2-GFP" expression plasmid. For stable expression of CRP2-HA in MCF7 cells, CRP2-HA fragment was inserted into empty pCDH vector via XhoI and BamHI restriction sites to generate the "pCDH-CRP2-HA" expression plasmid subsequently used for MCF7 cell lentiviral transduction. To produce the glutathione S-transferase (GST)-fused CRP2 recombinant protein, the coding sequence of CRP2 was subcloned into the bacterial expression vector pGEX-4T1 (GE Healthcare). GST-fused CRP2 was expressed in BL21 bacteria and purified using glutathione-agarose resin according to the manufacturer's instructions (Themo Scientific Pierce). Subsequently, GST was removed by thrombin cleavage. Lentivirus production was achieved by co-transfecting lentiviral pGIPZ shRNAs or expression plasmids with packaging and envelope plasmids in HEK293T cells using Xtreme transfection reagent (Roche). MDA-MB-231-luc-D3H2LN or MCF-7 cells (pCDH-CRP2-HA) were infected with virus, and transduced cells were selected with 0.5 µg/ml puromycin (Sigma-Aldrich; shCRP2a, b, sh-, L134_CRP2-GFP) or 1 mg/ml G418 (Sigma-Aldrich; shCRP2a/rescue; pCDH-CRP2-HA).

### RNA extraction and RT-qPCR

Total RNA was extracted with RNeasy Mini Kit (Qiagen) according to the manufacturer's instructions. Purified RNA was reverse-transcribed to cDNA using the SuperScript III cDNA synthesis kit (Invitrogen). qPCR reactions with specific primers for *MMP-9* (Qiagen), CRP1 (F:GAAGAGGTTCAGTGCGAAGG; R:CCAGATTCTTCTTGCAGACCA, Eurogentec), CRP3 (F: CTCGATGTGGCAAGTCAGTC; R:AGATGGCACAGCGGAAAC, Eurogentec) and *GAPDH* (F: AGCCACATCGCTCAGACAC; R: GCCCAATACGACCAAATCC, Eurogentec) were performed using SYBR Green I (Qiagen) in a Applied Biosystems ViiA™ 7 Real-Time PCR System (Life Technologies). The $2^{-\Delta\Delta Ct}$ method was used to determine relative gene transcript levels normalized to the *GAPDH* reference gene.

200

## Protein extraction and western blot

Extraction of total protein from cell lysates was prepared in RIPA lysis buffer (Millipore) supplemented with protease and phosphatase inhibitor mixture (Roche). Twenty micrograms of proteins were separated by SDS-PAGE and transferred to a PVDF membrane (Millipore). Primary antibodies against the following proteins were used: CRP1 (079K2866, Sigma-Aldrich), CRP2 (HPA045617, Sigma-Aldrich), CRP3 (sc-166930, Santa Cruz Biotechnology), MMP-9 (#13667, Cell Signaling Technology), GADPH (#5174, Cell Signaling Technology) and tubulin (T5168, Sigma Aldrich). As secondary antibodies we used HRP-conjugated goat anti-rabbit IgG (111-035-003, Jackson ImmunoResearch) and HRP-conjugated goat anti-mouse IgG (A4416, Sigma-Aldrich). Protein bands were detected using the SuperSignal™ West Femto Chemiluminescent Substrate (Thermo Scientific) and visualized by ImageQuant LAS 4000 (GE Healthcare Life Science). Protein levels were quantified using ImageJ (NIH, Bethesda, USA).

## Cell proliferation assays

For MTT-based colorimetric assay, $10^3$ cells per well were seeded in 96-well plates and their growth was monitored over 6 days. Briefly, cells were incubated for 4 h in 0.5 mg/ml Thiazolyl Blue Tetrazolium Bromide (Sigma-Aldrich) and lysed in dimethyl sulfoxide (DMSO). The optical density was measured at 540 nm with FLUOstar OPTIMA (BMG LABTECH). For [$^3$H]Thymidine incorporation-based assay, $3 \times 10^3$ cells per well in 96-well plates were starved in serum-free DMEM medium for 24 h, and subsequently stimulated for proliferation in complete medium for 18h. Cells were then labeled with 0.25 μCi [$^3$H]thymidine for 6 h and harvested onto UniFilter-96 GF/C plates using a Unifilter-96 Harvester (Perkin-Elmer). MicroScint-20 liquid scintillation cocktail was added to the dried filter plates at room temperature. The amount of incorporated tritium was measured using TopCount NXT™ (Perkin-Elmer) Microplate Scintillation and Luminescence Counter (Perkin Elmer). For 3D spheroid proliferation assay, spheroids were prepared in 96-well plates coated with 1.5% Noble agar (BD Difco) prepared in serum-free DMEM medium. One thousand cells per well were centrifuged at 500 x $g$ and incubated for 3 h at 37°C and 5% $CO_2$. An ECM gel was prepared from Engelbreth-Holm-Swarm murine sarcoma (EHS matrix, Sigma-Aldrich) diluted to 1 mg/ml in complete DMEM growth medium, and added to clustered cells to induce spheroid formation. Fresh medium was added on the top of spheroids and changed every three days. Spheroids growth was monitored during 6 days. Spheroid diameter was measured in ImageJ (NIH, Bethesda, USA), and an average spheroid volume was calculated from 25 spheroids for each cell line.

## Cell migration and invasion assays

### Scratch-wound migration assays

96-well plates were coated with rat tail collagen I (200 μg/ml, ibidi) in PBS and 2 mM acetic acid overnight at 37°C. After washing, $4 \times 10^4$ cells per well (shCRP2a and b, and sh-) were seeded to form a confluent monolayer for 4 h. Homogeneous scratch wounds were generated by using a 96-well tool WoundMaker™ (Essen BioScience). The cell free area was imaged every 3 h until the cells from both sides merged. Wound confluence was measured at each time point using the automated image acquisition and processing system IncuCyte (Essen BioScience). For scratch-wound invasion assays, cells and wounds were prepared as above described. After wounding, cells were embedded in a 3D collagen I gel (2 mg/ml, Ibidi) following manufacturer's instructions and the gap closure was measured after 72 h. Prior to chemotaxis assays, MDA-MB-231 and Hs578T cells were starved 24 h in serum-free DMEM medium without or with 1% FBS, respectively. After starvation, MDA-MB-231 cells ($1 \times 10^5$) and Hs578T cells ($0.5 \times 10^5$) were embedded in rat tail collagen I (Ibidi) gel (2 mg/ml and 1.5 mg/ml, respectively), and loaded in a μ-Slide Chemotaxis ³ᴰ slide (Ibidi) and incubated at 37°C for 1 h to induce collagen gel polymerization. After polymerization, the two chambers flanking the channel were filled with DMEM medium supplemented or not with 10% FBS (and EGF 50 ng/ml in case of Hs578T cells), respectively. For each condition, about 150 cells (3 x 50) were tracked over 2 days using the live cell imaging Cell-IQ™ system (CM Technologies; 1 picture every 20 minutes). Single cell tracking was performed in ImageJ with MTrackJ pluging (NIH, Bethesda, USA), and average velocities (μm/min⁻¹) were calculated. MDA-MB-231 cell 2D migration velocity was determined as above described except that cells were loaded on a collagen IV coated μ-Slide Chemotaxis²ᴰ slide (Ibidi).

For transwell analyses, 24-well inserts (Greigner) were filled with 100 μl of EHS matrix (330 μg/ml in DMEM medium) and incubated 2 h at 37°C. MDA-MB-231 cells ($5 \times 10^4$), Hs578T cells ($3 \times 10^4$), and MCF-7 cells ($5 \times 10^4$) were loaded on the insert in DMEM without serum (MDA-MD-231-luc cells) or supplemented with 1% FBS (HS578T cells) or 2% FBS (MCF-7 cells). The lower well was filled with DMEM supplemented with 10% FBS (MDA-MB-231 cells), or 10% FBS and 50 ng/ml EGF (HS578T and MCF-7 cells) as chemoattractant. The total number of cells and the number of cells that had invaded after 24 h (48 h in case of MCF-7 cells) were evaluated by MTT, and the percentage of invasion was calculated and normalized to siCtr cells (set to 100%).

201

## Gelatinase zymography

Gelatinase zymography assays were performed in 10% (v/v) SDS-PAGE gel in the presence of 1 mg/ml gelatin from bovine skin type B (Sigma-Aldrich). Conditioned media (20 μL/sample) from PMA-free or PMA-treated cells were prepared for electrophoresis under non-reducing conditions [46]. Gels were washed twice after electrophoresis in 2.5% (v/v) Triton X-100 for 30 min and incubated in a developing buffer containing 100 mM Tris-HCl, 5 mM CaCl$_2$ and 0.005% (v/v) Brij-35 (pH 8.0) (Sigma-Aldrich) overnight at 37°C. Gels were stained for 30 min in a staining buffer containing 0.5% Coomassie Brilliant Blue R-250 in 50% (v/v) methanol and 10% (v/v) acetic acid (Sigma-Aldrich).

## Confocal microscopy and immuno-fluorescence

Cells were fixed in 4% paraformaldehyde (PFA, Thermo Scientific), permeabilized with 0.1% (v/v) Tween 20, incubated in the blocking buffer (5% Bovine Serum Albumin, BSA and 5% Normal Goat Serum, NGS, Sigma-Aldrich) for 1 h and incubated with primary antibodies overnight at 4°C. Cells were incubated with appropriate secondary antibodies for 4 h at room temperature. Analyses were performed in mounting medium (Citifluor AF1, Agar Scientific) using a Zeiss LSM510 Meta laser scanning confocal microscope equipped with a ×63/1.4-numerical-aperture (NA) oil immersion Plan Apochromat objective. Stacks with 0.4 μm optical sections were captured and processed for deconvolution by using Huygens essential Software (SVI, Netherlands) to enhance the signal-to-noise ratio. To investigate CRP2 localization in invadopodia, cells were cultured on Cy3-conjugated gelatin-coated coverslips (QCM™ Gelatin Invadopodia Assay, Millipore) for 6 h and CRP2-GFP was co-localized with cortactin (antibody clone 4F11, Millipore) and actin (Acti-stain™ 670 phalloidin, Cytoskeleton). To localize CRP2 in elongated invadopodia, cells were grown on EHS matrix-coated ThinCert™ Tissue Culture Inserts (Greiner) with 1-μm-diameter pores [9]. Invadopodia elongation was stimulated with conditioned culture medium containing 15% FBS and 50 ng/ml EGF (Preprotech) for 24 h. For localization experiments in invading cells, we used a circular invasion assay similar as the one described in [37]. Briefly, 5 x 10$^5$ cells were plated around a silicone culture-insert (ibidi) in a round μ-dish (35mm, ibidi) to create a large cell free region. After 24 h, the insert was removed and cells were overlaid with 4.5 mg/ml EHS matrix. EHS matrix was polymerized during 4 h at 37°C prior addition of culture medium. After 48 h cells were fixed and CRP2-GFP was co-localized with cortactin and actin. In addition to CRP2-GFP detection, endogenous CRP2 was immunolocalized using the same antibodies as in western blot.

The skewness analysis for actin bundling quantification was performed as previously described [25]. In brief, regions of interest (ROI, 13 x 13 μm) containing stress fibers labeled with Acti-stain 555 phalloidin were acquired using optimized and identical settings. The skewness of signal intensity distribution of AF pixels was calculated using the software plug-in Kbi_Filter2d (ThinLine), developed by Higaki and coworkers [58] (available at http://hasezawa.ib.k.u-tokyo.ac.jp/zp/Kbi/HigStomata). Skewness average values were calculated from three independent experiments, including 200 ROI, for each condition.

## Fluorescent gelatin degradation assay

5 x 10$^4$ cells were seeded on a 16 mm coverslip coated with a 6:1 mix of unlabeled:Cy3-labelled gelatin according to the manufacturer's instructions (QCM™ Gelatin Invadopodia Assay; Millipore). After 18 h at 37°C, cells were fixed and stained for actin (Acti-stain™ 670 phalloidin, Cytoskeleton). ECM degrading cells were defined as cells with an underlying black area depleted of fluorescent gelatin. Active cells were scored and expressed as percentage of the total cell population. In addition, the degraded area per cell was measured using the threshold tool of ImageJ software, and a degradation index corresponding to the ratio of degraded gelatin surface per cell was calculated.

## Total internal reflection fluorescence (TIRF) microscopy

TIRF microscopy observations were performed as previously described in [25]. A 3:1 mix of cold (Cytoskeleton) and Alexa Fluor 488-labeled actin (1 μM; Invitrogen) was induced to polymerize in NEM-myosin-coated perfusion chambers as shown in [59]. The chamber was perfused with actin alone or in combination with 3 μM recombinant CRP2. Actin filaments were imaged by TIRF microscopy on a Zeiss Axiovert 200M inverted microscope equipped with a ×100/1.46-NA Alpha Plan-Apochromat TIRF objective. Time lapse images were acquired at 5 s intervals over 45min with a Zeiss Axiocam HR camera. Images were analyzed using ImageJ. Kymograph was built along actin bundles with the MultiKymograph plugin (http://www.embl.de/eamnet/html/body_kymograph.html).

## Immunohistochemistry

A triple negative breast cancer tissue array (BRC964) was purchased from Pantomics, Inc. (Richmond, CA, USA). Immunohistochemical staining was performed using rabbit anti-human CSRP2 (HPA045617, Sigma-

Aldrich) after an optimal dilution (1/250) was determined using a universal TMA UNC241 (Richmond, CA, USA). Rabbit anti-cytokeratin and normal rabbit serum were used as positive and negative controls. Heat-induced epitope retrieval was performed using a pressure cooker and Tris-EDTA buffer. Polymer-based detection system was used for detection according to Pantomics' standard protocol.

## Experimental and spontaneous metastasis breast cancer models

Animal work was conducted in accordance to the national and international regulations, and with protocols approved by the Ministry of Agriculture and Ministry of Health. Highly invasive MDA-MB-231-luc-cells expressing an shRNA targeting CRP2 (shCRP2a) or a control shRNA (sh-) were trypsinized, washed in PBS twice and filtered onto a 50 µm filter (Partec CellTrics). In the experimental metastasis model, $10^6$ cells in 0.1 ml PBS were injected into the lateral tail vein of 6-week-old female athymic nu/nu mice (Charles River). Cell implantation to the lungs was immediately controlled by bioluminescence imaging (IVIS imaging system). After 5 weeks, mice were sacrificed by cervical dislocation after isoflurane (2%) anesthesia. Lungs were collected and the number of GFP (transduction marker) positive metastatic lesions was analyzed under a fluorescent stereomicroscope and using ImageJ (NIH, Bethesda, USA). The other organs and tissues of mice from the two groups were also carefully checked for the presence of metastases. In the spontaneous metastasis model $5 \times 10^5$ cells in 50 µL EHS matrix diluted 1:1 in PBS were injected into one mammary fat pad of 6-week-old NOD.Cg-$Prkdc^{scid}$ $Il2rg^{tm1Wjl}$/SzJ (NSG) mice (Charles River). Primary tumor dimensions (length, width and height) were periodically measured using calipers and the tumor volume was calculated according to the formula: ½ x L x W x H. After 20 days, mice were sacrificed by cervical dislocation and lungs were collected and the number of GFP (transduction marker) positive metastatic lesions was analyzed as above described.

## Statistics

All numerical data are shown as mean ± SE. Error bars represent standard error. Kaplan-Meier survival plots [29], hazard ratio with 95% confidence intervals and Logrank P values were used to test for associations between CRP2 expression (Affy probe 207030_s_at), and metastasis-free survival in breast cancer patients. Statistical significance was determined by Mann-Whitney U test for the *in vivo* lung metastasis models, Z-test for two population proportions for the gelatin degradation assays (active cells), and unpaired two-tailed Student's *t* test for the other analyses. $P$ values < 0.05 were considered statistically significant.

## CONFLICTS OF INTEREST

The authors declare no conflict of interest.

## REFERENCES

1. Wan L, Pantel K and Kang Y. Tumor metastasis: moving new biological insights into the clinic. Nature medicine. 2013; 19:1450-1464.

2. Linder S. The matrix corroded: podosomes and invadopodia in extracellular matrix degradation. Trends in cell biology. 2007; 17:107-117.

3. Murphy DA and Courtneidge SA. The 'ins' and 'outs' of podosomes and invadopodia: characteristics, formation and function. Nature reviews Molecular cell biology. 2011; 12:413-426.

4. Chen WT, Chen JM, Parsons SJ and Parsons JT. Local degradation of fibronectin at sites of expression of the transforming gene product pp60src. Nature. 1985; 316:156-158.

5. Gligorijevic B, Wyckoff J, Yamaguchi H, Wang Y, Roussos ET and Condeelis J. N-WASP-mediated invadopodium formation is involved in intravasation and lung metastasis of mammary tumors. Journal of cell science. 2012; 125:724-

734.

6. Leong HS, Robertson AE, Stoletov K, Leith SJ, Chin CA, Chien AE, Hague MN, Ablack A, Carmine-Simmen K, McPherson VA, Postenka CO, Turley EA, Courtneidge SA, Chambers AF and Lewis JD. Invadopodia are required for cancer cell extravasation and are a therapeutic target for metastasis. Cell reports. 2014; 8:1558-1570.

7. Paz H, Pathak N and Yang J. Invading one step at a time: the role of invadopodia in tumor metastasis. Oncogene. 2014; 33:4193-4202.

8. Overall CM and Kleifeld O. Tumour microenvironment - opinion: validating matrix metalloproteinases as drug targets and anti-targets for cancer therapy. Nature reviews Cancer. 2006; 6:227-239.

9. Schoumacher M, Goldman RD, Louvard D and Vignjevic DM. Actin, microtubules, and vimentin intermediate filaments cooperate for elongation of invadopodia. The Journal of cell biology. 2010; 189:541-556.

10. Li A, Dawson JC, Forero-Vargas M, Spence HJ, Yu X, Konig I, Anderson K and Machesky LM. The actin-bundling protein fascin stabilizes actin in invadopodia and potentiates protrusive invasion. Curr Biol. 2010; 20:339-345.

11. Machesky LM and Li A. Fascin: Invasive filopodia promoting metastasis. Commun Integr Biol. 2010; 3:263-270.

12. Van Audenhove I, Boucherie C, Pieters L, Zwaenepoel O, Vanloo B, Martens E, Verbrugge C, Hassanzadeh-Ghassabeh G, Vandekerckhove J, Cornelissen M, De Ganck A and Gettemans J. Stratifying fascin and cortactin function in invadopodium formation using inhibitory nanobodies and targeted subcellular delocalization. FASEB journal : official publication of the Federation of American Societies for Experimental Biology. 2014; 28:1805-1818.

13. Chen L, Yang S, Jakoncic J, Zhang JJ and Huang XY. Migrastatin analogues target fascin to block tumour metastasis. Nature. 2010; 464:1062-1066.

14. Huang FK, Han S, Xing B, Huang J, Liu B, Bordeleau F, Reinhart-King CA, Zhang JJ and Huang XY. Targeted inhibition of fascin function blocks tumour invasion and metastatic colonization. Nature communications. 2015; 6:7465.

15. Weiskirchen R and Gunther K. The CRP/MLP/TLP family of LIM domain proteins: acting by connecting. Bioessays. 2003; 25:152-162.

16. Papuga J, Hoffmann C, Dieterle M, Moes D, Moreau F, Tholl S, Steinmetz A and Thomas C. Arabidopsis LIM proteins: a family of actin bundlers with distinct expression patterns and modes of regulation. The Plant cell. 2010; 22:3034-3052.

17. Louis HA, Pino JD, Schmeichel KL, Pomies P and Beckerle MC. Comparison of three members of the cysteine-rich protein family reveals functional conservation and divergent patterns of gene expression. J Biol Chem. 1997; 272:27484-

27491.

18. Kong Y, Flick MJ, Kudla AJ and Konieczny SF. Muscle LIM protein promotes myogenesis by enhancing the activity of MyoD. Molecular and cellular biology. 1997; 17:4750-4760.

19. Chang DF, Belaguli NS, Iyer D, Roberts WB, Wu SP, Dong XR, Marx JG, Moore MS, Beckerle MC, Majesky MW and Schwartz RJ. Cysteine-rich LIM-only proteins CRP1 and CRP2 are potent smooth muscle differentiation cofactors. Dev Cell. 2003; 4:107-118.

20. Knoll R, Hoshijima M, Hoffman HM, Person V, Lorenzen-Schmidt I, Bang ML, Hayashi T, Shiga N, Yasukawa H, Schaper W, McKenna W, Yokoyama M, Schork NJ, Omens JH, McCulloch AD, Kimura A, et al. The cardiac mechanical stretch sensor machinery involves a Z disc complex that is defective in a subset of human dilated cardiomyopathy. Cell. 2002; 111:943-955.

21. Geier C, Gehmlich K, Ehler E, Hassfeld S, Perrot A, Hayess K, Cardim N, Wenzel K, Erdmann B, Krackhardt F, Posch MG, Osterziel KJ, Bublak A, Nagele H, Scheffold T, Dietz R, et al. Beyond the sarcomere: CSRP3 mutations cause hypertrophic cardiomyopathy. Hum Mol Genet. 2008; 17:2753-2765.

22. Newman B, Cescon D, Woo A, Rakowski H, Erikkson MJ, Sole M, Wigle ED and Siminovitch KA. W4R variant in CSRP3 encoding muscle LIM protein in a patient with hypertrophic cardiomyopathy. Mol Genet Metab. 2005; 84:374-375.

23. Arber S, Hunter JJ, Ross J, Jr., Hongo M, Sansig G, Borg J, Perriard JC, Chien KR and Caroni P. MLP-deficient mice exhibit a disruption of cardiac cytoarchitectural organization, dilated cardiomyopathy, and heart failure. Cell. 1997; 88:393-403.

24. Knoll R, Kostin S, Klede S, Savvatis K, Klinge L, Stehle I, Gunkel S, Kotter S, Babicz K, Sohns M, Miocic S, Didie M, Knoll G, Zimmermann WH, Thelen P, Bickeboller H, et al. A common MLP (muscle LIM protein) variant is associated with cardiomyopathy. Circ Res. 2010; 106:695-704.

25. Hoffmann C, Moreau F, Moes M, Luthold C, Dieterle M, Goretti E, Neumann K, Steinmetz A and Thomas C. Human Muscle LIM Protein Dimerizes along the Actin Cytoskeleton and Cross-Links Actin Filaments. Molecular and cellular biology. 2014; 34:3053-3065.

26. Tran TC, Singleton C, Fraley TS and Greenwood JA. Cysteine-rich protein 1 (CRP1) regulates actin filament bundling. BMC Cell Biol. 2005; 6:45.

27. Jang HS and Greenwood JA. Glycine-rich region regulates cysteine-rich protein 1 binding to actin cytoskeleton. Biochem Biophys Res Commun. 2009; 380:484-488.

28. Hu Z, Fan C, Oh DS, Marron JS, He X, Qaqish BF, Livasy C, Carey LA, Reynolds E, Dressler L, Nobel A, Parker J, Ewend MG, Sawyer LR, Wu J, Liu Y, et al. The molecular portraits of breast tumors are conserved across microarray platforms. BMC Genomics. 2006; 7:96.

29. Gyorffy B, Lanczky A, Eklund AC, Denkert C, Budczies J, Li Q and Szallasi Z. An online survival analysis tool to rapidly assess the effect of 22,277 genes on breast cancer prognosis using microarray data of 1,809 patients. Breast cancer research and treatment. 2010; 123:725-731.

30. Neve RM, Chin K, Fridlyand J, Yeh J, Baehner FL, Fevr T, Clark L, Bayani N, Coppe JP, Tong F, Speed T, Spellman PT, DeVries S, Lapuk A, Wang NJ, Kuo WL, et al. A collection of breast cancer cell lines for the study of functionally distinct cancer subtypes. Cancer cell. 2006; 10:515-527.

31. Zyad A, Branellec D, Mahe Y, Tursz T and Chouaib S. The development of human tumor-cell resistance to TNF-alpha does not confer resistance to cytokine-induced cellular cytotoxic mechanisms. International journal of cancer Journal international du cancer. 1992; 52:953-958.

32. Akalay I, Janji B, Hasmim M, Noman MZ, Andre F, De Cremoux P, Bertheau P, Badoual C, Vielh P, Larsen AK, Sabbah M, Tan TZ, Keira JH, Hung NT, Thiery JP, Mami-Chouaib F, et al. Epithelial-to-mesenchymal transition and autophagy induction in breast carcinoma promote escape from T-cell-mediated lysis. Cancer research. 2013; 73:2418-2427.

33. Jenkins DE, Hornig YS, Oei Y, Dusich J and Purchio T. Bioluminescent human breast cancer cell lines that permit rapid and sensitive in vivo detection of mammary tumors and multiple metastases in immune deficient mice. Breast cancer research : BCR. 2005; 7:R444-454.

34. Ayala I, Baldassarre M, Giacchetti G, Caldieri G, Tete S, Luini A and Buccione R. Multiple regulatory inputs converge on cortactin to control invadopodia biogenesis and extracellular matrix degradation. Journal of cell science. 2008; 121:369-378.

35. Pignatelli J, Tumbarello DA, Schmidt RP and Turner CE. Hic-5 promotes invadopodia formation and invasion during TGF-beta-induced epithelial-mesenchymal transition. The Journal of cell biology. 2012; 197:421-437.

36. Kam Y, Guess C, Estrada L, Weidow B and Quaranta V. A novel circular invasion assay mimics in vivo invasive behavior of cancer cell lines and distinguishes single-cell motility in vitro. BMC cancer. 2008; 8:198.

37. Yu X and Machesky LM. Cells assemble invadopodia-like structures and invade into matrigel in a matrix metalloprotease dependent manner in the circular invasion assay. PloS one. 2012; 7:e30605.

38. Kubow KE and Horwitz AR. Reducing background fluorescence reveals adhesions in 3D matrices. Nature cell biology. 2011; 13:3-5; author reply 5-7.

39. Hoffmann C, Moes D, Dieterle M, Neumann K, Moreau F, Tavares Furtado A, Dumas D, Steinmetz A and Thomas C. Live cell imaging reveals actin-cytoskeleton-induced self-association of the actin-bundling protein WLIM1. Journal of cell science. 2014; 127:583-598.

40. Thomas C, Hoffmann C, Dieterle M, Van Troys M, Ampe C and Steinmetz A. Tobacco WLIM1 is a novel F-actin binding protein involved in actin cytoskeleton remodeling. The Plant cell. 2006; 18:2194-2206.

41. Wang HJ, Wan AR and Jauh GY. An actin binding protein, LlLIM1, mediates Ca and H regulation of actin dynamics in pollen tubes. Plant Physiol. 2008; 47:1619-1636.

42. Sand JM, Larsen L, Hogaboam C, Martinez F, Han M, Rossel Larsen M, Nawrocki A, Zheng Q, Karsdal MA and Leeming DJ. MMP mediated degradation of type IV collagen alpha 1 and alpha 3 chains reflects basement membrane remodeling in experimental and clinical fibrosis—validation of two novel biomarker assays. PloS one. 2013; 8:e84934.

43. Beliveau A, Mott JD, Lo A, Chen EI, Koller AA, Yaswen P, Muschler J and Bissell MJ. Raf-induced MMP-9 disrupts tissue architecture of human breast cells in three-dimensional culture and is necessary for tumor growth in vivo. Genes & development. 2010; 24:2800-2811.

44. Yousef EM, Tahir MR, St-Pierre Y and Gaboury LA. MMP-9 expression varies according to molecular subtypes of breast cancer. BMC cancer. 2014; 14:609.

45. Farina AR and Mackay AR. Gelatinase B/MMP-9 in Tumour Pathogenesis and Progression. Cancers. 2014; 6:240-296.

46. Roomi MW, Monterrey JC, Kalinovsky T, Rath M and Niedzwiecki A. Patterns of MMP-2 and MMP-9 expression in human cancer cell lines. Oncology reports. 2009; 21:1323-1333.

47. Cervero P, Himmel M, Kruger M and Linder S. Proteomic analysis of podosome fractions from macrophages reveals similarities to spreading initiation centres. European journal of cell biology. 2012; 91:908-922.

48. Yang S, Huang FK, Huang J, Chen S, Jakoncic J, Leo-Macias A, Diaz-Avalos R, Chen L, Zhang JJ and Huang XY. Molecular mechanism of fascin function in filopodial formation. J Biol Chem. 2013; 288:274-284.

49. Jansen S, Collins A, Yang C, Rebowski G, Svitkina T and Dominguez R. Mechanism of actin filament bundling by fascin. J Biol Chem. 2011; 286:30087-30096.

50. Konrat R, Krautler B, Weiskirchen R and Bister K. Structure of cysteine- and glycine-rich protein CRP2. Backbone dynamics reveal motional freedom and independent spatial orientation of the lim domains. J Biol Chem. 1998; 273:23233-23240.

51. Sedeh RS, Fedorov AA, Fedorov EV, Ono S, Matsumura F, Almo SC and Bathe M. Structure, evolutionary conservation, and conformational dynamics of Homo sapiens fascin-1, an F-actin crosslinking protein. Journal of molecular biology. 2010; 400:589-604.

52. Yu M, Bardia A, Wittner BS, Stott SL, Smas ME, Ting DT, Isakoff SJ, Ciciliano JC, Wells MN, Shah AM, Concannon KF, Donaldson MC, Sequist LV, Brachtel E, Sgroi D, Baselga J, et al. Circulating breast tumor cells exhibit dynamic changes in epithelial and mesenchymal

205

composition. Science. 2013; 339:580-584.

53. Wu ML, Chen CH, Lin YT, Jheng YJ, Ho YC, Yang LT, Chen L, Layne MD and Yet SF. Divergent signaling pathways cooperatively regulate TGFbeta induction of cysteine-rich protein 2 in vascular smooth muscle cells. Cell communication and signaling : CCS. 2014; 12:22.

54. Pang MF, Georgoudaki AM, Lambut L, Johansson J, Tabor V, Hagikura K, Jin Y, Jansson M, Alexander JS, Nelson CM, Jakobsson L, Betsholtz C, Sund M, Karlsson MC and Fuxe J. TGF-beta1-induced EMT promotes targeted migration of breast cancer cells through the lymphatic system by the activation of CCR7/CCL21-mediated chemotaxis. Oncogene. 2015.

55. Kim-Kaneyama JR, Suzuki W, Ichikawa K, Ohki T, Kohno Y, Sata M, Nose K and Shibanuma M. Uni-axial stretching regulates intracellular localization of Hic-5 expressed in smooth-muscle cells *in vivo*. Journal of cell science. 2005; 118:937-949.

56. Coussens LM, Fingleton B and Matrisian LM. Matrix metalloproteinase inhibitors and cancer: trials and tribulations. Science. 2002; 295:2387-2392.

57. Wei J, Gorman TE, Liu X, Ith B, Tseng A, Chen Z, Simon DI, Layne MD and Yet SF. Increased neointima formation in cysteine-rich protein 2-deficient mice in response to vascular injury. Circ Res. 2005; 97:1323-1331.

58. Higaki T, Kutsuna N, Sano T, Kondo N and Hasezawa S. Quantification and cluster analysis of actin cytoskeletal structures in plant cells: role of actin bundling in stomatal movement during diurnal cycles in Arabidopsis guard cells. Plant J. 2010; 61:156-165.

59. Breitsprecher D, Kiesewetter AK, Linkner J and Faix J. Analysis of actin assembly by *in vitro* TIRF microscopy. Methods in molecular biology. 2009; 571:401-415.

206

# Review 1

## Hypoxia: a key feature of the tumor microenvironment triggers several mechanisms of evasion from natural killer and cytotoxic T lymphocytes surveillance.

Mgrditchian T, Arakelian T, Paggetti J, Viry E, Al-Absi A, Medves S, Moussay E, Berchem G, Thomas C and Janji B. *Journal of Immunology Research*. 2014.

## Review Article

# Hypoxia: A Key Feature of the Tumor Microenvironment Triggers Several Mechanisms of Evasion from Natural Killer and Cytotoxic T Lymphocytes Surveillance

**Mgrditchian T[1], Arakelian T[1], Paggetti J[1], Viry E[1], Al-Absi A[2], Medves S[1], Moussay E[1], Berchem G[1,3], Thomas C[2] and Janji B[1*]**

[1]Laboratory of Experimental Hemato-Oncology, Department of Oncology, Public Research Center for Health

[2]Laboratory of Cellular and Molecular-Oncology, Department of Oncology, Public Research Center for Health, Luxembourg

[3]Centre Hospitalier de Luxembourg, Department of Hemato-Oncology, Luxembourg

**\*Corresponding author:** Bassam Janji, Laboratory of Experimental Hemato-Oncology, Department of Oncology, Public Research Center for Health, Luxembourg, Tel: +352 26 970 285; Fax: +352 26 970 390; Email: bassam.janji@crp-sante.lu

## Abstract

Since many years, the tumor microenvironment is recognized as an important promoter of cancer initiation and progression. Although tumors primarily consist in cancer cells, various components/factors of the microenvironment and more specifically the immune landscape, dramatically impact cancer progression. Comprehensive analyses conducted on diverse tumors have identified and characterized the most relevant components/factors of the tumor microenvironment that supports the malignant behavior of a growing primary tumor. Tumor hypoxia is a common characteristic of the tumor microenvironment that is associated with tumor progression, metastasis, treatment failure and escape from immune surveillance. Although immune cells are usually efficiently recruited into the tumor bed, hypoxic microenvironment was reported to compromise immune cell functions and, in some cases, switch immune cell activity towards a pro-tumorigenic profile. Mechanistic studies have highlighted that hypoxia acts as double-edged sword: it simultaneously impairs the function of immune cells in the tumor microenvironment and activates intrinsic cell resistance mechanisms in tumor cells. The present article aims at reviewing some recent findings on how hypoxia impairs the anti-tumor immune response by focusing on emerging mechanisms by which hypoxia damps the function of immune effectors cells and activates intrinsic immune resistance mechanisms in tumor cells including autophagy and actin cytoskeleton remodeling.

**Keywords:** Cancer; Hypoxia; Immune response; Tumor microenvironment; Autophagy; Actin cytoskeleton

## Abbreviations

AFs: Actin Filaments; APCs: Antigen Presenting Cells; ARP: Actin-Related Protein; ATG: Autophagy-Related Genes; Bcl-2: B Cell Lymphoma 2; CAFs: Cancer-Associated Fibroblasts; Cdc42: Cell Division Cycle 42; CTL: Cytotoxic T Lymphocyte; ECM: Extracellular Matrix; EMT: Epithelial-to-Mesenchymal Transition; FAK: Focal Adhesion Kinase; HIF: Hypoxia-Inducible Factors; HOXA1: Homeobox A1; HRE: *Hypoxia*-Response Element; IS, Immunological Synapse; LFA: Lymphocyte Function-Associated Antigen; MAPK: Mitogen-Activated Protein Kinases; MHC: Major Histocompatibility Complex; MICA: MHC Class I Polypeptide-Related Sequence A; miR: micro RNA; NK: Natural Killer; NKG2D: Natural Killer Group 2 Member D; PHD2: Prolyl Hydroxylase Domain Protein 2; PTPN1: Protein Tyrosine Phosphatase Non-Receptor Type 1; Rac1: Ras-Related C3 Botulinum Toxin Substrate 1; Rho: Ras Homolog; ROCK1: Rho-Associated Protein Kinase 1; STAT3: Signal Transducer and Activator of Transcription 3; TCR: T Cell Receptor; TNF: Tumor Necrosis Factor;TP53I11: Tumor Protein p53-inducible Protein 11; VEGF: Vascular Endothelial Growth Factor; VHL: Von Hippel–Lindau; WAS: Wiskott-Aldrich Syndrome; WASp: WAS Protein; YAP: Yes-associated Protein.

## Introduction

Research in tumor immunology has validated the concept of cancer immune surveillance which predicts that the immune system can recognize precursors of cancer and, in most cases, destroy them or slow their growth before they become clinically apparent [1, 2]. Several types of immune cells are involved in tumor immune surveillance. Briefly, key cells of the adaptive immune system recognizing cancer cells are cytotoxic T lymphocytes (CTL) which are able to identify tumor antigens *via* the T cell receptor (TCR) [3]. Some of these antigens are expressed exclusively by tumors and thus are called tumor-specific antigens [3]. Natural killer (NK) cells of the innate immune system also play an important role in tumor immune surveillance [3] by mechanisms called "missing-self" and "induced-self" recognitions [5]. In addition to CTL and NK cells, macrophages and neutrophil granulocytes are also involved in anti-tumor immunity [6]. Macrophages are antigen presenting cells (APCs) that display tumor antigens and stimulate other immune cells such as CTL, NK cells and other APCs [7]. While the molecular mechanism by which CTL and NK cells recognize their target tumor cells is fundamentally different, both immune cells kill their target following the establishment of immunological synapse (IS) [8]. The formation of IS requires cell polarization and extensive remodeling of the actin cytoskeleton at various stages [9]. It is now well established that CTL and NK cells recognize and kill target cells by two major pathways: either through the release of cytotoxic granules containing perforin and granzymes to the cytosol of target cells [10], or through

tumor necrosis factor (TNF) super family-dependent killing [11].

Many microenvironmental factors (*e.g.*hypoxia, composition/organization of the extracellular matrix (ECM), inflammation, immune suppressive tumor-associated cells) contribute to various aspects of cancer progression, including immune evasion of tumor cells [12, 13]. Recently, it has been reported that the immune system also sculpts the immunogenic phenotype of an established tumor to favor the emergence of resistant tumor cell variants [14]. Accumulating experimental and clinical evidence indicates that multiple mechanisms suppressing the anti-tumor immune functions are directly evolved in the tumor microenvironment [15]. Recently, attention has been focused on the mechanisms by which hypoxic stress within the tumor microenvironment alters tumor transcriptional profiles to modulate glycolysis, proliferation, survival and invasion [16].

In this review, we focus on recent progresses in understanding the influence of hypoxic stress on the tumor survival mechanisms and tumor escape from immune surveillance. We discuss how hypoxia impairs tumor cell killing mediated by both innate and adaptive immune cells. We also review how hypoxia confers resistance to immune attack by activating intrinsic resistance mechanisms in tumor cells. Particular attention is given to hypoxia-induced immune escape mechanisms that rely on actin cytoskeleton remodeling in tumor or immune cells. Finally, we briefly address how hypoxia-targeted strategies may have potential clinical application for restoring an efficient anti-tumor immune response.

## Hypoxia and Hypoxia-inducible Factors (HIF) Regulation

Hypoxic stress plays a major role in the acquisition of tumor resistance to immune cell-mediated apoptosis and in the impairment of immune cell activity. Tumor cells adapt to hypoxic microenvironment by inducing transcription factors of the hypoxia inducible factor (HIF) family [17]. The HIF family comprises three members, HIF-1,-2 and-3. HIF-1 is a hetero dimeric protein composed of a constitutively expressed HIF-1β subunit and an oxygen-regulated HIF-1α subunit. In the presence of oxygen, HIF-1α is hydroxylated on proline residue 402 and/or 564 by prolyl hydroxylase domain protein 2 (PHD2). Hydroxylated HIF-1α interacts with the Von Hippel–Lindau (VHL) tumor suppressor protein [18] and recruits an E3 ubiquitin-protein ligase to catalyze the polyubiquitination of HIF-1α and itssubsequent targeting to theubiquitin proteasome system for degradation [19] (**Figure 1**). Under hypoxic condition, the hydroxylation of HIF-1α is inhibited leading to HIF-1α accumulation. Subsequently, HIF-1α Trans locates to the nucleus, dimerizes with HIF-1βsubunit, binds to the *hypoxia*-response elements (HRE) present in the promoter of target genes, and recruits co-activators to activate gene transcription (**Figure 1**). Similar to HIF-1α, HIF-2α is regulated by oxygen-dependent hydroxylation [20]. Although they share structurally similar DNA-binding and dimerization domains, HIF-1α and -2α differ in their trans activation domains. Accordingly, HIF-1α and -2α share overlapping target genes, and each also regulates a set of specific targets [21]. HIF-3α lacks the trans activation domain and was proposed to function as an inhibitor of HIF-1α and HIF-2α. Interestingly, its expression is transcriptionally regulated by HIF-1[22].

## Influence of Hypoxia on Cancer Cell Sensitivity to CTL and NK-mediated Lysis

As previously mentioned, hypoxia modulates both the activity of immune effectors and the response of tumor cells to these effectors. It has been reported that hypoxia decreases the sensitivity of tumor cells to CTL-mediated killing by several mechanisms involving HIF-1. For example, Noman *et al.* showed that HIF-1α induces the phosphorylation of signal transducer and activator of transcription 3 (STAT3) in tumor cells by a mechanism involving at least in part, vascular endothelial growth factor (VEGF) secretion. Following its
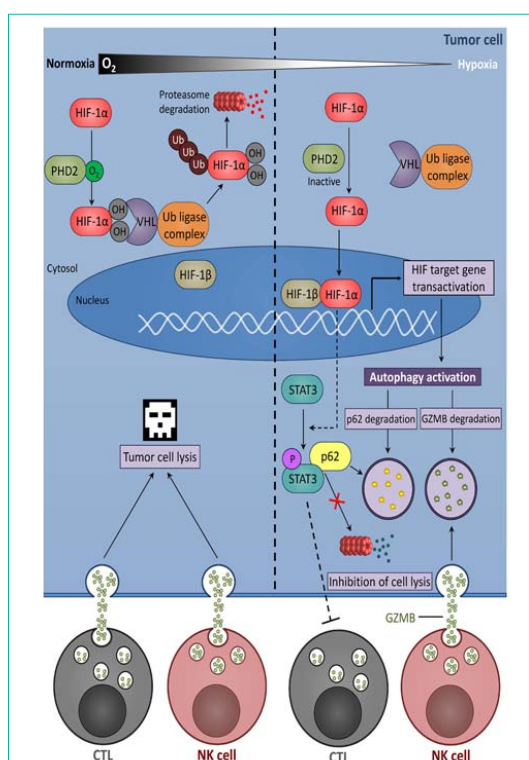


**Figure 1:** Hypoxia induces tumor cell resistance mechanisms leading to escape from CTL- or NK-mediated lysis. Under normoxic condition, the oxygen-sensitive prolyl hydroxylase domain protein 2 (PHD2) hydroxylatesHIF-1α subunit which is bound to *Von Hippel-Lindau protein (*VHL), ubiquitinated and subsequently degraded by the ubiquitin-proteasome system. Under hypoxia, PHD2 protein is inactivated, and HIF-1α is therefore stabilized. Stabilized HIF-1α translocated to the nucleus and formed with HIF-1β, a heterodimeric complex responsible for transcriptional activation of HIF-target genes including those responsible for the activation of autophagy. In addition, HIF induced the phosphorylation of the signal transducer and activator of transcription (STAT) 3 by a mechanism which is not fully described. The activation of autophagy leads to the degradation of the cargo protein p62, responsible for the elimination of phospho-STAT3 by the ubiquitin proteasome system. The degradation of phospho-STAT3 inhibits CTL-mediated lysis of tumor cells. Furthermore, excessive autophagy in hypoxic target cells leads to the selective degradation of granzyme B (GZMB), a serine protease contained into the cytotoxic granules released by natural killer (NK) cells, thereby inhibiting NK-mediated lysis.

210

translocation to the nucleus, HIF-1α cooperates with pSTAT3 to alter the susceptibility of non-small cell lung carcinoma to CTL-mediated killing [23] (**Figure 1**). A follow-up study has reported that the level of pSTAT3 is tightly controlled by the activation of autophagy in hypoxic cells. Indeed, the accumulation of pSTAT3 was no longer observed when the autophagic flux was inhibited in hypoxic tumor cells [24]. Briefly, autophagy is a catabolic process where a cell self-digests its own components. It can be activated in response to multiple stresses including hypoxia, nutrient starvation, growth factor withdrawal and endoplasmic reticulum stress. Autophagy primarily serves as an adaptive metabolic response providing nutrients, preventing accumulation of altered cell components [25], shaping the anti-tumor immune response [26] and the acquisition of resistance to TNF α [27]. Studies aimed at investigating the mechanisms by which autophagy controls pSTAT3 revealed that targeting autophagy decreases the level of pSTAT3, and that this decrease was mediated by the ubiquitin proteasome system [24, 28].

Another study showed that the transcription factor NANOG, which is involved in stem cell self-renewal, is a new mediator of hypoxia-induced resistance to CTL-lysis [29, 30]. NANOG is induced at both transcriptional and translational levels under hypoxic stress and its targeting leads to significant attenuation of hypoxia-induced tumor resistance to CTL-dependent killing. NANOG depletion results in inhibition of STAT3 phosphorylation and nuclear translocation. Furthermore, it has been shown that HIF-1 induces hypoxia-inducible micro RNA (miR)-210. Over expression of miR-210 in tumor cell stargets protein tyrosine phosphatase non-receptor type 1 (PTPN1), homeobox A1 (HOXA1), and tumor protein p53-inducible protein 11 (TP53I11), and thereby decreases tumor cell susceptibility to CTL [31]. Hypoxia has also been reported to increase the shedding of the major histocompatibility complex (MHC) class I polypeptide-related sequence A (MICA), a ligand for the activating receptor natural killer group 2 member D (NKG2D), at the surface of prostate cancer cells. This shedding is related to the impairment of NO signaling [32] and leads to tumor escape from NK and CTL cells. Furthermore, HIF-1 is able to down regulate MICA expression in osteosarcoma cells resulting in tumor resistance to NK-mediated lysis [33]. Recently, we showed that targeting autophagy under hypoxia restores NK-mediated lysis in breast cancer cells. We provided mechanistic evidence that activation of autophagy under hypoxia leads to the degradation of NK-derived granzyme B making hypoxic tumor cells less sensitive to NK-mediated killing [34, 35] (**Figure 1**). Taken together, it is now well documented that hypoxic microenvironment is an important determinant involved in the control of anti-tumor immune response. Indeed, its immune suppressive effect contributes not only in damping the immune cell function but also in conferring resistance mechanisms to tumor cells to resist immune cells attack [36].
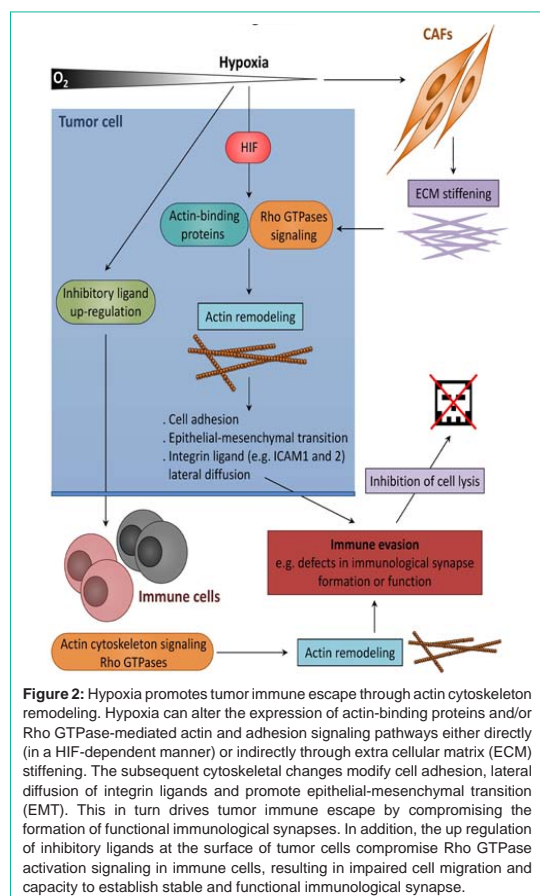
## The Actin Cytoskeleton: A Point of Convergence for Various Processes Involved in Tumor Immune Evasion

To fulfill their biological functions, immune cells require exceptional capabilities to proliferate, move through the entire body, infiltrate tissues, establish cell-cell contacts and exchange various types of compounds/signals with both other immune cells and their

targets. The related cellular processes, including cell division, cell migration and invasion, cell shape plasticity, intracellular transport, endo and exocytosis, membrane trafficking and phagocytosis, largely rely on dynamic re-arrangements of the actin cytoskeleton. Accordingly, dysregulation of the actin cytoskeleton organization or dynamics can compromise immune cell function and lead to severe diseases, including cancer [37]. A typical illustration is provided by the Wiskott-Aldrich syndrome (WAS) which is caused by alterations of WAS protein (WASp) activity. One major function of WASp is to stimulate actin polymerization through the actin-related proteins (ARP) 2/3 nucleation complex in response to signals from the cell surface [38, 39]. Although some signaling activities of WASp are independent of actin remodeling, most immune cell defects induced by the loss of WASp are at least to some extent, related to defective actin responses, including cell migration, activation, IS formation, and phagocytosis [40-43].

One important aspect of the anti-tumor immune response is the establishment of the IS between cytotoxic immune cells, such as CTL and NK cells, and their targets. Although the signaling pathways activating CTL and NK cell-mediated tumor cell death differ, the establishment of a functional IS and the directed secretion of cytolytic granules toward the tumor cell are relatively well conserved processes that require extensive cytoskeletal remodeling. Following immune cell activation, actin polymerization is activated [44, 45] and granules polarize toward the cell-cell contact region in a microtubule network and microtubule motor activity-dependent manner [46-48]. A critical feature of this process is the translocation of the microtubule-organizing center (upon which granules converge) from the rear of the immune cell to the leading edge where the immunological synapse is established. The presence of pre-docked granules at the cell cortex of CTL and NK cells, that can be exocytosed before centrosome polarization has been reported [49-51]. Both pharmacological and genetic studies indicate that immune cell activation, IS formation, and the steps following granule polarization largely rely on actin cytoskeleton remodeling [46, 48, 52-54]. A substantial remodeling event occurring simultaneously with centrosome translocation is the accumulation of actin toward the edge of the cell-cell contact region in the so-called distal supra molecular activation cluster where integrin proteins concentrate to mediate cell adhesion [55-57]. The central region of mature synapses was initially proposed to function as an actin-free clearance through which granules are passively released [47, 56]. Such a model was however challenged by studies supporting that granules associate with actin in a myosin IIA dependent manner prior to their delivery to the precise de-granulation sites [58, 59]. Recently, high-resolution microscopy has provided compelling evidence that an actin meshwork is present at the center of the IS from NK cells and that it functions as a facilitator for granule secretion rather than as a barrier [46, 60-62].

In contrast to the well-characterized configurations and roles of actin filaments (AFs) in NK and CTL cells during the cytolytic process, there is a relative gap of knowledge about AF organization and dynamics in target tumor cells. However growing evidence indicate that AF reorganization in tumor cells can promote resistance to anti-tumor immunity (**Figure 2**). Thus, knock-down of two actin-regulatory proteins, namely the actin-severing factor scinderin [63, 64] and the signaling molecule ephrin-A1 [65] that

211

**Figure 2:** Hypoxia promotes tumor immune escape through actin cytoskeleton remodeling. Hypoxia can alter the expression of actin-binding proteins and/or Rho GTPase-mediated actin and adhesion signaling pathways either directly (in a HIF-dependent manner) or indirectly through extra cellular matrix (ECM) stiffening. The subsequent cytoskeletal changes modify cell adhesion, lateral diffusion of integrin ligands and promote epithelial-mesenchymal transition (EMT). This in turn drives tumor immune escape by compromising the formation of functional immunological synapses. In addition, the up regulation of inhibitory ligands at the surface of tumor cells compromise Rho GTPase activation signaling in immune cells, resulting in impaired cell migration and capacity to establish stable and functional immunological synapse.

are over expressed in resistant lung tumor cells, was sufficient to restore normal cell morphology and to increase cell sensitivity to CTL-mediated cell death [66]. A follow-up study established that the focal adhesion kinase (FAK) signaling pathway, which controls actin organization and modulates cell adhesion and proliferation was defective in tumor resistant cells [67]. Remarkably, the suppression of FAK in tumor cell was sufficient to promote their resistance to CTL by blocking IS formation. Furthermore, increased AF rearrangement and adhesion following pharmacological activation of Ras homolog (Rho) GTP ases has been reported to induce tumor cell susceptibility to CTL mediated killing. These data further support the role of actin remodeling as a switch in the control of tumor cell susceptibility to cytotoxic immune cells. In addition, depolymerization of AFs in NK-sensitive target cells abrogates the conjugate formation mediated by lymphocyte associated antigen (LFA)-1 and subsequently affects granule polarization [68]. Experimental data point to a mechanism where actin cytoskeleton-dependent tethering of LFA-1 ligand such as intercellular adhesion molecules (ICAM)-1 and -2, is required for proper integrin signaling in NK cells [68]. Thus, the modulation of the lateral diffusion of integrin ligand by actin remodeling at the

tumor cell cortex represents a potential facet of the immune evasion.

Tumor cells do not only remodel their own actin cytoskeleton to escape from the immune system but are also capable of promoting cytoskeletal modifications in immune cells to impair their activity (**Figure 2**). Gene-expression profiling study revealed that genes involved in actin cytoskeleton formation and organization in peripheral blood CTL are considerably dysregulated in chronic lymphocytic leukemia patients [69]. Thus, leukemia cells were able to induce similar cytoskeletal defects in CTL from healthy allogeneic donors. Interestingly, the underlying process required cell-cell contact and was independent on cytokine release. Follow-up studies established that malignant cells up-regulate inhibitory ligands such as the B7 super family-related ligands CD200, CD274 and CD276, and TNF-receptor super family member CD270, to compromise the activation of key regulators of T cell synapse actin dynamics, including the Rho GTPases RhoA, Ras-related C3 botulinum toxin substrate 1 (Rac1) and cell division cycle protein 42 (Cdc42) and eventually compromise the establishment of a functional IS [70, 71]. Remarkably, similar inhibitory ligand signaling axes were found in a range of other hematologic and solid carcinoma cells, suggesting that tumor cell-induced T cell actin synapse dysfunction is a common immunosuppressive strategy. Recently, elegant work by Ramsay *et al* demonstrated that leukemia cells from patients impair T cell LFA-1-mediated migration by altering Rho GTPase activation signaling. Importantly, the immune modulating drug lenalidomide was shown to restore T cell Rho GTPase activity and LFA-1 activation, laying the ground for immunotherapy approaches promoting T cell motility in cancer patients [72].

## Tumor Microenvironment-induced Cancer Progression and Immune Evasion Involve Actin Cytoskeleton Remodeling

It has been reported that the physical properties of tumor stroma considerably differ from those of corresponding healthy tissues. Hypoxic stress within the tumor microenvironment induces an increase in ECM stiffness [73] and this increase is largely associated with the ability of hypoxia to induce the expression of ECM genes in cancer-associated fibroblasts, such as those involved in collagen fiber deposition and organization [74-76]. The perception of matrix stiffening by actin cytoskeleton-linked integrins activates signaling pathways that promote Rho GTPase-dependent cytoskeletal tension, focal adhesion assembly and cell migration [73, 77]. Interestingly, a recent study showed that an increase in matrix stiffness and actin cytoskeleton contractibility activates the transcription factor Yes-associated protein(YAP) in cancer-associated fibroblasts and that this activation is required for these fibroblasts to further increase matrix stiffening, cell invasion and angiogenesis [78]. Thus, by inducing a stiff microenvironment, hypoxia promotes actin remodeling in both tumor and cancer-associated fibroblasts (CAFs) leading to increased fibrillar collagen deposition and promoting tumorigenic functions of CAFs (**Figure 2**).

Hypoxic stress has been described to modify the expression and/or activity of Rho GTPases and/or of their downstream targets in both healthy and cancer cells. Recently, HIF-1 and -2 were shown to directly activate transcription of RhoA and Rho-associated

protein kinase 1 (ROCK1) genes, and subsequently promote actin cytoskeleton changes that underlie the invasive tumor cell phenotype [79]. Such coordination between HIF and RhoA-ROCK1 activation also induced FAK activation and focal adhesion formation, indicating that FAK is a major effectors of RhoA/ROCK1 in hypoxic breast cancer cells. Rac1 and Cdc42, two other major Rho GTPases controlling actin dynamics [80] and cancer progression [81] are up-regulated and activated by hypoxia in different tumor cells [82, 83]. In this context, it is worth noting that an immune functional screen identified Cdc42 as a key mediator of tumor resistance to CTL-mediated killing [84]. Remarkably, stable expression of constitutively active Cdc42 protected colorectal tumor cells against cytotoxicity and tumor suppression by allore active CTL *in vitro* and CTL and NK cells *in vivo*. However, the role of actin remodeling in the underlying mechanism remains uncertain. Instead, Cdc42 has been shown to promote immune resistance, at least in part, by mitogen-activated protein kinases (MAPK)-dependent inhibition of apoptosis and stabilization of the B cell lymphoma 2 (Bcl-2) anti apoptotic factor. In addition to modulating actin regulatory signaling pathways, hypoxia also drives changes in the expression level of specific actin-binding proteins [85]. However, how such changes influence the immune tumor response remains to be assessed.

As previously reported, hypoxia-induced autophagy plays important roles in tumor immune escape [86]. To our best knowledge, the role of the actin cytoskeleton in hypoxia-induced autophagy has not been extensively investigated in the specific context of tumor immune escape. Nevertheless, emerging evidence indicate that epithelial-to-mesenchymal transition (EMT), a biological process associated with dramatic morphologic changes and actin cytoskeleton remodeling, alters the susceptibility of tumor cells to CTL-mediated immune surveillance by a mechanism involving autophagy [87, 88]. There is also clear evidence that Rho family-dependent actin remodeling is required for proper autophagy induced by other environmental stresses, such as starvation [89]. Finally, several autophagy-related genes (ATG) proteins were reported to physically and/or functionally interact with actin cytoskeleton components, such as the actin motor myosin II [90] and the FA protein paxillin [91].

The ability of cancer cells to evade immune surveillance and resist immunotherapy raises fundamental questions about how tumor cells survive in the presence of a competent immune system. To address this issue, studies have primarily focused on the mechanisms by which tumor cells avoid recognition by the immune system without considering the impact of the tumor microenvironment. Thus, despite intense investigation, the relatively modest gains provided by immunotherapy can be in part attributed to the activation of mechanisms suppressing the anti-tumor immunity. It is now clearly established that the majority of these mechanisms are likely evolved in the local tumor microenvironment. In line with this, it may be more accurate to consider cancer, which was initially thought to be a disease of cells, then of genes, and then of genomes, as a disease of the microenvironment. While remarkable and fairly rapid progresses have been made over the past two decades regarding the role of the microenvironment in cancer biology and treatment, our understanding of its actual contribution in tumor resistance to immune cell attack is still fragmented.

Emerging data indicate that hypoxia in the tumor microenvironment plays key role in mediating tolerance to immune cell attack. Therefore, an understanding of the tumor microenvironment, and in particular of hypoxia-induced tumor resistance, may allow better understanding of tumor adaptation and evolution, and ultimately lead to improve the efficacy of potential therapeutics. Thus, it stands to reason that targeting hypoxia could have a substantial effect in evolving the properties of tumor microenvironment from immunosuppressive to immune permissive. In keeping with this, an extensive number of HIF inhibitory molecules are currently under development and being tested or in use in clinical settings. Such inhibitors comprise HIF-α antisense, dominant negative HIF-α and viral vectors as well as small molecules that inhibit HIF at multiple sites. Briefly, these inhibitors have been shown to block tumor xenograft growth and inhibit HIF activity through a wide variety of molecular mechanisms, including decreased HIF-1α mRNA levels, decreased HIF-1α protein synthesis, increased HIF-1α degradation, decreased HIF subunit hetero-dimerization, decreased HIF binding to DNA, and decreased HIF transcriptional activity. Notably, HIF-1α inhibitors would be expected to affect some parameters of the antitumor immunity such as CLT activity *in vivo* and *in vitro* (*i.e.,* cytokine production, proliferation, and activation). Indeed, several recent studies highlight that hypoxia is capable of mediating tumor cell resistance to CTL and NK cells [24, 31, 36]. In addition, it should be investigated whether HIF inhibitors could affect several other important mediators of immune tolerance such as myeloid-derived suppressor cells (MDSC) and T regulatory cells (*i.e.,* recruitment, function and differentiation). Overall, hypoxia inhibition in hypoxic tumors can be used as a cutting-edge approach to improve cancer immunotherapy and to formulate more effective cancer vaccine-based therapy.

significance in cancer- and non-cancer pathologies. Carcinogenesis. 2012;

213

immunological synapse: a molecular machine controlling T cell activation. Science. 1999; 285: 221-227.

9. Angus KL, Griffiths GM . Cell polarisation and the immunological synapse. Curr Opin Cell Biol. 2013; 25: 85-91.

10. Shresta S, MacIvor DM, Heusel JW, Russell JH, Ley TJ . Natural killer and lymphokine-activated killer cells require granzyme B for the rapid induction of apoptosis in susceptible target cells. Proc Natl Acad Sci U S A. 1995; 92: 5679-5683.

11. Cullen SP, Brunet M, Martin SJ . Granzymes in cancer and immunity. Cell Death Differ. 2010; 17: 616-623.

12. Quail DF, Joyce JA . Microenvironmental regulation of tumor progression and metastasis. Nat Med. 2013; 19: 1423-1437.

13. Palazon A, Goldrath AW2, Nizet V3, Johnson RS4 . HIF Transcription Factors, Inflammation, and Immunity. Immunity. 2014; 41: 518-528.

14. Hamai A, Benlalam H, Meslin F, Hasmim M, Carre T, Akalay I, et al. Immune surveillance of human cancer: if the cytotoxic T-lymphocytes play the music, does the tumoral system call the tune? Tissue antigens. 2010; 75:1-8.

15. Whiteside TL . The tumor microenvironment and its role in promoting tumor growth. Oncogene. 2008; 27: 5904-5912.

16. Majmundar AJ, Wong WJ, Simon MC . Hypoxia-inducible factors and the response to hypoxic stress. Mol Cell. 2010; 40: 294-309.

17. Semenza GL . Hypoxia-inducible factors: mediators of cancer progression and targets for cancer therapy. Trends Pharmacol Sci. 2012; 33: 207-214.

18. Baldewijns MM, van Vlodrop IJ, Vermeulen PB, Soetekouw PM, van Engeland M, de Bruïne AP . VHL and HIF signalling in renal cell carcinogenesis. J Pathol. 2010; 221: 125-138.

19. Salceda S, Caro J . Hypoxia-inducible factor 1alpha (HIF-1alpha) protein is rapidly degraded by the ubiquitin-proteasome system under normoxic conditions. Its stabilization by hypoxia depends on redox-induced changes. J Biol Chem. 1997; 272: 22642-22647.

20. Patel SA, Simon MC . Biology of hypoxia-inducible factor-2alpha in development and disease. Cell Death Differ. 2008; 15: 628-634.

21. Lau KW, Tian YM, Raval RR, Ratcliffe PJ, Pugh CW . Target gene selectivity of hypoxia-inducible factor-alpha in renal cancer cells is conveyed by post-DNA-binding mechanisms. Br J Cancer. 2007; 96: 1284-1292.

22. Makino Y, Uenishi R, Okamoto K, Isoe T, Hosono O, Tanaka H, et al. Transcriptional up-regulation of inhibitory PAS domain protein gene expression by hypoxia-inducible factor 1 (HIF-1): a negative feedback regulatory circuit in HIF-1-mediated signaling in hypoxic cells. The Journal of biological chemistry. 2007; 282:14073-14082.

23. Noman MZ, Buart S, Van Pelt J, Richon C, Hasmim M, Leleu N, et al. The cooperative induction of hypoxia-inducible factor-1 alpha and STAT3 during hypoxia induced an impairment of tumor susceptibility to CTL-mediated cell lysis. Journal of immunology. 2009; 182: 3510-3521.

24. Noman MZ, Janji B, Kaminska B, Van Moer K, Pierson S, Przanowski P, et al . Blocking hypoxia-induced autophagy in tumors restores cytotoxic T-cell activity and promotes regression. Cancer Res. 2011; 71: 5976-5986.

25. Mathew R, White E . Autophagy in tumorigenesis and energy metabolism: friend by day, foe by night. Curr Opin Genet Dev. 2011; 21: 113-119.

26. Viry E, Paggetti J, Baginska J, Mgrditchian T, Berchem G, Moussay E, et al . Autophagy: An adaptive metabolic response to stress shaping the antitumor immunity. Biochem Pharmacol. 2014; .

27. Moussay E, Kaoma T, Baginska J, Muller A, Van Moer K, Nicot N, et al. The acquisition of resistance to TNFalpha in breast cancer cells is associated with constitutive activation of autophagy as revealed by a transcriptome analysis using a custom microarray. Autophagy. 2011; 7: 760-770.

28. Noman MZ, Janji B, Berchem G, Mami-Chouaib F, Chouaib S . Hypoxia-induced autophagy: a new player in cancer immunotherapy? Autophagy. 2012; 8: 704-706.

29. Hasmim M, Noman MZ, Lauriol J, Benlalam H, Mallavialle A, Rosselli F, et al. Hypoxia-dependent inhibition of tumor cell susceptibility to CTL-mediated lysis involves NANOG induction in target cells. Journal of immunology. 2011; 187: 4031-4039.

30. Hasmim M, Noman MZ, Messai Y, Bordereaux D, Gros G, Baud V, et al . Cutting edge: Hypoxia-induced Nanog favors the intratumoral infiltration of regulatory T cells and macrophages via direct regulation of TGF-β1. J Immunol. 2013; 191: 5802-5806.

31. Noman MZ, Buart S, Romero P, Ketari S, Janji B, Mari B, et al. Hypoxia-inducible miR-210 regulates the susceptibility of tumor cells to lysis by cytotoxic T cells. Cancer Res. 2012; 72: 4629-4641.

32. Siemens DR, Hu N, Sheikhi AK, Chung E, Frederiksen LJ, Pross H, et al. Hypoxia increases tumor cell shedding of MHC class I chain-related molecule: role of nitric oxide. Cancer Res. 2008; 68: 4746-4753.

33. Yamada N, Yamanegi K, Ohyama H, Hata M, Nakasho K, Futani H, et al. Hypoxia downregulates the expression of cell surface MICA without increasing soluble MICA in osteosarcoma cells in a HIF-1alpha-dependent manner. International journal of oncology. 2012; 41: 2005-2012.

34. Baginska J, Viry E, Berchem G, Poli A, Noman MZ, van Moer K, et al. Granzyme B degradation by autophagy decreases tumor cell susceptibility to natural killer-mediated lysis under hypoxia. Proc Natl Acad Sci U S A. 2013; 110: 17450-17455.

35. Viry E, Baginska J, Berchem G, Noman MZ, Medves S, Chouaib S, et al. Autophagic degradation of GZMB/granzyme B: a new mechanism of hypoxic tumor cell escape from natural killer cell-mediated lysis. Autophagy. 2014; 10: 173-175.

36. Baginska J, Viry E, Paggetti J, Medves S, Berchem G, Moussay E, et al. The critical role of the tumor microenvironment in shaping natural killer cell-mediated anti-tumor immunity. Front Immunol. 2013; 4: 490.

37. Wickramarachchi DC, Theofilopoulos AN, Kono DH . Immune pathology associated with altered actin cytoskeleton regulation. Autoimmunity. 2010; 43: 64-75.

38. Blanchoin L, Amann KJ, Higgs HN, Marchand JB, Kaiser DA, Pollard TD . Direct observation of dendritic actin filament networks nucleated by Arp2/3 complex and WASP/Scar proteins. Nature. 2000; 404: 1007-1011.

39. Symons M, Derry JM, Karlak B, Jiang S, Lemahieu V, Mccormick F, et al. Wiskott-Aldrich syndrome protein, a novel effector for the GTPase CDC42Hs, is implicated in actin polymerization. Cell. 1996; 84: 723-734.

40. Bouma G, Burns SO, Thrasher AJ . Wiskott-Aldrich Syndrome: Immunodeficiency resulting from defective cell migration and impaired immunostimulatory activation. Immunobiology. 2009; 214: 778-790.

41. Bouma G, Mendoza-Naranjo A, Blundell MP, de Falco E, Parsley KL, Burns SO, et al. Cytoskeletal remodeling mediated by WASp in dendritic cells is necessary for normal immune synapse formation and T-cell priming. Blood. 2011; 118: 2492-2501.

42. Notarangelo LD, Ochs HD . Wiskott-Aldrich Syndrome: a model for defective actin reorganization, cell trafficking and synapse formation. Curr Opin Immunol. 2003; 15: 585-591.

43. Thrasher AJ, Burns SO . WASP: a key immunological multitasker. Nat Rev Immunol. 2010; 10: 182-192.

44. Bunnell SC, Kapoor V, Trible RP, Zhang W, Samelson LE . Dynamic actin polymerization drives T cell receptor-induced spreading: a role for the signal transduction adaptor LAT. Immunity. 2001; 14: 315-329.

45. Tskvitaria-Fuller I, Rozelle AL, Yin HL, Wülfing C . Regulation of sustained actin dynamics by the TCR and costimulation as a mechanism of receptor localization. J Immunol. 2003; 171: 2287-2295.

46. Mace EM, Dongre P, Hsu HT, Sinha P, James AM, Mann SS, et al. Cell biological steps and checkpoints in accessing NK cell cytotoxicity. Immunol Cell Biol. 2014; 92: 245-255.

47. Stinchcombe JC, Majorovits E, Bossi G, Fuller S, Griffiths GM . Centrosome polarization delivers secretory granules to the immunological synapse. Nature. 2006; 443: 462-465.

214

215

Stinchcombe JC, Griffiths GM . Secretory mechanisms in cell-mediated

Integrin-dependent organization and bidirectional vesicular traffic at cytotoxic

Ritter AT, Angus KL, Griffiths GM . The role of the cytoskeleton at the

conditions by inducing P4HA1, P4HA2, and PLOD2 expression in fibroblasts.

the generation and maintenance of cancer-associated fibroblasts. Nature cell

vesicle trafficking. Trends Cell Biol. 2006; 16: 522-529.

actin filaments in natural killer cells. Commun Integr Biol. 2012; 5: 184-186.

JP, Vitale ML, et al . Chromaffin cell scinderin, a novel calcium-dependent
actin filament-severing protein. EMBO J. 1990; 9: 43-52.

filament severing protein that controls cortical actin network dynamics during

Identification of target actin content and polymerization status as a mechanism

J Immun Res

216

# References

1    Schultz, K. T. & Grieder, F. Structure and function of the immune system. *Toxicol Pathol* **15**, 262-264, doi:10.1177/019262338701500301 (1987).

2    DeNardo, D. G. & Coussens, L. M. Inflammation and breast cancer. Balancing immune response: crosstalk between adaptive and innate immune cells during breast cancer progression. *Breast Cancer Res* **9**, 212, doi:10.1186/bcr1746 (2007).

3    den Haan, J. M., Arens, R. & van Zelm, M. C. The activation of the adaptive immune system: cross-talk between antigen-presenting cells, T cells and B cells. *Immunol Lett* **162**, 103-112, doi:10.1016/j.imlet.2014.10.011 (2014).

4    Mittrucker, H. W., Visekruna, A. & Huber, M. Heterogeneity in the differentiation and function of CD8(+) T cells. *Arch Immunol Ther Exp (Warsz)* **62**, 449-458, doi:10.1007/s00005-014-0293-y (2014).

5    Sun, B. & Zhang, Y. Overview of orchestration of CD4+ T cell subsets in immune responses. *Adv Exp Med Biol* **841**, 1-13, doi:10.1007/978-94-017-9487-9_1 (2014).

6    Kim, H. J. & Cantor, H. CD4 T-cell subsets and tumor immunity: the helpful and the not-so-helpful. *Cancer Immunol Res* **2**, 91-98, doi:10.1158/2326-6066.CIR-13-0216 (2014).

7    Gattinoni, L. *et al*. Removal of homeostatic cytokine sinks by lymphodepletion enhances the efficacy of adoptively transferred tumor-specific CD8+ T cells. *J Exp Med* **202**, 907-912, doi:10.1084/jem.20050732 (2005).

8    Berzins, S. P. & Ritchie, D. S. Natural killer T cells: drivers or passengers in preventing human disease? *Nat Rev Immunol* **14**, 640-646, doi:10.1038/nri3725 (2014).

9    Chamoto, K. *et al*. NKT cells act as regulatory cells rather than killer cells during activation of NK cell-mediated cytotoxicity by alpha-galactosylceramide in vivo. *Immunol Lett* **95**, 5-11, doi:10.1016/j.imlet.2004.04.012 (2004).

10   Pieper, K., Grimbacher, B. & Eibel, H. B-cell biology and development. *J Allergy Clin Immunol* **131**, 959-971, doi:10.1016/j.jaci.2013.01.046 (2013).

11   Marcus, A. *et al*. Recognition of tumors by the innate immune system and natural killer cells. *Adv Immunol* **122**, 91-128, doi:10.1016/B978-0-12-800267-4.00003-1 (2014).

12   Artis, D. & Spits, H. The biology of innate lymphoid cells. *Nature* **517**, 293-301, doi:10.1038/nature14189 (2015).

13   Nowarski, R., Gagliani, N., Huber, S. & Flavell, R. A. Innate immune cells in inflammation and cancer. *Cancer Immunol Res* **1**, 77-84, doi:10.1158/2326-6066.CIR-13-0081 (2013).

14   Kolaczkowska, E. & Kubes, P. Neutrophil recruitment and function in health and inflammation. *Nat Rev Immunol* **13**, 159-175, doi:10.1038/nri3399 (2013).

15   Dunkelberger, J. R. & Song, W. C. Complement and its role in innate and adaptive immune responses. *Cell Res* **20**, 34-50, doi:10.1038/cr.2009.139 (2010).

16   Toapanta, F. R. & Ross, T. M. Complement-mediated activation of the adaptive immune responses: role of C3d in linking the innate and adaptive immunity. *Immunol Res* **36**, 197-210, doi:10.1385/IR:36:1:197 (2006).

17   Vivier, E. & Medzhitov, R. Editorial overview: Innate immunity. *Curr Opin Immunol* **38**, v-vii, doi:10.1016/j.coi.2015.12.005 (2016).

18      Neyen, C. & Lemaitre, B. Sensing Gram-negative bacteria: a phylogenetic perspective. *Curr Opin Immunol* **38**, 8-17, doi:10.1016/j.coi.2015.10.007 (2016).

19      Soares, M. P. & Bozza, M. T. Red alert: labile heme is an alarmin. *Curr Opin Immunol* **38**, 94-100, doi:10.1016/j.coi.2015.11.006 (2016).

20      Stephenson, H. N., Herzig, A. & Zychlinsky, A. Beyond the grave: When is cell death critical for immunity to infection? *Curr Opin Immunol* **38**, 59-66, doi:10.1016/j.coi.2015.11.004 (2016).

21      Daeron, M. Innate myeloid cells under the control of adaptive immunity: the example of mast cells and basophils. *Curr Opin Immunol* **38**, 101-108, doi:10.1016/j.coi.2015.12.004 (2016).

22      Huntington, N. D., Carpentier, S., Vivier, E. & Belz, G. T. Innate lymphoid cells: parallel checkpoints and coordinate interactions with T cells. *Curr Opin Immunol* **38**, 86-93, doi:10.1016/j.coi.2015.11.008 (2016).

23      Kiessling, R., Klein, E. & Wigzell, H. "Natural" killer cells in the mouse. I. Cytotoxic cells with specificity for mouse Moloney leukemia cells. Specificity and distribution according to genotype. *Eur J Immunol* **5**, 112-117, doi:10.1002/eji.1830050208 (1975).

24      Topham, N. J. & Hewitt, E. W. Natural killer cell cytotoxicity: how do they pull the trigger? *Immunology* **128**, 7-15, doi:10.1111/j.1365-2567.2009.03123.x (2009).

25      Campbell, K. S. & Hasegawa, J. Natural killer cell biology: an update and future directions. *J Allergy Clin Immunol* **132**, 536-544, doi:10.1016/j.jaci.2013.07.006 (2013).

26      Stanietsky, N. & Mandelboim, O. Paired NK cell receptors controlling NK cytotoxicity. *FEBS Lett* **584**, 4895-4900, doi:10.1016/j.febslet.2010.08.047 (2010).

27      Ribatti, D. Historical overview on the morphological characterization of large granular lymphocytes/natural killer cells. *Immunol Lett* **190**, 58-63, doi:10.1016/j.imlet.2017.07.014 (2017).

28      Kiessling, R., Klein, E., Pross, H. & Wigzell, H. "Natural" killer cells in the mouse. II. Cytotoxic cells with specificity for mouse Moloney leukemia cells. Characteristics of the killer cell. *Eur J Immunol* **5**, 117-121, doi:10.1002/eji.1830050209 (1975).

29      Pross, H. F., Baines, M. G., Rubin, P., Shragge, P. & Patterson, M. S. Spontaneous human lymphocyte-mediated cytotoxicity against tumor target cells. IX. The quantitation of natural killer cell activity. *J Clin Immunol* **1**, 51-63 (1981).

30      Kedar, E., Ikejiri, B. L., Gorelik, E. & Herbermann, R. B. Natural cell-mediated cytotoxicity in vitro and inhibition of tumor growth in vivo by murine lymphoid cells cultured with T cell growth factor (TCGF). *Cancer Immunol Immunother* **13**, 14-23 (1982).

31      Zamai, L. *et al*. Natural killer (NK) cell-mediated cytotoxicity: differential use of TRAIL and Fas ligand by immature and mature primary human NK cells. *J Exp Med* **188**, 2375-2380 (1998).

32      Herberman, R. B. & Holden, H. T. Natural cell-mediated immunity. *Adv Cancer Res* **27**, 305-377 (1978).

33      Thornthwaite, J. T. & Leif, R. C. The plaque cytogram assay. I. Light and scanning electron microscopy of immunocompetent cells. *J Immunol* **113**, 1897-1908 (1974).

34      Timonen, T. & Saksela, E. Isolation of human NK cells by density gradient centrifugation. *J Immunol Methods* **36**, 285-291 (1980).

35    Geiger, T. L. & Sun, J. C. Development and maturation of natural killer cells. *Curr Opin Immunol* **39**, 82-89, doi:10.1016/j.coi.2016.01.007 (2016).

36    Gregoire, C. *et al*. The trafficking of natural killer cells. *Immunol Rev* **220**, 169-182, doi:10.1111/j.1600-065X.2007.00563.x (2007).

37    Yu, J., Freud, A. G. & Caligiuri, M. A. Location and cellular stages of natural killer cell development. *Trends Immunol* **34**, 573-582, doi:10.1016/j.it.2013.07.005 (2013).

38    Poli, A. *et al*. CD56bright natural killer (NK) cells: an important NK cell subset. *Immunology* **126**, 458-465, doi:10.1111/j.1365-2567.2008.03027.x (2009).

39    Amand, M. *et al*. Human CD56(dim)CD16(dim) Cells As an Individualized Natural Killer Cell Subset. *Front Immunol* **8**, 699, doi:10.3389/fimmu.2017.00699 (2017).

40    Vanherberghen, B. *et al*. Classification of human natural killer cells based on migration behavior and cytotoxic response. *Blood* **121**, 1326-1334, doi:10.1182/blood-2012-06-439851 (2013).

41    Maghazachi, A. A. Role of chemokines in the biology of natural killer cells. *Curr Top Microbiol Immunol* **341**, 37-58, doi:10.1007/82_2010_20 (2010).

42    Robertson, M. J. Role of chemokines in the biology of natural killer cells. *J Leukoc Biol* **71**, 173-183 (2002).

43    Berahovich, R. D., Lai, N. L., Wei, Z., Lanier, L. L. & Schall, T. J. Evidence for NK cell subsets based on chemokine receptor expression. *J Immunol* **177**, 7833-7840 (2006).

44    Pegram, H. J., Andrews, D. M., Smyth, M. J., Darcy, P. K. & Kershaw, M. H. Activating and inhibitory receptors of natural killer cells. *Immunol Cell Biol* **89**, 216-224, doi:10.1038/icb.2010.78 (2011).

45    Fassett, M. S., Davis, D. M., Valter, M. M., Cohen, G. B. & Strominger, J. L. Signaling at the inhibitory natural killer cell immune synapse regulates lipid raft polarization but not class I MHC clustering. *Proc Natl Acad Sci U S A* **98**, 14547-14552, doi:10.1073/pnas.211563598 (2001).

46    Purdy, A. K. & Campbell, K. S. Natural killer cells and cancer: regulation by the killer cell Ig-like receptors (KIR). *Cancer Biol Ther* **8**, 2211-2220 (2009).

47    Sivori, S. *et al*. TLR/NCR/KIR: Which One to Use and When? *Front Immunol* **5**, 105, doi:10.3389/fimmu.2014.00105 (2014).

48    Borrego, F., Masilamani, M., Marusina, A. I., Tang, X. & Coligan, J. E. The CD94/NKG2 family of receptors: from molecules and cells to clinical relevance. *Immunol Res* **35**, 263-278, doi:10.1385/IR:35:3:263 (2006).

49    Spear, P., Wu, M. R., Sentman, M. L. & Sentman, C. L. NKG2D ligands as therapeutic targets. *Cancer Immun* **13**, 8 (2013).

50    Mistry, A. R. & O'Callaghan, C. A. Regulation of ligands for the activating receptor NKG2D. *Immunology* **121**, 439-447, doi:10.1111/j.1365-2567.2007.02652.x (2007).

51    Sutherland, C. L. *et al*. ULBPs, human ligands of the NKG2D receptor, stimulate tumor immunity with enhancement by IL-15. *Blood* **108**, 1313-1319, doi:10.1182/blood-2005-11-011320 (2006).

52    Zhang, J., Basher, F. & Wu, J. D. NKG2D Ligands in Tumor Immunity: Two Sides of a Coin. *Front Immunol* **6**, 97, doi:10.3389/fimmu.2015.00097 (2015).

53     Andre, P. *et al.* Comparative analysis of human NK cell activation induced by NKG2D and natural cytotoxicity receptors. *Eur J Immunol* **34**, 961-971, doi:10.1002/eji.200324705 (2004).

54     Nausch, N. & Cerwenka, A. NKG2D ligands in tumor immunity. *Oncogene* **27**, 5944-5958, doi:10.1038/onc.2008.272 (2008).

55     Waldhauer, I. & Steinle, A. NK cells and cancer immunosurveillance. *Oncogene* **27**, 5932-5943, doi:10.1038/onc.2008.267 (2008).

56     Molfetta, R. *et al.* Regulation of NKG2D Expression and Signaling by Endocytosis. *Trends Immunol* **37**, 790-802, doi:10.1016/j.it.2016.08.015 (2016).

57     Hirayasu, K. & Arase, H. Functional and genetic diversity of leukocyte immunoglobulin-like receptor and implication for disease associations. *J Hum Genet* **60**, 703-708, doi:10.1038/jhg.2015.64 (2015).

58     Carosella, E. D., Rouas-Freiss, N., Tronik-Le Roux, D., Moreau, P. & LeMaoult, J. HLA-G: An Immune Checkpoint Molecule. *Adv Immunol* **127**, 33-144, doi:10.1016/bs.ai.2015.04.001 (2015).

59     Shemesh, A. *et al.* Splice variants of human natural cytotoxicity receptors: novel innate immune checkpoints. *Cancer Immunol Immunother*, doi:10.1007/s00262-017-2104-x (2017).

60     Bozzano, F. *et al.* Activating NK cell receptor expression/function (NKp30, NKp46, DNAM-1) during chronic viraemic HCV infection is associated with the outcome of combined treatment. *Eur J Immunol* **41**, 2905-2914, doi:10.1002/eji.201041361 (2011).

61     Cantoni, C. *et al.* The three-dimensional structure of the human NK cell receptor NKp44, a triggering partner in natural cytotoxicity. *Structure* **11**, 725-734 (2003).

62     Alvarez-Breckenridge, C. A. *et al.* NK cells impede glioblastoma virotherapy through NKp30 and NKp46 natural cytotoxicity receptors. *Nat Med* **18**, 1827-1834, doi:10.1038/nm.3013 (2012).

63     Herrmann, J. *et al.* Homo-oligomerization of the activating natural killer cell receptor NKp30 ectodomain increases its binding affinity for cellular ligands. *J Biol Chem* **289**, 765-777, doi:10.1074/jbc.M113.514786 (2014).

64     Matta, J. *et al.* Induction of B7-H6, a ligand for the natural killer cell-activating receptor NKp30, in inflammatory conditions. *Blood* **122**, 394-404, doi:10.1182/blood-2013-01-481705 (2013).

65     Li, Y., Wang, Q. & Mariuzza, R. A. Structure of the human activating natural cytotoxicity receptor NKp30 bound to its tumor cell ligand B7-H6. *J Exp Med* **208**, 703-714, doi:10.1084/jem.20102548 (2011).

66     Mandelboim, O. *et al.* Recognition of haemagglutinins on virus-infected cells by NKp46 activates lysis by human NK cells. *Nature* **409**, 1055-1060, doi:10.1038/35059110 (2001).

67     Hadad, U. *et al.* NKp46 Clusters at the Immune Synapse and Regulates NK Cell Polarization. *Front Immunol* **6**, 495, doi:10.3389/fimmu.2015.00495 (2015).

68     Baychelier, F. *et al.* Identification of a cellular ligand for the natural cytotoxicity receptor NKp44. *Blood* **122**, 2935-2942, doi:10.1182/blood-2013-03-489054 (2013).

69     Bialoszewska, A. *et al.* Constitutive expression of ligand for natural killer cell NKp44 receptor (NKp44L) by normal human articular chondrocytes. *Cell Immunol* **285**, 6-9, doi:10.1016/j.cellimm.2013.08.005 (2013).

70 Mathew, S. O., Rao, K. K., Kim, J. R., Bambard, N. D. & Mathew, P. A. Functional role of human NK cell receptor 2B4 (CD244) isoforms. *Eur J Immunol* **39**, 1632-1641, doi:10.1002/eji.200838733 (2009).

71 Ito, M. *et al.* Killer cell lectin-like receptor G1 binds three members of the classical cadherin family to inhibit NK cell cytotoxicity. *J Exp Med* **203**, 289-295, doi:10.1084/jem.20051986 (2006).

72 Shibuya, A. *et al.* DNAM-1, a novel adhesion molecule involved in the cytolytic function of T lymphocytes. *Immunity* **4**, 573-581 (1996).

73 Wang, F. *et al.* TIGIT expression levels on human NK cells correlate with functional heterogeneity among healthy individuals. *Eur J Immunol* **45**, 2886-2897, doi:10.1002/eji.201545480 (2015).

74 Kirkham, C. L. & Carlyle, J. R. Complexity and Diversity of the NKR-P1:Clr (Klrb1:Clec2) Recognition Systems. *Front Immunol* **5**, 214, doi:10.3389/fimmu.2014.00214 (2014).

75 Sedy, J. R. *et al.* A herpesvirus entry mediator mutein with selective agonist action for the inhibitory receptor B and T lymphocyte attenuator. *J Biol Chem* **292**, 21060-21070, doi:10.1074/jbc.M117.813295 (2017).

76 Ware, C. F. Targeting the LIGHT-HVEM pathway. *Adv Exp Med Biol* **647**, 146-155, doi:10.1007/978-0-387-89520-8_10 (2009).

77 Shao, J. Y. *et al.* Siglec-7 Defines a Highly Functional Natural Killer Cell Subset and Inhibits Cell-Mediated Activities. *Scand J Immunol* **84**, 182-190, doi:10.1111/sji.12455 (2016).

78 Wang, W., Erbe, A. K., Hank, J. A., Morris, Z. S. & Sondel, P. M. NK Cell-Mediated Antibody-Dependent Cellular Cytotoxicity in Cancer Immunotherapy. *Front Immunol* **6**, 368, doi:10.3389/fimmu.2015.00368 (2015).

79 Vivier, E., Tomasello, E., Baratin, M., Walzer, T. & Ugolini, S. Functions of natural killer cells. *Nat Immunol* **9**, 503-510, doi:10.1038/ni1582 (2008).

80 Fais, S. NK cell-released exosomes: Natural nanobullets against tumors. *Oncoimmunology* **2**, e22337, doi:10.4161/onci.22337 (2013).

81 Whiteside, T. L. Immune modulation of T-cell and NK (natural killer) cell activities by TEXs (tumour-derived exosomes). *Biochem Soc Trans* **41**, 245-251, doi:10.1042/BST20120265 (2013).

82 Lugini, L. *et al.* Immune surveillance properties of human NK cell-derived exosomes. *J Immunol* **189**, 2833-2842, doi:10.4049/jimmunol.1101988 (2012).

83 Screpanti, V., Wallin, R. P., Ljunggren, H. G. & Grandien, A. A central role for death receptor-mediated apoptosis in the rejection of tumors by NK cells. *J Immunol* **167**, 2068-2073 (2001).

84 Fellows, E., Gil-Parrado, S., Jenne, D. E. & Kurschus, F. C. Natural killer cell-derived human granzyme H induces an alternative, caspase-independent cell-death program. *Blood* **110**, 544-552, doi:10.1182/blood-2006-10-051649 (2007).

85 Kumar, R., Herbert, P. E. & Warrens, A. N. An introduction to death receptors in apoptosis. *Int J Surg* **3**, 268-277, doi:10.1016/j.ijsu.2005.05.002 (2005).

86 Vujanovic, N. L. Role of TNF superfamily ligands in innate immunity. *Immunol Res* **50**, 159-174, doi:10.1007/s12026-011-8228-8 (2011).

87 Volpe, E., Sambucci, M., Battistini, L. & Borsellino, G. Fas-Fas Ligand: Checkpoint of T Cell Functions in Multiple Sclerosis. *Front Immunol* **7**, 382, doi:10.3389/fimmu.2016.00382 (2016).

88      Salvesen, G. S. & Riedl, S. J. Structure of the Fas/FADD complex: a conditional death domain complex mediating signaling by receptor clustering. *Cell Cycle* **8**, 2723-2727, doi:10.4161/cc.8.17.9399 (2009).

89      Kayagaki, N. & Yagita, H. [Metalloproteinase-mediated release of human fas ligand]. *Nihon Rinsho* **54**, 1747-1752 (1996).

90      Tsutsui, H. *et al.* Caspase-1-independent, Fas/Fas ligand-mediated IL-18 secretion from macrophages causes acute liver injury in mice. *Immunity* **11**, 359-367 (1999).

91      Falschlehner, C., Schaefer, U. & Walczak, H. Following TRAIL's path in the immune system. *Immunology* **127**, 145-154, doi:10.1111/j.1365-2567.2009.03058.x (2009).

92      Walczak, H. Death receptor-ligand systems in cancer, cell death, and inflammation. *Cold Spring Harb Perspect Biol* **5**, a008698, doi:10.1101/cshperspect.a008698 (2013).

93      Dang, V. T. *et al.* Fasting enhances TRAIL-mediated liver natural killer cell activity via HSP70 upregulation. *PLoS One* **9**, e110748, doi:10.1371/journal.pone.0110748 (2014).

94      Yamashita, M. *et al.* A novel method for evaluating antibody-dependent cell-mediated cytotoxicity by flowcytometry using cryopreserved human peripheral blood mononuclear cells. *Sci Rep* **6**, 19772, doi:10.1038/srep19772 (2016).

95      Clynes, R. A., Towers, T. L., Presta, L. G. & Ravetch, J. V. Inhibitory Fc receptors modulate in vivo cytotoxicity against tumor targets. *Nat Med* **6**, 443-446, doi:10.1038/74704 (2000).

96      Wang, S. Y., Racila, E., Taylor, R. P. & Weiner, G. J. NK-cell activation and antibody-dependent cellular cytotoxicity induced by rituximab-coated target cells is inhibited by the C3b component of complement. *Blood* **111**, 1456-1463, doi:10.1182/blood-2007-02-074716 (2008).

97      Seidel, U. J., Schlegel, P. & Lang, P. Natural killer cell mediated antibody-dependent cellular cytotoxicity in tumor immunotherapy with therapeutic antibodies. *Front Immunol* **4**, 76, doi:10.3389/fimmu.2013.00076 (2013).

98      Voskoboinik, I., Whisstock, J. C. & Trapani, J. A. Perforin and granzymes: function, dysfunction and human pathology. *Nat Rev Immunol* **15**, 388-400, doi:10.1038/nri3839 (2015).

99      Chamkha, H., Li, X., Rouvet, G. & Thiery, J. [Perforin, granzyme and granulysin association to kill intracellular parasites]. *Med Sci (Paris)* **32**, 708-710, doi:10.1051/medsci/20163208015 (2016).

100     Hsu, H. T. *et al.* NK cells converge lytic granules to promote cytotoxicity and prevent bystander killing. *J Cell Biol* **215**, 875-889, doi:10.1083/jcb.201604136 (2016).

101     van den Broek, M. F., Kagi, D., Zinkernagel, R. M. & Hengartner, H. Perforin dependence of natural killer cell-mediated tumor control in vivo. *Eur J Immunol* **25**, 3514-3516, doi:10.1002/eji.1830251246 (1995).

102     Vahedi, F., Fraleigh, N., Vlasschaert, C., McElhaney, J. & Hanifi-Moghaddam, P. Human granzymes: related but far apart. *Med Hypotheses* **83**, 688-693, doi:10.1016/j.mehy.2014.09.019 (2014).

103     Trapani, J. A. Granzymes: a family of lymphocyte granule serine proteases. *Genome Biol* **2**, REVIEWS3014 (2001).

104    Arias, M. *et al.* The Untold Story of Granzymes in Oncoimmunology: Novel Opportunities with Old Acquaintances. *Trends Cancer* **3**, 407-422, doi:10.1016/j.trecan.2017.04.001 (2017).

105    Martinvalet, D. ROS signaling during granzyme B-mediated apoptosis. *Mol Cell Oncol* **2**, e992639, doi:10.4161/23723556.2014.992639 (2015).

106    de Poot, S. A. & Bovenschen, N. Granzyme M: behind enemy lines. *Cell Death Differ* **21**, 359-368, doi:10.1038/cdd.2013.189 (2014).

107    Perl, M., Denk, S., Kalbitz, M. & Huber-Lang, M. Granzyme B: a new crossroad of complement and apoptosis. *Adv Exp Med Biol* **946**, 135-146, doi:10.1007/978-1-4614-0106-3_8 (2012).

108    Rousalova, I. & Krepela, E. Granzyme B-induced apoptosis in cancer cells and its regulation (review). *Int J Oncol* **37**, 1361-1378 (2010).

109    Lau, A. *et al.* Serine protease inhibitor-6 inhibits granzyme B-mediated injury of renal tubular cells and promotes renal allograft survival. *Transplantation* **98**, 402-410, doi:10.1097/TP.0000000000000237 (2014).

110    Azzi, J. *et al.* Serine protease inhibitor 6 plays a critical role in protecting murine granzyme B-producing regulatory T cells. *J Immunol* **191**, 2319-2327, doi:10.4049/jimmunol.1300851 (2013).

111    Poe, M. *et al.* Human cytotoxic lymphocyte granzyme B. Its purification from granules and the characterization of substrate and inhibitor specificity. *J Biol Chem* **266**, 98-103 (1991).

112    Motyka, B. *et al.* Mannose 6-phosphate/insulin-like growth factor II receptor is a death receptor for granzyme B during cytotoxic T cell-induced apoptosis. *Cell* **103**, 491-500 (2000).

113    Galvin, J. P. *et al.* Apoptosis induced by granzyme B-glycosaminoglycan complexes: implications for granule-mediated apoptosis in vivo. *J Immunol* **162**, 5345-5350 (1999).

114    Menager, M. M. *et al.* Secretory cytotoxic granule maturation and exocytosis require the effector protein hMunc13-4. *Nat Immunol* **8**, 257-267, doi:10.1038/ni1431 (2007).

115    Fowler, K. T., Andrews, N. W. & Huleatt, J. W. Expression and function of synaptotagmin VII in CTLs. *J Immunol* **178**, 1498-1504 (2007).

116    Lord, S. J., Rajotte, R. V., Korbutt, G. S. & Bleackley, R. C. Granzyme B: a natural born killer. *Immunol Rev* **193**, 31-38 (2003).

117    Korsmeyer, S. J. *et al.* Pro-apoptotic cascade activates BID, which oligomerizes BAK or BAX into pores that result in the release of cytochrome c. *Cell Death Differ* **7**, 1166-1173, doi:10.1038/sj.cdd.4400783 (2000).

118    Pinkoski, M. J. *et al.* Granzyme B-mediated apoptosis proceeds predominantly through a Bcl-2-inhibitable mitochondrial pathway. *J Biol Chem* **276**, 12060-12067, doi:10.1074/jbc.M009038200 (2001).

119    MacDonald, G., Shi, L., Vande Velde, C., Lieberman, J. & Greenberg, A. H. Mitochondria-dependent and -independent regulation of Granzyme B-induced apoptosis. *J Exp Med* **189**, 131-144 (1999).

120    Adrain, C., Murphy, B. M. & Martin, S. J. Molecular ordering of the caspase activation cascade initiated by the cytotoxic T lymphocyte/natural killer (CTL/NK) protease granzyme B. *J Biol Chem* **280**, 4663-4673, doi:10.1074/jbc.M410915200 (2005).

121 Sebbagh, M., Hamelin, J., Bertoglio, J., Solary, E. & Breard, J. Direct cleavage of ROCK II by granzyme B induces target cell membrane blebbing in a caspase-independent manner. *J Exp Med* **201**, 465-471, doi:10.1084/jem.20031877 (2005).

122 Goping, I. S., Sawchuk, T., Underhill, D. A. & Bleackley, R. C. Identification of {alpha}-tubulin as a granzyme B substrate during CTL-mediated apoptosis. *J Cell Sci* **119**, 858-865, doi:10.1242/jcs.02791 (2006).

123 Yang, C. H., Lambie, E. J. & Snyder, M. NuMA: an unusually long coiled-coil related protein in the mammalian nucleus. *J Cell Biol* **116**, 1303-1317 (1992).

124 Zhang, D., Beresford, P. J., Greenberg, A. H. & Lieberman, J. Granzymes A and B directly cleave lamins and disrupt the nuclear lamina during granule-mediated cytolysis. *Proc Natl Acad Sci U S A* **98**, 5746-5751, doi:10.1073/pnas.101329598 (2001).

125 Bots, M. & Medema, J. P. Granzymes at a glance. *J Cell Sci* **119**, 5011-5014, doi:10.1242/jcs.03239 (2006).

126 McCormack, R., de Armas, L., Shiratsuchi, M. & Podack, E. R. Killing machines: three pore-forming proteins of the immune system. *Immunol Res* **57**, 268-278, doi:10.1007/s12026-013-8469-9 (2013).

127 Metkar, S. S. *et al.* Perforin rapidly induces plasma membrane phospholipid flip-flop. *PLoS One* **6**, e24286, doi:10.1371/journal.pone.0024286 (2011).

128 Voskoboinik, I., Dunstone, M. A., Baran, K., Whisstock, J. C. & Trapani, J. A. Perforin: structure, function, and role in human immunopathology. *Immunol Rev* **235**, 35-54, doi:10.1111/j.0105-2896.2010.00896.x (2010).

129 Law, R. H. *et al.* The structural basis for membrane binding and pore formation by lymphocyte perforin. *Nature* **468**, 447-451, doi:10.1038/nature09518 (2010).

130 Thiery, J. & Lieberman, J. Perforin: a key pore-forming protein for immune control of viruses and cancer. *Subcell Biochem* **80**, 197-220, doi:10.1007/978-94-017-8881-6_10 (2014).

131 Osinska, I., Popko, K. & Demkow, U. Perforin: an important player in immune response. *Cent Eur J Immunol* **39**, 109-115, doi:10.5114/ceji.2014.42135 (2014).

132 Okada, S., Li, Q., Whitin, J. C., Clayberger, C. & Krensky, A. M. Intracellular mediators of granulysin-induced cell death. *J Immunol* **171**, 2556-2562 (2003).

133 Leon, D. L., Fellay, I., Mantel, P. Y. & Walch, M. Killing Bacteria with Cytotoxic Effector Proteins of Human Killer Immune Cells: Granzymes, Granulysin, and Perforin. *Methods Mol Biol* **1535**, 275-284, doi:10.1007/978-1-4939-6673-8_18 (2017).

134 Mace, E. M. *et al.* Cell biological steps and checkpoints in accessing NK cell cytotoxicity. *Immunol Cell Biol* **92**, 245-255, doi:10.1038/icb.2013.96 (2014).

135 Dustin, M. L. The immunological synapse. *Cancer Immunol Res* **2**, 1023-1033, doi:10.1158/2326-6066.CIR-14-0161 (2014).

136 de la Roche, M., Asano, Y. & Griffiths, G. M. Origins of the cytolytic synapse. *Nat Rev Immunol* **16**, 421-432, doi:10.1038/nri.2016.54 (2016).

137 Kearney, C. J., Brennan, A. J., Darcy, P. K. & Oliaro, J. The Role of the immunological Synapse Formed by Cytotoxic Lymphocytes in Immunodeficiency and Anti-Tumor immunity. *Crit Rev Immunol* **35**, 325-347 (2015).

138 Dustin, M. L. What counts in the immunological synapse? *Mol Cell* **54**, 255-262, doi:10.1016/j.molcel.2014.04.001 (2014).

139     Mace, E. M. & Orange, J. S. New views of the human NK cell immunological synapse: recent advances enabled by super- and high-resolution imaging techniques. *Front Immunol* **3**, 421, doi:10.3389/fimmu.2012.00421 (2012).

140     Orange, J. S. *et al.* The mature activating natural killer cell immunologic synapse is formed in distinct stages. *Proc Natl Acad Sci U S A* **100**, 14151-14156, doi:10.1073/pnas.1835830100 (2003).

141     Comerci, C. J., Mace, E. M., Banerjee, P. P. & Orange, J. S. CD2 promotes human natural killer cell membrane nanotube formation. *PLoS One* **7**, e47664, doi:10.1371/journal.pone.0047664 (2012).

142     McNerney, M. E. & Kumar, V. The CD2 family of natural killer cell receptors. *Curr Top Microbiol Immunol* **298**, 91-120 (2006).

143     Mesecke, S., Urlaub, D., Busch, H., Eils, R. & Watzl, C. Integration of activating and inhibitory receptor signaling by regulated phosphorylation of Vav1 in immune cells. *Sci Signal* **4**, ra36, doi:10.1126/scisignal.2001325 (2011).

144     Mace, E. M., Zhang, J., Siminovitch, K. A. & Takei, F. Elucidation of the integrin LFA-1-mediated signaling pathway of actin polarization in natural killer cells. *Blood* **116**, 1272-1279, doi:10.1182/blood-2009-12-261487 (2010).

145     Mentlik, A. N., Sanborn, K. B., Holzbaur, E. L. & Orange, J. S. Rapid lytic granule convergence to the MTOC in natural killer cells is dependent on dynein but not cytolytic commitment. *Mol Biol Cell* **21**, 2241-2256, doi:10.1091/mbc.E09-11-0930 (2010).

146     Stinchcombe, J. C. & Griffiths, G. M. Communication, the centrosome and the immunological synapse. *Philos Trans R Soc Lond B Biol Sci* **369**, doi:10.1098/rstb.2013.0463 (2014).

147     Kupfer, A. & Kupfer, H. Imaging immune cell interactions and functions: SMACs and the Immunological Synapse. *Semin Immunol* **15**, 295-300, doi:10.1016/j.smim.2003.09.001 (2003).

148     Mace, E. M., Monkley, S. J., Critchley, D. R. & Takei, F. A dual role for talin in NK cell cytotoxicity: activation of LFA-1-mediated cell adhesion and polarization of NK cells. *J Immunol* **182**, 948-956 (2009).

149     Orange, J. S. *et al.* Wiskott-Aldrich syndrome protein is required for NK cell cytotoxicity and colocalizes with actin to NK cell-activating immunologic synapses. *Proc Natl Acad Sci U S A* **99**, 11351-11356, doi:10.1073/pnas.162376099 (2002).

150     Rak, G. D., Mace, E. M., Banerjee, P. P., Svitkina, T. & Orange, J. S. Natural killer cell lytic granule secretion occurs through a pervasive actin network at the immune synapse. *PLoS biology* **9**, e1001151, doi:10.1371/journal.pbio.1001151 (2011).

151     Vyas, Y. M. *et al.* Spatial organization of signal transduction molecules in the NK cell immune synapses during MHC class I-regulated noncytolytic and cytolytic interactions. *J Immunol* **167**, 4358-4367 (2001).

152     Riteau, B., Barber, D. F. & Long, E. O. Vav1 phosphorylation is induced by beta2 integrin engagement on natural killer cells upstream of actin cytoskeleton and lipid raft reorganization. *J Exp Med* **198**, 469-474, doi:10.1084/jem.20021995 (2003).

153     Burshtyn, D. N., Shin, J., Stebbins, C. & Long, E. O. Adhesion to target cells is disrupted by the killer cell inhibitory receptor. *Curr Biol* **10**, 777-780 (2000).

154 Coudert, J. D. *et al.* Altered NKG2D function in NK cells induced by chronic exposure to NKG2D ligand-expressing tumor cells. *Blood* **106**, 1711-1717, doi:10.1182/blood-2005-03-0918 (2005).

155 Hsu, H. T. & Orange, J. S. Distinct integrin-dependent signals define requirements for lytic granule convergence and polarization in natural killer cells. *Sci Signal* **7**, pe24, doi:10.1126/scisignal.2005816 (2014).

156 Carisey, A. F., Mace, E. M., Saeed, M. B., Davis, D. M. & Orange, J. S. Nanoscale Dynamism of Actin Enables Secretory Function in Cytolytic Cells. *Curr Biol*, doi:10.1016/j.cub.2017.12.044 (2018).

157 Banerjee, P. P. *et al.* Cdc42-interacting protein-4 functionally links actin and microtubule networks at the cytolytic NK cell immunological synapse. *J Exp Med* **204**, 2305-2320, doi:10.1084/jem.20061893 (2007).

158 Hsu, H. T., Carisey, A. F. & Orange, J. S. Measurement of Lytic Granule Convergence After Formation of an NK Cell Immunological Synapse. *Methods Mol Biol* **1584**, 497-515, doi:10.1007/978-1-4939-6881-7_31 (2017).

159 Tuli, A. *et al.* Arf-like GTPase Arl8b regulates lytic granule polarization and natural killer cell-mediated cytotoxicity. *Mol Biol Cell* **24**, 3721-3735, doi:10.1091/mbc.E13-05-0259 (2013).

160 Andzelm, M. M., Chen, X., Krzewski, K., Orange, J. S. & Strominger, J. L. Myosin IIA is required for cytolytic granule exocytosis in human NK cells. *J Exp Med* **204**, 2285-2291, doi:10.1084/jem.20071143 (2007).

161 Mace, E. M. *et al.* NK cell lytic granules are highly motile at the immunological synapse and require F-actin for post-degranulation persistence. *J Immunol* **189**, 4870-4880, doi:10.4049/jimmunol.1201296 (2012).

162 Liu, D., Martina, J. A., Wu, X. S., Hammer, J. A., 3rd & Long, E. O. Two modes of lytic granule fusion during degranulation by natural killer cells. *Immunol Cell Biol* **89**, 728-738, doi:10.1038/icb.2010.167 (2011).

163 Pardo, J. *et al.* The biology of cytotoxic cell granule exocytosis pathway: granzymes have evolved to induce cell death and inflammation. *Microbes Infect* **11**, 452-459, doi:10.1016/j.micinf.2009.02.004 (2009).

164 Balaji, K. N., Schaschke, N., Machleidt, W., Catalfamo, M. & Henkart, P. A. Surface cathepsin B protects cytotoxic lymphocytes from self-destruction after degranulation. *J Exp Med* **196**, 493-503 (2002).

165 Simhadri, V. R. *et al.* Human CD300a binds to phosphatidylethanolamine and phosphatidylserine, and modulates the phagocytosis of dead cells. *Blood* **119**, 2799-2809, doi:10.1182/blood-2011-08-372425 (2012).

166 Bhat, R. & Watzl, C. Serial killing of tumor cells by human natural killer cells-- enhancement by therapeutic antibodies. *PLoS One* **2**, e326, doi:10.1371/journal.pone.0000326 (2007).

167 Brady, J. *et al.* The interactions of multiple cytokines control NK cell maturation. *J Immunol* **185**, 6679-6688, doi:10.4049/jimmunol.0903354 (2010).

168 Huntington, N. D. *et al.* Interleukin 15-mediated survival of natural killer cells is determined by interactions among Bim, Noxa and Mcl-1. *Nat Immunol* **8**, 856-863, doi:10.1038/ni1487 (2007).

169 Dubois, S., Mariner, J., Waldmann, T. A. & Tagaya, Y. IL-15Ralpha recycles and presents IL-15 In trans to neighboring cells. *Immunity* **17**, 537-547 (2002).

170     Orange, J. S. *et al*. IL-2 induces a WAVE2-dependent pathway for actin reorganization that enables WASp-independent human NK cell function. *J Clin Invest* **121**, 1535-1548, doi:10.1172/JCI44862 (2011).

171     Voss, S. D., Sondel, P. M. & Robb, R. J. Characterization of the interleukin 2 receptors (IL-2R) expressed on human natural killer cells activated in vivo by IL-2: association of the p64 IL-2R gamma chain with the IL-2R beta chain in functional intermediate-affinity IL-2R. *J Exp Med* **176**, 531-541 (1992).

172     Mavropoulos, A., Sully, G., Cope, A. P. & Clark, A. R. Stabilization of IFN-gamma mRNA by MAPK p38 in IL-12- and IL-18-stimulated human NK cells. *Blood* **105**, 282-288, doi:10.1182/blood-2004-07-2782 (2005).

173     Chaix, J. *et al*. Cutting edge: Priming of NK cells by IL-18. *J Immunol* **181**, 1627-1631 (2008).

174     Brady, J., Hayakawa, Y., Smyth, M. J. & Nutt, S. L. IL-21 induces the functional maturation of murine NK cells. *J Immunol* **172**, 2048-2058 (2004).

175     Zwirner, N. W. & Domaica, C. I. Cytokine regulation of natural killer cell effector functions. *Biofactors* **36**, 274-288, doi:10.1002/biof.107 (2010).

176     Wu, L. & Van Kaer, L. Natural killer T cells in health and disease. *Front Biosci (Schol Ed)* **3**, 236-251 (2011).

177     Ferlazzo, G. & Morandi, B. Cross-Talks between Natural Killer Cells and Distinct Subsets of Dendritic Cells. *Front Immunol* **5**, 159, doi:10.3389/fimmu.2014.00159 (2014).

178     Wehner, R., Dietze, K., Bachmann, M. & Schmitz, M. The bidirectional crosstalk between human dendritic cells and natural killer cells. *J Innate Immun* **3**, 258-263, doi:10.1159/000323923 (2011).

179     Vitale, M. *et al*. NK-dependent DC maturation is mediated by TNFalpha and IFNgamma released upon engagement of the NKp30 triggering receptor. *Blood* **106**, 566-571, doi:10.1182/blood-2004-10-4035 (2005).

180     Pallmer, K. & Oxenius, A. Recognition and Regulation of T Cells by NK Cells. *Front Immunol* **7**, 251, doi:10.3389/fimmu.2016.00251 (2016).

181     Martin-Fontecha, A. *et al*. Induced recruitment of NK cells to lymph nodes provides IFN-gamma for T(H)1 priming. *Nat Immunol* **5**, 1260-1265, doi:10.1038/ni1138 (2004).

182     Ralainirina, N. *et al*. Control of NK cell functions by CD4+CD25+ regulatory T cells. *J Leukoc Biol* **81**, 144-153, doi:10.1189/jlb.0606409 (2007).

183     Palucka, K. & Banchereau, J. Cancer immunotherapy via dendritic cells. *Nat Rev Cancer* **12**, 265-277, doi:10.1038/nrc3258 (2012).

184     Farkona, S., Diamandis, E. P. & Blasutig, I. M. Cancer immunotherapy: the beginning of the end of cancer? *BMC Med* **14**, 73, doi:10.1186/s12916-016-0623-5 (2016).

185     Sharma, P., Wagner, K., Wolchok, J. D. & Allison, J. P. Novel cancer immunotherapy agents with survival benefit: recent successes and next steps. *Nat Rev Cancer* **11**, 805-812, doi:10.1038/nrc3153 (2011).

186     Mullard, A. New cancer vaccines show clinical promise. *Nat Rev Drug Discov* **16**, 519, doi:10.1038/nrd.2017.150 (2017).

187     Banchereau, J. & Palucka, K. Immunotherapy: Cancer vaccines on the move. *Nat Rev Clin Oncol* **15**, 9-10, doi:10.1038/nrclinonc.2017.149 (2018).

188     Hammerstrom, A. E., Cauley, D. H., Atkinson, B. J. & Sharma, P. Cancer immunotherapy: sipuleucel-T and beyond. *Pharmacotherapy* **31**, 813-828, doi:10.1592/phco.31.8.813 (2011).

189     Sabado, R. L. & Bhardwaj, N. Cancer immunotherapy: dendritic-cell vaccines on the move. *Nature* **519**, 300-301, doi:10.1038/nature14211 (2015).

190     Kaufman, H. L., Kohlhapp, F. J. & Zloza, A. Oncolytic viruses: a new class of immunotherapy drugs. *Nat Rev Drug Discov* **14**, 642-662, doi:10.1038/nrd4663 (2015).

191     Lichty, B. D., Breitbach, C. J., Stojdl, D. F. & Bell, J. C. Going viral with cancer immunotherapy. *Nat Rev Cancer* **14**, 559-567, doi:10.1038/nrc3770 (2014).

192     Liu, B. L. *et al.* ICP34.5 deleted herpes simplex virus with enhanced oncolytic, immune stimulating, and anti-tumour properties. *Gene Ther* **10**, 292-303, doi:10.1038/sj.gt.3301885 (2003).

193     Hinrichs, C. S. & Rosenberg, S. A. Exploiting the curative potential of adoptive T-cell therapy for cancer. *Immunol Rev* **257**, 56-71, doi:10.1111/imr.12132 (2014).

194     Rosenberg, S. A. *et al.* Durable complete responses in heavily pretreated patients with metastatic melanoma using T-cell transfer immunotherapy. *Clin Cancer Res* **17**, 4550-4557, doi:10.1158/1078-0432.CCR-11-0116 (2011).

195     Morgan, R. A., Dudley, M. E. & Rosenberg, S. A. Adoptive cell therapy: genetic modification to redirect effector cell specificity. *Cancer J* **16**, 336-341, doi:10.1097/PPO.0b013e3181eb3879 (2010).

196     Pagel, J. M. & West, H. J. Chimeric Antigen Receptor (CAR) T-Cell Therapy. *JAMA Oncol* **3**, 1595, doi:10.1001/jamaoncol.2017.2989 (2017).

197     Walseng, E. *et al.* A TCR-based Chimeric Antigen Receptor. *Sci Rep* **7**, 10713, doi:10.1038/s41598-017-11126-y (2017).

198     Orlowski, R. J., Porter, D. L. & Frey, N. V. The promise of chimeric antigen receptor T cells (CARTs) in leukaemia. *Br J Haematol* **177**, 13-26, doi:10.1111/bjh.14475 (2017).

199     Pardoll, D. M. The blockade of immune checkpoints in cancer immunotherapy. *Nat Rev Cancer* **12**, 252-264, doi:10.1038/nrc3239 (2012).

200     Kondo, Y. *et al.* Differential contribution of three immune checkpoint (VISTA, CTLA-4, PD-1) pathways to antitumor responses against squamous cell carcinoma. *Oral Oncol* **57**, 54-60, doi:10.1016/j.oraloncology.2016.04.005 (2016).

201     Sharma, P. & Allison, J. P. Immune checkpoint targeting in cancer therapy: toward combination strategies with curative potential. *Cell* **161**, 205-214, doi:10.1016/j.cell.2015.03.030 (2015).

202     Buchbinder, E. I. & Desai, A. CTLA-4 and PD-1 Pathways: Similarities, Differences, and Implications of Their Inhibition. *Am J Clin Oncol* **39**, 98-106, doi:10.1097/COC.0000000000000239 (2016).

203     Hodi, F. S. *et al.* Improved survival with ipilimumab in patients with metastatic melanoma. *N Engl J Med* **363**, 711-723, doi:10.1056/NEJMoa1003466 (2010).

204     Ishida, Y., Agata, Y., Shibahara, K. & Honjo, T. Induced expression of PD-1, a novel member of the immunoglobulin gene superfamily, upon programmed cell death. *EMBO J* **11**, 3887-3895 (1992).

205     Okazaki, T., Chikuma, S., Iwai, Y., Fagarasan, S. & Honjo, T. A rheostat for immune responses: the unique properties of PD-1 and their advantages for clinical application. *Nat Immunol* **14**, 1212-1218, doi:10.1038/ni.2762 (2013).

206    Le Mercier, I. *et al.* VISTA Regulates the Development of Protective Antitumor Immunity. *Cancer Res* **74**, 1933-1944, doi:10.1158/0008-5472.CAN-13-1506 (2014).

207    Li, N. *et al.* Immune-checkpoint protein VISTA critically regulates the IL-23/IL-17 inflammatory axis. *Sci Rep* **7**, 1485, doi:10.1038/s41598-017-01411-1 (2017).

208    Wang, L. *et al.* VISTA, a novel mouse Ig superfamily ligand that negatively regulates T cell responses. *J Exp Med* **208**, 577-592, doi:10.1084/jem.20100619 (2011).

209    Triebel, F. *et al.* LAG-3, a novel lymphocyte activation gene closely related to CD4. *J Exp Med* **171**, 1393-1405 (1990).

210    Sakuishi, K. *et al.* Targeting Tim-3 and PD-1 pathways to reverse T cell exhaustion and restore anti-tumor immunity. *J Exp Med* **207**, 2187-2194, doi:10.1084/jem.20100643 (2010).

211    Chiossone, L., Vienne, M., Kerdiles, Y. M. & Vivier, E. Natural killer cell immunotherapies against cancer: checkpoint inhibitors and more. *Semin Immunol* **31**, 55-63, doi:10.1016/j.smim.2017.08.003 (2017).

212    Moretta, L. *et al.* Human NK cells: from surface receptors to the therapy of leukemias and solid tumors. *Front Immunol* **5**, 87, doi:10.3389/fimmu.2014.00087 (2014).

213    Granzin, M. *et al.* Shaping of Natural Killer Cell Antitumor Activity by Ex Vivo Cultivation. *Front Immunol* **8**, 458, doi:10.3389/fimmu.2017.00458 (2017).

214    Tonn, T. *et al.* Treatment of patients with advanced cancer with the natural killer cell line NK-92. *Cytotherapy* **15**, 1563-1570, doi:10.1016/j.jcyt.2013.06.017 (2013).

215    Guillerey, C., Huntington, N. D. & Smyth, M. J. Targeting natural killer cells in cancer immunotherapy. *Nat Immunol* **17**, 1025-1036, doi:10.1038/ni.3518 (2016).

216    Dall'Ozzo, S. *et al.* Rituximab-dependent cytotoxicity by natural killer cells: influence of FCGR3A polymorphism on the concentration-effect relationship. *Cancer Res* **64**, 4664-4669, doi:10.1158/0008-5472.CAN-03-2862 (2004).

217    Kawaguchi, Y. *et al.* Cetuximab induce antibody-dependent cellular cytotoxicity against EGFR-expressing esophageal squamous cell carcinoma. *Int J Cancer* **120**, 781-787, doi:10.1002/ijc.22370 (2007).

218    Seo, Y. *et al.* Cetuximab-mediated ADCC activity is correlated with the cell surface expression level of EGFR but not with the KRAS/BRAF mutational status in colorectal cancer. *Oncol Rep* **31**, 2115-2122, doi:10.3892/or.2014.3077 (2014).

219    Ito, A. *et al.* Defucosylated anti-CCR4 monoclonal antibody exercises potent ADCC-mediated antitumor effect in the novel tumor-bearing humanized NOD/Shi-scid, IL-2Rgamma(null) mouse model. *Cancer Immunol Immunother* **58**, 1195-1206, doi:10.1007/s00262-008-0632-0 (2009).

220    Ishii, T. *et al.* Defucosylated humanized anti-CCR4 monoclonal antibody KW-0761 as a novel immunotherapeutic agent for adult T-cell leukemia/lymphoma. *Clin Cancer Res* **16**, 1520-1531, doi:10.1158/1078-0432.CCR-09-2697 (2010).

221    Knorr, D. A., Bachanova, V., Verneris, M. R. & Miller, J. S. Clinical utility of natural killer cells in cancer therapy and transplantation. *Semin Immunol* **26**, 161-172, doi:10.1016/j.smim.2014.02.002 (2014).

222    Cifaldi, L., Locatelli, F., Marasco, E., Moretta, L. & Pistoia, V. Boosting Natural Killer Cell-Based Immunotherapy with Anticancer Drugs: a Perspective. *Trends Mol Med* **23**, 1156-1175, doi:10.1016/j.molmed.2017.10.002 (2017).

223    Davies, F. E. *et al.* Thalidomide and immunomodulatory derivatives augment natural killer cell cytotoxicity in multiple myeloma. *Blood* **98**, 210-216 (2001).

224    Krieg, S. & Ullrich, E. Novel immune modulators used in hematology: impact on NK cells. *Front Immunol* **3**, 388, doi:10.3389/fimmu.2012.00388 (2012).

225    Siegel, R. L., Miller, K. D. & Jemal, A. Cancer Statistics, 2017. *CA Cancer J Clin* **67**, 7-30, doi:10.3322/caac.21387 (2017).

226    DeSantis, C., Ma, J., Bryan, L. & Jemal, A. Breast cancer statistics, 2013. *CA Cancer J Clin* **64**, 52-62, doi:10.3322/caac.21203 (2014).

227    Shah, R., Rosso, K. & Nathanson, S. D. Pathogenesis, prevention, diagnosis and treatment of breast cancer. *World J Clin Oncol* **5**, 283-298, doi:10.5306/wjco.v5.i3.283 (2014).

228    Lanfranchi, A. Normal breast physiology: the reasons hormonal contraceptives and induced abortion increase breast-cancer risk. *Issues Law Med* **29**, 135-146 (2014).

229    Abdulkareem, I. H. & Zurmi, I. B. Review of hormonal treatment of breast cancer. *Niger J Clin Pract* **15**, 9-14, doi:10.4103/1119-3077.94088 (2012).

230    Yip, C. H. & Rhodes, A. Estrogen and progesterone receptors in breast cancer. *Future Oncol* **10**, 2293-2301, doi:10.2217/fon.14.110 (2014).

231    Anders, C. K. & Carey, L. A. Biology, metastatic patterns, and treatment of patients with triple-negative breast cancer. *Clin Breast Cancer* **9 Suppl 2**, S73-81, doi:10.3816/CBC.2009.s.008 (2009).

232    Katz, H. & Alsharedi, M. Immunotherapy in triple-negative breast cancer. *Med Oncol* **35**, 13, doi:10.1007/s12032-017-1071-6 (2017).

233    Howard, J. H. & Bland, K. I. Current management and treatment strategies for breast cancer. *Curr Opin Obstet Gynecol* **24**, 44-48, doi:10.1097/GCO.0b013e32834da4b1 (2012).

234    Ye, J. C. & Formenti, S. C. Integration of radiation and immunotherapy in breast cancer - Treatment implications. *Breast* **38**, 66-74, doi:10.1016/j.breast.2017.12.005 (2017).

235    Bellavance, E. C. & Kesmodel, S. B. Decision-Making in the Surgical Treatment of Breast Cancer: Factors Influencing Women's Choices for Mastectomy and Breast Conserving Surgery. *Front Oncol* **6**, 74, doi:10.3389/fonc.2016.00074 (2016).

236    Rossi, S. *et al.* Maintenance hormonal and chemotherapy treatment in metastatic breast cancer: a systematic review. *Future Oncol* **12**, 1299-1307, doi:10.2217/fon-2015-0065 (2016).

237    Solinas, C. *et al.* Targeting immune checkpoints in breast cancer: an update of early results. *ESMO Open* **2**, e000255, doi:10.1136/esmoopen-2017-000255 (2017).

238    Alsuliman, A. *et al.* Bidirectional crosstalk between PD-L1 expression and epithelial to mesenchymal transition: significance in claudin-low breast cancer cells. *Mol Cancer* **14**, 149, doi:10.1186/s12943-015-0421-2 (2015).

239    Tolba, M. F. & Omar, H. A. Immunotherapy, an evolving approach for the management of triple negative breast cancer: Converting non-responders to

responders. *Crit Rev Oncol Hematol* **122**, 202-207, doi:10.1016/j.critrevonc.2018.01.005 (2018).

240    Richards, J. O., Albers, A. J., Smith, T. S. & Tjoe, J. A. Erratum to: NK cell-mediated antibody-dependent cellular cytotoxicity is enhanced by tamoxifen in HER2/neu non-amplified, but not HER2/neu-amplified, breast cancer cells. *Cancer Immunol Immunother* **65**, 1337, doi:10.1007/s00262-016-1903-9 (2016).

241    Diessner, J. *et al.* Targeting breast cancer stem cells with HER2-specific antibodies and natural killer cells. *Am J Cancer Res* **3**, 211-220 (2013).

242    Wang, M. *et al.* Mechanism of immune evasion in breast cancer. *Onco Targets Ther* **10**, 1561-1573, doi:10.2147/OTT.S126424 (2017).

243    Mittal, D., Gubin, M. M., Schreiber, R. D. & Smyth, M. J. New insights into cancer immunoediting and its three component phases--elimination, equilibrium and escape. *Curr Opin Immunol* **27**, 16-25, doi:10.1016/j.coi.2014.01.004 (2014).

244    Hou, S. Y. *et al.* Expressions of MAGE-A9 and MAGE-A11 in breast cancer and their expression mechanism. *Arch Med Res* **45**, 44-51, doi:10.1016/j.arcmed.2013.10.005 (2014).

245    Xu, X. *et al.* Overexpression of MAGE-A9 predicts unfavorable outcome in breast cancer. *Exp Mol Pathol* **97**, 579-584, doi:10.1016/j.yexmp.2014.11.001 (2014).

246    Baric, M. *et al.* Circulating Her-2/neu extracellular domain in breast cancer patients-correlation with prognosis and clinicopathological parameters including steroid receptor, Her-2/neu receptor coexpression. *Pathol Oncol Res* **21**, 589-595, doi:10.1007/s12253-014-9859-6 (2015).

247    Bubenik, J. MHC class I down regulation, tumour escape from immune surveillance and design of therapeutic strategies. *Folia Biol (Praha)* **51**, 1-2 (2005).

248    Bebenek, M., Dus, D. & Kozlak, J. Prognostic value of the Fas/Fas ligand system in breast cancer. *Contemp Oncol (Pozn)* **17**, 120-122, doi:10.5114/wo.2013.34612 (2013).

249    Fulda, S., Meyer, E. & Debatin, K. M. Inhibition of TRAIL-induced apoptosis by Bcl-2 overexpression. *Oncogene* **21**, 2283-2294, doi:10.1038/sj.onc.1205258 (2002).

250    Marsicano, S. R. *et al.* Survinin expression in patients with breast cancer during chemotherapy. *Tumour Biol* **36**, 3441-3445, doi:10.1007/s13277-014-2979-5 (2015).

251    Li, C. W. *et al.* Glycosylation and stabilization of programmed death ligand-1 suppresses T-cell activity. *Nat Commun* **7**, 12632, doi:10.1038/ncomms12632 (2016).

252    Li, Z. *et al.* PD-L1 Expression Is Associated with Tumor FOXP3(+) Regulatory T-Cell Infiltration of Breast Cancer and Poor Prognosis of Patient. *J Cancer* **7**, 784-793, doi:10.7150/jca.14549 (2016).

253    Beatty, G. L. & Gladney, W. L. Immune escape mechanisms as a guide for cancer immunotherapy. *Clin Cancer Res* **21**, 687-692, doi:10.1158/1078-0432.CCR-14-1860 (2015).

254    Vinay, D. S. *et al.* Immune evasion in cancer: Mechanistic basis and therapeutic strategies. *Semin Cancer Biol* **35 Suppl**, S185-S198, doi:10.1016/j.semcancer.2015.03.004 (2015).

255    Freier, C. P. *et al.* FOXP3+ Cells Recruited by CCL22 into Breast Cancer Correlates with Less Tumor Nodal Infiltration. *Anticancer Res* **36**, 3139-3145 (2016).

256    Hossain, D. M. *et al.* MEK inhibition prevents tumour-shed transforming growth factor-beta-induced T-regulatory cell augmentation in tumour milieu. *Immunology* **144**, 561-573, doi:10.1111/imm.12397 (2015).

257    Deng, W. *et al.* Antitumor immunity. A shed NKG2D ligand that promotes natural killer cell activation and tumor rejection. *Science* **348**, 136-139, doi:10.1126/science.1258867 (2015).

258    Vitale, M., Cantoni, C., Pietra, G., Mingari, M. C. & Moretta, L. Effect of tumor cells and tumor microenvironment on NK-cell function. *Eur J Immunol* **44**, 1582-1592, doi:10.1002/eji.201344272 (2014).

259    Thiery, J. P. Epithelial-mesenchymal transitions in tumour progression. *Nat Rev Cancer* **2**, 442-454, doi:10.1038/nrc822 (2002).

260    Nieto, M. A., Huang, R. Y., Jackson, R. A. & Thiery, J. P. Emt: 2016. *Cell* **166**, 21-45, doi:10.1016/j.cell.2016.06.028 (2016).

261    Huang, K. X., Iwakami, N., Fujii, I., Ebizuka, Y. & Sankawa, U. Transformations of Penicillium islandicum and Penicillium frequentans that produce anthraquinone-related compounds. *Curr Genet* **28**, 580-584 (1995).

262    Lamouille, S., Xu, J. & Derynck, R. Molecular mechanisms of epithelial-mesenchymal transition. *Nat Rev Mol Cell Biol* **15**, 178-196, doi:10.1038/nrm3758 (2014).

263    Lim, J. & Thiery, J. P. Epithelial-mesenchymal transitions: insights from development. *Development* **139**, 3471-3486, doi:10.1242/dev.071209 (2012).

264    Liu, F., Gu, L. N., Shan, B. E., Geng, C. Z. & Sang, M. X. Biomarkers for EMT and MET in breast cancer: An update. *Oncol Lett* **12**, 4869-4876, doi:10.3892/ol.2016.5369 (2016).

265    Heimann, R., Lan, F., McBride, R. & Hellman, S. Separating favorable from unfavorable prognostic markers in breast cancer: the role of E-cadherin. *Cancer Res* **60**, 298-304 (2000).

266    Creighton, C. J., Chang, J. C. & Rosen, J. M. Epithelial-mesenchymal transition (EMT) in tumor-initiating cells and its clinical implications in breast cancer. *J Mammary Gland Biol Neoplasia* **15**, 253-260, doi:10.1007/s10911-010-9173-1 (2010).

267    Vleminckx, K., Vakaet, L., Jr., Mareel, M., Fiers, W. & van Roy, F. Genetic manipulation of E-cadherin expression by epithelial tumor cells reveals an invasion suppressor role. *Cell* **66**, 107-119 (1991).

268    Mendez, M. G., Kojima, S. & Goldman, R. D. Vimentin induces changes in cell shape, motility, and adhesion during the epithelial to mesenchymal transition. *FASEB J* **24**, 1838-1851, doi:10.1096/fj.09-151639 (2010).

269    van Meeteren, L. A. & ten Dijke, P. Regulation of endothelial cell plasticity by TGF-beta. *Cell Tissue Res* **347**, 177-186, doi:10.1007/s00441-011-1222-6 (2012).

270    Choi, Y. *et al.* Epithelial-mesenchymal transition increases during the progression of in situ to invasive basal-like breast cancer. *Hum Pathol* **44**, 2581-2589, doi:10.1016/j.humpath.2013.07.003 (2013).

271    Sarrio, D. *et al.* Epithelial-mesenchymal transition in breast cancer relates to the basal-like phenotype. *Cancer Res* **68**, 989-997, doi:10.1158/0008-5472.CAN-07-2017 (2008).

272 Tan, T. Z. *et al.* Epithelial-mesenchymal transition spectrum quantification and its efficacy in deciphering survival and drug responses of cancer patients. *EMBO Mol Med* **6**, 1279-1293, doi:10.15252/emmm.201404208 (2014).

273 Shankar, J. & Nabi, I. R. Actin Cytoskeleton Regulation of Epithelial Mesenchymal Transition in Metastatic Cancer Cells. *PLoS One* **10**, e0119954, doi:10.1371/journal.pone.0119954 (2015).

274 Thiery, J. P. & Sleeman, J. P. Complex networks orchestrate epithelial-mesenchymal transitions. *Nat Rev Mol Cell Biol* **7**, 131-142, doi:10.1038/nrm1835 (2006).

275 Hansen, S. M., Berezin, V. & Bock, E. Signaling mechanisms of neurite outgrowth induced by the cell adhesion molecules NCAM and N-cadherin. *Cell Mol Life Sci* **65**, 3809-3821, doi:10.1007/s00018-008-8290-0 (2008).

276 Cieply, B. *et al.* Suppression of the epithelial-mesenchymal transition by Grainyhead-like-2. *Cancer Res* **72**, 2440-2453, doi:10.1158/0008-5472.CAN-11-4038 (2012).

277 Wu, Z. Q. *et al.* Canonical Wnt signaling regulates Slug activity and links epithelial-mesenchymal transition with epigenetic Breast Cancer 1, Early Onset (BRCA1) repression. *Proc Natl Acad Sci U S A* **109**, 16654-16659, doi:10.1073/pnas.1205822109 (2012).

278 Ye, L. Y. *et al.* Hypoxia-Induced Epithelial-to-Mesenchymal Transition in Hepatocellular Carcinoma Induces an Immunosuppressive Tumor Microenvironment to Promote Metastasis. *Cancer Res* **76**, 818-830, doi:10.1158/0008-5472.CAN-15-0977 (2016).

279 Teng, Y. & Li, X. The roles of HLH transcription factors in epithelial mesenchymal transition and multiple molecular mechanisms. *Clin Exp Metastasis* **31**, 367-377, doi:10.1007/s10585-013-9621-6 (2014).

280 Cieply, B., Farris, J., Denvir, J., Ford, H. L. & Frisch, S. M. Epithelial-mesenchymal transition and tumor suppression are controlled by a reciprocal feedback loop between ZEB1 and Grainyhead-like-2. *Cancer Res* **73**, 6299-6309, doi:10.1158/0008-5472.CAN-12-4082 (2013).

281 Zhang, J. & Ma, L. MicroRNA control of epithelial-mesenchymal transition and metastasis. *Cancer Metastasis Rev* **31**, 653-662, doi:10.1007/s10555-012-9368-6 (2012).

282 Chung, V. Y. *et al.* GRHL2-miR-200-ZEB1 maintains the epithelial status of ovarian cancer through transcriptional regulation and histone modification. *Sci Rep* **6**, 19943, doi:10.1038/srep19943 (2016).

283 Wang, Y., Shi, J., Chai, K., Ying, X. & Zhou, B. P. The Role of Snail in EMT and Tumorigenesis. *Curr Cancer Drug Targets* **13**, 963-972 (2013).

284 Xue, J. *et al.* Sustained activation of SMAD3/SMAD4 by FOXM1 promotes TGF-beta-dependent cancer metastasis. *J Clin Invest* **124**, 564-579, doi:10.1172/JCI71104 (2014).

285 Janji, B. *et al.* The actin filament cross-linker L-plastin confers resistance to TNF-alpha in MCF-7 breast cancer cells in a phosphorylation-dependent manner. *J Cell Mol Med* **14**, 1264-1275, doi:10.1111/j.1582-4934.2009.00918.x (2010).

286 Akalay, I. *et al.* EMT impairs breast carcinoma cell susceptibility to CTL-mediated lysis through autophagy induction. *Autophagy* **9**, 1104-1106, doi:10.4161/auto.24728 (2013).

287    Akalay, I. *et al.* Epithelial-to-mesenchymal transition and autophagy induction in breast carcinoma promote escape from T-cell-mediated lysis. *Cancer Res* **73**, 2418-2427, doi:10.1158/0008-5472.CAN-12-2432 (2013).

288    Baginska, J. *et al.* Granzyme B degradation by autophagy decreases tumor cell susceptibility to natural killer-mediated lysis under hypoxia. *Proc Natl Acad Sci U S A* **110**, 17450-17455, doi:10.1073/pnas.1304790110 (2013).

289    Akalay, I. *et al.* Targeting WNT1-inducible signaling pathway protein 2 alters human breast cancer cell susceptibility to specific lysis through regulation of KLF-4 and miR-7 expression. *Oncogene* **34**, 2261-2271, doi:10.1038/onc.2014.151 (2015).

290    Terry, S. *et al.* Acquisition of tumor cell phenotypic diversity along the EMT spectrum under hypoxic pressure: Consequences on susceptibility to cell-mediated cytotoxicity. *Oncoimmunology* **6**, e1271858, doi:10.1080/2162402X.2016.1271858 (2017).

291    Le Floc'h, A. *et al.* Alpha E beta 7 integrin interaction with E-cadherin promotes antitumor CTL activity by triggering lytic granule polarization and exocytosis. *J Exp Med* **204**, 559-570, doi:10.1084/jem.20061524 (2007).

292    Lopez-Soto, A. *et al.* Epithelial-mesenchymal transition induces an antitumor immune response mediated by NKG2D receptor. *J Immunol* **190**, 4408-4419, doi:10.4049/jimmunol.1202950 (2013).

293    Puhr, M. *et al.* Epithelial-to-mesenchymal transition leads to docetaxel resistance in prostate cancer and is mediated by reduced expression of miR-200c and miR-205. *Am J Pathol* **181**, 2188-2201, doi:10.1016/j.ajpath.2012.08.011 (2012).

294    Dave, B., Mittal, V., Tan, N. M. & Chang, J. C. Epithelial-mesenchymal transition, cancer stem cells and treatment resistance. *Breast Cancer Res* **14**, 202, doi:10.1186/bcr2938 (2012).

295    Zheng, X. *et al.* Epithelial-to-mesenchymal transition is dispensable for metastasis but induces chemoresistance in pancreatic cancer. *Nature* **527**, 525-530, doi:10.1038/nature16064 (2015).

296    Saxena, M., Stephens, M. A., Pathak, H. & Rangarajan, A. Transcription factors that mediate epithelial-mesenchymal transition lead to multidrug resistance by upregulating ABC transporters. *Cell Death Dis* **2**, e179, doi:10.1038/cddis.2011.61 (2011).

297    Takai, S., Schlom, J., Tucker, J., Tsang, K. Y. & Greiner, J. W. Inhibition of TGF-beta1 signaling promotes central memory T cell differentiation. *J Immunol* **191**, 2299-2307, doi:10.4049/jimmunol.1300472 (2013).

298    Chen, L. *et al.* Metastasis is regulated via microRNA-200/ZEB1 axis control of tumour cell PD-L1 expression and intratumoral immunosuppression. *Nat Commun* **5**, 5241, doi:10.1038/ncomms6241 (2014).

299    Noman, M. Z. *et al.* The immune checkpoint ligand PD-L1 is upregulated in EMT-activated human breast cancer cells by a mechanism involving ZEB-1 and miR-200. *Oncoimmunology* **6**, e1263412, doi:10.1080/2162402X.2016.1263412 (2017).

300    Terry, S. *et al.* New insights into the role of EMT in tumor immune escape. *Mol Oncol* **11**, 824-846, doi:10.1002/1878-0261.12093 (2017).

301    Byers, L. A. *et al.* An epithelial-mesenchymal transition gene signature predicts resistance to EGFR and PI3K inhibitors and identifies Axl as a therapeutic target

for overcoming EGFR inhibitor resistance. *Clin Cancer Res* **19**, 279-290, doi:10.1158/1078-0432.CCR-12-1558 (2013).

302     Mizushima, N. Autophagy: process and function. *Genes Dev* **21**, 2861-2873, doi:10.1101/gad.1599207 (2007).

303     Levy, J. M. M., Towers, C. G. & Thorburn, A. Targeting autophagy in cancer. *Nat Rev Cancer* **17**, 528-542, doi:10.1038/nrc.2017.53 (2017).

304     Boya, P., Reggiori, F. & Codogno, P. Emerging regulation and functions of autophagy. *Nat Cell Biol* **15**, 713-720, doi:10.1038/ncb2788 (2013).

305     Ezaki, J. *et al.* Liver autophagy contributes to the maintenance of blood glucose and amino acid levels. *Autophagy* **7**, 727-736 (2011).

306     Chen, Y. & Klionsky, D. J. The regulation of autophagy - unanswered questions. *J Cell Sci* **124**, 161-170, doi:10.1242/jcs.064576 (2011).

307     Matsui, Y. *et al.* Molecular mechanisms and physiological significance of autophagy during myocardial ischemia and reperfusion. *Autophagy* **4**, 409-415 (2008).

308     White, E., Karp, C., Strohecker, A. M., Guo, Y. & Mathew, R. Role of autophagy in suppression of inflammation and cancer. *Curr Opin Cell Biol* **22**, 212-217, doi:10.1016/j.ceb.2009.12.008 (2010).

309     Matsuzawa-Ishimoto, Y., Hwang, S. & Cadwell, K. Autophagy and Inflammation. *Annu Rev Immunol*, doi:10.1146/annurev-immunol-042617-053253 (2017).

310     Schmid, D., Pypaert, M. & Munz, C. Antigen-loading compartments for major histocompatibility complex class II molecules continuously receive input from autophagosomes. *Immunity* **26**, 79-92, doi:10.1016/j.immuni.2006.10.018 (2007).

311     Laddha, S. V., Ganesan, S., Chan, C. S. & White, E. Mutational landscape of the essential autophagy gene BECN1 in human cancers. *Mol Cancer Res* **12**, 485-490, doi:10.1158/1541-7786.MCR-13-0614 (2014).

312     Wang, C., Wang, Y., McNutt, M. A. & Zhu, W. G. Autophagy process is associated with anti-neoplastic function. *Acta Biochim Biophys Sin (Shanghai)* **43**, 425-432, doi:10.1093/abbs/gmr028 (2011).

313     Hamurcu, Z. *et al.* Targeting LC3 and Beclin-1 autophagy genes suppresses proliferation, survival, migration and invasion by inhibition of Cyclin-D1 and uPAR/Integrin beta1/ Src signaling in triple negative breast cancer cells. *J Cancer Res Clin Oncol* **144**, 415-430, doi:10.1007/s00432-017-2557-5 (2018).

314     Rubinsztein, D. C., Shpilka, T. & Elazar, Z. Mechanisms of autophagosome biogenesis. *Curr Biol* **22**, R29-34, doi:10.1016/j.cub.2011.11.034 (2012).

315     Tanida, I., Ueno, T. & Kominami, E. LC3 and Autophagy. *Methods Mol Biol* **445**, 77-88, doi:10.1007/978-1-59745-157-4_4 (2008).

316     Pugsley, H. R. Quantifying autophagy: Measuring LC3 puncta and autolysosome formation in cells using multispectral imaging flow cytometry. *Methods* **112**, 147-156, doi:10.1016/j.ymeth.2016.05.022 (2017).

317     Kast, D. J. & Dominguez, R. The Cytoskeleton-Autophagy Connection. *Curr Biol* **27**, R318-R326, doi:10.1016/j.cub.2017.02.061 (2017).

318     Aplin, A., Jasionowski, T., Tuttle, D. L., Lenk, S. E. & Dunn, W. A., Jr. Cytoskeletal elements are required for the formation and maturation of autophagic vacuoles. *J Cell Physiol* **152**, 458-466, doi:10.1002/jcp.1041520304 (1992).

319  Zhuo, C. *et al.* Proteomics analysis of autophagy-deficient Atg7-/- MEFs reveals a close relationship between F-actin and autophagy. *Biochem Biophys Res Commun* **437**, 482-488, doi:10.1016/j.bbrc.2013.06.111 (2013).

320  Moreau, K. *et al.* Transcriptional regulation of Annexin A2 promotes starvation-induced autophagy. *Nat Commun* **6**, 8045, doi:10.1038/ncomms9045 (2015).

321  Kast, D. J., Zajac, A. L., Holzbaur, E. L., Ostap, E. M. & Dominguez, R. WHAMM Directs the Arp2/3 Complex to the ER for Autophagosome Biogenesis through an Actin Comet Tail Mechanism. *Curr Biol* **25**, 1791-1797, doi:10.1016/j.cub.2015.05.042 (2015).

322  Mi, N. *et al.* CapZ regulates autophagosomal membrane shaping by promoting actin assembly inside the isolation membrane. *Nat Cell Biol* **17**, 1112-1123, doi:10.1038/ncb3215 (2015).

323  Lee, J. Y. *et al.* HDAC6 controls autophagosome maturation essential for ubiquitin-selective quality-control autophagy. *EMBO J* **29**, 969-980, doi:10.1038/emboj.2009.405 (2010).

324  Xia, P. *et al.* WASH inhibits autophagy through suppression of Beclin 1 ubiquitination. *EMBO J* **32**, 2685-2696, doi:10.1038/emboj.2013.189 (2013).

325  Aguilera, M. O., Beron, W. & Colombo, M. I. The actin cytoskeleton participates in the early events of autophagosome formation upon starvation induced autophagy. *Autophagy* **8**, 1590-1603, doi:10.4161/auto.21459 (2012).

326  Maycotte, P. *et al.* STAT3-mediated autophagy dependence identifies subtypes of breast cancer where autophagy inhibition can be efficacious. *Cancer Res* **74**, 2579-2590, doi:10.1158/0008-5472.CAN-13-3470 (2014).

327  Starobinets, H. *et al.* Antitumor adaptive immunity remains intact following inhibition of autophagy and antimalarial treatment. *J Clin Invest* **126**, 4417-4429, doi:10.1172/JCI85705 (2016).

328  Pietrocola, F. *et al.* Caloric Restriction Mimetics Enhance Anticancer Immunosurveillance. *Cancer Cell* **30**, 147-160, doi:10.1016/j.ccell.2016.05.016 (2016).

329  Liang, X. *et al.* Inhibiting systemic autophagy during interleukin 2 immunotherapy promotes long-term tumor regression. *Cancer Res* **72**, 2791-2801, doi:10.1158/0008-5472.CAN-12-0320 (2012).

330  Levy, J. M. *et al.* Autophagy inhibition improves chemosensitivity in BRAF(V600E) brain tumors. *Cancer Discov* **4**, 773-780, doi:10.1158/2159-8290.CD-14-0049 (2014).

331  Noman, M. Z. *et al.* Blocking hypoxia-induced autophagy in tumors restores cytotoxic T-cell activity and promotes regression. *Cancer Res* **71**, 5976-5986, doi:10.1158/0008-5472.CAN-11-1094 (2011).

332  Mgrditchian, T. *et al.* Targeting autophagy inhibits melanoma growth by enhancing NK cells infiltration in a CCL5-dependent manner. *Proc Natl Acad Sci U S A* **114**, E9271-E9279, doi:10.1073/pnas.1703921114 (2017).

333  Lazarides, E. & Weber, K. Actin antibody: the specific visualization of actin filaments in non-muscle cells. *Proc Natl Acad Sci U S A* **71**, 2268-2272 (1974).

334  Taylor, D. L. & Wang, Y. L. Molecular cytochemistry: incorporation of fluorescently labeled actin into living cells. *Proc Natl Acad Sci U S A* **75**, 857-861 (1978).

335     Holmes, K. C., Popp, D., Gebhard, W. & Kabsch, W. Atomic model of the actin filament. *Nature* **347**, 44-49, doi:10.1038/347044a0 (1990).

336     Blanchoin, L., Boujemaa-Paterski, R., Sykes, C. & Plastino, J. Actin dynamics, architecture, and mechanics in cell motility. *Physiol Rev* **94**, 235-263, doi:10.1152/physrev.00018.2013 (2014).

337     Davidson, A. J. & Wood, W. Unravelling the Actin Cytoskeleton: A New Competitive Edge? *Trends Cell Biol* **26**, 569-576, doi:10.1016/j.tcb.2016.04.001 (2016).

338     Pollard, T. D. Actin and Actin-Binding Proteins. *Cold Spring Harb Perspect Biol* **8**, doi:10.1101/cshperspect.a018226 (2016).

339     Pollard, T. D. & Cooper, J. A. Actin and actin-binding proteins. A critical evaluation of mechanisms and functions. *Annu Rev Biochem* **55**, 987-1035, doi:10.1146/annurev.bi.55.070186.005011 (1986).

340     Pollard, T. D. & Quirk, S. Profilins, ancient actin binding proteins with highly divergent primary structures. *Soc Gen Physiol Ser* **49**, 117-128 (1994).

341     Pollard, T. D., Almo, S., Quirk, S., Vinson, V. & Lattman, E. E. Structure of actin binding proteins: insights about function at atomic resolution. *Annu Rev Cell Biol* **10**, 207-249, doi:10.1146/annurev.cb.10.110194.001231 (1994).

342     Pollard, T. D., Blanchoin, L. & Mullins, R. D. Molecular mechanisms controlling actin filament dynamics in nonmuscle cells. *Annu Rev Biophys Biomol Struct* **29**, 545-576, doi:10.1146/annurev.biophys.29.1.545 (2000).

343     Campellone, K. G. & Welch, M. D. A nucleator arms race: cellular control of actin assembly. *Nat Rev Mol Cell Biol* **11**, 237-251, doi:10.1038/nrm2867 (2010).

344     Takenawa, T. & Suetsugu, S. The WASP-WAVE protein network: connecting the membrane to the cytoskeleton. *Nat Rev Mol Cell Biol* **8**, 37-48, doi:10.1038/nrm2069 (2007).

345     Goode, B. L. & Eck, M. J. Mechanism and function of formins in the control of actin assembly. *Annu Rev Biochem* **76**, 593-627, doi:10.1146/annurev.biochem.75.103004.142647 (2007).

346     Pollard, T. D. Regulation of actin filament assembly by Arp2/3 complex and formins. *Annu Rev Biophys Biomol Struct* **36**, 451-477, doi:10.1146/annurev.biophys.35.040405.101936 (2007).

347     Bamburg, J. R. & Bernstein, B. W. Roles of ADF/cofilin in actin polymerization and beyond. *F1000 Biol Rep* **2**, 62, doi:10.3410/B2-62 (2010).

348     Moriyama, K. *et al.* Destrin, a mammalian actin-depolymerizing protein, is closely related to cofilin. Cloning and expression of porcine brain destrin cDNA. *J Biol Chem* **265**, 5768-5773 (1990).

349     Duan, X. *et al.* The small GTPase RhoA regulates the LIMK1/2-cofilin pathway to modulate cytoskeletal dynamics in oocyte meiosis. *J Cell Physiol*, doi:10.1002/jcp.26450 (2018).

350     Sun, H. Q., Yamamoto, M., Mejillano, M. & Yin, H. L. Gelsolin, a multifunctional actin regulatory protein. *J Biol Chem* **274**, 33179-33182 (1999).

351     Khurana, S. & George, S. P. The role of actin bundling proteins in the assembly of filopodia in epithelial cells. *Cell Adh Migr* **5**, 409-420, doi:10.4161/cam.5.5.17644 (2011).

352     Bartles, J. R. Parallel actin bundles and their multiple actin-bundling proteins. *Curr Opin Cell Biol* **12**, 72-78 (2000).

353     Otto, J. J. Actin-bundling proteins. *Curr Opin Cell Biol* **6**, 105-109 (1994).

354     Jansen, S. *et al.* Mechanism of actin filament bundling by fascin. *J Biol Chem* **286**, 30087-30096, doi:10.1074/jbc.M111.251439 (2011).

355     Al-Alwan, M. *et al.* Fascin is a key regulator of breast cancer invasion that acts via the modification of metastasis-associated molecules. *PLoS One* **6**, e27339, doi:10.1371/journal.pone.0027339 (2011).

356     Van Audenhove, I. *et al.* Fascin Rigidity and L-plastin Flexibility Cooperate in Cancer Cell Invadopodia and Filopodia. *J Biol Chem* **291**, 9148-9160, doi:10.1074/jbc.M115.706937 (2016).

357     Machacek, M. *et al.* Coordination of Rho GTPase activities during cell protrusion. *Nature* **461**, 99-103, doi:10.1038/nature08242 (2009).

358     Hanna, S. & El-Sibai, M. Signaling networks of Rho GTPases in cell motility. *Cell Signal* **25**, 1955-1961, doi:10.1016/j.cellsig.2013.04.009 (2013).

359     Sit, S. T. & Manser, E. Rho GTPases and their role in organizing the actin cytoskeleton. *J Cell Sci* **124**, 679-683, doi:10.1242/jcs.064964 (2011).

360     Spiering, D. & Hodgson, L. Dynamics of the Rho-family small GTPases in actin regulation and motility. *Cell Adh Migr* **5**, 170-180 (2011).

361     Girouard, M. P., Pool, M., Alchini, R., Rambaldi, I. & Fournier, A. E. RhoA Proteolysis Regulates the Actin Cytoskeleton in Response to Oxidative Stress. *PLoS One* **11**, e0168641, doi:10.1371/journal.pone.0168641 (2016).

362     Zhang, W., Huang, Y. & Gunst, S. J. The small GTPase RhoA regulates the contraction of smooth muscle tissues by catalyzing the assembly of cytoskeletal signaling complexes at membrane adhesion sites. *J Biol Chem* **287**, 33996-34008, doi:10.1074/jbc.M112.369603 (2012).

363     Li, H. *et al.* Simulation of crosstalk between small GTPase RhoA and EGFR-ERK signaling pathway via MEKK1. *Bioinformatics* **25**, 358-364, doi:10.1093/bioinformatics/btn635 (2009).

364     Rihet, S. *et al.* Mutation status of genes encoding RhoA, Rac1, and Cdc42 GTPases in a panel of invasive human colorectal and breast tumors. *J Cancer Res Clin Oncol* **127**, 733-738 (2001).

365     Pichot, C. S. *et al.* Cdc42-interacting protein 4 promotes breast cancer cell invasion and formation of invadopodia through activation of N-WASp. *Cancer Res* **70**, 8347-8356, doi:10.1158/0008-5472.CAN-09-4149 (2010).

366     Zins, K., Gunawardhana, S., Lucas, T., Abraham, D. & Aharinejad, S. Targeting Cdc42 with the small molecule drug AZA197 suppresses primary colon cancer growth and prolongs survival in a preclinical mouse xenograft model by downregulation of PAK1 activity. *J Transl Med* **11**, 295, doi:10.1186/1479-5876-11-295 (2013).

367     Prasad, C. P., Chaurasiya, S. K., Axelsson, L. & Andersson, T. WNT-5A triggers Cdc42 activation leading to an ERK1/2 dependent decrease in MMP9 activity and invasive migration of breast cancer cells. *Mol Oncol* **7**, 870-883, doi:10.1016/j.molonc.2013.04.005 (2013).

368     Chrysanthou, E. *et al.* Phenotypic characterisation of breast cancer: the role of CDC42. *Breast Cancer Res Treat* **164**, 317-325, doi:10.1007/s10549-017-4267-8 (2017).

369     Arias-Romero, L. E. & Chernoff, J. Targeting Cdc42 in cancer. *Expert Opin Ther Targets* **17**, 1263-1273, doi:10.1517/14728222.2013.828037 (2013).

370    Butler, B., Kastendieck, D. H. & Cooper, J. A. Differently phosphorylated forms of the cortactin homolog HS1 mediate distinct functions in natural killer cells. *Nat Immunol* **9**, 887-897, doi:10.1038/ni.1630 (2008).

371    Jankowska, K. I. & Burkhardt, J. K. Analyzing Actin Dynamics at the Immunological Synapse. *Methods Mol Biol* **1584**, 7-29, doi:10.1007/978-1-4939-6881-7_2 (2017).

372    Butler, B. & Cooper, J. A. Distinct roles for the actin nucleators Arp2/3 and hDia1 during NK-mediated cytotoxicity. *Curr Biol* **19**, 1886-1896, doi:10.1016/j.cub.2009.10.029 (2009).

373    Dustin, M. L. & Cooper, J. A. The immunological synapse and the actin cytoskeleton: molecular hardware for T cell signaling. *Nat Immunol* **1**, 23-29, doi:10.1038/76877 (2000).

374    Comrie, W. A., Babich, A. & Burkhardt, J. K. F-actin flow drives affinity maturation and spatial organization of LFA-1 at the immunological synapse. *J Cell Biol* **208**, 475-491, doi:10.1083/jcb.201406121 (2015).

375    Mace, E. M. & Orange, J. S. Dual channel STED nanoscopy of lytic granules on actin filaments in natural killer cells. *Commun Integr Biol* **5**, 184-186, doi:10.4161/cib.18818 (2012).

376    Ritter, A. T., Angus, K. L. & Griffiths, G. M. The role of the cytoskeleton at the immunological synapse. *Immunol Rev* **256**, 107-117, doi:10.1111/imr.12117 (2013).

377    Ritter, A. T. *et al.* Actin depletion initiates events leading to granule secretion at the immunological synapse. *Immunity* **42**, 864-876, doi:10.1016/j.immuni.2015.04.013 (2015).

378    Mace, E. M. & Orange, J. S. Lytic immune synapse function requires filamentous actin deconstruction by Coronin 1A. *Proc Natl Acad Sci U S A* **111**, 6708-6713, doi:10.1073/pnas.1314975111 (2014).

379    Ritter, A. T. *et al.* Cortical actin recovery at the immunological synapse leads to termination of lytic granule secretion in cytotoxic T lymphocytes. *Proc Natl Acad Sci U S A* **114**, E6585-E6594, doi:10.1073/pnas.1710751114 (2017).

380    Smyth, M. J., Hayakawa, Y., Takeda, K. & Yagita, H. New aspects of natural-killer-cell surveillance and therapy of cancer. *Nat Rev Cancer* **2**, 850-861, doi:10.1038/nrc928 (2002).

381    Vivier, E., Ugolini, S., Blaise, D., Chabannon, C. & Brossay, L. Targeting natural killer cells and natural killer T cells in cancer. *Nature reviews. Immunology* **12**, 239-252, doi:10.1038/nri3174 (2012).

382    Malmberg, K. J. *et al.* Natural killer cell-mediated immunosurveillance of human cancer. *Semin Immunol*, doi:10.1016/j.smim.2017.08.002 (2017).

383    Long, E. O., Kim, H. S., Liu, D., Peterson, M. E. & Rajagopalan, S. Controlling natural killer cell responses: integration of signals for activation and inhibition. *Annu Rev Immunol* **31**, 227-258, doi:10.1146/annurev-immunol-020711-075005 (2013).

384    Moretta, A. *et al.* Early liaisons between cells of the innate immune system in inflamed peripheral tissues. *Trends Immunol* **26**, 668-675, doi:10.1016/j.it.2005.09.008 (2005).

385     Mocikat, R. *et al*. Natural killer cells activated by MHC class I(low) targets prime dendritic cells to induce protective CD8 T cell responses. *Immunity* **19**, 561-569 (2003).

386     Walzer, T., Dalod, M., Vivier, E. & Zitvogel, L. Natural killer cell-dendritic cell crosstalk in the initiation of immune responses. *Expert Opin Biol Ther* **5 Suppl 1**, S49-59, doi:10.1517/14712598.5.1.S49 (2005).

387     Rosenberg, S. A. *et al*. Observations on the systemic administration of autologous lymphokine-activated killer cells and recombinant interleukin-2 to patients with metastatic cancer. *N Engl J Med* **313**, 1485-1492, doi:10.1056/NEJM198512053132327 (1985).

388     Miller, J. S. *et al*. Successful adoptive transfer and in vivo expansion of human haploidentical NK cells in patients with cancer. *Blood* **105**, 3051-3057, doi:10.1182/blood-2004-07-2974 (2005).

389     Geller, M. A. *et al*. A phase II study of allogeneic natural killer cell therapy to treat patients with recurrent ovarian and breast cancer. *Cytotherapy* **13**, 98-107, doi:10.3109/14653249.2010.515582 (2011).

390     Carlsten, M. & Childs, R. W. Genetic Manipulation of NK Cells for Cancer Immunotherapy: Techniques and Clinical Implications. *Frontiers in immunology* **6**, 266, doi:10.3389/fimmu.2015.00266 (2015).

391     Burga, R. A. *et al*. Improving efficacy of cancer immunotherapy by genetic modification of natural killer cells. *Cytotherapy* **18**, 1410-1421, doi:10.1016/j.jcyt.2016.05.018 (2016).

392     Hanahan, D. & Weinberg, R. A. Hallmarks of cancer: the next generation. *Cell* **144**, 646-674, doi:10.1016/j.cell.2011.02.013 (2011).

393     Katz, P., Zaytoun, A. M. & Lee, J. H., Jr. Mechanisms of human cell-mediated cytotoxicity. III. Dependence of natural killing on microtubule and microfilament integrity. *Journal of immunology* **129**, 2816-2825 (1982).

394     Brown, A. C., Dobbie, I. M., Alakoskela, J. M., Davis, I. & Davis, D. M. Super-resolution imaging of remodeled synaptic actin reveals different synergies between NK cell receptors and integrins. *Blood* **120**, 3729-3740, doi:10.1182/blood-2012-05-429977 (2012).

395     Sanborn, K. B. *et al*. Myosin IIA associates with NK cell lytic granules to enable their interaction with F-actin and function at the immunological synapse. *J Immunol* **182**, 6969-6984, doi:10.4049/jimmunol.0804337 (2009).

396     Cai, Z. *et al*. Alteration of the sphingomyelin/ceramide pathway is associated with resistance of human breast carcinoma MCF7 cells to tumor necrosis factor-alpha-mediated cytotoxicity. *The Journal of biological chemistry* **272**, 6918-6926 (1997).

397     Riedl, J. *et al*. Lifeact: a versatile marker to visualize F-actin. *Nat Methods* **5**, 605-607, doi:nmeth.1220 [pii]
10.1038/nmeth.1220 (2008).

398     Prehoda, K. E., Scott, J. A., Mullins, R. D. & Lim, W. A. Integration of multiple signals through cooperative regulation of the N-WASP-Arp2/3 complex. *Science* **290**, 801-806 (2000).

399     Alter, G., Malenfant, J. M. & Altfeld, M. CD107a as a functional marker for the identification of natural killer cell activity. *J Immunol Methods* **294**, 15-22, doi:10.1016/j.jim.2004.08.008 (2004).

400     Krzewski, K., Gil-Krzewska, A., Nguyen, V., Peruzzi, G. & Coligan, J. E. LAMP1/CD107a is required for efficient perforin delivery to lytic granules and NK-cell cytotoxicity. *Blood* **121**, 4672-4683, doi:10.1182/blood-2012-08-453738 (2013).

401     Castellano, F. *et al.* Inducible recruitment of Cdc42 or WASP to a cell-surface receptor triggers actin polymerization and filopodium formation. *Curr Biol* **9**, 351-360 (1999).

402     Rohatgi, R. *et al.* The interaction between N-WASP and the Arp2/3 complex links Cdc42-dependent signals to actin assembly. *Cell* **97**, 221-231 (1999).

403     Nobes, C. D. & Hall, A. Rho, rac, and cdc42 GTPases regulate the assembly of multimolecular focal complexes associated with actin stress fibers, lamellipodia, and filopodia. *Cell* **81**, 53-62 (1995).

404     Kozma, R., Ahmed, S., Best, A. & Lim, L. The Ras-related protein Cdc42Hs and bradykinin promote formation of peripheral actin microspikes and filopodia in Swiss 3T3 fibroblasts. *Mol Cell Biol* **15**, 1942-1952 (1995).

405     Schirenbeck, A., Bretschneider, T., Arasada, R., Schleicher, M. & Faix, J. The Diaphanous-related formin dDia2 is required for the formation and maintenance of filopodia. *Nat Cell Biol* **7**, 619-625, doi:10.1038/ncb1266 (2005).

406     Vignjevic, D. *et al.* Role of fascin in filopodial protrusion. *The Journal of cell biology* **174**, 863-875, doi:jcb.200603013 [pii]
10.1083/jcb.200603013 (2006).

407     Viry, E. *et al.* Hijacker of the Antitumor Immune Response: Autophagy Is Showing Its Worst Facet. *Front Oncol* **6**, 246, doi:10.3389/fonc.2016.00246 (2016).

408     Yilmaz, M. & Christofori, G. EMT, the cytoskeleton, and cancer cell invasion. *Cancer metastasis reviews* **28**, 15-33, doi:10.1007/s10555-008-9169-0 (2009).

409     Viry, E. *et al.* Autophagic degradation of GZMB/granzyme B: a new mechanism of hypoxic tumor cell escape from natural killer cell-mediated lysis. *Autophagy* **10**, 173-175, doi:10.4161/auto.26924 (2014).

410     Moussay, E. *et al.* The acquisition of resistance to TNFalpha in breast cancer cells is associated with constitutive activation of autophagy as revealed by a transcriptome analysis using a custom microarray. *Autophagy* **7**, 760-770 (2011).

411     Gugnoni, M., Sancisi, V., Manzotti, G., Gandolfi, G. & Ciarrocchi, A. Autophagy and epithelial-mesenchymal transition: an intricate interplay in cancer. *Cell Death Dis* **7**, e2520, doi:10.1038/cddis.2016.415 (2016).

412     Hansen, T. E. & Johansen, T. Following autophagy step by step. *BMC Biol* **9**, 39, doi:10.1186/1741-7007-9-39 (2011).

413     Raulet, D. H., Gasser, S., Gowen, B. G., Deng, W. & Jung, H. Regulation of ligands for the NKG2D activating receptor. *Annu Rev Immunol* **31**, 413-441, doi:10.1146/annurev-immunol-032712-095951 (2013).

414     Pentcheva-Hoang, T., Chen, L., Pardoll, D. M. & Allison, J. P. Programmed death-1 concentration at the immunological synapse is determined by ligand affinity and availability. *Proc Natl Acad Sci U S A* **104**, 17765-17770, doi:10.1073/pnas.0708767104 (2007).

415     Jang, J. H. *et al.* Imaging of Cell-Cell Communication in a Vertical Orientation Reveals High-Resolution Structure of Immunological Synapse and Novel PD-1 Dynamics. *J Immunol* **195**, 1320-1330, doi:10.4049/jimmunol.1403143 (2015).

416    Gross, C. C., Brzostowski, J. A., Liu, D. & Long, E. O. Tethering of intercellular adhesion molecule on target cells is required for LFA-1-dependent NK cell adhesion and granule polarization. *J Immunol* **185**, 2918-2926, doi:10.4049/jimmunol.1000761 (2010).

417    Eissmann, P. & Davis, D. M. Inhibitory and regulatory immune synapses. *Curr Top Microbiol Immunol* **340**, 63-79, doi:10.1007/978-3-642-03858-7_4 (2010).

418    Ding, H., Yang, X. & Wei, Y. Fusion Proteins of NKG2D/NKG2DL in Cancer Immunotherapy. *Int J Mol Sci* **19**, doi:10.3390/ijms19010177 (2018).

419    Klingemann, H., Boissel, L. & Toneguzzo, F. Natural Killer Cells for Immunotherapy - Advantages of the NK-92 Cell Line over Blood NK Cells. *Front Immunol* **7**, 91, doi:10.3389/fimmu.2016.00091 (2016).

420    Zuo, Y., Wu, Y. & Chakraborty, C. Cdc42 negatively regulates intrinsic migration of highly aggressive breast cancer cells. *J Cell Physiol* **227**, 1399-1407, doi:10.1002/jcp.22853 (2012).

421    Humphries-Bickley, T. *et al.* Characterization of a Dual Rac/Cdc42 Inhibitor MBQ-167 in Metastatic Cancer. *Mol Cancer Ther* **16**, 805-818, doi:10.1158/1535-7163.MCT-16-0442 (2017).

422    Carlin, L. M. *et al.* A targeted siRNA screen identifies regulators of Cdc42 activity at the natural killer cell immunological synapse. *Sci Signal* **4**, ra81, doi:10.1126/scisignal.2001729 (2011).

423    Sinai, P., Nguyen, C., Schatzle, J. D. & Wulfing, C. Transience in polarization of cytolytic effectors is required for efficient killing and controlled by Cdc42. *Proc Natl Acad Sci U S A* **107**, 11912-11917, doi:10.1073/pnas.0913422107 (2010).

424    Rane, C. K. & Minden, A. P21 activated kinase signaling in cancer. *Semin Cancer Biol*, doi:10.1016/j.semcancer.2018.01.006 (2018).

425    Smirnova, T. D., Danilenko, D. M. & Slita, A. V. [Role of cellular cytoskeleton in influenza A infectious cycle]. *Tsitologiia* **55**, 92-100 (2013).

426    Ritchey, L. & Chakrabarti, R. Aurora A kinase modulates actin cytoskeleton through phosphorylation of Cofilin: Implication in the mitotic process. *Biochim Biophys Acta* **1843**, 2719-2729, doi:10.1016/j.bbamcr.2014.07.014 (2014).

427    Benz, P. M. *et al.* Differential VASP phosphorylation controls remodeling of the actin cytoskeleton. *J Cell Sci* **122**, 3954-3965, doi:10.1242/jcs.044537 (2009).

**Antoun AL ABSI**

# Rôle du cytosquelette d'actine dans la résistance des cellules de cancer du sein à la lyse induite par les cellules « natural killer »

## Résumé

L'évasion immunitaire tumorale joue un rôle central dans la progression tumorale et représente un obstacle majeur au succès des immunothérapies. Dans cette Thèse nous avons étudié le rôle du cytosquelette d'actine dans la résistance des cellules de cancer du sein à la lyse induite par les cellules "natural killers" (NKs). Nous avons trouvé que les cellules de cancer du sein résistantes échappent à l'attaques des cellules NKs par une accumulation importante et rapide d'actine près de la synapse immunologique, un processus que nous avons nommé "réponse actine". Nos analyses mécanistiques suggèrent que la réponse actine induit la polarisation d'autophagosomes vers la synapse immunologique et facilite ainsi la dégradation des molécules cytotoxiques sécrétées par les cellules NKs, tel que le ganzyme B, par autophagie. De plus, la réponse actine est associée au regroupement de ligands inhibiteurs à la synapse, suggérant qu'elle est au centre de plusieurs mécanismes de résistance. Dans leur ensemble, nos résultats constituent une base pour le développement d'approches thérapeutiques visant à interférer avec la réponse actine et à restaurer une réponse immunitaire anti tumorale efficace.

Mots-clés : Cancer du sein, cellules Natural Killer, cytosquelette d'actine, Cytotoxicité, évasion immunitaire, granzyme B.

## Résumé en anglais

Tumor immune evasion plays a central role in cancer progression and is a major hurdle to effective immunotherapy. In this Thesis, we examine the role of the actin cytoskeleton in breast cancer cell resistance to natural killer (NK) cell-mediated cell lysis. We found that resistant breast cancer cells escape from NK-cell attack through a rapid and prominent accumulation of actin near the immunological synapse, a process we termed the "actin response". Our mechanistic investigations suggest that the actin response drives autophagosome polarization toward the immunological synapse and thereby facilitates the autophagy-mediated degradation of NK cell-derived cytotoxic molecules such as granzyme B. In addition, the actin response was associated with inhibitory ligand clustering at the immunological synapse, suggesting that it is a common driver of different immune evasion mechanisms. Taken together, our data lays the groundwork for therapeutic approaches aimed at interfering with the actin response and restoring an effective anti-tumor immune response.

Key words: Actin cytoskeleton, breast cancer, cytotoxicity, granzyme B, immune escape, natural killer.